Isolated Elliptical Galaxies

Fatma Mohamed Reda Mahmoud Mohamed
(M.Sc.)

A thesis presented in fulfilment of the requirements of
Doctor of Philosophy.

Faculty of Information and Communication Technology

Swinburne University of Technology

2007

Abstract

This thesis presents a detailed study of a well defined sample of isolated early-type galaxies. We define a sample of 36 nearby isolated early-type galaxies using a strict isolation criteria. New wide-field optical imaging of 20 isolated galaxies confirms their early-type morphology and relative isolation. We find that the isolated galaxies reveal a colour-magnitude relation similar to cluster ellipticals, which suggests that they formed at a similar epoch to cluster galaxies, such that the bulk of their stars are very old. However, several galaxies of our sample reveal evidence for dust lanes, plumes, shells, boxy and disk isophotes. Thus at least some isolated galaxies have experienced a recent merger/accretion event which may have also induced a small burst of star formation.

Using new long-slit spectra of 12 galaxies we found that, isolated galaxies follow similar scaling relations between central stellar population parameters, such as age, metallicity [Z/H] and α-element abundance [E/Fe], with galaxy velocity dispersion to their counterparts in high density environments. However, isolated galaxies tend to have slightly younger ages, higher metallicities and lower abundance ratios. Such properties imply an extended star formation history for galaxies in lower density environments.

We measure age gradients that anticorrelate with the central galaxy age. Thus as a young starburst evolves, the age gradient flattens from positive to almost zero. Metallicity gradients range from near zero to strongly negative. For our high mass galaxies, metallicity gradients are shallower with increasing galaxy mass. Such behaviour is expected in the remnants of multiple mergers. The metallicity gradients are also found to be correlated with the central age and metallicity, as well as to the age gradients. We generally find flat [E/Fe] gradients.

We also examine the Fundamental Plane in both traditional R_e, μ_e and σ space and κ-space. Most isolated galaxies follow the same Fundamental Plane tilt and scatter for galaxies in high density environments. However, a few galaxies notably deviate from the plane in the sense of having smaller M/L ratios. This can be understood in terms of their younger stellar populations, which are presumably induced by a gaseous merger.

In conclusion, our results are compatible with an extended merger/accretion history for most isolated elliptical galaxies. However, for those galaxies which show no fine structures nor any young stellar populations, an early formation epoch followed by passive evolution is more probable.

Acknowledgements

First and foremost I would like to thank my supervisor Duncan Forbes for giving me the opportunity to join his team at Swinburne University. I appreciate his incredible support starting from the stage of writing my first paper in astronomy and ending with this thesis. I greatly appreciate his unstinting sharing of expertise, knowledge and his suggestions, input, calm encouragement and remarkable patience. Thanks Duncan.

I am also very grateful to my co-advisor Robert Proctor for being very supportive and encouraging during my work with the stellar populations part of this study. He did not only provide me with his programming codes which were essential for this study, but also his advise and discussions were of great impact on my understanding of the details of this area of astrophysics. Thanks also to his insightful comments on the earlier drafts, unending patience and encouragements. Thanks Rob.

My deep thanks to George Hau whose discussions and consultation, during his visits to Swinburne or via email, significantly assisted me to accomplish this thesis. Thanks also to George for supplying me with the reduced 2-D spectra.

In particular I would like to thank Matthew Bailes for approving me as a visitor to the Center for more than two years and then as a formal student at Swinburne. I am really grateful to him for supplying me with all facilities that I needed.

I would also like to express my thanks to Lee Spitler, Max Spolaor, Trevor Mendel, Virginia Kilborn, Sarah Brough and Michael Pierce for the useful discussions and brainstorming during our regular meetings as well as other casual talks and conversations.

I greatly appreciate and thank Michael Beasley, Ewan O'Sullivan and Søren Larsen for participating with various aspects throughout this study.

I am also grateful to the supporting team at the Anglo Australian Observatory. I would like also to thank Paul Goudfrooij and Vera Kozhurina-Platais for supplying us with the reduced images observed with the ESO/MPG telescope and Ale Terlevich for his help with the observations.

I acknowledge and thank the generous support from the sponsors of my PhD scholarship. My living expenses for the first two years and travel fares were provided by The Egyptian Ministry of Higher Education. The Centre for Astrophysics & Supercomputing, the Faculty

of Information and Communication Technology and Swinburne University provided a full scholarship for the last year. I would also like to acknowledge a travel fund provided by the IAU Travel Grant Program.

Next, I want to thank all my good friends whom I met in Melbourne: Yasmine, Roza, Ika, Aisha, Dayana, Nora, Suzanne and Shereen. We shared lots of fun, happiness, laughter as well as tears. Their love and care was very supportive during my studying years, although, that make it more painful when I am leaving now.

Last but not least, I am very thankful and dedicate this thesis to my beloved family who, although very far in distance, are always in my heart. They gave me a huge support, encouragement and everlasting love and trust throughout every stage of my life.

Declaration

This thesis contains no material that has been accepted for the award of any other degree or diploma. To the best of my knowledge, this thesis contains no material previously published or written by another author, except where due reference is made in the text of the thesis. All work presented is primarily that of the author with paper co-authors making contributions to the relevant chapters.

Chapter 3 includes all the photometric measurements published in Reda et al., 2004, MNRAS, 354, 851 and Reda, Forbes & Hau, 2005, MNRAS, 360, 693. The CCD images of galaxies obtained at the ESO/MPG 2.2-m telescope were observed by Ale Terlevich and Duncan Forbes and reduced by Paul Goudfrooij and Vera Kozhurina-Platais.

Chapter 4 is an extract from the submitted paper Reda, Proctor, Forbes, Hau & Larsen, 2007, MNRAS, in press. The spectroscopic observations for galaxies and standard stars and basic data reduction including bias, dark current and flat field subtraction, wavelength calibration and correction for the S-distortion and sky subtraction, carried out by G.K.T Hau and D.A.Forbes and published in their paper Hau & Forbes, 2006, MNRAS, 371, 633. Their 2-D spectra are used by the author to produce results discussed in this chapter. The radial profile of the recession velocity in figure 4.3 and velocity dispersion in the top panels of figures 4.4 are based on new measurements by the author and included in this chapter.

Chapter 5 is based upon the published paper Reda, Forbes & Hau (2005). The velocity dispersion measurements from Hau & Forbes (2006) are replaced by new measurements by the author from chapter 4.

Minor alterations have been made to the published works in order to maintain consistency of style.

Fatma M. Reda

Contents

List of Figures

List of Tables

Chapter 1

Introduction

1.1 General overview

In this thesis we investigate the morphological structure and stellar population content of isolated early-type galaxies. Our aim is to understand how these galaxies formed and evolved. We define a sample of isolated early-type galaxies in the local universe ($z < 0.03$). Comparing the properties of these galaxies to their counterparts in higher density environments, we can obtain deeper insight into the parameters affecting their past formation and evolution.

Observations show that various properties of galaxies vary with their environment. Since the discovery of galaxies and their classification according to their appearance as ellipticals (E), spirals (S) and lenticular (S0), observations suggested a relation between galaxy morphology and the density of the host environment (e.g. Hubble & Humason 1931; Oemler 1974; Dressler 1980; Goto et al. 2003; Tanaka et al. 2004; Postman et al. 2005). While spiral galaxies are more numerous in the field, early-type galaxies, i.e. ellipticals and S0, are more commonly found in dense environments such as clusters and groups. Within a cluster, the dense core regions are richer with early-type galaxies than the lower-density outskirts. This distribution of galaxy morphology with environment is known as the morphology-density relation (Dressler 1980). Within galaxy groups, Domínguez et al. (2002) studied groups in the 2dF Galaxy Redshift Survey to explore the verification of both of the morphology-density relation and morphology-group centric radius relation. Both of the two previous relations were found to correlate with the total mass of the hosting group. Domínguez *et al.,* found that both the morphology-density relation and morphology-group centric radius are clearly seen in massive groups ($M \geq 10^{13.5}\ M_{\odot}$), while in groups of lower masses neither relation is apparent.

Environmental dependencies have also been seen in galaxy scaling relations such as the colour-magnitude relation (CMR) and the fundamental plane (FP), which is a 2-dimensional relation in 3-dimensional space determined by the galaxy size, luminosity and central velocity dispersion (see Sec. 1.5.2). For example, in a comparison study of early-type galaxies in the

field, groups and rich clusters, de Carvalho & Djorgovski (1992) found field galaxies to have a FP of higher intrinsic scatter than those in clusters, especially when stellar population variables were included. For a sample of 35 field early-type galaxies at a median redshift of 0.9, Kodama, Bower & Bell (1999) found these galaxies to have greater scatter in the CMR than that obtained by Stanford, Eisenhardt & Dickinson (1998) for cluster galaxies at a similar redshift of $z \sim 0.9$. This suggests a slightly more extended star formation period for early-type galaxies in the field than in clusters. Kodama at al. also found *some* of their sample galaxies to have redder colours than Coma cluster galaxies in the local Universe, indicating CMR evolution. These authors concluded that at least half of the field early-type galaxies at these redshifts formed their stars at $z > 2$.

The environment also plays a role in galaxy stellar populations. Studies of the stellar populations in early-type galaxies in different environments suggests that field galaxies tend to be bluer, and have spectral indices indicating stellar population of slightly younger mean ages and more metal rich than their cluster counterparts (e.g. de Carvalho & Djorgovski 1992; Kuntschner et al. 2002; Terlevich & Forbes 2002; Graham et al. 2003; Collobert et al. 2006).

In all environments, early-type galaxies show morphological fine structures such as tidal tails, dust lanes, discy or boxy components (Schweizer et al. 1990), while some other structures such as shells and irregular isophotes are more preferentially exist in the field and groups rather than in clusters (Malin & Carter 1983; Zepf & Whitmore 1993). These results suggests an environmental role in the formation of these morphological structures.

Theoretical models often attempt to explain these morphological structures as a result of past merging in earlier galaxy formation stages or, alternatively, by tidal interactions with close neighbours (Thomson 1991; Hernquist & Weil 1992; Schweizer 1992; Hjorth & Madsen 1995). In dense cluster environments, merging was more likely at earlier epochs when the cluster was still forming and velocity dispersions were low enough to allow outright mergers, while mergers in the field are expected to occur at high redshift as well as in the present Universe (Kauffmann 1995). Therefore long lasting morphological structures are expected to exist in all environments, while short life structures are predicted to be more common in low density environments.

Most previous studies of early-type galaxies in different environments have not been extended to the very low-densities of truly isolated galaxies. In such extreme low-density environments we can eliminate the effects of many physical processes which may affect the evolution of galaxies in denser environments.

In this study we define a new sample of 36 candidate isolated early-type galaxies with strict isolation conditions to ensure the absence of any strong tidal effects from a massive neighbour. Using the Wide Field Imager (WFI) on the 3.9-m Anglo-Australian Telescope (AAT) and the WFI on the ESO/MPG 2.2-m telescope we obtained imaging in the B and R filters for a wide area surrounding 20 galaxies in the sample. This allows us to study the number density distribution and photometric parameters of the faint galaxies in these fields as well as the

isolated galaxies themselves. Spectroscopic observations for twelve galaxies of the sample were collected using EFOSC2 at the ESO 3.6-m telescope on the La Silla Observatory in two observing runs. The long slit was positioned along the major axis of each galaxy. Using these spectra we obtain radial profiles of both kinematics and stellar population parameters for these 12 galaxies. The photometric, kinematical and stellar population parameters are supplemented by data from the literature to construct galaxy scaling relations.

The main aspect of this work, however is to investigate the observational properties of isolated early-type galaxies and compare them to those for galaxies in higher density environments. Based on the results of this study, we briefly discuss the implications for the formation of isolated early-type galaxies. Although this work does not give a full answer to all questions related to the formation and evolution of early-type galaxies, we aim to add number of useful constraints.

1.2 Formation and evolution scenarios

The observed homogeneity of the elliptical galaxy properties such as their luminosity profile, colour and velocity dispersion allow these galaxies to follow tight scaling relations with very small intrinsic scatter (see Sec. 1.5). Examining the slope and scatter of these scaling relations in the local universe and up to high redshifts (e.g. Stanford, Eisenhardt & Dickinson 1998; Saglia et al. 2000) suggests a uniform formation and evolution process for these galaxies. Furthermore, the existence of old, fully assembled massive elliptical galaxies at moderate redshifts of $1.6 < z < 1.9$, such as those observed by Cimatti et al. (2004), strongly suggest the formation of these galaxies in the early universe.

The formation scenario known as the dissipative "monolithic collapse" model, which we shall refer to as "collapse" model, postulates that elliptical galaxies were formed at high redshift on a short time scale during a rapid collapse of gaseous material in the form of a single cloud (Eggen, Lynden-Bell & Sandage 1962; Larson 1974; Chiosi & Carraro 2002; Kawata & Gibson 2003; Matteucci 2003). Their stars were formed in a short intense starburst last for less than 1 Gyr, followed by galactic wind which evacuates the galaxy of any extra gas and prevents any further star formation. The strength of the galactic wind ejecting the gas and ceasing star formation depends on the depth of the potential well of the galaxy, or its mass. Massive galaxies can hold their gas components longer to perform complete synthetic processes and produce heavier elements which is observed as a higher metallicity for these massive galaxies than less massive ones, and is known as the mass-metallicity relation. The end product of these models is an elliptical galaxy composed of mainly stars and no significant gas fraction. Another set of models are dedicated to follow the continuing collapse of these stellar components. These subsequent evolution is considered as a pure stellar dynamical problem or dissipationless collapse (e.g. van Albada 1982; Trenti, Bertin & van Albada 2005). The dissipationless collapse models can reproduce number of the observed properties

of elliptical galaxies such as their de Vaucouleurs $r^{1/4}$ surface brightness profile as well as the projected radial profiles of the line-of-sight velocity dispersion and the rotational velocity (see Sec. 1.3 for more details).

Moreover, recent high resolution N-body simulation of dissipationless collapse in pre-existing dark matter haloes (Nipoti, Londrillo & Ciotti 2006) are able to reproduce elliptical galaxies with surface brightness profiles resembling the observed characteristics, such as the Sérsic profile with a range of n index values and central cores (see Sec. 1.3.1).

However, according to the collapse scenario, a galaxy's photometric and morphological parameters are independent of the local environment of the galaxy, and consequently it does not explain the observed morphology-density relation. Moreover, this formation scenario does not explain the observed evidence of a substantial intermediate-age stellar population in early-type galaxies (e.g. Terlevich & Forbes 2002; McDermid et al. 2006), or the fine morphological structure such as shells, plumes and tidal tails (Malin & Carter 1983) which are found in a significant number of galaxies.

The other suggested model is the "hierarchical merging", which we shall refer to as "merging", model. This scenario provides a logical explanation for these observational features and is supported by the observations of interacting galaxies at different stages of the merging process (Vorontsov-Velyaminov 1959; Arp 1966a,b; Schweizer 1980; Schweizer & Seitzer 1988; Barnes & Hernquist 1992).

The merger scenario for galaxy formation and evolution at different redshifts is a natural extension of the hierarchical clustering theory, such as the Cold Dark Matter cosmological model. In all models, the Universe started as small-amplitude density fluctuations which were then amplified by gravitational instability acting on Cold Dark Matter until they became non-linear. The resulting bound clumps collapsed to form almost relaxed virialized Cold Dark Matter haloes. In the merger scenario, smaller haloes formed first and became progressively more massive by merging together and/or accreting surrounding material (Peebles 1982; Blumenthal et al. 1984). A fraction of the baryonic content of the halo starts cooling down by radiating a large amount of its energy and transfers to the halo centre cold, star-forming condensations (Rees & Ostriker 1977; Silk 1977; White & Rees 1978). Dissipative collapse continues until the cold gas settles into rotationally supported discs (Fall & Efstathiou 1980; Mo, Mao & White 1998). Merger/accretion processes continue to form larger structures on different scales, such as more massive galaxies, galaxy groups, clusters and super-clusters. However, formation of early-type galaxies through mergers was more probable in a cluster only at the early stages of the cluster formation where the relative velocity between galaxies was slow enough to allow mergers. On the other hand, galaxy mergers in the field are possible at high redshifts as well as in the present Universe.

If a galaxy consumes its gas content in star forming processes, followed by a galactic wind which rejects the remaining gas to the inter-galactic medium, then a dissipationless major merger between two such galaxies (a dry merger) will produce a massive elliptical galaxy

of uniformly old stellar population. Furthermore, numerical simulations of dissipationless mergers can reproduce the observed scaling relations of elliptical galaxies (Capelato, de Carvalho & Carlberg 1995; Dantas et al. 2003; González-García & van Albada 2003; Boylan-Kolchin, Ma & Quataert 2005). For example, the recent model of Naab, Khochfar & Burkert (2006) can reproduce the galaxy kinematics and isophotal shapes as a function its mass.

However, other simulations emphasize the importance of the gas component during mergers to obtain the observed scatter and slope of the scaling relations (Ciotti & van Albada 2001; Evstigneeva et al. 2004; Boylan-Kolchin, Ma & Quataert 2006). In addition, the recent numerical simulations by Robertson et al. (2006) found that gas dissipation significantly contributes to the tilt of the observed FP. Nevertheless, Robertson et al. found that the impact of dissipation on the remnant properties is mass dependent. During the first pericentric passage of a massive progenitor, the gas is heated and driven to the halo leading to a dissipationless like merger. On the other hand, low-mass galaxies experience rapid conversion of gas into stars which increases the impact of gas dissipation on the central properties of the remnant.

Since the early work by Larson & Tinsley (1978) and Lavery & Henry (1988), gaseous mergers are known to induce secondary star formation events as well as other morphological and kinematical substructures (Mihos & Hernquist 1996; Barnes 2004; see Sec. 1.3 for more details). Therefore, more massive galaxies are expected to have younger and more metal-rich central stellar populations, which formed during mergers over longer time scales, than smaller galaxies. However, these predictions are in contradiction with the observed scaling relations between the absolute magnitude (or central velocity dispersion) and both the age and metallicity of the central stellar populations (Bender & Saglia 1999; Mehlert et al. 2003; Collobert et al. 2006). The observed mass-age and mass-metallicity relations are in the sense that more massive elliptical galaxies are older and more metal-rich than the less massive ones. This phenomena is found to be stronger at higher redshifts than in the present Universe, and is known as “the down-sizing” phenomenon (Cowie et al. 1996; Madau et al. 1996; Shaver et al. 1996).

This observational evidence was the motivation for mechanisms to suppress the star formation processes in more massive galaxies. De Lucia, Kauffmann & White (2004) suggest that the dependence of the star formation rate on the circular velocity of the galaxy is able to accelerate star formation in massive galaxies more than in less massive ones. Another suggestion of a central massive black hole and AGN feedback in massive galaxies can also lead to the observed mass-age relation (Springel, Di Matteo & Hernquist 2005; Croton et al. 2006).

In the following sections the basic properties, stellar population parameters of elliptical galaxies and their scaling relations are explained and discussed in the context of these two formation and evolution scenarios.

1.3 Basic properties of early-type galaxies

In the following subsections we describe a number of the properties of early-type galaxies and discuss how they may be explained in the context of different formation scenarios.

1.3.1 Surface brightness profiles

The radial surface brightness profiles of elliptical galaxies show a high degree of regularity. de Vaucouleurs (1948) found that the isophotal surface-brightness μ (in magnitude/arcsec^2) follows the form

$$\mu(r) = \mu_e + 8.327\ [(\frac{r}{r_e})^{1/4} - 1], \tag{1.1}$$

called the de Vaucouleurs law. The quantity r_e is the radius of the isophote enclosing half the total light of the galaxy and is known as the effective radius. A related quantity to r_e is the mean surface-brightness μ_e at the effective radius.

The de Vaucouleurs $r^{1/4}$ law was found to be valid over a surface-brightness range of $17.8 < \mu < 27.8$ mag/arcsec^2 (de Vaucouleurs & Capaccioli 1979). The $r^{1/4}$ law fits most luminous elliptical galaxies, however for the brightest cluster elliptical galaxies, the $r^{1/4}$ law is only valid for the inner region, with the outer envelope of these giant galaxies showing enhanced light. On the other hand, the outer regions of small ellipticals are truncated below the $r^{1/4}$ law. Sérsic (1968) introduced his formula by replacing de Vaucouleurs $\frac{1}{4}$ by $\frac{1}{n}$, where n lies between 1 (exponential profile) up to more than 10. Therefore, the index n is a shape parameter measures the curvature of the galaxy light profile. Prugniel & Simien (1997) found that the index n is strongly correlated to the mass and size of small galaxies. However, for more luminous ($M_B < -20$), or large galaxies, n is found to be fairly constant at the de Vaucouleurs value.

The importance of the Sérsic index, as a measure of the central concentration of the galaxy light, has increased significantly in the last few years due to its strong relations to other physical properties of elliptical galaxies. In a series of papers by Graham and collaborators, the Sérsic index is found to show a tight correlation with the mass of the central black hole, with more massive black holes residing in more centrally concentrated galaxies (e.g. Graham et al. 2003; Erwin, Graham & Caon 2004; Graham & Driver 2007). This tight correlation of the mass of the central black hole and the Sérsic index represents another scaling relation which requires explanation by theoretical models of galaxy formation and evolution.

Using ground based observations it is difficult to study the light profile of the most inner regions of galaxies. Nevertheless, some evidence beyond the seeing limits indicated the presence of cores which could not be described by the isothermal King model (e.g. Lauer

1985; Kormendy 1985). Using the high spatial resolution of the *Hubble Space Telescope*, it became possible to investigate the true shape of galaxy cores. Inner to a break radius (r_b), the central surface brightness profiles of most galaxies are found to be either shallower or steeper than the global profile of the galaxy. Galaxies with shallow cusps are known as "core" galaxies, while those with steep cusps are called "power-law" galaxies.

Simulations show that the shape of the central light profile is correlated to the galaxy's formation history and the properties of its progenitors. For example, the simulations of Milosavljević & Merritt (2001) show that mergers of two power-law systems with central massive black holes produce a core profile galaxy.

We observe galaxies, such as NGC 1316 (Schweizer 1980) and NGC 7252 (Schweizer 1982), which are in the late stage of merging. However, despite their highly distorted isophotes, tidal tails and other evidence of a dramatic recent merger, the distribution of their light profiles in the inner parts follow perfectly the standard de Vaucouleurs law. Such galaxies present strong evidence that two merged disk galaxies can produce a typical elliptical galaxy with an $r^{1/4}$ de Vaucouleurs profile. During the gravitational collapse of a galaxy, or after a galaxy merger, the gravitational potential of the system fluctuates rapidly and irregularly. In such a time dependent potential, the collisionless process known as violent relaxation (Lynden-Bell 1967), redistributes the energies and angular momenta of stars and dark matter particles producing the observed uniformity and dynamical equilibrium of the final collisionless stellar systems – an elliptical galaxy.

1.3.2 Morphological fine structure

As well as the dominant elliptical shape of elliptical galaxies, the majority of them have morphological fine structures (e.g. Malin & Carter 1983; Schweizer & Seitzer 1988; Seitzer & Schweizer 1990; Barnes & Hernquist 1992). These structures are in the form of extra light regions which are usually detected as distortions in the isophotal shapes of the galaxies. The extra light regions take several forms such as shells, tails and extended plumes (Malin & Carter 1983; Schweizer & Seitzer 1988; Reid, Boisson & Sansom 1994).

Another types of fine structure observed in elliptical galaxies are discy and boxy isophotal shapes. Discy isophotes are found to be the result of extra light extending along the major/minor axis, while boxy isophotes are due to light at an angle of 45° to these axes. If the radial profile of the isophotal shape changes between discy and boxy, it is called an irregular isophote. In a detailed study of isophotal shapes in massive ellipticals, Bender et al. (1989) and Nieto & Bender (1989) found that the shape showed little or no correlation with the classic photometric parameters such as effective radius or ellipticity. However, galaxies which were radio-loud and/or surrounded by gaseous X-ray halos generally had boxy or irregular isophotes. Bender et al. also found that galaxies with boxy or irregular isophotes seem to have higher mass-to-light ratios ($\sim 11.5 \pm 0.9\ M_\odot/L_\odot$) than discy galaxies

($\sim 6.4 \pm 0.6\ M_{\odot}/L_{\odot}$). As a function of galaxy luminosity, low-luminosity galaxies show tendency to be discy, while more luminous galaxies are found to have boxy shapes. These observed correlations emphasise the intrinsic origin of the boxy/discy dichotomy and their dependence on the formation history of the galaxy (Bekki & Shioya 1997).

Central dust lanes are another common feature observed in a significant fraction of elliptical galaxies (e.g. Sadler & Gerhard 1985; Ebneter, Davis & Djorgovski 1988). The origin of dust in early-type galaxies is controversial. Some studies suggest an internal source such as the collective outflow of dusty gas from evolving red giant stars. However, Forbes (1991) found no strong correlation between the FIR dust emission in elliptical galaxies and their optical luminosities. This result argues in favour of an external origin for the dust in early-type galaxies, e.g. brought in during the accretion of a gas-rich galaxy. This result was confirmed by Goudfrooij & de Jong (1995) and Trinchieri & Goudfrooij (2002).

The majority of elliptical galaxies with these fine structures are found in the field rather than the higher density environments of clusters (e.g. Malin & Carter 1983; Colbert, Mulchaey & Zabludoff 2001). With the high probability of recent merger/interaction events occurring in the field at $z < 2$ rather than in high density clusters, these observational results are consistent with the numerical simulations which demonstrated that these fine structures can be reproduced by either a weak interaction with another galaxy (Thomson & Wright 1990; Thomson 1991) or minor/major mergers (Hernquist & Spergel 1992; Schweizer 1992; Hjorth & Madsen 1995). Mergers and interactions of galaxies with gas are expected to trigger star formation producing young stellar populations in the remnant galaxy. Estimating the age of galaxies using both spectroscopic indices and global colours, young galaxies are found to have stronger fine structures than older galaxies (Schweizer et al. 1990; Schweizer & Seitzer 1992).

Taking these observational results and theoretical expectations into consideration, isolated early-type galaxies would be expected to show a higher frequency of fine structures such as shells, tails and extended plumes than those galaxies in clusters and compact groups.

1.3.3 Internal kinematics

Analysis of the spectra of elliptical galaxies shows that the distribution of stellar velocities is generally close to a symmetric Gaussian. In addition to the ordered rotation velocity (V_r), the stars are also moving with random velocities known as velocity dispersion (σ) (Illingworth 1977). The net rotation of the galaxy is often characterized by the quantity $(\frac{V}{\sigma_o})^*$, where V is the maximum observed rotational velocity and σ_o is the central velocity dispersion of the galaxy, corrected for the galaxy ellipticity (Binney 1978; Kormendy 1982). While low-luminosity galaxies are found to be rotationally supported systems (with $(\frac{V}{\sigma_o})^* \sim 1$), massive elliptical galaxies are kinematically hot systems which are mainly supported by random velocities rather than rotation (Illingworth 1977; Davies et al. 1983). The internal kinematics

of galaxies are found to be correlated to their mass and isophotal shapes. For example, low-luminosity elliptical galaxies with discy isophotes have relatively higher rotational velocities than massive ellipticals of boxy isophotes which are found to be more dynamically hot systems (Bender 1988; Binney & Merrifield 1998; their Fig. 4.39).

Whereas collapse models are not likely to reproduce the kinematic substructures of elliptical galaxies, numerical simulations such as those by Burkert & Naab (2005), González-García & Balcells (2005), Cox et al. (2006), Jesseit et al. (2006), Naab, Jesseit & Burkert (2006) and Naab, Khochfar & Burkert (2006) can reproduce the observed kinematical substructures and their correlation with mass of the elliptical galaxies by mergers of progenitors with different mass ratios and gas fractions.

Observations suggest the presence of many other more complicated kinematical structures in elliptical galaxies. In some galaxies, the radial profile of the rotational velocity shows a strong central antisymmetric profile. This can indicate the presence of a kinematically-distinct rapidly rotating core (KDC) with an angular momentum vector that lies perpendicular to that of the bulk of the galaxy (Forbes 1992). Elliptical galaxies can also show intrinsic minor axis rotation (Bender 1988; Carter, Thomson & Hau 1998).

KDCs are predicted to be created either by accretion of a gas-rich satellite galaxy (Franx & Illingworth 1988) or mergers of elliptical galaxies (Balcells & Quinn 1990). KDCs also can be a counter-rotating central gas disks created during a merger of two gas-rich disk galaxies of equal mass (Hernquist & Barnes 1991). However Hau & Thomson (1994) suggested that mergers are not required to form KDC, which can be a result of a retrograde flyby encounter of an elliptical galaxy with an embedded highly rotating disk. In this case, the rotation of the outer regions of the galaxy is reversed, whereas the central disk is relatively unaffected.

1.3.4 Interstellar media

Observations have shown that the interstellar media in early-type galaxies takes several forms (Bregman, Hogg & Roberts 1992) such as dust (Ebneter & Balick 1985; Ferrari et al. 1999), cold neutral HI gas of temperature $T \sim 10$ K (Knapp, Turner & Cunniffe 1985; Morganti et al. 2006; Serra et al. 2007), ionised gas of $T \sim 10^4$ K (Phillips et al. 1986; Goudfrooij et al. 1994b) and hot X-ray emitting gas of $T \sim 10^{6-7}$ K (Forman, Jones & Tucker 1985; O'Sullivan, Forbes & Ponman 2001).

The amount of hot X-ray gas bound to an early-type galaxy is found to correlate to other properties such as the flatness of the galaxy, with more round galaxies being more X-ray luminous (Eskridge, Fabbiano & Kim 1995) than flattened galaxies of similar optical luminosity. Similar correlations have been detected in the radio bands with more round galaxies are also being more radio-loud.

Comparing the kinematics of the stellar and gaseous components of a galaxy gives a clue

to the origin of the gas. If the gas was produced internally due to stellar evolution, then it is expected to observe a similar rotation for both stars and gas. On the other hand, the accreted gas from outside the galaxy due to merger/accretion events may be counter-rotating compared to the stellar body of the galaxy.

The dust and gas in elliptical galaxies are usually found to be co-spatial, suggesting the same origin for both components. They are found to be oriented along the major and/or minor axes of the galaxies (Martel et al. 2004). Both the orientation and dynamics of dust and gas, compared to the stellar content of early-type galaxies, indicates an external origin (Forbes 1991; Ferrari et al. 1999; Caon, Macchetto & Pastoriza 2000). In this scenario, the cool cloud of gas and dust has been brought in during the accretion or merger with a gas-rich galaxy (Barnes & Hernquist 1992; Hau & Thomson 1994; Serra et al. 2007). However, the recent study of Sarzi et al. (2006) found that highly rotating elliptical and S0 galaxies show evidence of co-rotating stars and gas which indicates an internal origin for the gas. These results suggest that in addition to an external origin for the dust and gas, internal production processes are not completely eliminated.

1.4 Stellar populations

The stellar populations within galaxies offer a fossil record of their star formation and chemical evolution. Comparing the spatial distribution of different stellar populations in galaxies with the predictions of theoretical models therefore helps to differentiate between competing scenarios of formation and evolution. In the following sections we will define the basic stellar population parameters and their extraction from different observational techniques such as photometry and spectroscopy. We will also discuss these parameters in the context of the collapse and "hierarchical" formation scenarios.

1.4.1 Stellar population parameters

Age, metallicity and α-elements abundance are three key parameters to describe the stellar population content of galaxies. Young ages indicates a recent star formation history, while metallicity [Z/H] indicates the sum of all elements (Z) heavier than helium relative to hydrogen (H) and defined as

$$[Z/H] = \log(Z/H) - \log(Z/H)_{\odot} \tag{1.2}$$

where $(Z/H)_{\odot}$ is the solar ratio.

[E/Fe] is an another quantity which describes the metal content of the stellar population. This parameter quantifies the relative abundance of the so-called 'α-elements' to the Fe-

peak elements, and is defined in similar way as in Eq. 1.2 for [Z/H]. The importance of the [E/Fe] parameter arises from the fact that different supernovae types eject different types of elements. For example, the so-called 'α-elements' (N, O, Mg, Ca, Na, Ne, S, Si and Ti) which are used in the definition of [E/Fe], are predicted to be delivered mainly by the Type II supernovae which explode due to the core collapse of massive stars. Supernovae type II take place in the early stages of star formation bursts due to the short life time of their massive progenitor stars (Hashimoto, Iwamoto & Nomoto 1993; Thielemann, Nomoto & Hashimoto 1996). On the other hand, the elements Cr, Mn, Fe, Co, Ni, Cu, and Zn, referred to as Fe-peak elements, are suggested to be produced by exploding white dwarfs in binary systems as Type Ia supernovae (Greggio & Renzini 1983). Type Ia supernovae are delayed by to later stages of galaxy evolution (Kirshner & Oke 1975; Nomoto, Thielemann & Yokoi 1984; Matteucci & Greggio 1986). Therefore, early-formed stars are predicted to be rich in α-elements, while stars which formed later, after the delayed explosion of Type Ia supernovae, will be formed out of gas which was enriched with the Fe-peak elements. Thus, stars with high [E/Fe] ratios are implied to be formed in a sort time scale, while late star formation events are indicated by low [E/Fe] ratios. (Matteucci 1994; Thomas, Greggio & Bender 1999). Therefore, the parameter [E/Fe] is often used to betoken the duration of star formation in a galaxy.

1.4.2 Stellar population colours

Early attempts to study the stellar population of galaxies were performed via the interpretation of their observed colours. Since the early finding of Baade (1944), the integrated colours of early-type galaxies are found to be consistent with the typical colour of G-K dwarf and giant stars (see also Peletier et al. 1990), which suggests that the main bulk of stellar populations in early-type galaxies consists of these stars.

The colours of early-type galaxies are found to correlate very well with their luminosity (or mass), with more luminous galaxies tending to be redder (Baum 1959). This is known as the colour-magnitude relation (CMR). Assuming that elliptical galaxies mainly consist of old stellar populations, the slope of the CMR has been assumed to be primarily a metallicity, rather than an age, effect (e.g. Ferreras, Charlot & Silk 1999; Vazdekis et al. 2001). This suggestion also arises from the observed relation between the strength of metal absorption features such as those of CN and Mg (see Sec. 1.4.3) and galaxy luminosity (Faber 1973). These two correlations, CMR and line strength-magnitude relation, therefore imply that red luminous galaxies are more metal-rich than bluer less luminous ones. Bower, Lucey & Ellis (1992) explain the scatter of the relation as a result of scatter in age. As function of look back time, the slope of the CMR is found to be constant to high redshifts (Aragon-Salamanca et al. 1993; Ellis et al. 1997; Kodama et al. 1998; Stanford, Eisenhardt & Dickinson 1998; Holden et al. 2004), which again supports the metallicity interpretation.

Within a galaxy, colour gradients give clues to the radial distribution of its stellar populations. Ellipticals generally show a negative radial gradient (i.e. redder towards smaller radii; de Vaucouleurs 1961; Strom et al. 1976; Sandage & Visvanathan 1978; Peletier et al. 1990; Bernardi et al. 2003d). If colour is again assumed to correlate with metallicity, then central stellar populations are of higher metallicity than those in the outer regions. The concentration of high metallicity stellar populations in the central regions of elliptical galaxies can be explained in the collapse model as a result of the metal-enriched driven gas towards the galaxy centre, which in turn produces the central metal-rich stellar populations.

As a function of the local environment density (i.e. the number of galaxies per pc^3) colour gradients are found to be steeper for galaxies in lower density environments while galaxies in high density environments show shallower colour gradients (Tamura & Ohta 2000; Trager et al. 2000; La Barbera et al. 2005). Again, recalling the assumed correlation of colour with stellar metallicity, the reduced colour gradient indicates shallower metallicity gradients, which in turn could be a consequence of late mergers (White 1980), as such mergers between gas poor galaxies are expected to 'wash out' the radial metallicity gradient in the remnant elliptical galaxy. However, mergers with a gas-rich galaxy provide the forming elliptical galaxy with fresh fuel to produce young stellar populations in the central region and hence change both age and metallicity gradients. Both age and metallicity have effects on the integrated colours of galaxies (e.g. Worthey 1994). Therefore, the secondary central star formation induced by mergers is expected to alter the colour gradient of the elliptical galaxy in an unpredictable way. To complicate matters more, Worthey (1998) showed that these effects can be balanced if the ratio of age to metallicity changes is equal to 3/2. This is known as the age-metallicity degeneracy.

While galaxy colour failed to break the age-metallicity degeneracy, absorption features of the galaxy stellar spectra, such as Lick/IDS system, are found to be more promising.

1.4.3 Lick/IDS indices

As explained above, both age and chemical abundance information of early-type galaxies give important clues to understand their formation and evolutionary history. As both age and metallicity have similar effects on the integrated colour of galaxies (O'Connell 1994; Worthey 1994), it is necessary to introduce another set of observables to separate their effects and break the degeneracy.

At the Lick Observatory between 1972 and 1984, the strength of strong absorption-line features in the wavelength region 4000-6000 Å of Galactic stars were measured and quantified. All observations had been done using same Cassegrain spectrograph and the Image Dissector Scanner (IDS; Robinson & Wampler 1972). That Lick/IDS system included 11 absorption-line indices for a sample of 460 stars in the field and in globular clusters. These indices are defined and measured in a series of publications (e.g. Faber et al. 1985; Burstein,

Table 1.1: List of Lick/IDS indices shows the original Lick resolution from Trager et al. (1998)

Index	Resolution	Pseudocontinuum		Bandpass		Unit
$H_{\delta A}$	10.9	4041.600	4079.750	4083.500	4122.250	Å
		4128.500	4161.000			
$H_{\delta F}$	10.9	4057.250	4088.500	4091.000	4112.250	Å
		4114.750	4137.250			
CN_1	10.6	4080.125	4117.625	4142.125	4177.125	mag
		4244.125	4284.125			
CN_2	10.6	4083.875	4096.375	4142.125	4177.125	mag
		4244.125	4284.125			
Ca 4227	10.2	4211.000	4219.750	4222.250	4234.750	Å
		4241.000	4251.000			
G 4300	9.8	4266.375	4282.625	4281.375	4316.375	Å
		4318.875	4335.125			
$H_{\gamma A}$	9.5	4283.500	4319.750	4319.750	4363.500	Å
		4367.250	4419.750			
$H_{\gamma F}$	9.5	4283.500	4319.750	4331.250	4352.250	Å
		4354.750	4384.750			
Fe 4383	9.2	4359.125	4370.375	4369.125	4420.375	Å
		4442.875	4455.375			
Ca 4455	9.1	4445.875	4454.625	4452.125	4474.625	Å
		4477.125	4492.125			
Fe 4531	9.0	4504.250	4514.250	4514.250	4559.250	Å
		4560.500	4579.250			
C 4668	8.8	4611.500	4630.250	4634.000	4720.250	Å
		4742.750	4756.500			
H_β	8.5	4827.875	4847.875	4847.875	4876.625	Å
		4876.625	4891.625			
Fe 5015	8.4	4946.500	4977.750	4977.750	5054.000	Å
		5054.000	5065.250			
Mg_1	8.4	4895.125	4957.625	5069.125	5134.125	mag
		5301.125	5366.125			
Mg_2	8.4	4895.125	4957.625	5154.125	5196.625	mag
		5301.125	5366.125			
Mg_b	8.4	5142.625	5161.375	5160.125	5192.625	Å
		5191.375	5206.375			
Fe 5270	8.4	5233.150	5248.150	5245.650	5285.650	Å
		5285.650	5318.150			
Fe 5335	8.4	5304.625	5315.875	5312.125	5352.125	Å
		5353.375	5363.375			
Fe 5406	8.4	5376.250	5387.500	5387.500	5415.000	Å
		5415.000	5425.000			
Fe 5709	9.1	5672.875	5696.625	5696.625	5720.375	Å
		5722.875	5736.625			
Fe 5782	9.3	5765.375	5775.375	5776.625	5796.625	Å
		5797.875	5811.625			
Na_D	9.5	5860.625	5875.625	5876.875	5909.375	Å
		5922.125	5948.125			
TiO_1	9.7	5816.625	5849.125	5936.625	5994.125	mag
		6038.625	6103.625			
TiO_2	9.7	6066.625	6141.625	6189.625	6272.125	mag
		6372.625	6415.125			

Faber & Gonzalez 1986; Gorgas et al. 1993) and collected and summarized by Worthey et al. (1994) who also added 10 new indices to the list. Another four indices that measure the higher Balmer lines $H_{\delta A}$, $H_{\gamma A}$, $H_{\delta F}$, $H_{\gamma F}$ were added later to the Lick system by Worthey & Ottaviani (1997). The final full IDS index strengths was presented by Trager et al. (1998) for 381 galaxies, 38 globular cluster and 460 stars based on 7417 spectra observed in the 4000-6400 Å region. Trager et al. also describe the method of measuring Lick/IDS absorptions line strengths for galaxies accounting for the effect of their internal velocity dispersions. Table 1.1 gives the final list of the 25 Lick indices from Trager et al. (1998).

Each index is defined by the bandpass of the feature of interest and two pseudocontinuum bandpasses bracketing the spectral absorption feature to the blue and red sides. Seven of these indices measure the molecular bands CN_2, CN_1, Mg_1, Mg_2, Mg_b, TiO_1, TiO_2, while the other 18 indices measure atomic absorption lines.

The strength of the spectral feature is quantified by comparing the average flux within the absorption feature with the average flux in the two pseudocontinuum. Therefore, precise definition for the red and blue pseudocontinuum for each spectral index is required to obtain adequate measurement of its strength.

1.4.4 Lick/IDS indices and stellar population parameters

Absorption lines of galaxy spectra represent the fingerprints of the chemical elements of its stellar populations. However, the Lick system (Burstein et al. 1984; Faber et al. 1985) defines absorption-line indices at medium resolution of about 8 Å at $\lambda = 5000$ Å. The passband of the Lick indices are very broad and include number of absorption features from various elements. Therefore each Lick index is not directly correlated to a specific one element (Greggio 1997; Tantalo, Chiosi & Bressan 1998). Instead, it was more useful to study how the strength of each index correlates with the stellar parameters such as the temperature, surface gravity and overall metallicity. Such correlations are known as the fitting functions.

To quantify the power of the absorption line indices of the Lick/IDS system to break the age-metallicity degeneracy in galaxies, Worthey (1994) measured the relative size of changes in the age and metallicity that produce the same change in index. Balmer lines, D4000, G4300, $H_{\delta A}$, $H_{\delta F}$, $H_{\gamma HR}$, $H_{\gamma A}$ $H_{\gamma F}$ and H_{β} are found to be sensitive to the age with negligible sensitivity to the metallicity. On the other hand, indices such as Fe5015, Fe5709, Fe5782 and C4668 are highly metallicity sensitive, while some other indices (e.g. Ca4227, Fe4383 and TiO_1) can not individually break the degeneracy. The indices Mg_1, Mg_2 and Mgb are oftenly used to measure the Mg enrichment with respect to Fe indices, i.e. the [E/Fe] parameter (e.g. Kuntschner 2000; Trager et al. 2000). The two indices CN_1 and CN_2 are also found to correlate with the [E/Fe] values (Thomas, Maraston & Bender 2003; TMB03).

1.4.5 Stellar evolutionary isochrones

Estimating galaxy stellar population parameters from their integrated light can be achieved by using stellar population synthesis models. In order to generate these models it is necessary to build a series of stellar evolutionary tracks or isochrones (e.g. Maeder & Meynet 1989; Fagotto et al. 1994; Kim et al. 2002; Yi, Kim & Demarque 2003). These isochrones give stellar parameters such as the bolometric luminosities L, effective temperature T_{eff} and surface gravity g as functions of evolutionary time and chemical composition.

Converting the stellar parameters L, T_{eff} and g into observables such as line indices is possible either empirically or theoretically. Empirically, the colours and spectroscopic observations of large stellar libraries are used to find fitting functions for the strength of different spectral indices as a function of L, T_{eff} and g (e.g. Buzzoni, Gariboldi & Mantegazza 1992; Buzzoni, Mantegazza & Gariboldi 1994; Worthey et al. 1994). Stars in the solar neighbourhood of the Milky Way disk are metal-rich and have [E/Fe] ratios decreasing from 0.3 at a metallicity of –1 and below to 0.0 (solar) at solar metallicity and above (McWilliam 1997; and references therein). Therefore, any stellar population model adopting these calibrations must allow for this pattern of abundance ratios before the abundance of α-elements can be measured in populations such as elliptical galaxies.

The use of synthetic stellar spectra allows us to not only make this allowance but also to estimate [E/Fe] in galaxy populations. For example, Tripicco & Bell (1995; TB95) built their synthetic spectra by computing model atmosphere and synthetic spectra at 56 closely spaced intervals along a 5 Gyr solar abundance isochrone of Tripicco, Dorman & Bell (1993). This isochrone was found to provide a good fit to the colour-magnitude diagram of the well-studied old Galactic open cluster M67. TB95 models are distributed over a range of effective temperature and surface gravity and simulate the full set of Lick/IDS spectral indices. Calibration of their synthetic spectra is performed by allocating their model sequence on the T_{eff} - log(g) plane along with number of field stars and few dwarfs from the Coma and other stars from the M67 cluster from the Lick/ISD database. Further comparison was done by projecting their isochrones into spectral indices versus temperature, gravity and metallicity parameters and comparing them to the fitting function of Worthey et al. (1994). TB95 carefully defined three pairs of T_{eff} and g to represent the evolutionary phases of dwarfs, turn-off and giant stars. For each of these phases, TB95 used their synthetic spectra to quantify the dependence of the synthetic indices on the abundance of individual elements or alternatively, which chemical element significantly affect a particular index. In fact, using synthetic stellar spectra (see also Kurucz 1979; Lejeune, Cuisinier & Buser 1997; Westera et al. 2002), it is possible to avoid the over abundance issue and many other limitations caused by using empirical models.

1.4.6 Single stellar population models

Stellar population synthesis models can be used to predict the age and chemical composition of external galaxies from their observed integrated light by assuming single stellar populations (SSPs), i.e. all stars are assumed to be formed at once with identical chemical compositions and their mass distribution is given by a specific initial mass function (IMF). In fact stellar populations in galaxies are a mixture of stars with range of ages and metallicities. The strength of the line indices reflects the luminosity weighted sum of these source stellar populations. Since young stars are significantly more luminous than old stars at the blue wavelengths of the Lick indices, then their spectra will dominate the integrated spectra of the galaxy. Therefore, if a galaxy contains even a small population of young stars, comparing the galaxy spectra to SSP models will lead to measuring stellar parameters which reflect the small portion of these young stars, rather than the main bulk of old populations. Therefore the measured ages and metallicities are often refer to as *luminosity weighted* parameters.

TMB03 built their stellar population model using the SSP models presented in Maraston (1998) and Maraston et al. (2003). The stellar isochrones are from Bono et al. (1997), Cassisi et al. (1999) and Salasnich et al. (2000) and the initial mass function slope is adopted from Salpeter (1955).

The fitting functions of Worthey et al. (1994) is used to describe the stellar indices of the isochrones as functions of T_{eff}, g and metallicity. In the previous section we explained the abundance pattern of the stellar library, from which the fitting functions are calculated, toward high [E/Fe] at low metallicities. To avoid the effect of this pattern, TMB03 assign well-defined [E/Fe] ratios at all metallicities. TMB03 consider various element mixtures by increasing the abundances of the α-elements and decreasing the Fe-peak elements at a given total metallicity. This allows them to quantify the variation of the iron abundance [Fe/H] and the α-elements to iron ratio [E/Fe] at fixed total metallicity [Z/H]. The effect on the Lick indices due to these element abundance changes is quantified using the response functions of Tripicco & Bell (1995).

The model calibration is carried out with Milky Way globular clusters. Since the globular cluster stars are coeval and have same chemical composition, they are considered as an observed simple stellar population (SSP). Using photometric and spectroscopic observations of individual stars of the Galactic globular clusters, it is possible to determine their age, metallicity and α-element abundance independently from any model (e.g. Feltzing & Gilmore 2000; Puzia et al. 2002; Carretta et al. 2001; Coelho et al. 2001; De Angeli et al. 2005). Using the Lick indices of metal-rich globular cluster stars of the Galactic bulge measured by Puzia et al. (2002), Maraston et al. (2003) found that the Mg indices are stronger than predicted by the SSP models at a given iron index, i.e. their stars are α-elements enhanced. This confirms the previous studies that measured [E/Fe] of up to 0.3 (e.g. Barbuy et al. 1999; Coelho et al. 2001; Origlia, Rich & Castro 2002). Furthermore, several globular clusters, such as NGC 6528 and NGC 6553 are found to have high metallicity. Therefore these objects are

adequate for calibrating the SSP models toward the range most relevant to elliptical galaxies. Globular clusters of old ages between 9 and 14 Gyrs, derived from colour-magnitude diagrams (VandenBerg 2000), are used to calibrate the models of TMB03.

This stellar population model of TMB03 provide the whole set of Lick indices in the wavelength range $4000 \leq \lambda \leq 6500$ Å. It covers ages between 1 and 15 Gyr and [Z/H] from of -2.3 to super-solar metallicity of 0.5. It also gives a well-defined [E/Fe] ratio at all metallicities and avoids the intrinsic α-elements bias of the other models which are built using Milky Way template stars.

Korn, Maraston & Thomas (2005) extended the work of Tripicco & Bell (1995) and computed model atmosphere calculations including the wavelength of the higher order Balmer lines H_γ and H_δ. Using the results of these model atmospheres and following the recipe of TMB03, Thomas, Maraston & Korn (2004; TMK04) quantify the effect of changing the element abundance on the Lick $H_{\delta A}$, $H_{\gamma A}$, $H_{\delta F}$, $H_{\gamma F}$ indices. The final product of TMB03 and TMK04 work is a SSP model of the 25 Lick/IDS indices, which allows estimates of age, metallicity and α-element abundances of the integrated spectra of elliptical galaxies. This is the model used through out this thesis.

1.4.7 Internal radial gradients of stellar populations

Comparing the radial gradient of stellar population age, [Z/H], [E/Fe] and velocity dispersion σ within a galaxy, to the prediction of different theoretical models represents a key tool to differentiate between their suggested formation scenarios.

For example, the collapse scenario predicts uniformally old stellar populations with steeper metallicity gradients in more massive galaxies (Carlberg 1984; Chiosi & Carraro 2002; Kawata & Gibson 2003). Furthermore, an 'inside-out' formation scenario implies a negative [E/Fe] gradient as central stars are formed on a shorter time scale than those in the outer regions, and viz versa for 'outside-in' formation (Ferreras & Silk 2002). On the other hand, age gradients indicate the presence of relatively young stellar populations which can be a result of a secondary star formation epoch induced by recent dissipative merger/interaction event. Kobayashi & Arimoto (1999) compiled a list of models of 80 early-type galaxies with radial metallicity gradient measurements; the average value being –0.3 dex per dex, while they found difficulties measuring the age and [E/Fe] parameters for their galaxies.

For Coma cluster ellipticals, Mehlert et al. (2003) confirmed significant radial metallicity gradients but, on average, found no radial age or [E/Fe] gradients. In contrast, Sánchez-Blázquez, Gorgas & Cardiel (2006a) found significant age gradients in a sample of cluster, group and field early-type galaxies. A weak correlation between metallicity gradient and galaxy mass was found by Forbes, Sánchez-Blázquez & Proctor (2005) and Sánchez-Blázquez et al. (2007) for cluster ellipticals.

From these results we see that, different galaxy samples show different gradients of their stellar population parameters. Therefore the environmental effect on the galaxy stellar populations requires further investigations. Furthermore, non of these studies explore the stellar population gradients of galaxies in extremely low density environments.

1.5 Scaling relations

Despite the large variety in their internal dynamics, structure and stellar content, early-type galaxies also show a high degree of homogeneity. Their fundamental parameters are strongly correlated with a very small intrinsic scatter. Beside the colour-magnitude relation which we discussed in Sec. 1.4.2, there are other scaling relations connecting the observed properties of early-type galaxies. These are the FP and its projection in the surface brightness-size plane, known as Kormendy relation, and the Mg_2-σ_o relation.

These are the surface brightness-size relation, know as Kormendy relation, the fundamental plane and the Mg_2-σ_o relation. In the following subsection we will discuss these relations and their observed dependence on the local density of the galaxy environment.

1.5.1 The surface brightness-size relation

Kormendy (1977) found that the effective radius (r_e) of elliptical galaxies is correlated with the surface brightness at r_e (μ_e). Based on a larger sample, Hamabe & Kormendy (1987) found this correlation in the V-band to be:

$$\mu_e = 2.94 \log(r_e) + 19.48 \tag{1.3}$$

i.e. larger galaxies have lower surface brightness. Many studies have used this relation to investigate galaxy evolution with environment and look-back time. For example, Hoessel, Oegerle & Schneider (1987) studied 372 elliptical galaxies in 97 nearby ($z < 0.1$) Abell clusters and found that the brightest cluster galaxies to have a r_e-μ_e relation very similar to that in Hamabe & Kormendy (1987). However they also found that the less luminous ellipticals in the cluster cores had a steeper relation with a slope of 4.56, in the sense that at a given surface brightness these galaxies have smaller effective sizes. The distinction of the two different luminosity groups became more obvious in a later study by Capaccioli, Caon & D'Onofrio (1992) with a larger sample of Virgo cluster galaxies and other data collected from the literature. They confirmed that, unlike the low luminosity galaxies, the brightest cluster galaxies fit perfectly on the Hamabe & Kormendy relation. In a recent study by Khosroshahi et al. (2004), the Kormendy relation was explored for early-type galaxies in groups that have a range of X-ray luminosities. They found that group early-type galaxies show a similar relation to those in clusters. Up to redshifts of $z \sim 1.5$, elliptical galaxies in

clusters show a similar relation to cluster galaxies in the local universe, with no significant change in the slope or scatter (Ziegler et al. 1999; Waddington et al. 2002; La Barbera et al. 2003).

1.5.2 The fundamental plane

The observational studies of Djorgovski & Davis (1987) and Dressler (1987) found that elliptical galaxies are confined to a tight plane defined by: $r_e \propto < \mu_e >^{\beta} \sigma^{\alpha}$ in the 3 dimensional space of central velocity dispersion (σ), effective radius (r_e) and mean surface brightness ($< \mu_e >$) enclosed by r_e, where α and β are coefficients. This plane is known as the fundamental plane (FP), and it has a small intrinsic scatter in its edge-on projection suggesting a strong regularity in the process of elliptical galaxy formation (Jørgensen, Franx & Kjaergaard 1993; JFK93).

Theoretically, the FP can be derived from the scalar form of the virial theorem as: $r_e = K_s\ \sigma^2 < \mu_e >^{-1} (M/L)^{-1}$, where K_s is a structure parameter which depends on the luminosity, kinematic and density structure of a galaxy, and (M/L) is the mass-to-light ratio (Djorgovski, de Carvalho & Han 1988). The observed and theoretical forms of the FP are identical only if the term $K_s\ (M/L)^{-1}$ is a power-law function of σ and/or $< \mu_e >$. The observed intrinsic scatter of the FP implies a deviation of the relation from the pure power-law form. These deviations reflect the effects of galaxy formation and evolutionary processes. Assuming that early-type galaxies are homologous, i.e. have similar kinematic, luminosity, and density distributions so that K_s = constant, then the FP reflects the evolution of the M/L ratio, i.e. their stellar population and dark matter content, as a function of the galaxy mass or luminosity. However, a combination of stellar population and non-homology dependence of the FP tilt is also plausible (Trujillo, Burkert & Bell 2004).

The observed small scatter of the FP implies high regularity of the formation and evolution of the galaxies such as the scenario suggested by the collapse model. However, many numerical simulations based on the hierarchical merger scenario were able to reproduce galaxies location on a FP of similar scatter and tilt to the observed values either by dissipationless merger (Dantas et al. 2003; González-García & van Albada 2003; Nipoti, Londrillo & Ciotti 2003), or mergers of gas-rich disks (Aceves & Velázquez 2005; Bekki 1998).

The recent numerical simulations of Robertson et al. (2006) discuss the merger of progenitors of different structure and components such as stellar disk, fraction of gas and all subsequent processes including gas cooling, star formation, supernova feedback, and central super-massive black hole considering its growth and feedback. This model also examines the effect of these components on the tilt and scatter of the FP of the merger remnants. While the dissipationless merger of two galaxies composed of an exponential stellar disk embedded in a dark matter halo produces a FP similar to the virial theory prediction, dissipation mergers of gaseous disks produces a FP with a tilt and scaling similar to the observed near-

IR photometric FP. Introducing central super-massive black holes to the progenitors, while increasing the radius of the remnant galaxy by moving the central gaseous material outward due to the feedback-driven winds, does not change the final FP which remains similar to observed near-IR photometric FP. That is because the central black hole also affects the central velocity dispersion and surface mass density to compensate for larger radii to roughly maintain the FP scaling. Robertson et al. also note that changing the gas fraction of the progenitors or the total angular momentum of the merged bodies does not strongly influence the FP of the remnants. Merging spherical galaxies resulting from the previous disk mergers gave final remnants with a FP similar to that of their progenitors. The major conclusion of these simulations is that gas-rich disk mergers can reproduce FP with the observed tilt and scaling, which is not the case for dissipationless mergers.

1.5.3 Central stellar populations

Another type of scaling relation that early-type galaxies follow are the observed correlations between some line indices and the central velocity dispersion σ_o. Considering σ_o as a proxy for galaxy mass (Faber & Jackson 1976), such observed correlations determine constraints on the chemical evolution as a function of galaxy mass. Furthermore, changes of these correlations with the density of the local environment of the galaxy (e.g. Jørgensen 1997) highlight the environmental role on galaxy formation and evolution.

For example, the classical relation between the Mg_2 index and σ_o (Dressler 1984) for cluster galaxies was revisited by Guzmán et al. (1992) who studied this Mg_2-σ_o correlation for a sample of 51 elliptical galaxies in Coma cluster. They found a zero point offset of 0.017 ± 0.005 between the correlation for galaxies in the cluster centre and those in the outskirts.

However, later studies suggested that this offset to be mainly driven by low mass galaxies rather than the massive ones. For example, Bernardi et al. (1998) studied the Mg_2-σ_o relation for a sample of 931 galaxy in clusters, groups and in the field. While luminous massive galaxies of $\log(\sigma_o) > 1.5$ (or $M_B < -18.5$) in both environments are found to follow similar Mg_2-σ_o correlation with insignificant offset of 0.005 ± 0.004, smaller galaxies show more pronounced zero point offset of 0.011 ± 0.006 between cluster and field galaxies. Bernardi et al. interpreted this offset as a result of luminosity-weighted age difference of about 1 Gyr with field galaxies being younger.

While both cluster and field galaxies of Bernardi et al. (1998) sample show similar scatter for the Mg_2-σ_o relation, that was not the case for the sample galaxies of Denicoló et al. (2005a; D05a). Comparing a sample of galaxies in low density environments such as groups and in the field to the Fornax cluster galaxies, from Kuntschner (2000), D05a found their galaxies to have Mg_2-σ_o relation with higher scatter than those in Fornax cluster. These results of D05a are consistent with the previous explanation of the scatter of the Mg_2-σ_o correlation as a result of recent star formation triggered by recent merger/interaction events (Schweizer

et al. 1990; Worthey & Collobert 2003), as such events are more probable in the low density environments than clusters in the local Universe.

On the other hand, eliminating the age effect by including old galaxies only, Kuntschner (2000) found, for 22 early-type galaxies in the Fornax cluster, the Mg_2 index as well as other Fe-line, Balmer lines and Ca4455 indices have clear positive correlations with σ_o. Kuntschner found that galaxies in Fornax cluster show correlation between both Mg_2 and $C_2$4668 with σ_o consistent to those of galaxies in the dense environment of the Coma (Jørgensen 1999) and other clusters (Jørgensen 1997). However $\log(\langle Fe \rangle)$-σ_o and $\log(H\beta)$-σ_o relations show different slopes (far steeper and shallower respectively) in Fornax cluster compared to Coma. Kuntschner relates the presence of these index-σ_o relations to the effect of galaxy metallicity rather than age. In fact, the interpretation of the Mg_2-σ_o relation in terms of age or metallicity is complicated due to the degeneracy of these two parameters on the line indices.

As explained in Sec. 1.4.6, the luminosity-weighted stellar population parameters such as age, metallicity [Z/H] and enhanced element abundances [E/Fe], can be measured by comparing the absorption line indices to stellar population models. The central stellar populations in cluster galaxies are found to be older and less metal-rich than those for field and loose groups galaxies (Kuntschner et al. 2002; Terlevich & Forbes 2002; Proctor et al. 2004b). These parameters are also found to correlate strongly to the central velocity dispersion σ_o of galaxies, in the sense that galaxies of high σ_o being older, more metal-rich and have higher [E/Fe] than those with lower σ_o (Bernardi et al. 2003d; Mehlert et al. 2003). The dispersion of these correlations are found to be related to the local environment density with galaxies in field and loose groups showing higher scatter than those in clusters (Collobert et al. 2006).

1.6 Outline of the thesis

In this chapter we have shown that several properties of elliptical galaxies are correlated to the local density of their environments. In order to disentangle the relative secular and environmental effects on the formation and evolution of these galaxies and also to examine the predictions of different formation scenarios, we study a sample of extremely isolated elliptical galaxies in the local universe.

In Chapter 2, previous studies of isolated early-type galaxies are summarized stating their selection criterion and briefly mentioning their results. Our improved selection criteria and the sample of 36 candidates are also presented with a number of galaxies in environments of higher density as a comparison sample.

Chapter 3 introduces the photometric imaging for a subsample of 20 isolated galaxies and the comparison sample and satellites in the field. Considering the results of this photometric study we discuss a number of possible formation scenarios for the isolated elliptical galaxies.

Chapter 4 details the long-slit observations of 12 isolated galaxies which were obtained using EFOSC2 at the ESO 3.6m telescope on the La Silla Observatory in two observing runs. Lick spectral indices are measured and fitted to a single stellar population model to estimated the stellar population parameters and their radial distribution for these galaxies. The results are used to discuss a number of outstanding issues related to the formation scenarios of isolated elliptical galaxies.

The scaling relations between the observable parameters of the elliptical galaxies such as the fundamental plane and its projection in the r_e-$< \mu_e >$ plane, know as Kormendy relation, are investigated in Chapter 5.

Finally, we summariez our results and draw conclusions from the whole study in Chapter 6. This chapter also includes suggested future work to follow up on understanding the past history of isolated elliptical galaxies.

Chapter 2

Isolated early-type galaxies

2.1 Introduction

Isolated galaxies represent the 'extreme field' galaxy population and thus provide additional insight to those environment related processes. A carefully selected sample of isolated early-type galaxies will offer a useful tool to tackle many of the outstanding issues in galaxy formation. For example, in dense environments, separating the effects of secular and environmental evolution ("nature versus nurture") is challenging. However, in such extremely low-density environments as those of isolated galaxies, one can eliminate the interaction processes that affect the evolution of galaxies in high-density environments such as ram-pressure stripping (Gunn & Gott 1972), strangulation (Balogh & Morris 2000; Fujita 2004), high-speed galaxy-galaxy encounters and tidal interactions with the cluster gravitational potential (Moore et al. 1996; 1999; Moore, Lake & Katz 1998).

2.2 Previous studies of early-type galaxies in low-density environments

Here we briefly review previous studies of galaxies in low-density environments. Each study had its advantages and limitations.

Karachentseva (1973) - a catalogue of ∼1000 galaxies with $m_B < 15.7$ and declination $> -3°$. The catalogue was chosen from the Zwicky et al. (1957) catalogue which is known to be biased against low surface brightness galaxies. The environment of each galaxy was inspected using the Palomar Observatory Sky Survey (POSS) for large neighbours. Isolation was established as the absence of companions within 20 galaxy diameters that have less than a ±2 magnitude difference from the primary galaxy (Stocke et al. 2004). For a number of reasons, including saturation and poor resolution in the POSS plates, one half of ellipticals in this catalogue appear to be morphologically misclassified (Saucedo-Morales & Bieging

2001).

Reduzzi, Longhetti & Rampazzo (1996) - a sample of 61 galaxies was selected from 'The Surface Photometry Catalogue' of the ESO-Uppsala Galaxies survey (Lauberts & Valentijn 1989). The galaxies were considered as isolated when the average number of galaxies of any morphology type was ≤ 1.5 within a radius of 1°. The sample of 61 galaxies were imaged for 20 min each at the 0.9-m ESO-Dutch telescope at La Silla, Chile. They noted that ten of the galaxies (i.e. 16 per cent of their galaxy sample) contained spiral arms or bars, indicating they were of late-type morphology. The isolation of the galaxies was quantified using the ratio of the separation between the target and the nearest galaxy in units of the target galaxy diameter, i.e. S/D_{25}. For galaxies with $S/D_{25} \leq 20$, they examined an additional parameter, i.e. the luminosity ratio between the target and the nearest galaxy L_B/L_B^n. Using these two parameters S/D_{25} and L_B/L_B^n, they suggested that three galaxies had significant companions. One of these was a misclassified spiral. Based on the S/D_{25} and L_B/L_B^n values given in their paper, we determined that another 7 galaxies have significant companions. This leaves a total of 42 galaxies that can be considered isolated and of early-type. For their total sample of 61 galaxies, they found about 40 per cent to have fine structures such as shells, dust, tidal tails, etc. Considering only the 42 isolated early-type galaxies, this percentage increases to 52 per cent.

Colbert, Mulchaey & Zabludoff (2001) - a sample of 30 early-type galaxies, selected from the Third Reference Catalogue (RC3; de Vaucouleurs et al. 1991) catalogue. Galaxies were selected to have no catalogued neighbours within 1 h_{100}^{-1} Mpc and ± 1000 km s^{-1}. Imaging of fields surrounding each galaxy was then used to confirm the lack of large galaxies within 200 h_{100}^{-1} kpc. However, some of the target galaxies themselves had luminosities only slightly greater than the catalogue limit. This means that some candidate isolated galaxies actually have nearby neighbours of quite similar luminosity. Our examination of this sample with the Digitised Sky Survey (DSS) suggests that $\sim$50 per cent of the candidate isolated galaxies have nearby neighbours.

Aars, Marcum & Fanelli (2001) - a sample of nine isolated elliptical galaxies selected from Karachentseva (1973). Two selection criteria were adopted for the initial identification of the isolated elliptical candidates. Firstly, elliptical galaxies were selected from the NASA Extragalactic Database (NED) that have separations of 2.5 Mpc from any other galaxy in the RC3. Secondly, the galaxy should have no neighbours with a known redshift (from NED) brighter than $M_V = -16.5$, within a projected separation of 2.5 Mpc. Only one galaxy in the RC3 and 13 in the Karachentseva (1973) catalogue meet these isolation criteria. From this sample of 14 galaxies, wide-field CCD images in the V-band were obtained using the 2.1-m telescope at McDonald Observatory. The one RC3 galaxy was a southern object which could not be imaged from McDonald Observatory and was therefore not included in the final sample. The images were used to check the isolation of these galaxies and to confirm the morphological type. This process identified that three were actually spiral galaxies and one was an irregular-type galaxy. These were excluded from further study leaving a

final sample of nine isolated elliptical galaxies. Aars et al. defined a characteristic number density of projected galaxies on the sky for known loose groups and clusters. Comparing the number density of galaxies detected in the field of their 9 galaxies with these characteristic densities, they identified 5 galaxies to be in environments similar to those of loose groups. The environments of the remaining four galaxies were confirmed to be of low density.

Kuntschner et al. (2002) - a sample of nine nearby early-type galaxies in low-density environments (strictly speaking this is not an isolated galaxy sample). They were selected from the Hydra-Centaurus Catalogue of Raychaudhury (1989; 1990) to be early-type (T < -3) with velocities $< 7,000$ km s^{-1} and apparent magnitudes of $b_J \leq 16.1$. Their sample completeness at this magnitude is ~ 50 per cent. These galaxies were then required to have a maximum of two neighbours with $b_J \leq 16.7$, within a radius of 1.3 Mpc and a velocity difference 350 km s^{-1}. The result was a sample of 40 E and S0 galaxies. Visual inspection of the DSS images revealed that some of the galaxies have late-type morphologies leaving a sample of 30 early-type galaxies in low-density environments. Spectroscopic observations of 24 galaxies of this sample were obtained at the 2.3-m telescope at the Siding Spring Observatory, Australia. Kuntschner et al. found 5 galaxies to have emission line spectra typical of spiral galaxies, 3 have red shifts beyond 7,000 km s^{-1} (the adopted redshift limit in their work), 4 galaxies were classified as group/cluster members and 2 had spectra of poor signal-to-noise. Kuntschner et al. also obtained optical UVR and near-infrared K_s imaging data for their sample with the CTIO 1.5-m telescope in Chile. By inspecting the model-subtracted images of the sample, one galaxy showed clearly visible spiral arms. In their final sample of 9 galaxies, 6 are members of the Arp & Madore (1987) catalogue of peculiar galaxies, i.e. they have indications of a past merger. The spectra indicate the presence of young stellar populations in several of these galaxies.

Smith, Martínez & Graham (2004) - a sample of 32 isolated early-type galaxies (T < -4). The Lyon-Meudon Extragalactic Data Archive (LEDA) catalogue was used to find ellipticals which have velocities $< 10,000$ km s^{-1}, absolute magnitudes $M_B \leq -19$ and Galactic latitudes $b >| 25^\circ |$. The LEDA database was also used to identify the faint neighbours in the field of the selected galaxies. The isolation criteria include a B-band magnitude difference > 0.7 between the primary galaxy and the neighbouring galaxies within a projected distance of 1 Mpc, or > 2.2 magnitudes within 500 kpc. They did not include any redshift information in their isolation criteria. They used the published data from the UK and Palomar Schmidt Sky Survey plates to select all detected dwarf galaxies with absolute magnitudes of $M_B \leq -14.6$ in the field of the primary galaxies. The sample of dwarfs brighter than $M_B = -16.8$ or with low surface brightness are incomplete.

Stocke et al. (2004) - a sample of early-type galaxies were selected from the Karachentseva (1973) catalogue. Thirteen galaxies were eliminated from the initially selected sample after checking the POSS plates and finding some comparably sized companions missed by Karachentseva (1973). Some of the sample galaxies are too faint and compact to be classified correctly by POSS. So for 80 per cent of the Es and 86% of the S0s galaxies, the morphology

and isolation were examined by Stocke et al. using optical imaging taken at Mt. Hopkins 0.6-m telescope and from images included in Adams, Jensen & Stocke (1980). That lead to the elimination of a further seven galaxies. Thus the final sample consists of 62 E and 36 S0 galaxies.

Collobert et al. (2006) - This sample of 41 galaxies are extracted from two sources. The first was the Anglo-Australian Observatory (AAO) two-degree field galaxy redshift survey (Colless et al. 2001; 2dFGRS). Galaxies were selected to be of absolute magnitude higher than $M_B = -19.13$ and with recession velocity $cz < 10\,000$ km s^{-1}, and their spectra from the 2dFGRS does not show strong emission lines. The field of these galaxy sample were required to have a maximum of 1 galaxy, not brighter than the candidate galaxy, within a sphere of radius 1 Mpc h^-1 or five galaxies within radius of 2 Mpc h^-1. Therefore binary systems are probably included in this sample. The galaxy morphology was checked using images from the DSS, NED and the 2 Micron All Sky Survey (2MASS) and galaxies with obvious spiral arms or disturbed morphology were excluded. The final list included 30 galaxies. Another 11 galaxies were added to this sample from the sample of Colbert, Mulchaey & Zabludoff (2001). These galaxies were selected from the RC3 to have a recession velocity $\leq$ 10 000km s^{-1} and have no catalogued companion galaxy within a projected radius of 1 Mpc h^-1 and velocity of $\pm$1000 km s^{-1}.

Having decided that most of the previous isolated galaxy samples were not suitable for our purpose, we have then designed our own definition.

2.3 Sample selection and the isolation criteria

Our sample of candidate isolated early-type galaxies was taken from the LEDA. This catalogue contains information on $\sim 100,000$ galaxies, of which $\sim 40,000$ have enough information recorded to be of use in this work. From this sample, we selected galaxies which satisfied the following criteria:

- Morphological type $T \leq -3$, i.e. early-type.
- Virgo corrected recession velocity $V \leq 9,000$ km s^{-1}, i.e. within 120 Mpc.
- Apparent magnitude $B \leq$ 14.0.
- Galaxy not listed as a member of a Lyon Galaxy Group (Garcia 1993).

The restrictions on apparent magnitude and recession velocity were imposed to minimize the effect of incompleteness in the catalogue. The LEDA catalogue is known to be 90 per cent complete at $B = 14.5$ (Amendola et al. 1997), so our sample should be close to being 100 per cent statistically complete. The selection process produced 330 galaxies which could

be considered as potential candidates. These were compared to the rest of the catalogue and accepted as being isolated if they had no neighbours which were within:

- 700 km s^{-1} in recession velocity,
- 0.67 Mpc in the plane of the sky, and
- 2.0 B-band magnitudes of the isolated galaxy.

These criteria were imposed to ensure that the galaxies did not lie in groups or clusters and that any neighbouring galaxies were too small and too distant to have any significant effect on the primary galaxy.

To check the results of this process, all galaxies were compared to the NED and the DSS. A NED search in the area within 0.67 Mpc of the galaxy identified galaxies which are not listed in LEDA. We also examined the DSS images for galaxies of similar brightness to the target which are not listed in either catalogue. This process produced 36 candidate isolated early-type galaxies. Basic data for this sample are listed in Table 2.1.

2.4 Comparison sample

As a comparison sample to our isolated galaxies for the photometric part of this study, we consider five galaxies in different environments. The galaxy IC 4320 is a part of an interacting isolated galaxy pair (with the spiral ESO509-G100). They have a B-magnitude difference of 0.88 and recession velocity difference of 260 km s^{-1}. The projected distance between them is 8.2 arcmin or 212 kpc (Soares et al. 1995). We also include imaging of a few galaxy groups to act as a comparison to our isolated galaxies. These are the NGC 3557 (LGG 229), NGC 4697 (LGG 314) and NGC 5266 (LGG 356) groups. In our comparison group sample, we also have included NGC 3528. Although it is not in the Garcia (1993) group catalogue, it has a luminous late-type galaxy (NGC 3529) at a projected distance of 5 arcmin or 70 kpc with B-band magnitude difference of 1 and recession velocity difference of 77 km s^{-1}. There is also a galaxy group (USGC S160) located at a projected distance of 14.8 arcmin or 207 kpc from NGC 3528, with a recession velocity difference of 30 km/s. In addition, there are many intermediate luminosity galaxies in the field of NGC 3528 with no published magnitude and/or velocity. The basic data for our comparison sample are summarized in Table 2.2.

Table 2.1: The sample of 36 isolated galaxies.

Galaxy	Type	B_T (mag)	Magnitude source	Dist. (Mpc)	Previous samples
NGC 682	E/S0	14.36	LEDA	73	
NGC 821	E	11.33	LEDA	23	SMG04
NGC 1041	E/S0	14.28	LEDA	93	
NGC 1045	E/S0	13.45	LEDA	60	
NGC 1132	E	13.03	LEDA	92	CMZ01
NGC 1162	E	12.88	LEDA	51	SMG04
NGC 2110	E/S0	12.21	LEDA	28	CMZ01
NGC 2128	E/S0	12.66	NED	44	
NGC 2271	E/S0	12.52	LEDA	32	
NGC 2865	E	11.98	LEDA	35	RLR96
NGC 3562	E	12.99	LEDA	93	
NGC 4240	E	13.31	LEDA	26	
NGC 4271	E/S0	13.48	NED	66	
NGC 4555	E	13.05	LEDA	90	
NGC 6172	E	13.75	LEDA	67	CMZ01
NGC 6411	E	12.47	LEDA	53	SMG04
NGC 6653	E	13.02	LEDA	66	SMG04
NGC 6702	E	12.61	LEDA	66	CMZ01
NGC 6776	E	12.51	LEDA	70	PR04
NGC 6799	E	12.98	LEDA	65	RLR96, CMZ01
NGC 6849	E/S0	12.93	LEDA	79	CMZ01
NGC 7330	E	12.66	NED	74	
NGC 7796	E	12.08	LEDA	42	
MCG-01-27-013	E/S0	14.71	LEDA	121	
MCG-01-03-018	E/S0	14.13	LEDA	77	
MCG-02-13-009	E	13.04	LEDA	73	
MCG-03-26-030	E/S0	14.26	LEDA	119	
ESO 107-G004	E	12.55	LEDA	39	
ESO 153-G003	E	13.66	NED	84	
ESO 194-G021	E/S0	13.34	LEDA	41	
ESO 218-G002	E	13.66	LEDA	54	
ESO 318-G021	E	13.24	LEDA	62	RLR96
ESO 462-G015	E	12.46	LEDA	77	
IC 1211	E	13.48	LEDA	78	
UGC 1735	E	13.42	NED	109	
UGC 2328	E	13.11	NED	68	

Notes: Hubble types are from LEDA. B_T is the total B magnitude corrected for Galactic extinction from Schlegel, Finkbeiner & Davis (1998). The sources of the B magnitude are listed in the next column. Distances obtained using the Virgo corrected recession velocities (from LEDA) with $H_0 = 75$ km s^{-1} Mpc^{-1}. Some galaxies were listed in previous samples such as: Reduzzi, Longhetti & Rampazzo (1996; RLR96), Colbert, Mulchaey & Zabludoff (2001; CMZ01) and Smith, Martínez & Graham (2004; SMG04), Pierfederici & Rampazzo (2004; PR04).

Table 2.2: The comparison sample.

Galaxy	Type	B_T (mag)	Magnitude source	Dist. (Mpc)	Environment
IC 4320	S0	13.85	NED	89	Isolated pair
NGC 3528	S0	12.88	LEDA	48	Group
NGC 3557	E	10.79	NED	38	Group
NGC 4697	E	10.02	LEDA	17	Group
NGC 5266	E/S0	11.17	LEDA	38	Group

Notes: Same as Table 2.1 for the comparison sample. The table includes the environment of each galaxy.

Chapter 3

Photometric properties

3.1 Introduction

In the previous chapter we introduced a sample of 36 highly isolated early-type galaxies. Here we present imaging for a subsample of these isolated galaxies and the comparison group galaxies in the B and R-bands. Using these images we measure the galaxy magnitudes, colour and effective parameters such as radius and mean surface brightness. We also investigate the internal morphological structure of these galaxies. The wide field imaging and the multi exposure time allow to detect satellite galaxies in the field of several isolated galaxies and study their luminosity function, number density distribution and also their gravitational effect on the primary galaxy. Comparing our results to the predictions of different formation models we discuss the possible formation scenarios.

3.2 Observations and data reduction

Imaging of 20 isolated galaxies of the sample in Table 2.1 and the 5 galaxies of the comparison sample in Table 2.2 have been observed for the purpose of this study. For 10 isolated galaxies and the comparison sample, B and R-band images were obtained using the Wide Field Imager (WFI) on the 3.9-m Anglo-Australian Telescope (AAT) on 2002 February 17th-19th. The WFI on the AAT is an 8-CCD imaging mosaic, of 2048 $\times$ 4096 pixels thinned back-illuminated CCDs with a pixel scale of $0.229''$ pix^{-1} giving a field-of-view of 30.6 $\times$ 30.6 sq. arcmins. Over the three nights there was some partial cloud and typical seeing conditions of about $2.0''$ in B and $1.5''$ in R. The exposure times for the galaxies and the number of observations are listed in Table 3.1. In addition to the galaxies, several standard star fields from Landolt (1992) were obtained during the observing run. These consisted of 10 sec exposures for both B and R-bands.

All galaxy and standard star images observed at the AAT telescope were reduced in an

identical manner using IRAF tasks. Six of the WFI CCD's have one or two bad columns which were corrected by interpolating the pixel values on both sides of the bad column. Data reduction included subtraction of the overscan regions. These regions were then trimmed before correcting the frames by master bias subtraction, dark frame subtraction and flat fielding using combined dome flats. The final images are flat to ≤ 2 per cent. We multiplicatively corrected for the different gains between CCDs using measurements of the mean sky level in each CCD, relative to the 'best' CCD (i.e. CCD6 which is cosmetically the cleanest). Finally, multiple exposures for several galaxies are combined to give an average integration time.

After determining an optimal aperture size of 10 pixels ($\sim 2.3"$), based on a curve-of-growth type analysis, raw magnitudes of between 7 and 25 stars were obtained for each filter using the IRAF task QPHOT. The zero-point for each filter was determined by a simple linear fit to the stellar raw magnitude versus their colours published by Landolt (1992) and corrected for airmass. The atmospheric extinction coefficients used were $k_B = 0.22$ and $k_R = 0.08$ mag/airmass. The final photometric zero-points are $Z_B = 25.19 \pm 0.06$ and $Z_R = 25.93 \pm 0.04$.

For another 10 isolated galaxies, imaging in the B and R-bands were obtained using the WFI on the ESO/MPG 2.2-m telescope on 2001 August 7th-10th. This WFI is an 8-CCD mosaic, focal reducer-type digital camera with 67-million pixel and a pixel scale of $0.227''$ pix^{-1} giving a field-of-view of 34×33 sq. arcmins. It has a high light sensitivity that allow more than 90 per cent of all incoming photons to be recorded. Each galaxy had several equal exposures which were combined to give an average integration time similar to the individual exposure time as summarized in Table 3.1. The median seeing conditions over the three nights were $1.3''$ in B and $1.1''$ in the R-band. To estimate the zero point for the magnitude measurements, standard star fields from Landolt (1992) were also obtained during the observing run on the ESO/MPG telescopes. These consisted of 10 sec exposures for both B and R-bands. For imaging obtained on the ESO/MPG telescope, the CCD frames reduction including overscaned correction and trimming, bias and dark frame subtraction, flat fielding, multi exposure combining and photometric zero-points estimation were carried out by D.A. Forbes and A.I. Terlevich.

3.3 Measuring photometric parameters of the isolated galaxies

In this section we use the reduced CCD images and the adopted photometric zero-points Z_B and Z_R to measure the B and R magnitude, colour and size of the isolated galaxies. We also investigate their inner morphological fine structures.

Table 3.1: Observational data of the combined sample.

Galaxy	A_B (mag)	A_R (mag)	Telescope	Exp. Time (sec)
NGC 1045	0.18	0.11	AAT	(B) 1×240
				(R) 1×120
NGC 1132	0.27	0.17	AAT	(B) 1×240
				(R) 1×120
NGC 2110	1.62	1.00	AAT	(B) 1×240
				(R) 1×120
NGC 2865	0.36	0.22	AAT	(B) 1×240
				(R) 1×120
NGC 4240	0.23	0.15	AAT	(B) 1×240
				(R) 1×120
NGC 6172	0.51	0.31	AAT	(B) 1×240
				(R) 1×120
NGC 6653	0.38	0.23	ESO	(B) 120
				(R) 120
NGC 6776	0.23	0.14	ESO	(B) 180
				(R) 300
NGC 6799	0.26	0.16	ESO	(B) 120
				(R) 120
NGC 6849	0.32	0.19	ESO	(B) 120
				(R) 120
NGC 7796	0.04	0.03	ESO	(B) 120
				(R) 120
ESO107-G004	0.19	0.12	ESO	(B) 120
				(R) 120
ESO153-G003	0.12	0.08	ESO	(B) 120
				(R) 120
ESO194-G021	0.07	0.04	ESO	(B) 120
				(R) 120
ESO218-G002	0.75	0.46	AAT	(B) 2×120
				(R) 2×60
ESO318-G021	0.35	0.22	AAT	(B) 1×120
				(R) 1×60
ESO462-G015	0.31	0.19	ESO	(B) 120
				(R) 120
MCG-01-03-018	0.25	0.16	ESO	(B) 180
				(R) 120
MCG-01-27-013	0.19	0.12	AAT	(B) 2×240
				(R) 2×120
MCG-03-26-030	0.22	0.14	AAT	(B) 1×240
				(R) 1×120
IC 4320	0.26	0.16	AAT	(B) 1×240
				(R) 1×120
NGC 3528	0.17	0.11	AAT	(B) 1×240
				(R) 1×120
NGC 3557	0.43	0.26	AAT	(B) 1×60, 3×600
				(R) 1×60, 3×420
NGC 4697	0.13	0.08	AAT	(B) 1×60, 3×600
				(R) 1×60, 3×420
NGC 5266	0.38	0.24	AAT	(B) 2×240
				(R) 2×120

Notes: The Galactic extinctions A_B and A_R are from Schlegel, Finkbeiner & Davis (1998). The exposure time for galaxies observed at the ESO/MGP telescope are the total integrated times. The table has been divided into three sections based on environment.

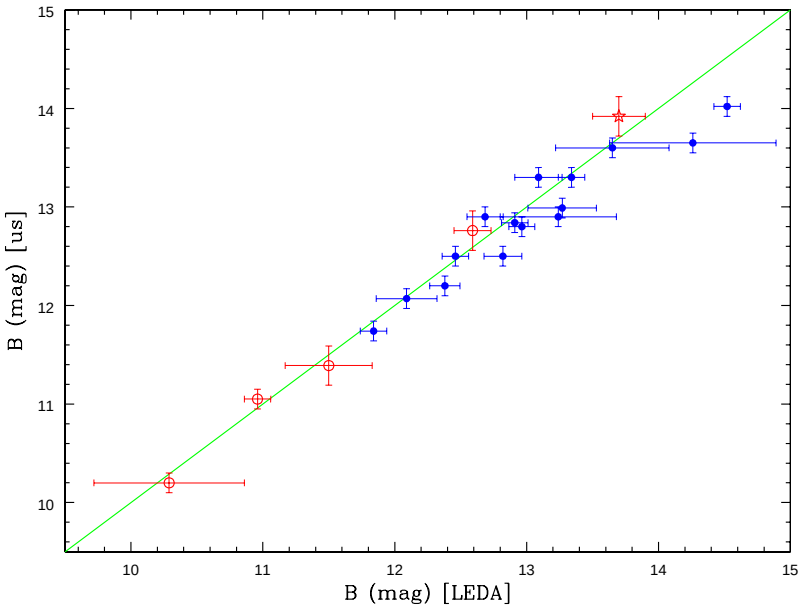

Figure 3.1: Comparison between our measured B magnitudes and the published values in LEDA. Filled and open circles represent group and isolated galaxies respectively, while the star is the primary galaxy of an isolated pair (IC 4320). The solid line is the one-to-one relation. Our measurements show good consistency with values from LEDA.

3.3.1 Magnitudes and colours

The QPHOT task in IRAF was used to obtain total magnitudes for the 25 primary galaxies in our sample. The sky was generally computed in an annulus of radius 1000 pixels and width of 50 pixels. Total magnitudes were derived by fitting a curve-of-growth to galaxy aperture magnitudes from 3× the seeing radius to large radii. Finally, the total magnitudes B and R were corrected for Galactic extinction using values from Schlegel, Finkbeiner & Davis (1998) as given in Table 3.1.

For ESO318-G021 and NGC 4240, the B frame is dominated by the light from a close bright star which prevented us measuring total B magnitudes. Considering the typical colour for galaxies in the present sample and the B magnitude quoted by LEDA, then our measured R magnitude for both of these two galaxies seems reasonable. A mean total (B–R) colour of 1.47 ± 0.03 was obtained for the 18 remaining galaxies. Our measured total B and R magnitudes, corrected for Galactic extinction, are given in Table 3.2. Fig. 3.1 shows the good agreement between our B magnitudes compared to the published values from LEDA.

3.3.2 Modelling and surface brightness profile fitting

Visual inspection of our CCD images of the galaxies in our sample confirms their early-type morphology as published in LEDA. The ISOPHOTE package in IRAF was used to fit a

Table 3.2: Measured photometric and size parameters.

Galaxy	B (mag)	±	R (mag)	±	$(B–R)_e$ (mag)	±	$r_e(B)$ (arcsec)	±	$r_e(R)$ (arcsec)	±
NGC 1045	13.0	0.1	11.4	0.1	1.63	0.14	15.7	4.2	16.7	1.6
NGC 1132	12.9	0.1	11.6	0.1	1.70	0.14	29.8	3.6	32.0	3.5
NGC 2110	11.7	0.1	10.3	0.1	1.47	0.14	28.3	1.4	24.3	1.2
NGC 2865	12.1	0.1	10.8	0.1	1.26	0.14	28.3	0.8	27.7	0.2
NGC 4240	-	-	11.3	0.1	-	-	-	-	-	-
NGC 6172	13.6	0.1	12.3	0.1	1.44	0.14	12.4	1.9	11.1	1.2
NGC 6653	12.8	0.1	11.4	0.1	1.62	0.14	26.0	1.4	25.2	0.2
NGC 6776	12.5	0.1	10.9	0.1	1.52	0.14	23.4	6.4	18.3	4.4
NGC 6799	13.3	0.1	11.8	0.1	1.60	0.14	18.7	0.9	19.3	0.2
NGC 6849	12.9	0.1	11.6	0.1	1.87	0.14	37.7	1.1	34.5	2.8
NGC 7796	12.2	0.1	10.6	0.1	1.53	0.14	25.2	1.3	22.7	3.1
ESO107-G004	12.6	0.2	11.2	0.2	1.79	0.20	25.3	3.8	17.5	4.2
ESO153-G003	13.7	0.1	12.1	0.1	1.53	0.14	10.2	1.5	17.4	6.1
ESO194-G021	13.3	0.1	11.6	0.1	1.38	0.14	14.8	0.7	17.6	0.8
ESO218-G002	12.8	0.1	11.4	0.1	1.58	0.14	22.0	6.6	20.1	5.0
ESO318-G021	-	-	12.1	0.1	-	-	-	-	21.7	3.2
ESO462-G015	12.5	0.2	11.0	0.1	1.59	0.17	21.3	0.9	18.7	1.3
MCG-01-27-013	14.0	0.1	12.5	0.1	1.58	0.14	16.1	2.1	13.8	0.9
MCG-01-03-018	13.4	0.1	12.0	0.1	1.64	0.14	24.4	0.5	19.1	1.3
MCG-03-26-030	13.7	0.1	12.1	0.1	1.63	0.14	14.3	0.6	15.6	2.5
IC 4320	13.9	0.2	12.3	0.1	1.59	0.22	27.6	9.5	22.4	4.5
NGC 3528	12.8	0.2	11.2	0.1	1.63	0.22	43.2	15.	45.6	0.9
NGC 3557	11.1	0.1	9.6	0.1	1.57	0.14	29.7	4.2	24.8	4.8
NGC 4697	10.2	0.1	8.8	0.1	1.46	0.14	86.9	9.9	65.3	6.5
NGC 5266	11.4	0.2	9.9	0.1	1.31	0.22	-	-	53.4	11.7

Notes: The table lists total magnitudes, colour at the effective radius and the effective radius itself.

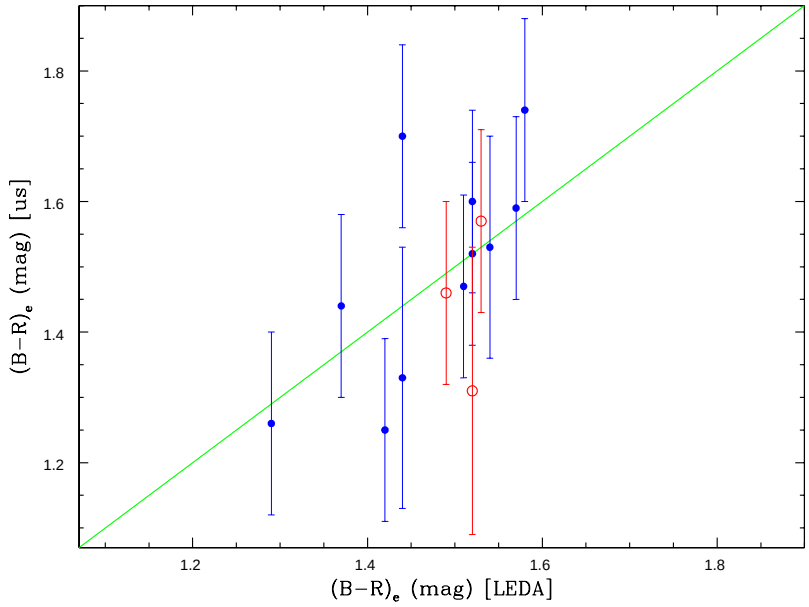

Figure 3.2: Comparison between our measured colour at the effective radius $(B–R)_e$ and the published values in LEDA. Generally, the two measurements are comparable. Symbols as in Fig. 3.1.

Table 3.3: Derived photometric parameters.

Galaxy	M_B (mag)	±	M_R (mag)	±	$< \mu_e >_B$ (mag/sq.")	±	$< \mu_e >_R$ (mag/sq.")	±
NGC 1045	-20.9	0.1	-22.5	0.1	20.8	0.1	19.4	0.1
NGC 1132	-21.4	0.1	-23.2	0.1	22.5	0.1	21.0	0.1
NGC 2110	-20.5	0.1	-21.9	0.1	20.7	0.1	19.0	0.1
NGC 2865	-20.6	0.1	-21.9	0.1	20.8	0.1	19.5	0.1
NGC 4240	-	-	-20.8	0.1	-	-	-	-
NGC 6172	-20.5	0.1	-21.8	0.1	20.8	0.1	19.1	0.1
NGC 6653	-21.1	0.1	-22.7	0.1	21.6	0.1	20.2	0.1
NGC 6776	-21.7	0.1	-23.3	0.1	21.1	0.1	19.4	0.1
NGC 6799	-21.1	0.1	-22.3	0.1	21.3	0.1	20.0	0.1
NGC 6849	-21.6	0.1	-22.9	0.1	22.2	0.1	21.4	0.1
NGC 7796	-21.0	0.1	-22.5	0.1	21.1	0.1	19.4	0.1
ESO107-G004	-20.4	0.2	-21.8	0.2	21.4	0.2	19.6	0.2
ESO153-G003	-20.9	0.1	-22.5	0.1	20.6	0.1	19.9	0.1
ESO194-G021	-19.7	0.1	-21.5	0.1	21.0	0.1	19.5	0.1
ESO218-G002	-20.9	0.1	-22.3	0.1	21.5	0.1	19.8	0.1
ESO318-G021	-	-	-21.9	0.1	-	-	20.6	0.2
ESO462-G015	-22.	0.1	-23.4	0.1	21.3	0.2	19.4	0.1
MCG-01-03-018	-21.0	0.1	-22.4	0.1	22.3	0.1	20.2	0.1
MCG-01-27-013	-21.4	0.1	-22.9	0.1	22.0	0.1	20.1	0.1
MCG-03-26-030	-21.7	0.1	-23.3	0.1	21.4	0.1	19.9	0.1
IC 4320	-20.9	0.2	-22.5	0.1	22.7	0.2	20.8	0.1
NGC 3528	-20.6	0.2	-22.2	0.1	22.4	0.2	20.9	0.1
NGC 3557	-21.8	0.1	-23.3	0.1	20.5	0.1	18.6	0.1
NGC 4697	-21.0	0.1	-22.4	0.1	21.4	0.1	19.5	0.1
NGC 5266	-21.5	0.2	-23.0	0.1	-	-	20.1	0.1

Notes: The table lists the absolute magnitudes and the mean surface brightness within the effective radius.

smooth elliptical model to the galaxy image (e.g. Forbes & Thomson 1992). In this package the isophotes are fit using an iterative method described by Jedrzejewski (1987). Before modelling the galaxy, the sky value was determined and subtracted. The program starts at a small radius and increases to large radii in a geometrical progression. The galaxy centre, position angle and ellipticity were allowed to vary.

Since our sample consists of early-type galaxies with absolute magnitudes in the range $-19.2 > M_B > -22.1$, their surface brightness profiles can be well fit by a de Vaucouleurs $R^{1/4}$ law (Prugniel & Simien 1997; Kuehn & Ryden 2005; see also Sec 1.3.1). By fitting the surface brightness profiles we derived the effective radii (r_e) and mean surface brightnesses ($< \mu_e >$) within r_e. To avoid resolution effects, the fitting was applied from a radius of about 3× the seeing to large radii. In the case of NGC 5266 there is a strong dust ring around the galaxy (see also Goudfrooij et al. 1994a). This prevented us from deriving a reliable surface brightness profile and parameters in the B-band. However for the R-band, only a small region of the profile was affected. This was masked and excluded from the fit. We were also unable to measure reliable profiles in the B and R-bands for NGC 4240 and the

Table 3.4: Derived effective radii in kpc.

Galaxy	$\log(r_e)_B$ (kpc)	$\pm$	$\log(r_e)_R$ (kpc)	$\pm$
NGC 1045	0.66	0.10	0.69	0.04
NGC 1132	1.12	0.05	1.14	0.06
NGC 2110	0.59	0.02	0.52	0.02
NGC 2865	0.68	0.01	0.67	0.01
NGC 4240	-	-	-	-
NGC 6172	0.61	0.06	0.56	0.06
NGC 6653	0.92	0.02	0.91	0.01
NGC 6776	0.90	0.11	0.79	0.09
NGC 6799	0.77	0.02	0.78	0.01
NGC 6849	1.16	0.01	1.12	0.03
NGC 7796	0.71	0.02	0.66	0.06
ESO107-G004	0.68	0.06	0.52	0.09
ESO153-G003	0.62	0.06	0.85	0.13
ESO194-G021	0.47	0.02	0.54	0.02
ESO218-G002	0.76	0.11	0.72	0.10
ESO318-G021	-	-	0.81	0.06
ESO462-G015	0.90	0.02	0.84	0.03
MCG-01-03-018	0.96	0.01	0.85	0.03
MCG-01-27-013	0.97	0.05	0.91	0.03
MCG-03-26-030	0.92	0.02	0.95	0.07
IC 4320	1.08	0.13	0.99	0.08
NGC 3528	1.00	0.13	1.03	0.01
NGC 3557	0.74	0.06	0.66	0.08
NGC 4697	0.86	0.05	0.73	0.04
NGC 5266	-	-	0.99	0.09

B-band for ESO318-G021, due to the bright nearby stars, and in the B and R-bands for the galaxy ESO153-G003 because the images are saturated.

Using the ellipticity (ϵ) and the effective semi-major axis (a_e) from the galaxy model, the effective radius r_e was calculated, i.e. $r_e = a_e\sqrt{1-\epsilon}$. The values of r_e, and its error estimate based on the variation during the fitting procedure, are given in Table 3.2. There is generally good agreement between the B and R-band effective radii determinations.

The $(B–R)_e$ colours at r_e (Table 3.2) are obtained from the models using the difference between the B and R-band surface brightness profiles. The exact radius used does not strongly affect the $(B–R)_e$ colour because of the shallow slope in the colour gradient. Fig. 3.2 shows good agreement between our derived colours and those given in LEDA, when available.

The mean surface brightness within r_e in each filter is calculated as:

$$< \mu_e >= 2.5\log(\pi r_e^2) + m(r_e) \tag{3.1}$$

where m(r_e) is the enclosed magnitude within r_e estimated from the model. Table 3.3 lists the mean surface brightnesses within the effective radius in the B and R-bands, while the effective radius in kpc is given in Table 3.4 in the two bands.

Table 3.5: Isophotal shape parameters

Galaxy	4^{th} cosine%	ΔPA (°)
NGC 1045	-3.5	0
NGC 1132	-1.5	10
NGC 2110	irr	12
NGC 2865	+1.5	14
NGC 6172	irr	25
NGC 6653	-2.0	10
NGC 6776	-2.0	30
NGC 6799	0	0
NGC 6849	+2.5	0
NGC 7796	-1.3	0
ESO107-G004	+1.0	20
ESO153-G003	-	
ESO194-G021	+5.0	20
ESO218-G002	0	70
ESO318-G021	0	8
ESO462-G015	+1.5	0
MCG-01-03-018	0	15
MCG-01-27-013	+1.0	14
MCG-03-26-030	+2.0	2
IC 4320	irr	30
NGC 3528	+3.2	10
NGC 3557	0	0
NGC 4697	+2.0	2
NGC 5266	irr	8

Notes: The percentage 4^{th} cosine term of the Fourier series is normalised to the semi-major axis. The difference between the maximum and minimum position angles are quoted for radii greater than 10 arcsec.

3.3.3 Isophotal shape parameters

The modelling process fits elliptical isophotes to the galaxy images and measures their isophotal shape parameters. Figures 3.3 show the radial profile of these parameters in the R-band for the twenty three galaxies which could be successfully modelled (i.e. excluding NGC 4240 and ESO153-G003). These isophotal shape parameters help define the morphology of the galaxy. For example, by fitting the isophote to the Fourier series, the 4^{th}-order cosine term is a useful parameter to express the deviation from a perfect ellipse due to the presence of additional light (Bender & Moellenhoff 1987). An excess of light along the major and/or minor axes (called discy) is indicated by positive values, while negative values indicate excess light at 45° with respect to these axes (called boxy).

To quantify the 4^{th}-order cosine parameter we applied a technique similar to that of Bender et al. (1989). When the 4^{th}-order cosine profile shows a peak or a minimum, then the

maximum amplitude is taken, while in case of a monotonically changing profile we use the value at r_e. In the case of more complicated profiles indicated by a radial change from discy to boxy (or vice versa), such galaxies are classified as irregular (irr). Table 3.5 lists the 4^{th}-order cosine values normalised to the semi-major axis. It also lists the difference between the maximum and minimum values of the position angle for each galaxy after avoiding the inner, seeing-affected regions.

3.3.4 Residual images

Another way to study the morphology or fine structure of an elliptical galaxy is by examining the residual image, i.e. the original image minus the galaxy model. Using the BMODEL task in IRAF we created a 2D model of the galaxy. This model represents the smooth elliptical structure of each galaxy. Subtracting this model from the original image gives the residual image which better reveals any fine structure (e.g. dust, shells, tidal tails, boxy or discy structure, etc.) hidden underneath the dominant elliptical light of the galaxy. Figures 3.4 display the residual images of the sample galaxies (excluding NGC 4240 and ESO153-G003).

3.4 Faint galaxy detection

As our images cover a field-of-view of hundreds of square kiloparsec surrounding each galaxy, they allow us to probe the distribution of galaxies in their fields. With the strict isolation criteria used to select galaxies in this study, the area surrounding the primary galaxy will contain no bright galaxies (within ~ 2 mags) but may still contain many faint ones. For the fifteen galaxies observed at the AAT telescope (see Table 3.1), the detection of these faint galaxies was performed using SExtractor version 2.3 (Bertin & Arnouts 1996). From the deeper R-band images, all objects with more than 10 connected pixels that are 3σ above the sky background were identified. To estimate the background level of the images, as well as the RMS noise in the background, we set the mesh size to 200 pixels. This value of the mesh size was found to be suitable for extended object detection. The image was then smoothed with a median filter of 10×10 pixels to remove any fluctuations resulting from bright or extended objects. The photometric parameter MAG_BEST was used as a measure of the total magnitude. A comparison between MAG_BEST magnitudes and the corresponding total magnitudes measured with the IRAF task QPHOT showed good agreement.

For star-galaxy separation, we used the CLASS_STAR parameter (ICLASS) defined by SExtractor. Running SExtractor on the 60 sec and the combined (1320 sec) R band mosaic frames of the NGC 3557 group, we obtained two sets of detected bright objects, i.e. stars and galaxies with ICLASS parameters of 1 and 0 respectively. For faint objects (R $\geqslant$ 18), ICLASS values ranged from 0 to 1. Visual inspectation of the 60 sec and combined images revealed that an ICLASS value of 0.09 provided a good separation between resolved galaxies

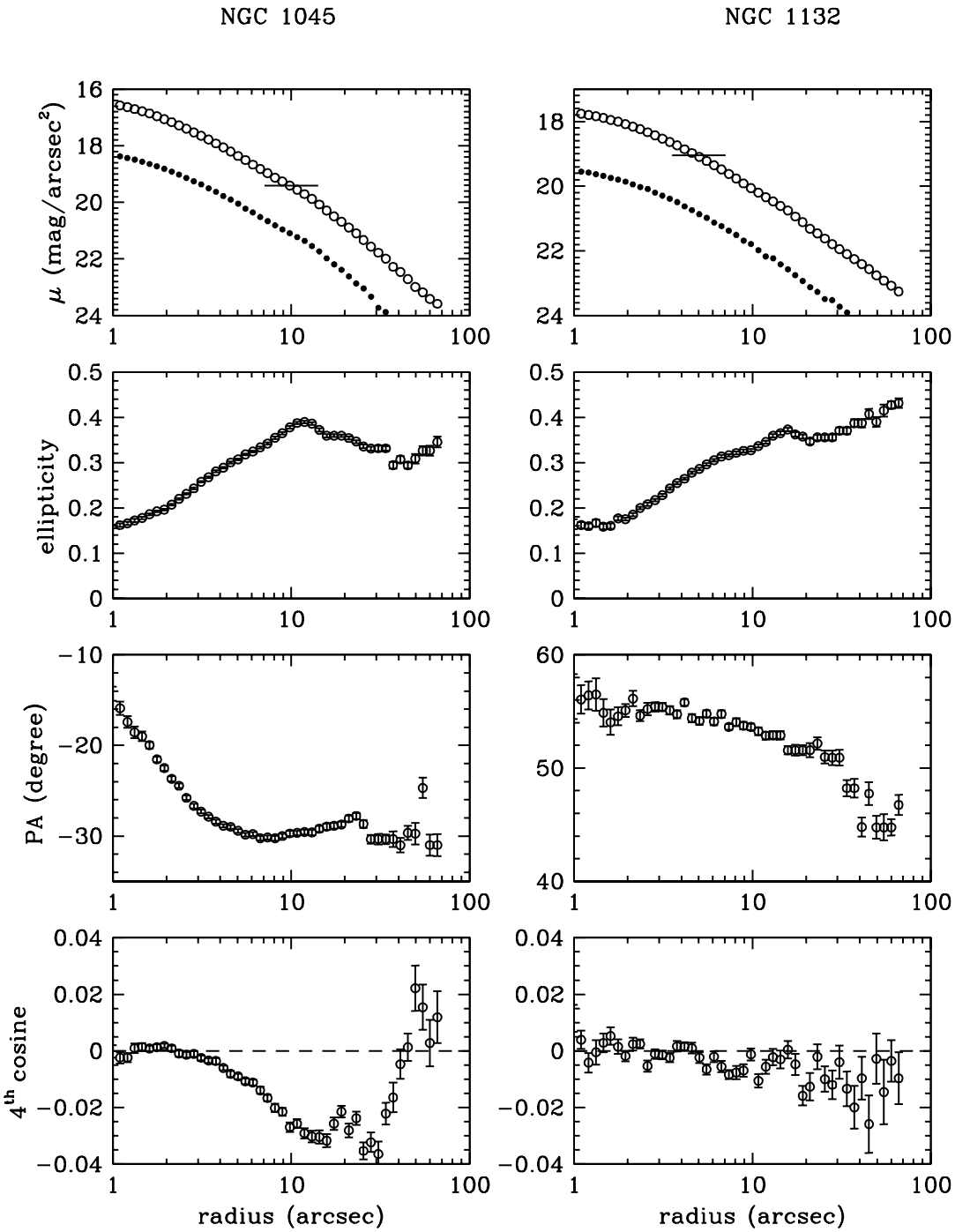

Figure 3.3: The radial profiles of the R-band (open circles) surface brightness, ellipticity, position angle and 4^{th}-order cosine. The upper panel for each galaxy shows also the B-band surface brightness (solid circles) and the thin horizontal line shows the sky brightness in the R-band. The name of each galaxy is written above each set of four panels.

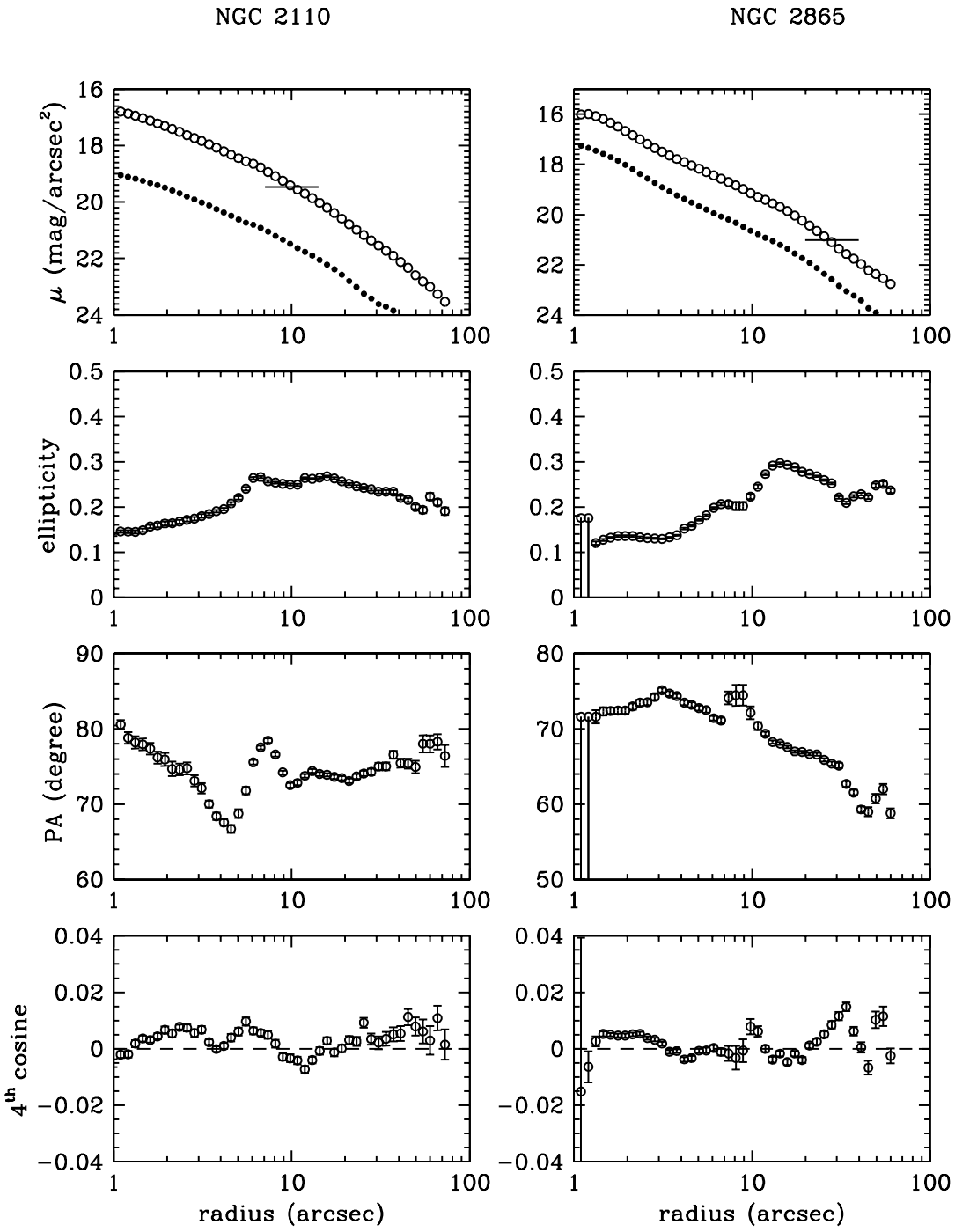

Figure 3.3: (continue)

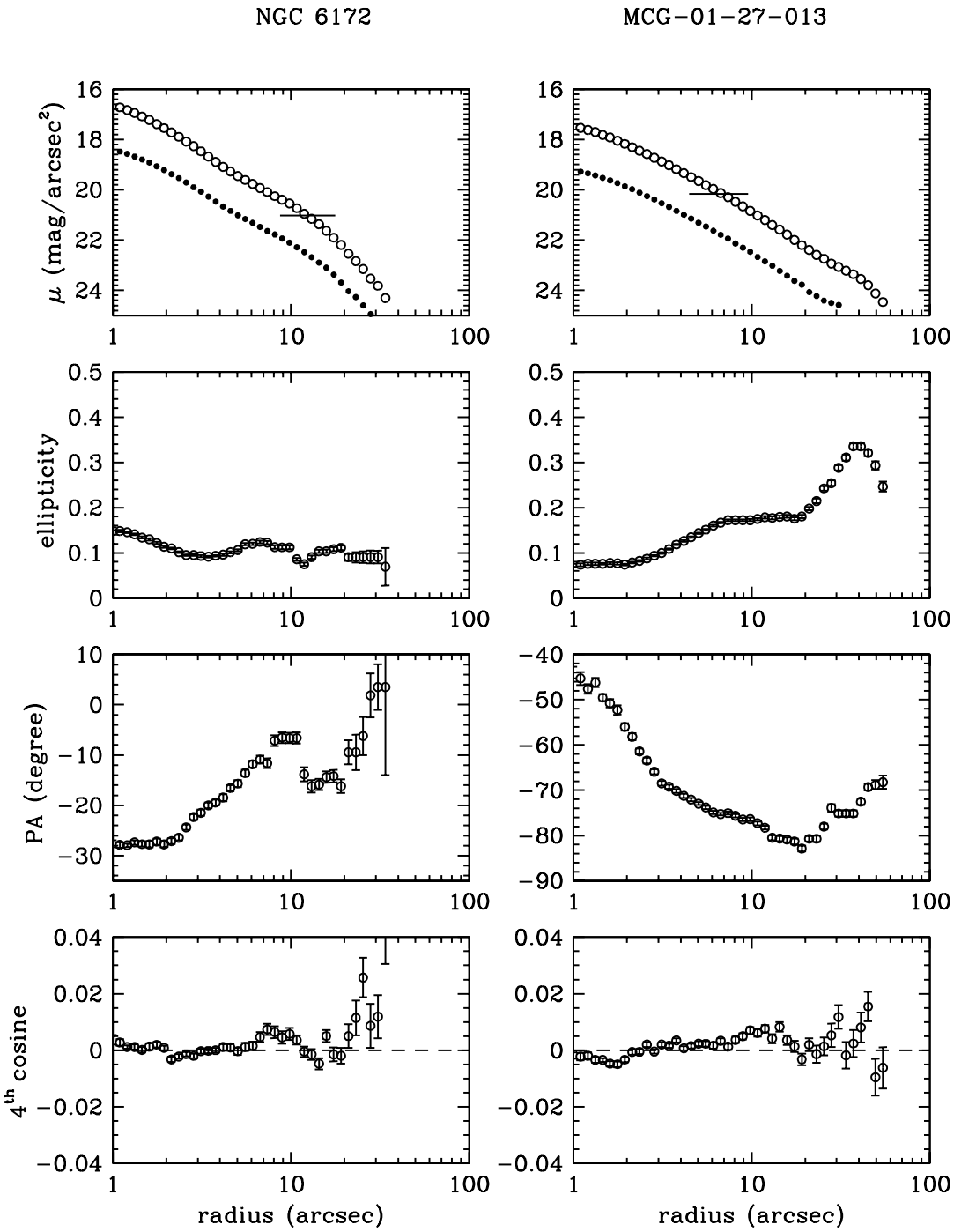

Figure 3.3: (continue)

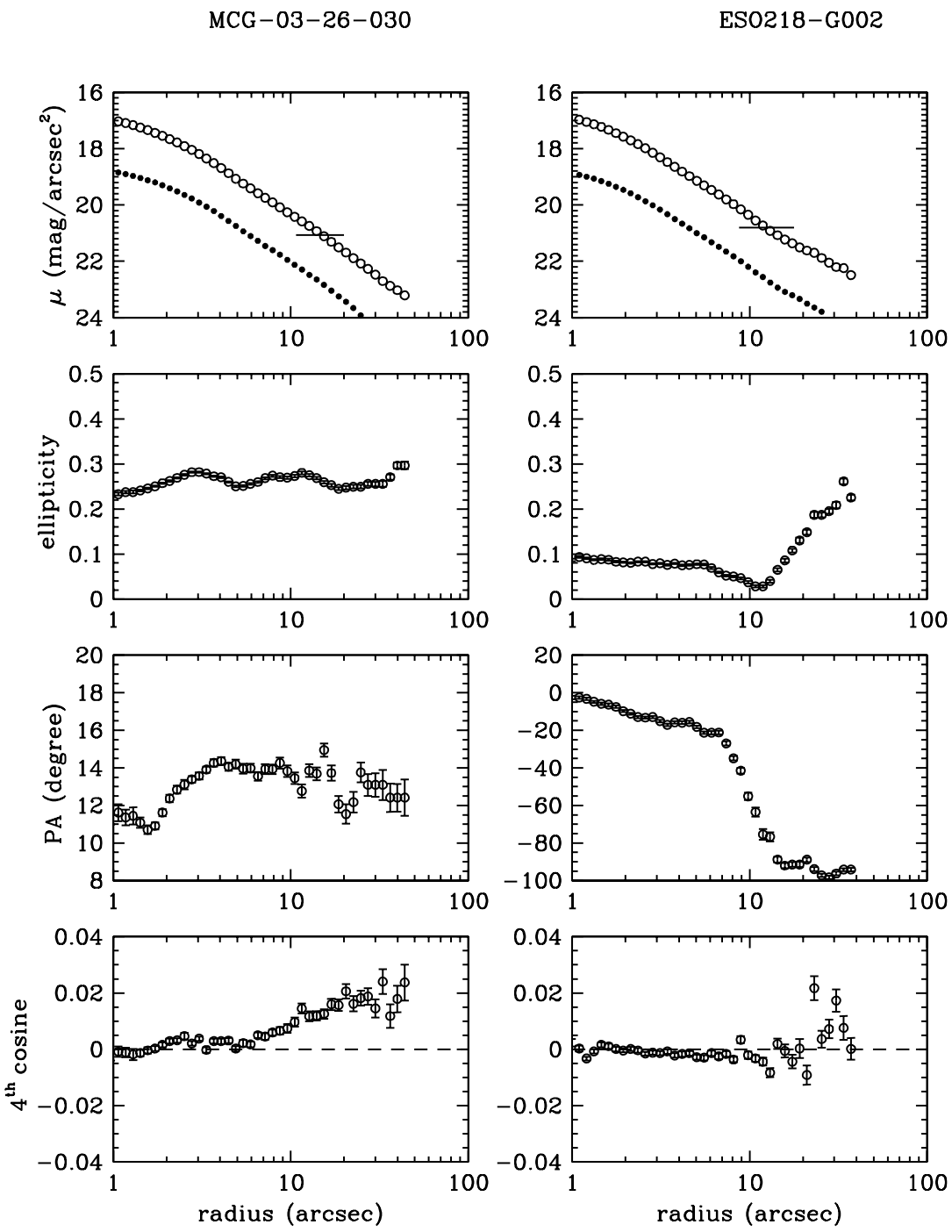

Figure 3.3: (continue)

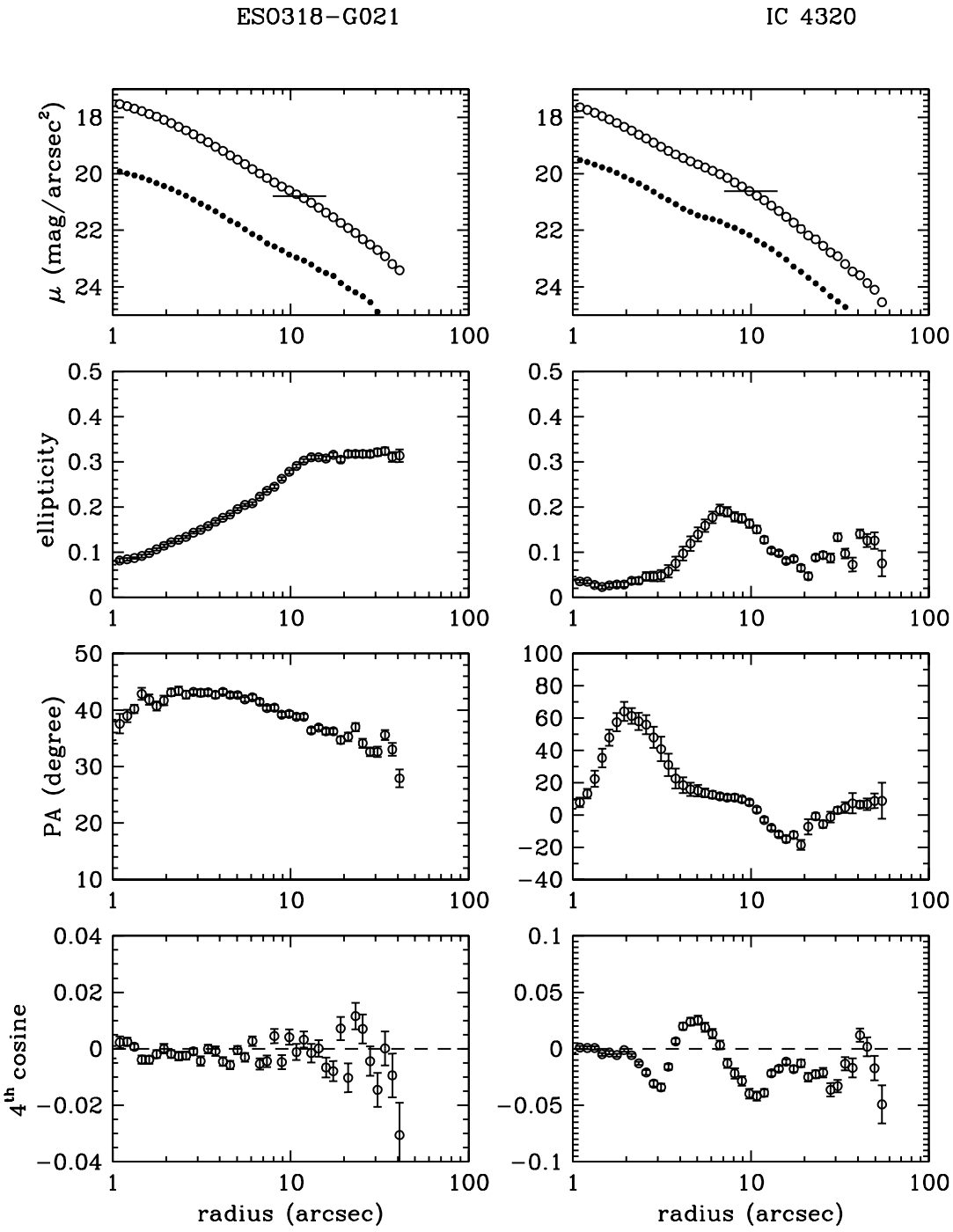

Figure 3.3: (continue)

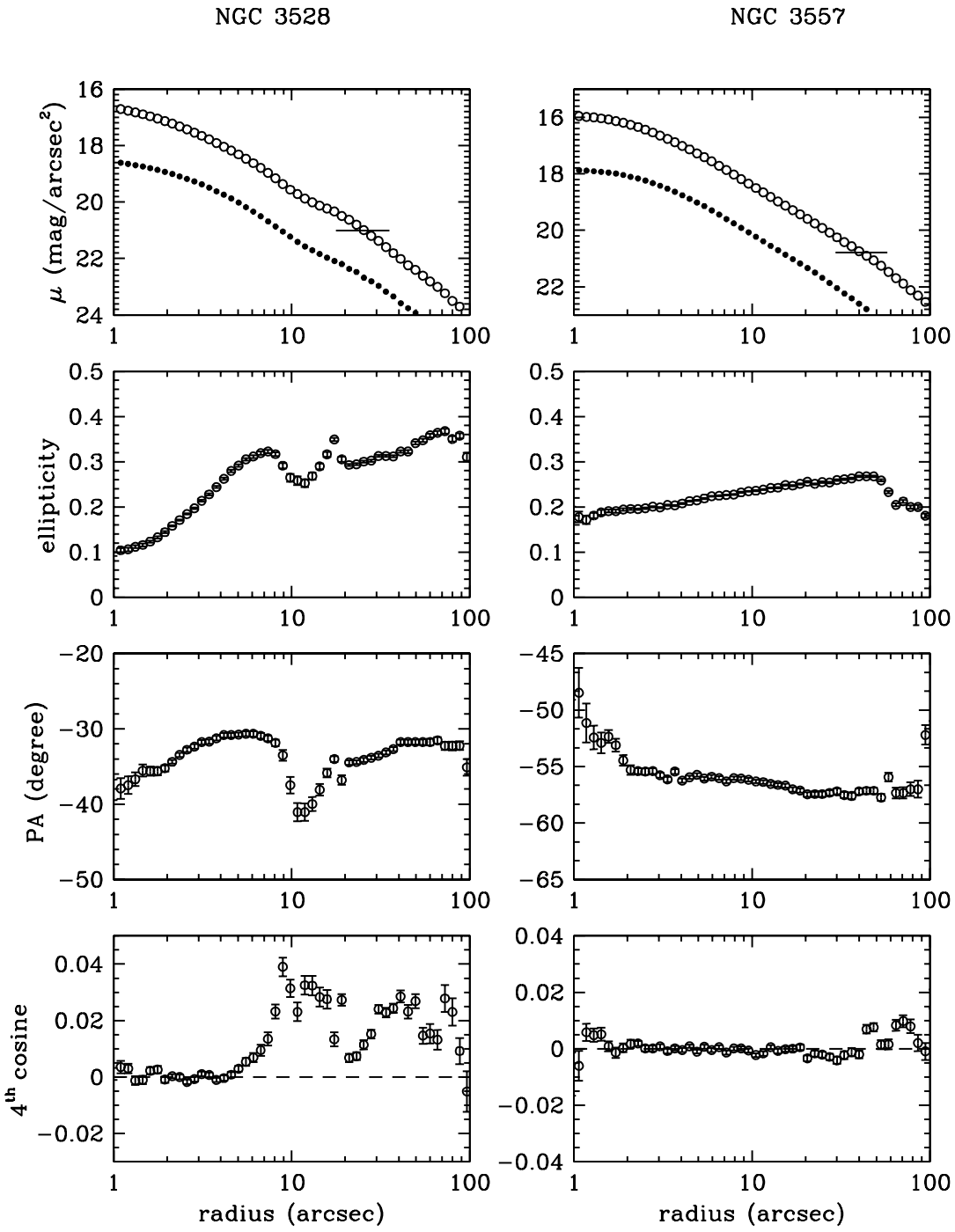

Figure 3.3: (continue)

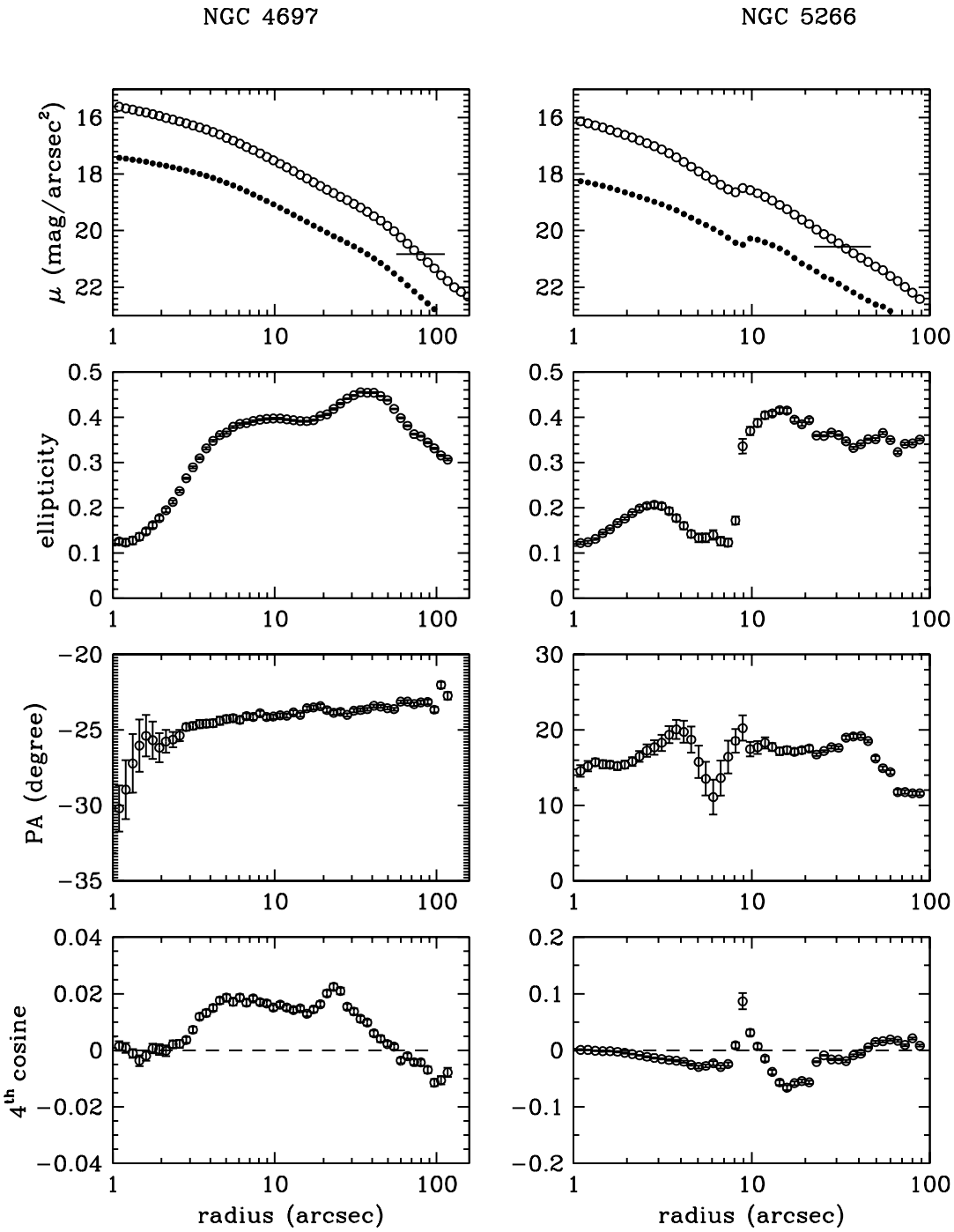

Figure 3.3: (continue)

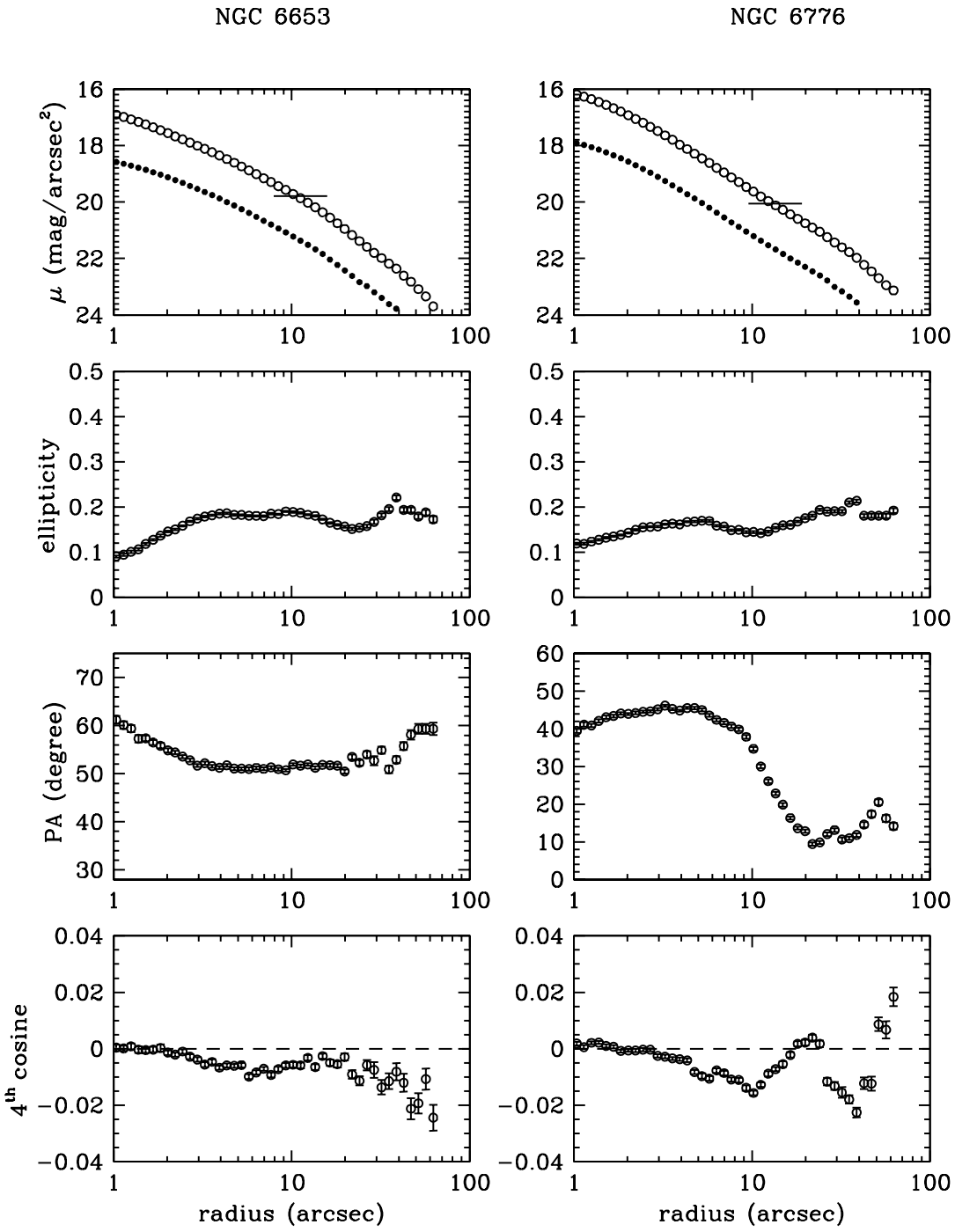

Figure 3.3: (continue)

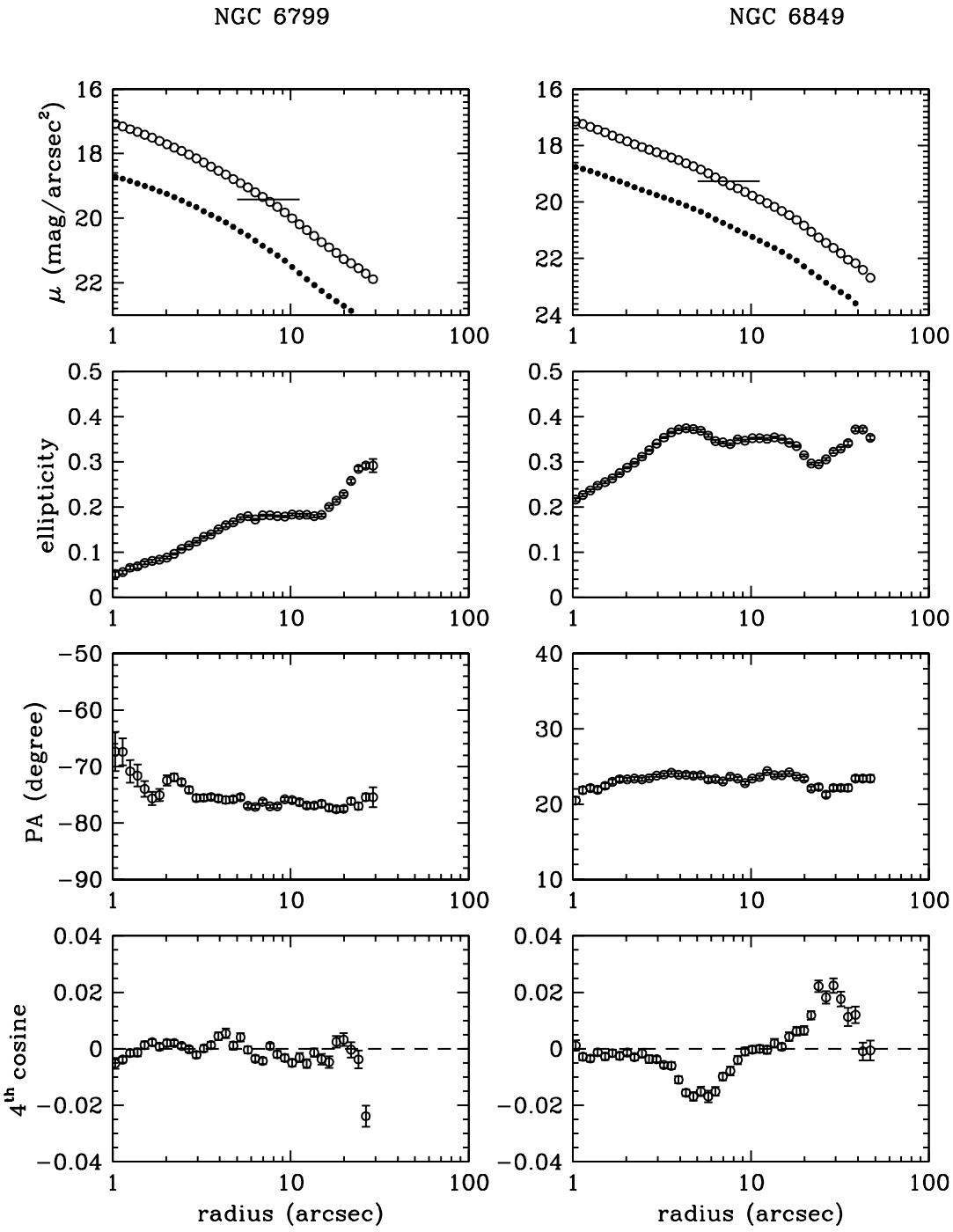

Figure 3.3: (continue)

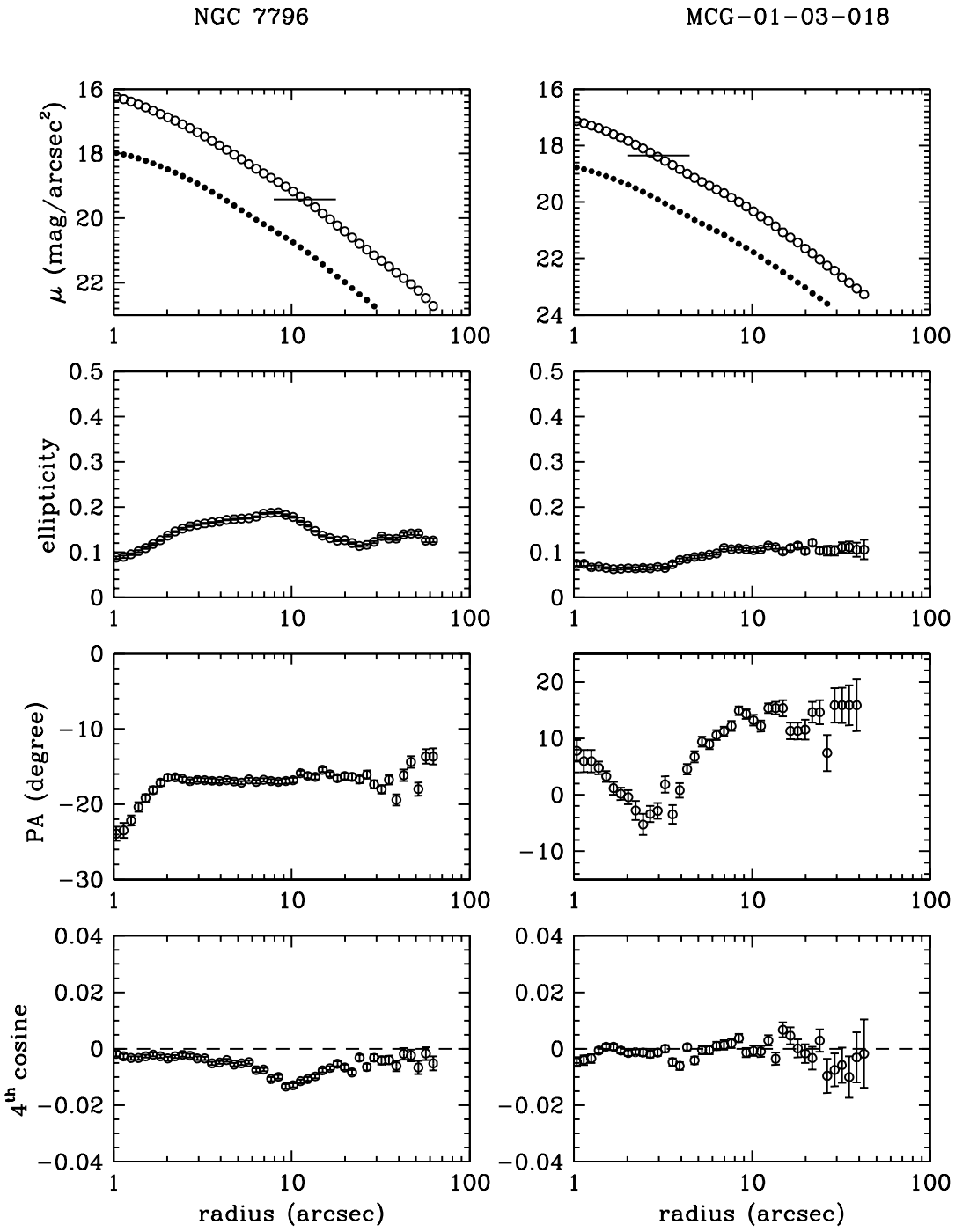

Figure 3.3: (continue)

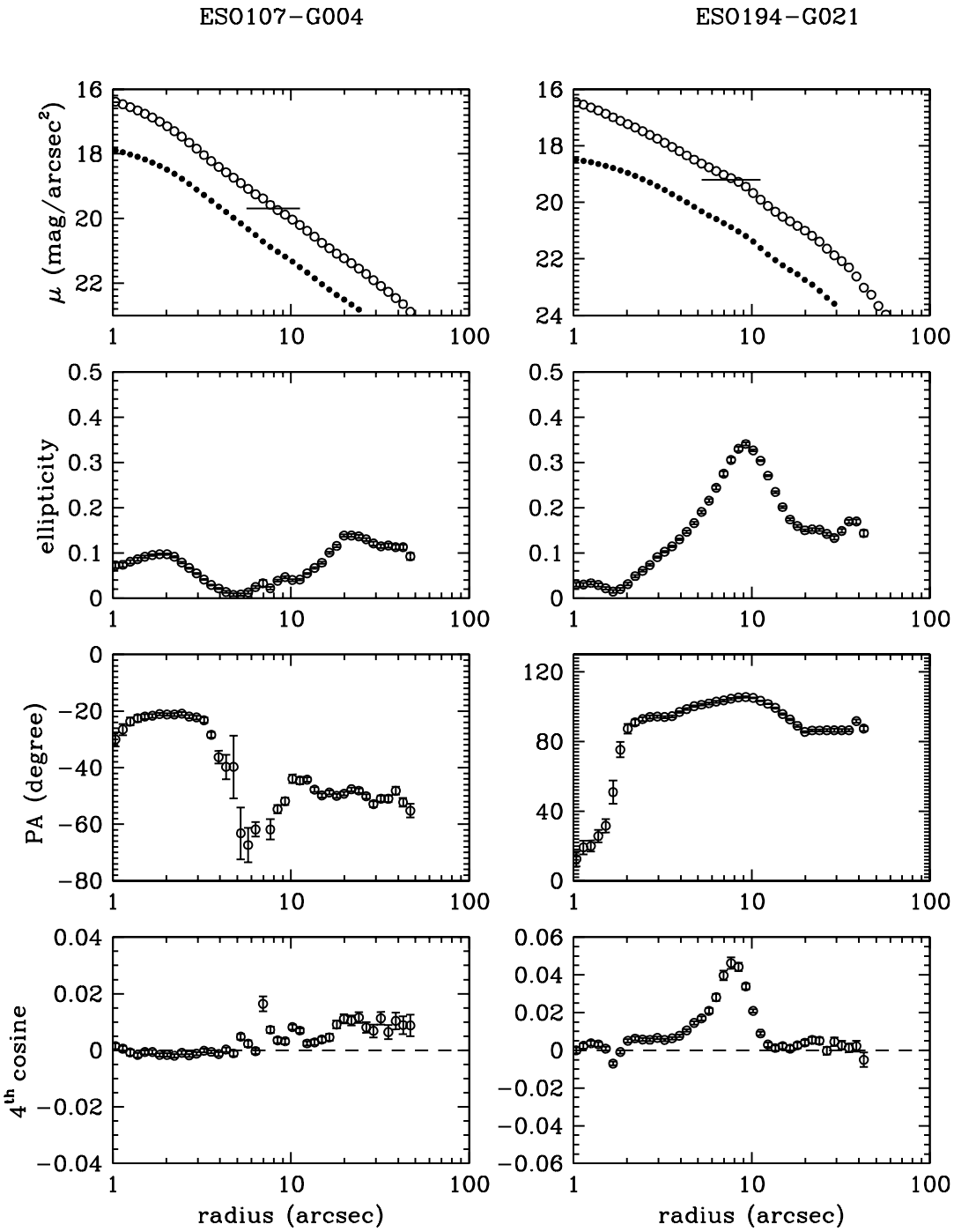

Figure 3.3: (continue)

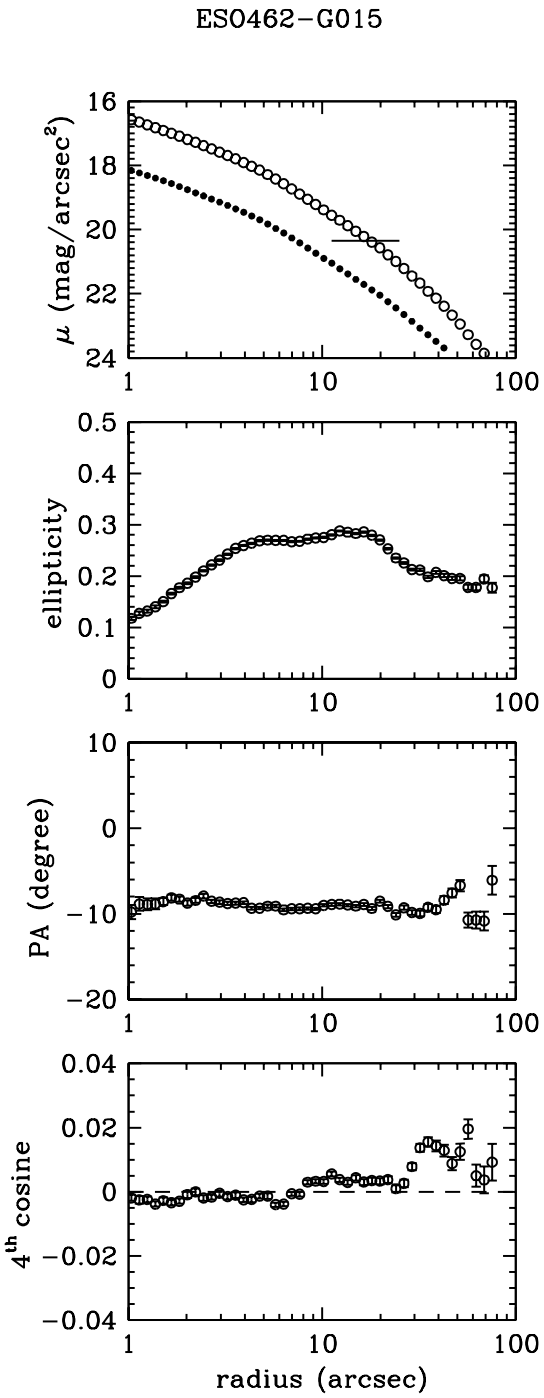

Figure 3.3: (continue)

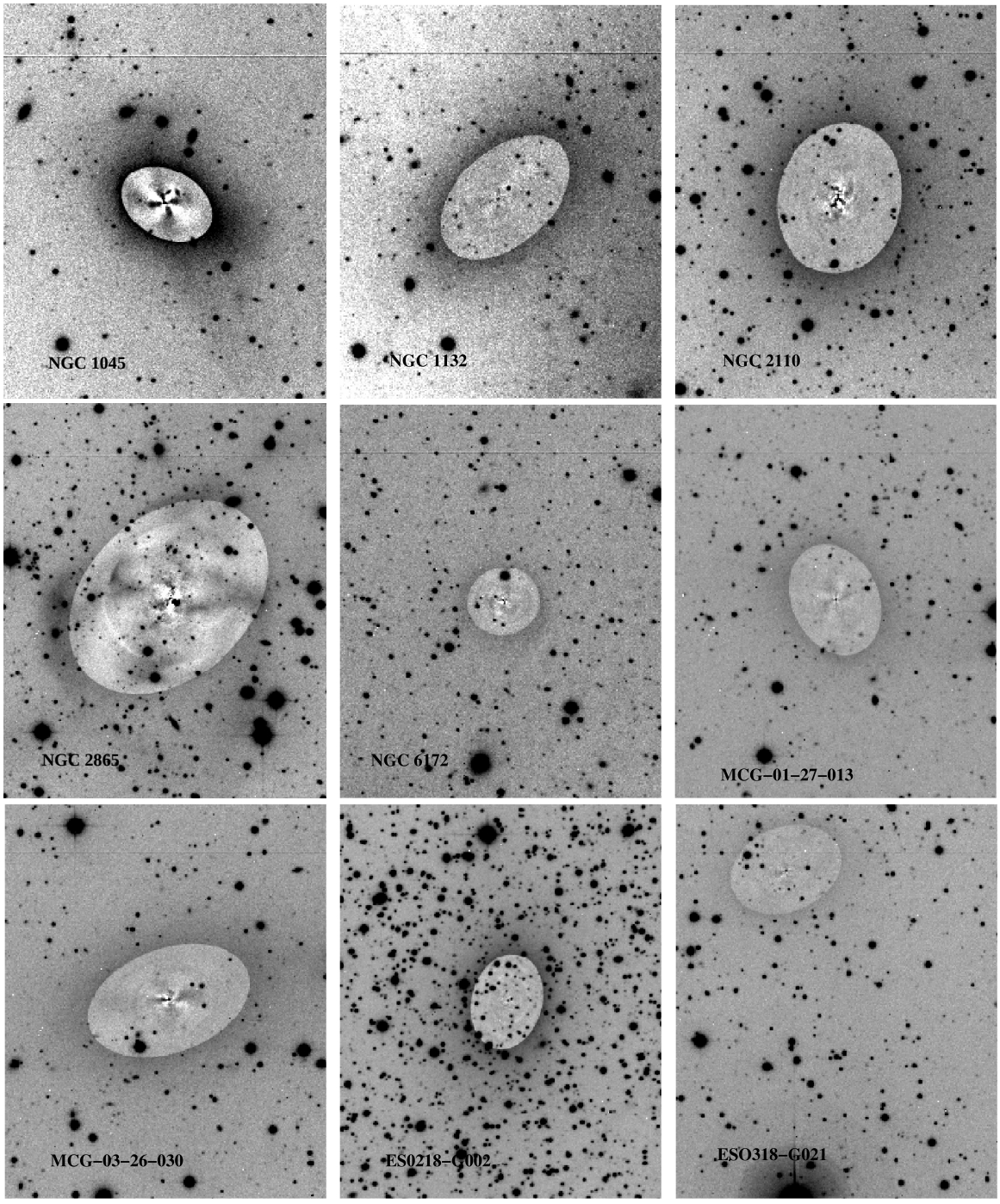

Figure 3.4: Residual images of galaxies (with filters given in brackets): NGC 1045(R), NGC 1132(R), NGC 2110(R), NGC 2865(R), NGC 6172(R), MCG-01-27-013(R), MCG-03-26-030(R), ESO218-G002(R) and ESO318-G021(R) (left to right, top to bottom). Dust regions can be seen as bright features and extra light as dark features. All images have the same size of 188 × 155 sq. arcsec and oriented as North up and East to the left.

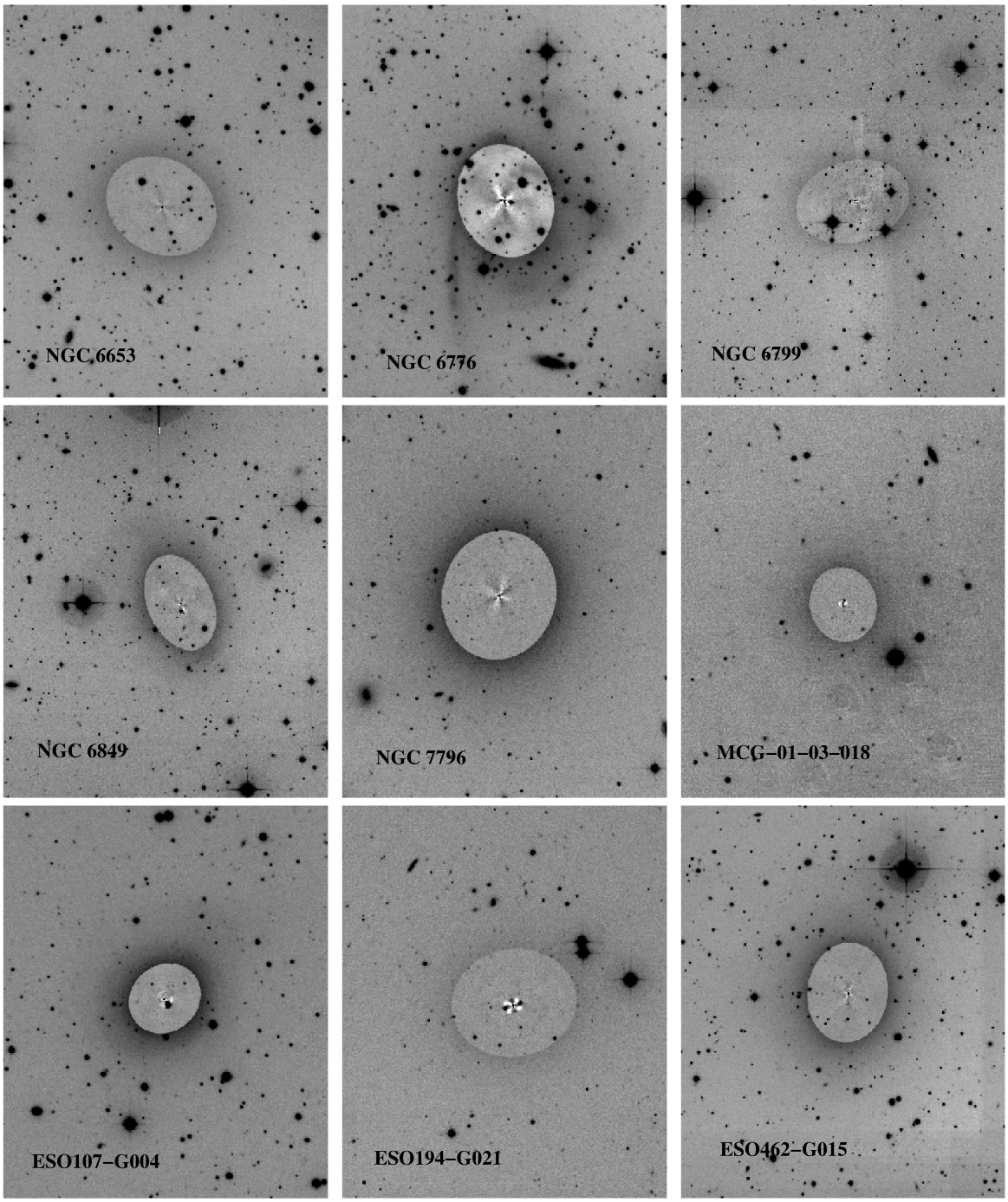

Figure 3.4: (Continue) Residual images of NGC 6653 (R), NGC 6776 (R), NGC 6799 (R), NGC 6849 (R), NGC 7796 (R), MCG-01-03-018 (R) , ESO107-G004 (R), ESO194-G021 (R) and ESO462-G015 (R).

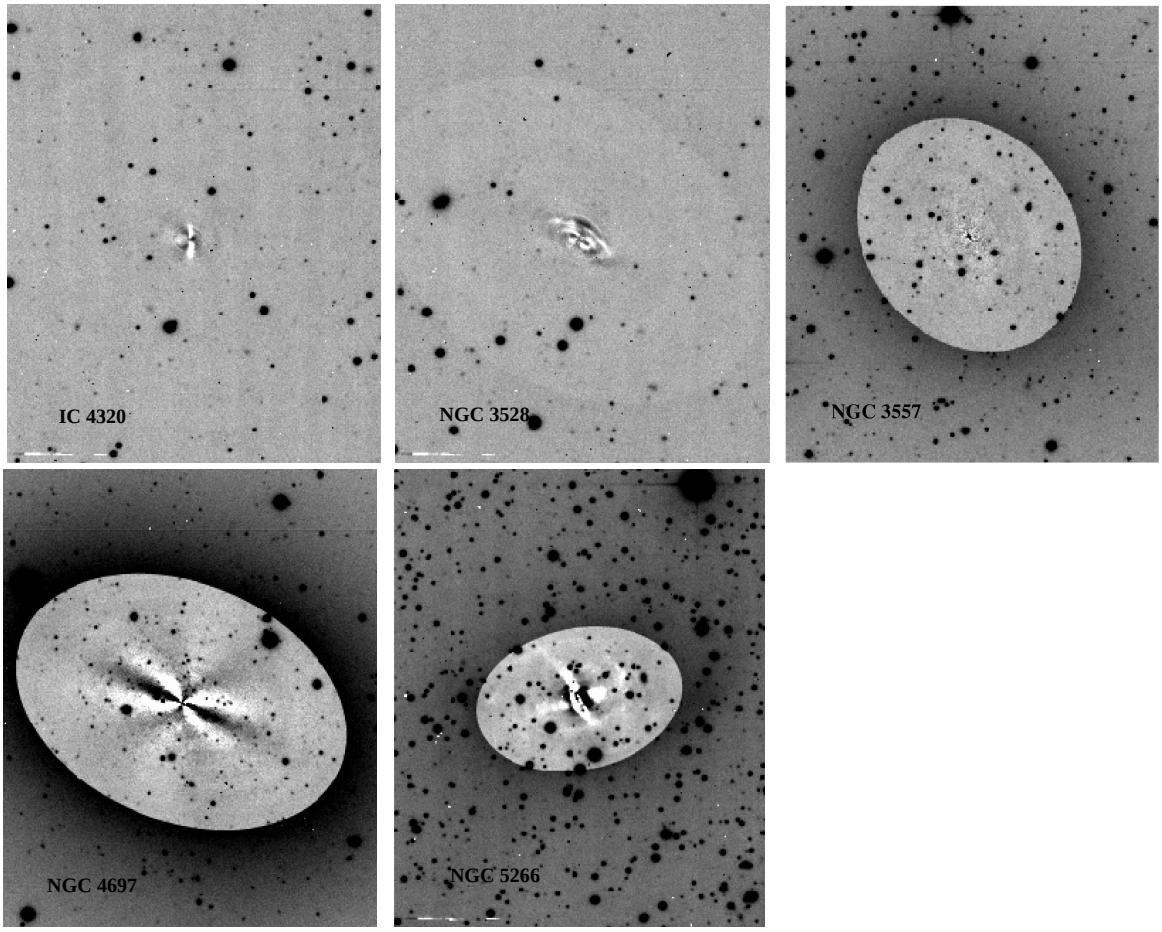

Figure 3.4: (Continue) Residual images of IC 4320(B), NGC 3528(B), NGC 3557(R), NGC 4697(R) and NGC 5266(B) (left to right, top to bottom).

and stellar-like objects. Thus objects with ICLASS > 0.09 were removed from all of our object lists. After displaying all the remaining detections, we removed the small number of obvious mis-identifications (e.g. bad columns, diffraction spikes, halos of bright stars, etc.). Finally, for the isolated galaxies, we searched the NED database and excluded any of the detected faint galaxies that have a published velocity difference of greater than 700 km s^{-1} from the parent galaxy. This resulted in only a handful of galaxies being removed for the isolated galaxy sample.

In order to estimate our magnitude completeness limits, we compared the 60 and 420 sec to the combined (1320 sec) frame of the NGC 3557 group. This allows us to estimate our completeness as a function of exposure time. For example, a typical 120 sec exposure has an estimated 100 per cent completeness limit of $R = 18.75$. Except for ESO318-G021, all other galaxies have a total exposure time of at least 120 sec (Table 3.1).

Using the SExtractor parameter A_IMAG as a measure of galaxy size, Fig. 3.5 shows the size-magnitude distribution after our selection criteria and visual inspection are applied.

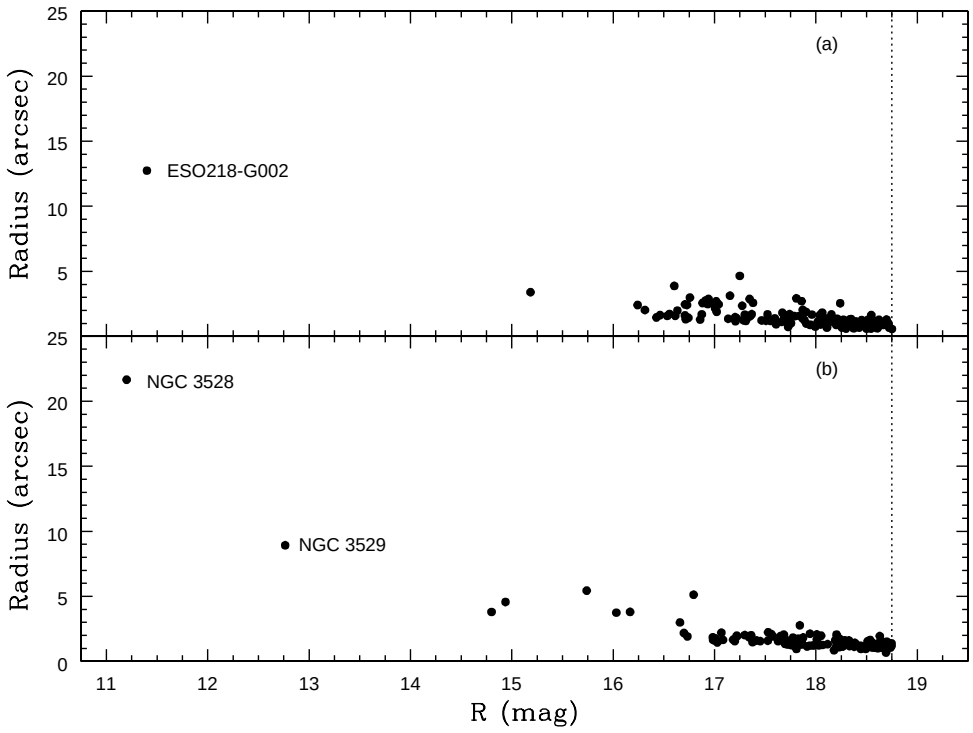

Figure 3.5: The size-magnitude relation for detected galaxies in the field of (a) the isolated galaxy ESO218-G002 and (b) the NGC 3528 group. The SExtractor parameters A_IMAG and MAG_BEST were used as a measure of size and magnitude respectively. The vertical dotted line represents our 100 per cent completeness limit of R = 18.75. For ESO218-G002 the brightest galaxy in the field is ~ 4 mags fainter and $\sim 1/3$ the size of ESO218-G002 itself.

The figure shows the isolated galaxy ESO218-G002 and the NGC 3528 group which are at almost same distance and have the same exposure time of 120 sec. The vertical line indicates our 100 per cent completeness limit of $R = 18.75$. For ESO218-G002 the brightest galaxy in the field is ~ 4 mag fainter and $\sim 1/3$ the size of ESO218-G002 itself. As a result of the SExtractor process, we have a list of apparent magnitudes, projected distances in kpc from the primary galaxy and angular sizes of galaxies in the field of the primary galaxy (see Appendix A for the complete list).

3.5 Results and discussion

3.5.1 Colours of isolated galaxies

Prugniel & Heraudeau (1998; PH98), using a sample of 5,169 galaxies, measured the colour for S0 galaxies to be $(B–R)_e = 1.52 \pm 0.2$ and for ellipticals $(B–R)_e = 1.57 \pm 0.2$. These values are consistent with the measured effective colours of our sample (see Table 3.2) which have a mean of $(B–R)_e = 1.58 \pm 0.03$. We note that NGC 2865 is quite blue with (B–

$R)_e = 1.26 \pm 0.14$.

The colour-magnitude relation (CMR) of ellipticals was discovered by Baum (1959) when he studied the stellar content for a sample of elliptical galaxies and globular clusters. He found more luminous ellipticals to be redder. Further studies of cluster ellipticals have shown that the CMR is a linear relation with a small intrinsic scatter (e.g. Bower, Lucey & Ellis 1992). A comparison of the observed slope and scatter of the CMR with that expected from theoretical models, has been used by many authors to constrain the formation epoch of the bulk of stars in early-type cluster galaxies to be at $z > 2$ (e.g. Ellis et al. 1997; Bower, Kodama & Terlevich 1998; Stanford, Eisenhardt & Dickinson 1995; 1998; Bernardi et al. 2003d; Tantalo & Chiosi 2004). The constant slope out to high redshifts means that the CMR indicates a relation of mass with metallicity (Kodama 2001); while the scatter, although small, is due to ongoing star formation (Bower, Lucey & Ellis 1992).

Fig. 3.6 presents the CMR for the 18 isolated elliptical galaxies measured in this study. We also include the four isolated galaxies NGC 821, NGC 2271, NGC 6702 and ESO318-G021, which have available colours from PH98. The isolated galaxies are reasonably well matched by a B–R CMR of slope and intrinsic scatter similar to that of early-type galaxies in the denser environment of the Coma cluster found by Gladders et al. (1998). We used total B–R colours as they are the closest match to the aperture magnitudes of Gladders et al. Fixing the slope to the Gladders et al. value, we measure a scatter of ~ 0.12 mag for the isolated galaxies, which is similar to our photometric errors. Thus the scatter is largely intrinsic and consistent with the estimated low scatter found for early-type galaxies in clusters (Bower, Lucey & Ellis 1992; Stanford, Eisenhardt & Dickinson 1998). None of our isolated galaxies show the extremely blue colours seen in the isolated galaxy sample of Marcum, Aars & Fanelli (2004). On the other hand the isolated galaxy ESO194-G021 shows a very red colour of $B-R = 1.73 \pm 0.14$ for its luminosity ($M_R = -21.5$). The residuals of our isolated galaxies from the CMR of galaxies in Coma cluster show a mean value of 0.05 with 1σ dispersion of 0.12 (see the inset in Fig. 3.6).

3.5.2 Morphological fine structure

Many studies have found that elliptical galaxies have light distributions which deviate from perfect ellipticity (Lauer 1985; Bender, Doebereiner & Moellenhoff 1988; Franx, Illingworth & Heckman 1989; Peletier et al. 1990; Bender & Moellenhoff 1987; Forbes & Thomson 1992; Goudfrooij et al. 1994b). These deviations can be due to dust lanes or extra-light structures. The isophotal shape is found to correlate to intrinsic properties of the galaxies such as their total luminosity, mass-to-light ratio, X-ray and radio emission (Bender et al. 1989; Nieto & Bender 1989). These correlations imply that these morphological structures are intrinsic and not due to galaxy orientation or projection effects. Numerical simulations suggest that such morphological features could be a result of the tidal disruption of a small companion

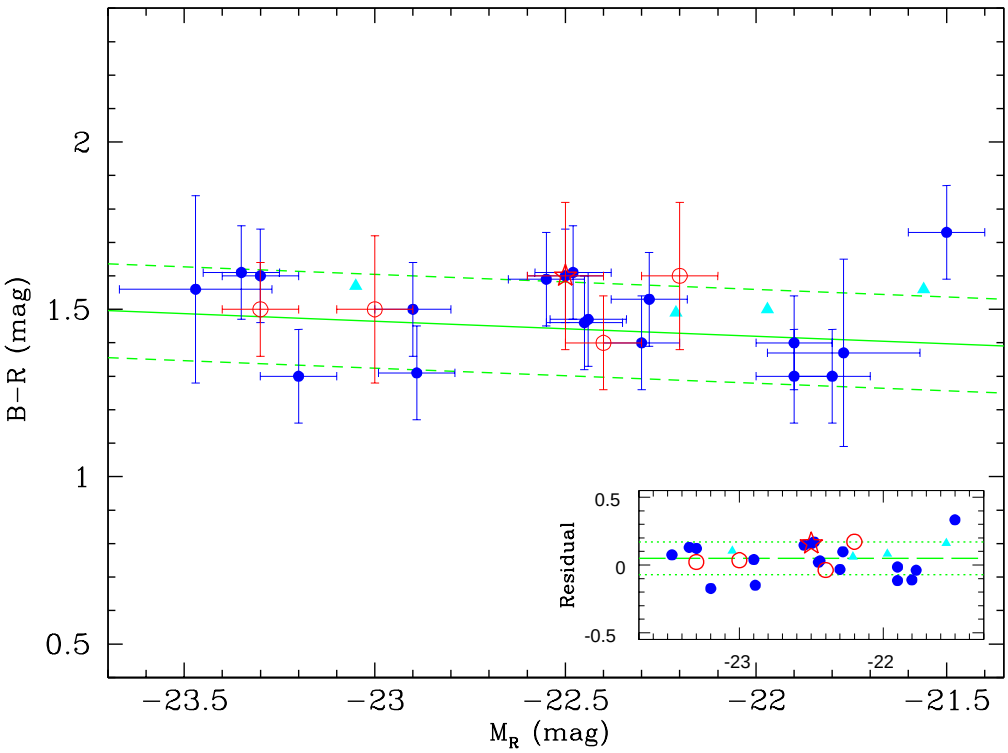

Figure 3.6: Colour-magnitude relation for the sample galaxies. The solid line (Gladders et al. 1998) represents the CMR of elliptical galaxies in the Coma cluster, while the short-dashed lines indicate the mean error in the colour measurements for our sample galaxies. Solid triangles are galaxies from PH98 (error bars are not shown) and other symbols are as in Fig. 3.1. The inset shows the distribution of the residuals of galaxies colour from the relation. The long-dashed line is the mean value of the residuals and the dotted lines represent the 1σ dispersion. The isolated galaxies are consistent with the Coma cluster CMR.

(Binney & Petrou 1985; Nieto & Bender 1989) or a major merger (Schweizer et al. 1990). Past mergers are also predicted to produce other morphological structures such as plumes, shells and tidal tails (Forbes 1991; Barnes & Hernquist 1992).

Our isolated galaxy sample reveals a range of fine structure from plumes and shells to dust lanes, and some galaxies with no detectable fine structure. Good examples of boxy and discy isophotes can be seen in NGC 1045 and NGC 4697 respectively. Shells (in the case of NGC 2865 and NGC 6776) and dust lanes (e.g. ESO194-G021) appear to affect the 4^{th}-order cosine profile of many galaxies, while ESO218-G002, ESO318-G021 and NGC 6799 are good examples of no obvious fine structure. From the radial profiles (Figures 3.3) and the residual images of each galaxy (Figures 3.4), the following features were revealed:

NGC 1045: The isophotes are strongly boxy out to a semi-major axis radius of $35''$. Probable dust along the semi-major and semi-minor axes. There is extensive extra tidal light surrounding the galaxy. This galaxy is a probable merger remnant.
NGC 1132: No obvious features. Classified as a fossil galaxy by Mulchaey & Zabludoff (1999).

NGC 2110: Probable dust traces in the central region. Contains a seyfert nucleus (Pfefferkorn, Boller & Rafanelli 2001).
NGC 2865: Extra tidal light (shells) to the east and north east. Probable dust in the inner region. This galaxy is a probable merger remnant (see also Hau, Carter & Balcells 1999).
NGC 4240: Nearby bright star. No obvious features.
NGC 6172: No obvious features.
NGC 6653: shows a boxy structure in its outer part.
NGC 6776: has probable dust within the central region of radius $\lesssim 3$ kpc ($8''$). It also reveals shell structures and extensive extra tidal light to the West and South. There is also a tidal tail extending in the southern direction.
NGC 6799: In both the B and R-bands, our images of NGC 6799 show a smooth elliptical profile and no morphological fine structure.
NGC 6849: is discy in the outer part and there is some extra tidal light to the North. The 4^{th} cosine parameter shows negative values in the inner 4 kpc ($10''$) due to the effect of a foreground star located near the centre of the galaxy. Using multi-colour photometry, Saraiva, Ferrari & Pastoriza (1999) found that the isophotes in the B-band showed stronger variations in ellipticity, position angle and elliptical shape compared to the isophotes in the other bands. They suggested that NGC 6849 has traces of dust in the central part. Comparing the isophotal parameters for NGC 6849 from our B and R-band imaging, we find no evidence of such differences.
NGC 7796: is a boxy galaxy reaching maximum boxiness in the inner region within a radius of 2 kpc ($10''$).
ESO107-G004: has a weak discy structure in the outer part at radii greater than 2 kpc ($10''$).
ESO153-G003: is saturated in our images which prevents us detecting any internal fine structure and it shows no obvious extra tidal light.
ESO194-G021: shows a disk structure between 1 and 3 kpc ($5'' - 15''$).
ESO218-G002: No obvious features. Large position angle twist seen.
ESO318-G021: Nearby bright star. No obvious features.
ESO462-G015: shows a uniform elliptical structure of ellipticity ≈ 0.3 within a radius of 9 kpc ($25''$), but becomes discy at larger radii.
MCG-01-03-018: shows traces of probable dust in central region.
MCG-01-27-013: Weak discy structure at radius $\sim 15''$.
MCG-03-26-030: Discy beyond $10''$. Probable dust.
IC 4320: Strong dust lane within central $20''$. Probably a merger remnant.
NGC 3528: Strong dust lane extending from the north east to south west. Probably a merger remnant.
NGC 3557: No obvious features.
NGC 4697: Strong discy structure extending to $\sim 40''$.
NGC 5266: Dust ring around galaxy. Probably a merger remnant (see also Morganti et al. 1997).

Thus, some isolated galaxies reveal signatures of a past interaction/merger while others look featureless and undisturbed. If evidence of a past merger includes shells, dust, plumes, discy and boxy structures, then we detected mergers in 60 per cent (11/18) of our isolated galaxies. This is a higher fraction than the 44 per cent quoted by Reduzzi, Longhetti & Rampazzo (1996) for their sample of 61 early-type galaxies in low-density environments. Also, a recent study by Michard & Prugniel (2004) found the frequency of galaxies with perturbed morphologies in poor group environments to be ≈ 35 per cent compared to only ≈ 19 per cent in the Virgo cluster.

About 28 per cent (5/18) of our galaxies contain dust which is comparable to the 24.6 per cent of dusty galaxies quoted by Reduzzi, Longhetti & Rampazzo (1996). Colbert, Mulchaey & Zabludoff (2001) detected 75 per cent of early-type galaxies in low-density environments to have dust.

Only two galaxies (11 per cent), NGC 2865 and NGC 6776, show obvious shell structures. Although this is comparable to the frequency found by Malin & Carter (1983) (11 percent) and Reduzzi, Longhetti & Rampazzo (1996) (16.4 per cent), it is much less than the frequency of > 50 which found by Seitzer & Schweizer (1990). On the other hand, we find more shells than Marcum, Aars & Fanelli (2004) who detected no shells in any of their 8 isolated early-type galaxies.

Zepf & Whitmore (1993) found 50 per cent of their Hickson compact group elliptical sample to have irregular isophotes compared to $\lesssim 21$ per cent in loose groups and clusters. Our sample, although small, does not show a predominance of irregular isophotes, and appears similar to the distribution of isophotal shapes for loose groups and cluster ellipticals suggesting a similar frequency of mergers and interactions. We speculate that the high density of Hickson Compact Groups and the resultant high interaction rate gives rise to irregular isophotes whereas in isolated environments such interactions do not occur.

3.5.3 The gravitational effects of dwarfs

Here, we have assumed that all detected faint galaxies in the field surrounding a galaxy lie at the same redshift as the primary galaxy (in reality many will be background objects) and have calculated their luminosity L_R in the R-band. For an assumed mass-to-light ratio of $M/L_R = 10\ M_\odot/L_\odot$ (Geha, Guhathakurta & van der Marel 2002), we estimated the mass M of each faint galaxy. For all faint galaxies in the field of a primary galaxy, we have calculated the dynamical friction timescale using equation 7-27 in Binney & Tremaine (1987). We assumed a velocity dispersion of $\sigma = 250$ km s^{-1} for the galaxies in the field of the isolated galaxy (Faber & Jackson 1976). As galaxies with dynamical friction times that are significantly less than the Hubble time should have merged with the primary galaxy, and hence not be visible, their existence suggests that they may actually lie in the foreground

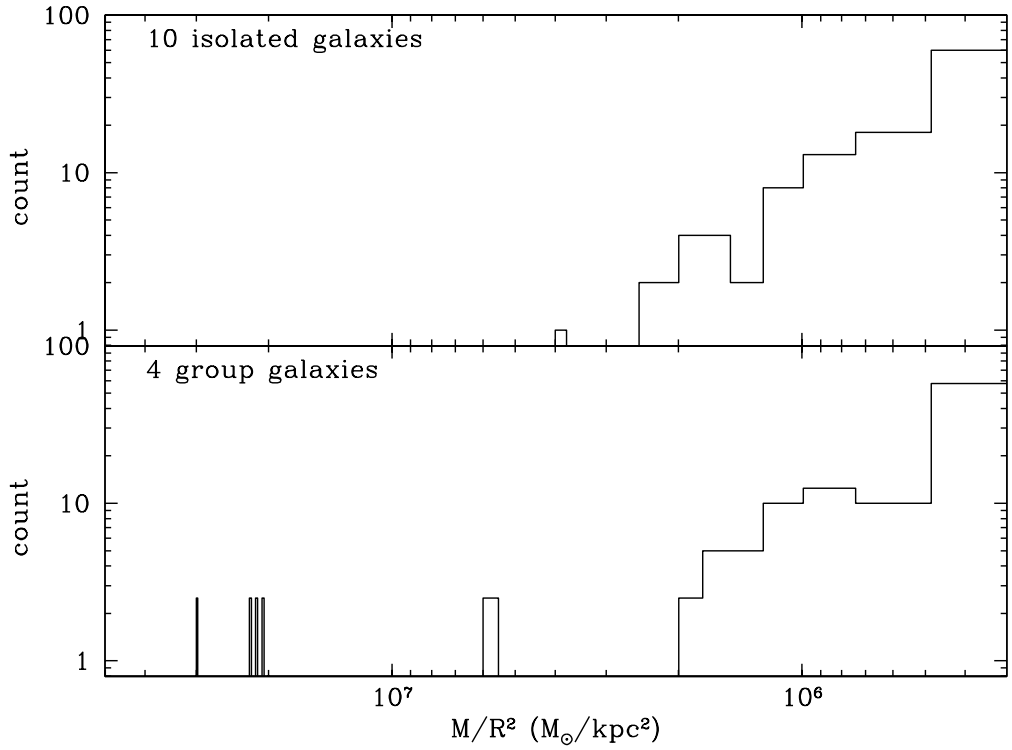

Figure 3.7: Number distribution of M/R^2 values for the 10 isolated and 4 group galaxies observed at the AAT telescope. The group galaxies have been scaled up in number by a factor of 2.5× to match the isolated galaxy sample. M is the mass of the detected galaxy in solar masses and R is the projected distance of the galaxy from the primary galaxy in kpc. The value M/R^2 represents the gravitational force applied on the primary galaxy by the faint galaxies in its local environment (assuming they lie at the same redshift). Unlike the group galaxies, the isolated galaxies are not influenced by the gravitational effects of faint neighbours with $M/R^2 \gtrsim 4 \times 10^6\ M_\odot/\mathrm{kpc}^2$.

or background. In the case of the four groups, we used the published velocities in NED to remove the non-group members.

The gravitational effect applied on the primary galaxy by each of the faint galaxies in its field is proportional to M/R^2, where R is the projected distance of the faint galaxy from the primary galaxy. Except for the faint dwarfs with short dynamical friction times and non-group members, we calculate the parameter M/R^2 for all detected galaxies in the field of the 10 isolated and 4 group galaxies. Fig. 3.7 shows the number distribution of the M/R^2 values for the isolated and the group galaxies. In the case of groups, the distribution has been scaled up by a factor of 2.5×. Comparing the fields of the isolated and group galaxies we notice the absence of galaxies with M/R^2 greater than $\sim 4 \times 10^6\ M_\odot/\mathrm{kpc}^2$ for isolated galaxies. This is a further indication that our isolated galaxies are indeed gravitationally isolated.

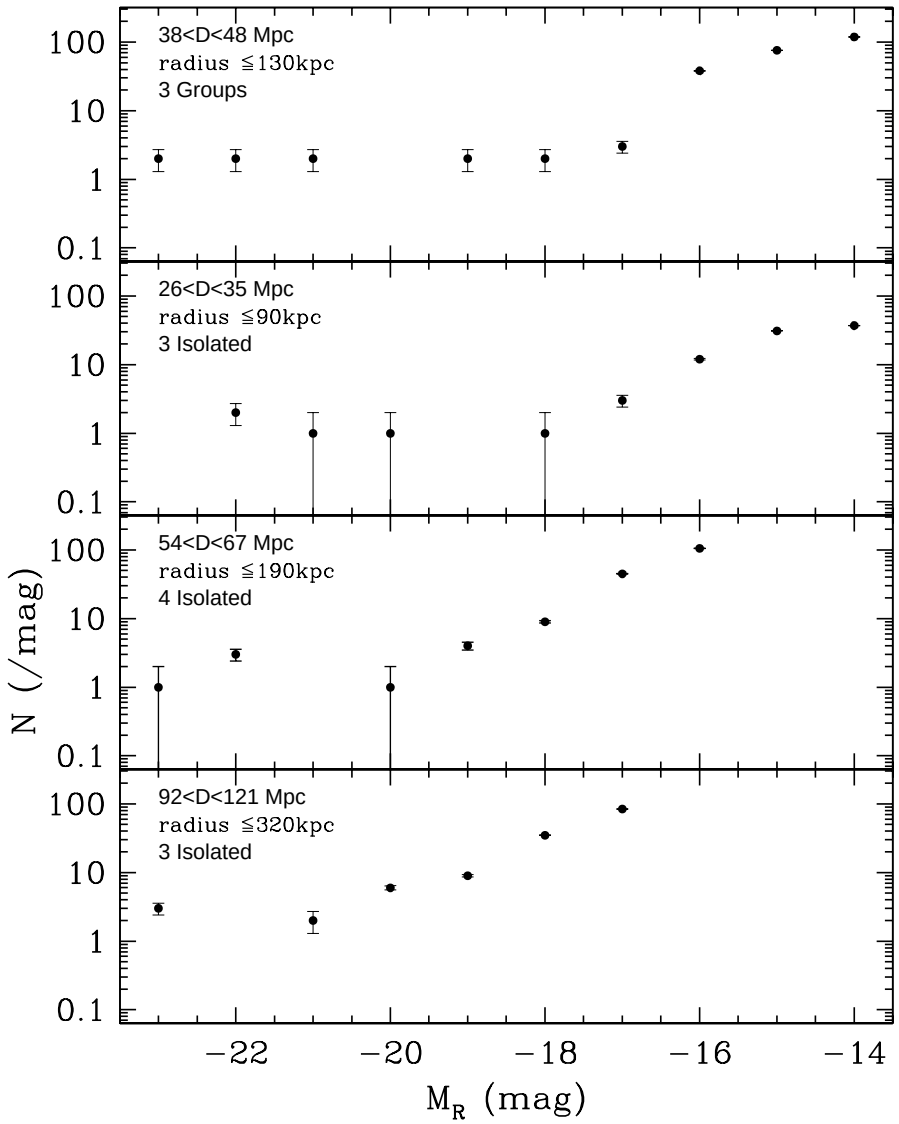

Figure 3.8: Differential luminosity function in the R-band for faint galaxies in the field of the ten isolated galaxies divided into three categories according to their distance. The top panel is the LF for three groups with distances comparable with the nearest isolated galaxies. Luminosity functions show a common faint end slope of about -1.2.

3.5.4 Luminosity function of dwarfs

The Luminosity Function (LF) represents the number distribution of galaxies in a given magnitude interval. Traditionally, this distribution is fit with a function of the form:

$$\phi(L) = (\phi^*/L^*)(L/L^*)^{\alpha} e^{(L/L^*)} \tag{3.2}$$

with L^* and α representing a characteristic bright magnitude and the slope of the faint end respectively (Schechter 1976). The importance of the LF lies in its strong correlation

with the mass function of the galaxy distribution, which is one of the observable tests of any theoretical cosmological model. It may also provide clues to the evolutionary history of galaxies. There have been several studies of the LF for high-density cluster environments (Trentham & Hodgkin 2002; Mobasher et al. 2003; Christlein & Zabludoff 2003) and lower density regions such as groups (Zabludoff & Mulchaey 2000; Flint, Bolte & Mendes de Oliveira 2003) and the field (Blanton et al. 2001; 2003; Drory et al. 2003).

Due to the different distances to the isolated galaxies, our data cover different physical areas with different absolute magnitude limits (under the assumption that all faint galaxies lie at the same redshift as the primary galaxy). To deal with this situation we divided the isolated galaxy sample into three distance intervals, and derived the LF separately for each (see Fig. 3.7). Excluding the nearby group NGC 4697, our imaging of the other three groups covers a comparable area to that of the isolated galaxies. We note that in driving the LFs, we assume that the faint galaxies are at the same redshift as the primary galaxy. Spectra are required to determine the true redshift distribution of these galaxies. We find that the isolated galaxies and groups have similar luminosity functions. They all show a faint end slope of ~ -1.2, and a change in the slope around $M_R \approx -18$. Such features are fairly common across a range of environments (Flint 2001; Trentham & Tully 2002; Miles et al. 2004). We note that fossil groups (Jones, Ponman & Forbes 2000) also reveal a similar luminosity function. This universality of isolated galaxy luminosity functions indicates that they are not a useful tool in discriminating between competing ideas for the origin of isolated galaxies.

3.5.5 Space number density of dwarfs

To calculate the space number density of the detected faint galaxies surrounding the primary galaxy we divided the field into concentric annuli centred on each primary galaxy. The density measures in the outer annuli were corrected for the missing area with the largest correction being a factor of 2, i.e. 50 per cent of the annulus was covered by the WFI field-of-view. The different magnitude limits in each field, determined by the exposure time, give rise to different background density levels.

In Figures 3.9, we display the space number density distribution of faint galaxies in the field of each primary galaxy. Seven out of ten isolated galaxies show almost constant density levels at all radii, indicating that the faint galaxies are mostly background objects and not associated with the isolated galaxies. The remaining three galaxies are NGC 2110, NGC 2865 and NGC 4240. Both NGC 2110 and NGC 4240 show a fairly continuous density decrease from the central region outwards. The outer most radial bin has a relatively high density suggesting that the background level has not been reached even at ~ 150 kpc. NGC 2865 shows a sharp decline from a high central density to a background level at a radius of ~ 60 kpc.

We note that these three galaxies are the closest in our sample, and for which we could detect

lower luminosity dwarfs with magnitudes down to $M_R \sim -13.5$. The mean faint magnitude limit that could be detected for the other 7 isolated galaxies is $M_R \sim -15.5$. If we include only luminous dwarfs with $M_R \lesssim -15.5$, then these three galaxies show no central excess, giving similar space densities to those of other galaxies (Fig. 3.10). This indicates that the majority of dwarf galaxies associated with the isolated galaxies are less luminous than $M_R \sim -15.5$, while more luminous dwarfs are likely to be background objects.

In their study of the NGC 1132 environment, Mulchaey & Zabludoff (1999) measured a higher central density of dwarf galaxies, with magnitudes of 17.22 <R< 19.22, than we have. From their density distribution we calculate the number of dwarfs within the central 80 kpc to be ~ 30 galaxies. We identify only 8 galaxies within the same area. Our magnitude limit for the NGC 1132 field is $R = 18.75$. This magnitude difference is not enough to explain the density distribution difference between the two studies. Considering all detected objects down to their magnitude limit of $R = 19.22$ and with ICLASS parameters up to 0.95, we find 19 objects. This number of detected dwarf galaxies is still less than that found by Mulchaey & Zabludoff. This smaller number could be due to the incompleteness of our detections for objects fainter than $R = 18.75$. The background level in the outer region (i.e. distances > 100 kpc) is consistent between the two studies.

As groups are distributed over a few megaparsecs, which is beyond our observed field-of-view, it is not surprising that the density levels remain high at all radii for our four group galaxies, i.e. none reach the background level. For IC 4320, after excluding its pair galaxy ESO509-G100, shows a constant density indicating no associated galaxies.

3.5.6 Comparison with 'fossil galaxies'

Jones et al. (2003) defined a 'fossil' to be a giant isolated elliptical galaxy with group-like X-ray emission and luminosities of $L_{X,bol} \geq 10^{42} h_{50}^{-2}$ erg s^{-1}. Fossils are required to be ≥ 2.0 R magnitudes brighter than the second brightest galaxy in the system within half the projected virial radius. According to the hierarchical model of galaxy formation these elliptical galaxies are believed to be the end result of merging many small galaxies of a X-ray luminous group (Ponman et al. 1994; Jones, Ponman & Forbes 2000; Jones et al. 2003).

We have searched the literature for X-ray observations of our sample galaxies, finding only NGC 2865, NGC 3557 and NGC 4697 (O'Sullivan, Forbes & Ponman 2001), NGC 2110 (Bradt et al. 1978; Pfefferkorn, Boller & Rafanelli 2001) and NGC 1132 (Mulchaey & Zabludoff 1999) to have published X-ray luminosities. Only NGC 1132 has an X-ray luminosity ($L_X = 2.5 \times 10^{42} h_{50}^{-2}$ erg s^{-1}) that is comparable to a fossil.

In a study of 6 fossils, Jones et al. (2003) and Jones, Ponman & Forbes (2000) measured the R magnitude difference between the primary elliptical galaxy and the second brightest galaxy in the field to be $\Delta R_{12} = 2.0 - 3.3$. They considered all objects within ~ 600 kpc of the primary galaxy. Excluding MCG-03-26-030, for the entire observed field around each of

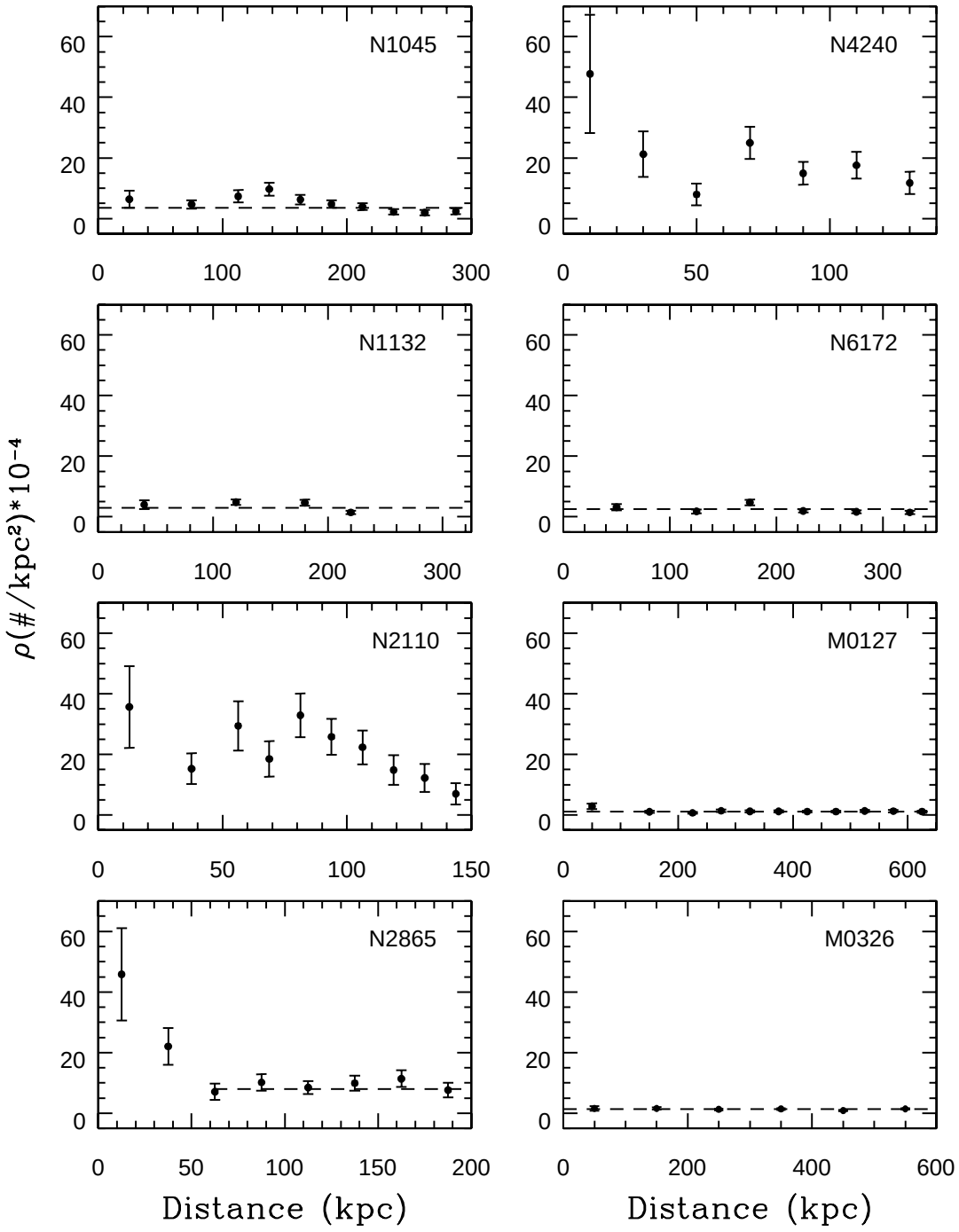

Figure 3.9: Space number density of detected faint galaxies in the field of each primary galaxy. We show Poisson error bars. The horizontal dashed lines represent the estimated background density level. The name of each primary galaxy is indicated (N=NGC, M=MCG, and E=ESO).

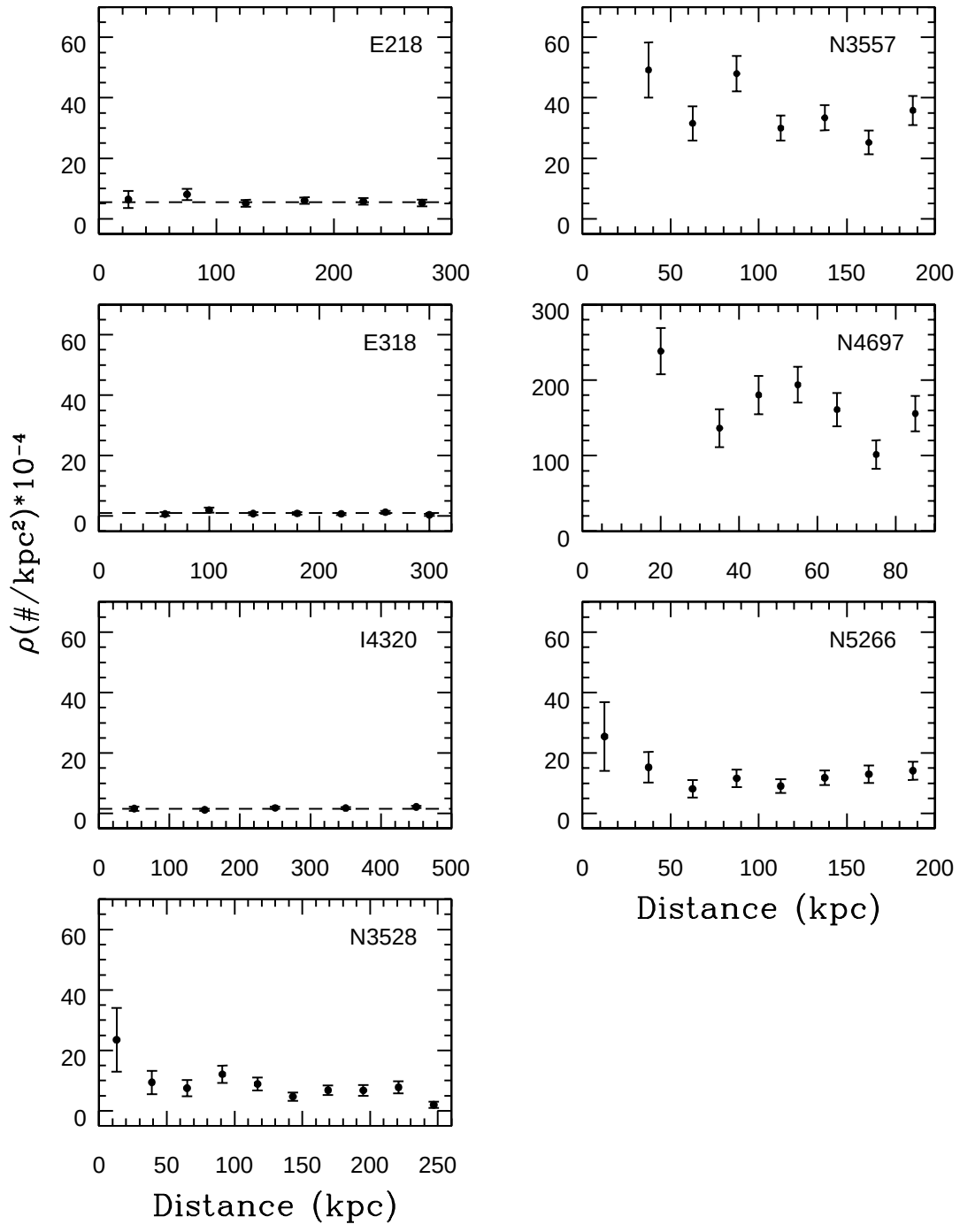

Figure 3.9: (Continue). Note the different vertical scale for NGC 4697.

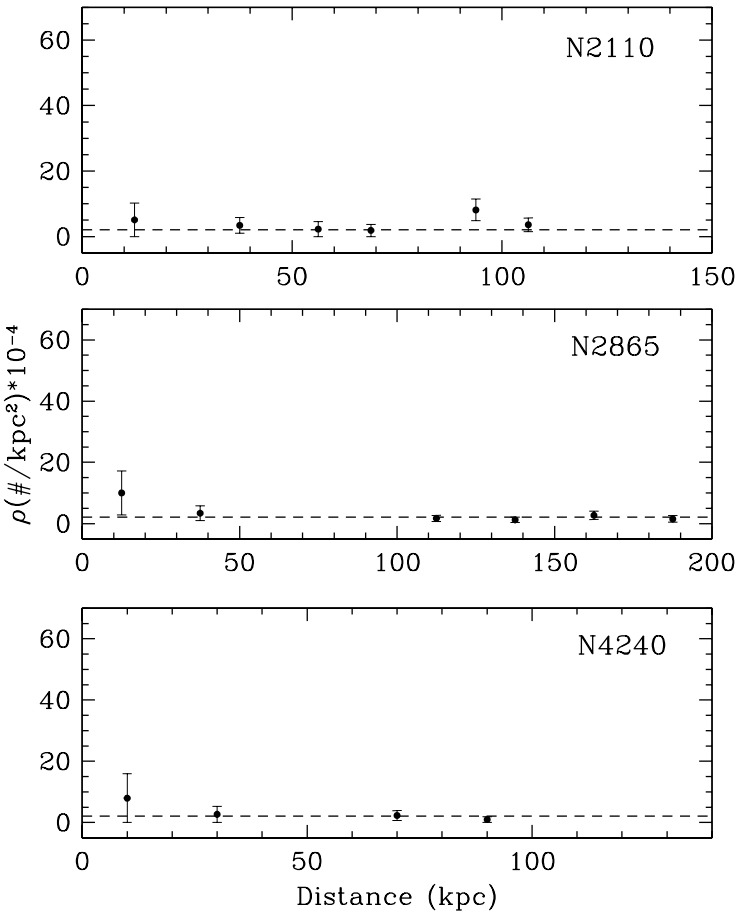

Figure 3.10: Space number density of the detected dwarf galaxies in the fields of the three galaxies NGC 2110, NGC 2865 and NGC 4240. In this figure only luminous dwarfs of $M_R \lesssim -15.5$ are included. The horizontal dashed lines represent the estimated background density level after this magnitude selection is applied. The luminous dwarfs are consistent with being background objects for all three galaxies.

our isolated galaxies, we find $\Delta R_{12} = 1.9-5.2$ and $\Delta B_{12} = 2.3-4.8$. If we use the maximum common radius for our sample of 116 kpc (which corresponds to the closest galaxy NGC 4240), we obtain similar values of $\Delta R_{12} = 1.9 - 5.3$ and $\Delta B_{12} = 2.3 - 5.4$. The galaxy MCG-03-26-030 is the least isolated in our sample with a magnitude difference of 1.8 in the *B*-band. Thus our isolated galaxies have a similar, and some times even greater, luminosity isolation than 'fossils'.

3.5.7 Possible formation scenarios

We now discuss the implications of our results in terms of various 'straw-man scenarios' for how isolated early-type galaxies may have formed. Our isolated galaxy images cover hundreds of square kiloparsecs of their surrounding fields. Using these images we are not only able to study the morphological structure of the galaxies themselves but also the magnitude and

spatial distribution of the dwarf galaxies in their environments. Our selection criteria ensure that the galaxies are not currently undergoing a strong interaction with any other galaxy. The possible scenarios for isolated galaxies formation are:

1) *Clumpy collapse at an early epoch.* The early-type galaxy may have formed at an early epoch from the clumpy collapse or gaseous merger of many fragments. However the incidence of dust lanes, plumes and shells indicates that if the galaxy is very old, then it must have experienced a recent merger/accretion event. The low-density environment sample of Kuntschner et al. (2002) revealed much fine structure and young central ages indicating recent star formation – presumably induced by a recent merger/accretion. Thus if isolated galaxies formed a long time ago, some of them have undergone strong subsequent evolution.

2) *An equal-mass merger of two massive galaxies.* If we consider merging of two galaxies as the simple addition of their contents, without taking into account any star formation during the merger, then the merger of two progenitors of $M_B \sim -20.25$ would produce an elliptical galaxy with magnitude of $M_B \sim -21$. The latter is a typical magnitude for our isolated galaxy sample. Furthermore the models of Bower, Kodama & Terlevich (1998) indicate that the merger of equal-mass galaxies will reproduce the slope and scatter of the CMR as we observe in Fig. 3.6. The 28 per cent of isolated galaxies with dust would seem to require that at least one of the progenitors was a spiral galaxy. We note that in a detailed study of NGC 2865, Hau, Carter & Balcells (1999) concluded that it is the result of a merger involving one spiral and one early-type galaxy. The plume seen in NGC 1045 also requires the merger to have involved a spiral galaxy (e.g. Toomre & Toomre 1972). In the collisionless N-body simulations of Naab & Burkert (2003), mergers of two disks of equal-mass may produce a boxy elliptical, while higher mass-ratios may create low-luminosity, rapidly-rotating discy ellipticals. We find 11 per cent (one galaxy; NGC 1045) to have boxy isophotes and 22 per cent to have discy isophotes in our isolated galaxy sample. We conclude that the merger of two near-equal-mass galaxies, with at least one being a spiral, is a plausible scenario for several of our isolated galaxies.

3) *A large elliptical accretes several dwarf galaxies.* If the elliptical galaxy was initially located on the CMR, then the accretion of small dwarfs will not have a strong effect on its mass nor on its overall colour. However, we would expect low-luminosity dwarfs (with long dynamical friction timescales) to avoid accretion and be located close to the isolated galaxy. Such a trend is seen in the high central space density for three isolated galaxies (Fig. 3.9). Perhaps the main difficulty with this scenario is explaining the observed fine structure. In three galaxies, the morphological disturbance (e.g. plume, shells, dust lanes) is quite strong suggesting the accretion of a fairly large galaxy. For the remaining 6 isolated galaxies, this scenario can not be excluded.

4) *A group of galaxies collapses with its luminous galaxies merging together.* Such a scenario would give rise to a giant elliptical galaxy (Barnes 1989) with a magnitude comparable to the total magnitude of the original group. The magnitudes of our isolated galaxies are similar

to poor groups but not typical of loose groups which have a total $M_B \approx -22$. The merged galaxies could explain the incidence of dust and other fine structure in our sample. However, we would again expect low-luminosity dwarfs to avoid the merger process, leaving a giant galaxy surrounded by a population of such dwarfs. In the case of a virialised X-ray group, its collapse is expected to produce an isolated early-type galaxy with an extended group-like X-ray emission (called a fossil) because the hot gas cooling time is very long. For our sample only NGC 1132, out of three galaxies with published X-ray luminosities, has a group-like X-ray emission. Thus most isolated early-type galaxies do not appear to be the result of a merged large group, but the possibility remains that they may be the product of a merged poor group.

Chapter 4

The spatially resolved stellar population

This chapter is based upon Reda et al. 2007, MNRAS, in press. The radial profile of the recession velocity and velocity dispersion based on new measurements by the author are included in this chapter.

4.1 Introduction

The stellar population properties of early-type galaxies (e.g. age, metallicity [Z/H] and α-element abundance [E/Fe]) provide crucial clues to their evolutionary history. Most work to date has concentrated on galaxy central regions. While useful, such data only sample a small fraction of the galaxy mass and do not provide any radial gradient information.

Radial gradients can help discriminate between different formation models. For example, dissipational collapse models (Larson 1974; Carlberg 1984; Kawata & Gibson 2003) predict strong metallicity gradients that correlate with galaxy mass, whereas mergers tend to result in shallow gradients (White 1980; Bekki & Shioya 1999) with little galaxy mass dependence. As [E/Fe] may be an indicator of star formation timescale, a positive gradient indicates outside-in formation and a negative one the opposite (e.g. Ferreras & Silk 2002). Age gradients indicate whether any young stars are confined to the central regions, and hence an indication of their mass contribution.

Here we extend the previous work by examining the radial stellar population properties to around 1 effective radius in a sample of a 12 isolated galaxies. Our new data are supplemented by data for 5 isolated galaxies from the literature. We also utilize the latest SSP models and fitting methods.

4.2 The data

In Chapter 2, we defined a sample of 36 isolated early-type galaxies in the local universe ($z < 0.03$). Here we present new data on the stellar populations of a subsample for 12 galaxies from that sample. The basic data of these galaxies and their sources are summarised in Table 4.1.

We supplement our data with data from the literature for other isolated galaxies of our sample. D05a extracted 21 Lick spectral indices for the central $r_e/8$ region for a sample of 86 early-type galaxies. Six of our 36 isolated galaxies were included in their study. D05a applied an emission correction to the indices where the galaxy spectra show evidence of emission lines. Comparing their extracted stellar population parameters to the literature, their measurements tend to be younger and more metal-rich (Denicoló et al. 2005b; D05b). Using their published indices of the six isolated galaxies, and applying the multi-index χ^2 minimization technique which we are using for our observations and the same SSP model (see Sec. 4.2.5), we have extracted the central stellar population parameters for these galaxies which are listed in Table 4.2.

The spatially resolved stellar population of the isolated galaxy NCG 821 was previously studied by Proctor et al. (2005). Here we used their data to extract the central values of the age, total metallicity [Z/H] and α-elements abundance [E/Fe] within $r_e/8$ which are also listed in Table 4.2. These measurements of the central parameters are consistent to our measurements using the indices from D05a. We also measured the radial gradient of these parameters, considering all apertures beyond the seeing limit, to be 0.29 ± 0.05, -0.06 ± 0.03, -0.72 ± 0.04 for log(age), [E/Fe] and [Z/H] respectively.

Table 4.1: Basic data for the observed isolated galaxies.

Galaxy	M_K (mag)	log (r_e) (kpc)	$\pm$	log (r_e) source
NGC 682	–24.88	0.73	0.10	PS97
NGC 1045	–25.02	0.66	0.10	T3.4
NGC 1162	–24.53	0.63	0.10	2MASS
NGC 2271	–23.84	0.47	0.07	R05
NGC 2865	–24.26	0.68	0.01	T3.4
NGC 4240	–22.71	0.29	0.10	2MASS
ESO 153-G003	–25.04	0.62	0.06	T3.4
ESO 218-G002	–24.51	0.76	0.11	T3.4
ESO 318-G021	–24.43	0.77	0.01	T3.4
MCG-01-27-013	–25.08	0.97	0.05	T3.4
MCG-02-13-009	–24.58	0.67	0.10	2MASS
MCG-03-26-030	–25.79	0.92	0.02	T3.4

Note: M_K is the absolute magnitudes in the K-band from 2MASS catalogue. Effective radius r_e values are from Table 3.4 (T3.4) and Reda, Forbes & Hau (2005; R05). Effective radius r_e from the 2MASS catalogue is the isophotal radius r_{20} in the K-band (via LEDA database) converted to effective radius using the correlation in Jarrett et al. (2003, Fig. 11). For NGC 682 the effective radius is derived from the fundamental plane (Prugniel & Simien 1997; PS97).

Table 4.2: Central (r<r_e/8) stellar populations of isolated galaxies from literature.

Galaxy	log(σ_o) (km/s)	age$_o$ (Gyr)	[E/Fe]$_o$	[Z/H]$_o$
NGC 821	2.33± 0.06	4.7 ± 1.9	0.15± 0.02	0.48± 0.05
NGC 1045	2.36± 0.06	5.3 ± 1.4	0.12± 0.02	0.43± 0.03
NGC 1132	2.37± 0.05	11.2 ± 4.7	0.36± 0.04	0.10± 0.07
NGC 2128	2.25± 0.06	2.8 ± 1.2	0.27± 0.03	0.48± 0.09
NGC 6172	2.13± 0.05	2.5 ± 0.5	0.00± 0.03	0.13± 0.04
NGC 6411	2.25± 0.03	10.6 ± 0.8	0.18± 0.04	–0.05± 0.02
NGC 821	2.29± 0.01	5.6 ± 0.5	0.22±0.01	0.41± 0.06

Notes: Parameters of the first six galaxies are obtained using the published Lick indices of Denicoló et al. (2005a) and refit to a SSP model for this work. For NGC 821 (in the last row), the parameters are the average of all apertures within r<r_e/8 from Proctor et al. (2005).

4.2.1 Observations

Our spectroscopic observations were carried out using EFOSC2 at the ESO 3.6-m telescope on the La Silla Observatory in two observing runs, 2002 Jan. 16-18 and 2004 Dec. 11-12. The observational set up and slit position are described in detail by Hau & Forbes (2006; HF06). Lick and spectrophotometric standard stars were observed at the parallactic angle. The observing nights were photometric and the seeing was generally better than 1.0″.

Observations of the first run (2002) were collected using a slit of 300″ length and 1.5″ width which was positioned along the major axis of each galaxy, with exception for the S0 galaxy ESO 153-G003 where the slit was positioned along the minor axis to avoid the disc. Using the ESO grism#8 of 600 line/mm provides a spectral resolution of 9.3 Å FWHM. The accumulated exposure time was 2 × 1200 seconds for each galaxy. In the 2004 run we used a 300″ × 1.2″ slit which provides a spectral resolution of 7.8 Å FWHM. The accumulated exposure time was 3 × 1200 seconds for each galaxy. The multiple observations of each galaxy are combined to increase the S/N ratio.

Additionally, a number of spectrophotometric stars were observed for flux calibration and Lick standard stars of type between K0 and K5 to be used as templates for velocity dispersion measurements and for calibration of the line-strength indices to the Lick/IDS system. A number of bias, dark current and dome flat were recorded each night. Observations of all galaxies and stars gave a wavelength coverage of 4300-6300 Å.

4.2.2 Basic data reduction

Data reduction, including bias, dark current and flat field subtraction, is performed using tasks within IRAF. Wavelength calibration is done using Helium-Argon lamp and is good to within 0.5 Å, while the flux standard stars are used to calibrate the spectra. The 2-D spectra are corrected for the S-distortion and sky subtracted. For more details about the

data reduction refer to HF06.

Finally the 2-D spectra of the galaxies are spatially binned using the STARLINK task EXTRACT to obtain 1-D spectra of S/N ratio greater than 20. We will refer to these 1-D spectra of each galaxy as *apertures*.

4.2.3 Velocity measurements

The heliocentric recession velocity of the standard stars are obtained by comparing their spectra to the solar spectrum. The *fxcor* task within IRAF is used to fit a Gaussian to the cross-correlation function to determine the maximum peak. The position of the maximum peak centre gives the required heliocentric recession velocity of the stars.

Once the heliocentric recession velocity of the standard stars were measured, the redshifts and velocity dispersions of the galaxies are determined by comparing their spectra to the spectra of the standard stars. The *fxcor* task of IRAF is used to compute the cross-corelation of the galaxy spectra with the spectra of each template star. Once the correlation is computed, the position of the maximum peak centre gives the recession velocity V_r and the velocity dispersion σ. The final V_r and σ are the average of the values estimated from all the template stars. The radial kinematics for the same sample of galaxies are discussed in HF06.

4.2.4 Absorption line-strength measurements

We adopted the definition of Lick/IDS absorption line indices from Trager et al. (1998). They defined each index using a pair of pseudocontinua bracketing the line feature and the central passbands of the line itself.

Our observations cover a wavelength range of 4300-6300 Å which includes 16 Lick/IDS index. These are one Balmer index (Hβ), three Magnesium indices (Mg_1, Mg_2 and Mg_b), Calcium (Ca4455), Sodium (NaD), Titanium Oxide (TiO_1) indices plus nine Iron indices Fe4383, Fe4531, Fe4668 (referred to as C4668), Fe5015, Fe5270, Fe5335, Fe5406, Fe5709 and Fe5782.

Five Lick standard stars were observed during each observing run and will be used in the following sections to calibrated the measured indices to the Lick system.

Matching to the Lick resolution

Lick absorption indices are affected by a wavelength dependent instrumental resolution. This resolution ranges from minimum value of $\sim$ 8.4 Å in the range 4900- 5400 Å and degrade at the blue and red sides reaching above $\sim$ 10 Å (see Fig. 7 in Worthey & Ottaviani 1997). Our observed instrumental resolutions (9.3 Å and 7.8 Å for 2002 and 2004 runs respectively)

are different from those of the standard Lick system. The galaxy velocity dispersion will also alter the observed resolution of the absorption lines.

To transform to the standard Lick system, two different methods are used according to the observed total resolution of the spectra (including both instrumental and velocity dispersion effects). For indices with combined resolution higher than that of the Lick system, spectra are degraded to the resolution of the Lick/IDS library by convolving the spectra with a wavelength dependent Gaussian. While for indices with resolution lower than the Lick/IDS system, a correction factor is measured by convolving the spectra of five Lick standard stars with a series of Gaussians widths from 0 to 500 km/s. Comparing the indices from the artificially broadened stellar spectra to the un-broadened indices, we estimate the index corrections for the broadening effect of velocity dispersion in galaxies. This factor is then used to transform the indices measured in the galaxies of low resolution spectra to the Lick resolution (Proctor & Sansom 2002; Proctor, Forbes & Beasley 2004a).

Zero-point offset due to flux calibration

Furthermore, the original Lick/IDS spectra were not flux calibrated while our spectra are. To compensate for the resulting effect on the shape of the spectral continuum, the differences between the measured and the published indices values are obtained for each observed calibration star. For each index, the values from all stars are averaged and compared to the literature values to give the mean offset. The error of the mean is obtained as: $\frac{\sigma_{offset}}{\sqrt{N}}$ where σ_{offset} is the rms of the scatter about offset and N is the number of the standard stars. The adopted offset of each index and its error are given in Table 4.3.

Table 4.3: Offset of the Lick indices from the published values.

		2002 run		2004 run	
Index	unit	mean offset	error of the mean	mean offset	error of the mean
Fe4383	Å	–0.031	0.329	–0.229	0.120
Ca4455	Å	0.214	0.152	–0.054	0.171
Fe4531	Å	–0.163	0.132	–0.342	0.103
C4668	Å	–0.828	0.097	–0.598	0.187
Hβ	Å	–0.018	0.088	–0.041	0.113
Fe5015	Å	–0.284	0.079	–0.357	0.185
Mg_1	mag	0.013	0.002	0.019	0.007
Mg_2	mag	0.019	0.003	0.018	0.006
Mg_b	Å	–0.083	0.071	0.039	0.195
Fe5270	Å	–0.135	0.053	–0.412	0.147
Fe5335	Å	–0.214	0.093	–0.274	0.215
Fe5406	Å	–0.121	0.035	–0.302	0.059
Fe5709	Å	–0.006	0.128	0.031	0.065
Fe5782	Å	0.084	0.026	0.027	0.067
Na_D	Å	0.058	0.132	–0.239	0.138
TiO_1	Å	0.004	0.005	0.006	0.003

4.2.5 Galaxy stellar population parameters

The age, total metallicity [Z/H] and α-element abundance [E/Fe] properties of our sample galaxies are estimated by comparing the Lick absorption lines indices to the single stellar population (SSP) model of Thomas, Maraston & Korn (2004; TMK04). The [E/Fe] parameter measures the ratio of the α-elements (N, O, Mg, Na, Si, Ti) to the Fe-peak elements (Cr, Mn, Fe, Co, Ni, Cu, Zn).

The multi-index χ^2 minimization technique (Proctor & Sansom 2002; Proctor, Forbes & Beasley 2004a) is used to obtain the corresponding SSP model values of the age, [Z/H] and [E/Fe] abundance ratios for the galaxies. In this technique as many indices as possible are fit to the model. Because most indices contain some information regarding each of the stellar parameters (Proctor & Sansom 2002), using this fitting technique has advantages of including all possible information recorded in all absorption line indices to measure these parameters. Another advantage of this fitting technique is that it identifies indices that are highly deviant from model values, permitting their exclusion from the fitting process. In addition, we note that parameters measured in this way are less prone to uncertainties in data reduction such as flux calibration, stray cosmic ray and also less prone to weak emission effects (Proctor, Forbes & Beasley 2004a). Therefore we start by fitting all 16 indices. The indices which deviate by more than 3σ are clipped and the χ^2 fit recalculated. After clipping the highly deviated indices ($> 3\sigma$), we notice that, for some apertures within each galaxy, the fitting is still not stable and the estimated values of the age, metallictiy and [E/Fe] are significantly affected by clipping different indices. Also, after this initial fitting process, many spectral indices show a significant range of deviations from the best fitting values. Considering NGC 2271 as a typical galaxy of the sample, the left panel of Fig. 4.1 shows the average deviation in units of error (i.e. χ) of the 16 indices from the best fit values.

Furthermore, we notice that some indices lie outside the model grid which can be due to residual offsets between the measured indices and the standard system, unknown dependencies of the line strength predictions on any abundance ratio or inaccuracies in SSP models. To eliminate the effects of the remaining offsets, we implemented the technique described by Kelson et al. (2006) to shift the zero points of the model to our data. Kelson et al. defined the reference point as a set of previously published stellar population parameters for the central massive early-type galaxy in the cluster of their study. To apply this technique to our galaxy sample we define a local reference point for each galaxy by choosing two central apertures with high S/N ratios that show higher stability during the initial fitting to the model. The initial measured age, [Z/H] and [E/Fe] of these two central apertures are considered as a reference zero point for that galaxy. We measure the offset between each index from the corresponding values in the model, at fixed age and metallicity as estimated by the initial fit. Then we apply similar shifts to the indices of all other apertures. Considering NGC 2271 as a typical galaxy of our sample, the applied shifts to its indices due to applying this method are shown in Table 4.4.

Table 4.4: Offset of the Lick indices due to applying Kelson method.

Index	Fe4383	Ca4455	Fe4531	Fe4668	Hβ	Fe5015	Mg1	Mg2
Offset	-0.7674	-0.3591	-0.036	1.8346	-0.129	-0.7202	-0.0012	0.0265
Index	Mgb	Fe5270	Fe5335	Fe5406	Fe5709	Fe5782	Na_D	TiO_1
Offset	-0.1635	-0.1449	-0.6445	0.1579	0.2859	-0.4157	-0.5614	0.022

After applying this shift, the number of highly deviant indices from the model is reduced and consequently larger number of indices are used during the fitting process which become much faster. Examining the extracted stellar population parameters before and after shifting the indices, we find that they are similar. That means applying Kelson et al. method only reduces the scatter of the indices around the model. Fig. 4.1 shows the average deviation of the indices before and after applying Kelson et al. technique. Errors in the derived parameters are estimated using Monte Carlo type realizations of the best-fitting SSP models perturbed by the index error estimates. Hence, the average estimated errors of stellar population parameters based on the observational errors are about $\pm$0.1 dex for the log(age), [Z/H] and [E/Fe] and $\pm$0.05 for log(σ).

The weak [O III] and/or Hβ emission in the two galaxies ESO318-G021 and MCG-02-13-009 (see HF06) is found to have no significant effect on our measurements of the stellar population parameters, again because of our use of all available indices and the multi-index χ^2 minimization technique to fit the indices to the SSP model.

4.3 Results

4.3.1 Central stellar population parameters

The central stellar population parameters of each galaxy are obtained by averaging the values of all apertures within the central $r_e/8$. The values are listed in Table 4.4 with the error on the mean. In the following sections we will investigate these values and their correlations compared to those for galaxies in high density environments (HDEs).

The stellar populations of three isolated galaxies NGC 821, NGC 1045 and NGC 2865 were previously measured in the literature. Comparing our measurements of NGC 2865 to those of Sánchez-Blázquez et al. (2007), we found comparable values of the central age (1.7 vs. 1.0 Gyrs), $[Z/H]_o$ (0.48 vs. 0.52) and $[E/Fe]_o$ (0.07 vs. 0.13). On the other hand, comparing our measurements for NGC 1045 to those obtained by using the data of D05a, their data indicate a younger age (5 vs. 10 Gyrs), more metal-rich (0.43 vs. 0.31) and less enhanced $[E/Fe]_o$ (0.12 vs. 0.36). We note that this galaxy does not show emission lines and D05a. did not apply any emission corrections to its indices. For NGC 821, both measurements of

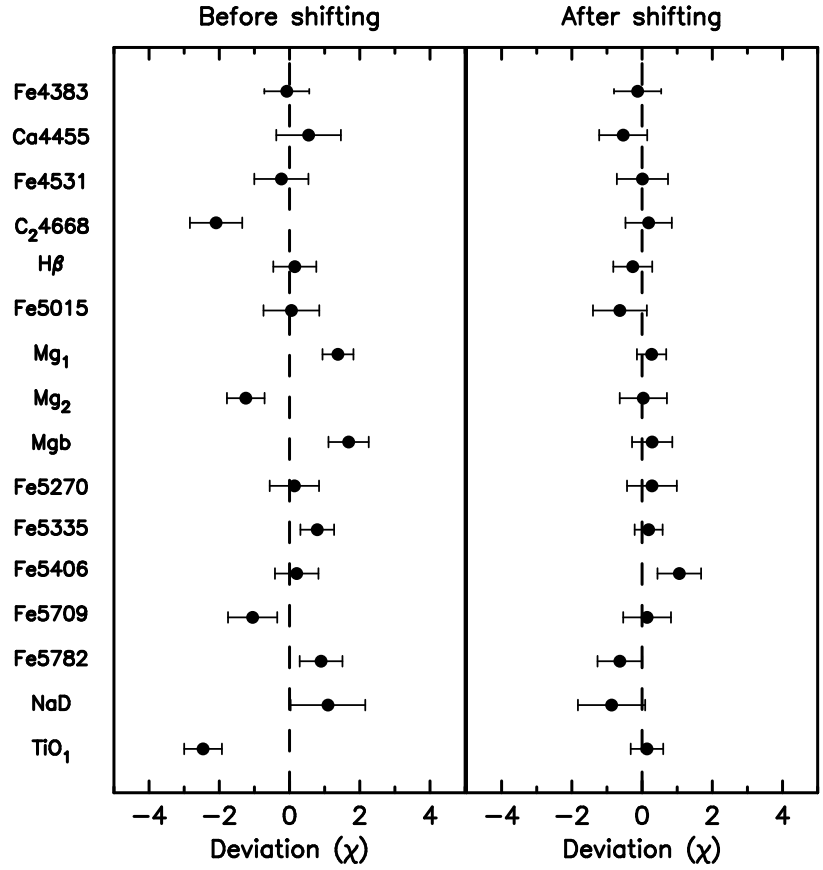

Figure 4.1: The average deviation in units of error (i.e. χ) of the 16 indices from the best fit values of NGC 2271 as a typical galaxy of the sample. Indices of the 31 apertures of the galaxy are shown before (left) and after (right) applying the shifting technique (see text for details). Error bars represent the rms scatter in the deviation.

Proctor et al. (2005) and those we obtained by using the data of D05a are comparable (see Table 4.2). Through out this paper we will consider our measurements for NGC 1045 and NGC 2865 and Proctor et al. values for NGC 821.

Central values

Including the additional data from Table 4.2, the seventeen isolated galaxies show a range of central luminosity-weighted ages. Roughly half (9 out of 17) are older than 9 Gyr, five galaxies are between 5 and 8 Gyrs, and 3 with ages younger than 3 Gyrs. The sample has an average age of 8.6 ± 0.9 Gyrs. This is younger than the average age of about 11 Gyr for galaxies in the Coma cluster found by Mehlert et al. (2003). Younger average luminosity-weighted ages for galaxies in low density environments were also found by Proctor, Forbes & Beasley (2004a; see also references therein) in comparison of galaxies in high density environments (HDEs) such as clusters and Hickson compact groups to those in loose groups and field. Similar results were also found in the large sample study of Terlevich & Forbes (2002).

Table 4.5: Central ($r<r_e/8$) stellar population parameters and the error on the mean.

Galaxy	$\log(\sigma_o)$	age$_o$ (Gyr)	$[E/Fe]_o$	$[Z/H]_o$
NGC 682	2.30 ± 0.01	8.0 ± 0.6	0.30 ± 0.01	0.33 ± 0.02
NGC 1045	2.42 ± 0.01	10.4 ± 0.6	0.36 ± 0.02	0.31 ± 0.02
NGC 1162	2.29 ± 0.01	6.8 ± 0.4	0.31 ± 0.01	0.29 ± 0.02
NGC 2271	2.37 ± 0.01	11.5 ± 0.5	0.14 ± 0.01	0.44 ± 0.02
NGC 2865	2.25 ± 0.02	1.7 ± 0.1	0.07 ± 0.01	0.48 ± 0.05
NGC 4240	2.09 ± 0.01	7.4 ± 0.5	–0.07 ± 0.01	0.23 ± 0.02
ESO153-G003	2.34 ± 0.01	11.2 ± 0.4	0.28 ± 0.01	0.19 ± 0.01
ESO218-G002	2.43 ± 0.01	14.8 ± 0.1	0.26 ± 0.01	0.35 ± 0.01
ESO318-G021	2.37 ± 0.01	8.9 ± 0.9	0.08 ± 0.01	0.34 ± 0.03
MCG-01-27-013	2.39 ± 0.01	8.0 ± 1.6	–0.03 ± 0.01	0.34 ± 0.04
MCG-02-13-009	2.33 ± 0.02	9.6 ± 1.2	0.05 ± 0.02	0.36 ± 0.02
MCG-03-26-030	2.47 ± 0.01	14.5 ± 0.2	0.15 ± 0.03	0.27 ± 0.01

On average, our isolated galaxies have central luminosity-weighted total metallicities of $[Z/H]_o = 0.29 \pm 0.03$. Mehlert et al. (2003) quotes values of 0.24 ± 0.06 and 0.12 ± 0.17 for the Coma cluster galaxies of types E and E/S0 respectively and Collobert et al. (2006) found an average of $[Z/H]_o = 0.27$ for their cluster galaxies. Using the published stellar population parameters in Thomas et al. (2005), we find that the early-type galaxies in their HDE subsample have an average of $[Z/H]_o = 0.29 \pm 0.02$, while their galaxies in low density environments are more metal-rich by about 0.05-0.1 dex.

The average central luminosity-weighted $[E/Fe]_o$ of our isolated galaxies is 0.17 ± 0.03. Comparing to the mean value of $[E/Fe]_o \sim 0.26 \pm 0.06$ reported by Mehlert et al. (2003) for cluster galaxies, our isolated galaxies show lower values by order of 0.1 dex. Although, if we arbitrarily divide our sample in half, then 8 out of 17 of our galaxies are significantly enhanced with $0.20 < [E/Fe] < 0.36$. These eight galaxies are comparable to those measured by Proctor, Forbes & Beasley (2004a) for galaxies in massive and compact groups ($[E/Fe]_o = 0.26 \pm 0.04$). The other nine galaxies resemble the solar element abundance with $[E/Fe]_o \sim 0.06 \pm 0.03$ which is lower than what Proctor et al. obtained for field galaxies ($[E/Fe] = 0.12 \pm 0.02$).

Central parameters correlations

Above we have compared the central stellar population parameters of the isolated galaxies with their counterparts in HDEs. However, such parameters are known to vary with galaxy velocity dispersion (e.g. Kuntschner et al. 2001; 2002; Mehlert et al. 2003; Collobert et al. 2006; Sánchez-Blázquez et al. 2006b; Brough et al. 2007). Next we compare the correlatio ns between central stellar population parameters of our isolated galaxies to those in HDEs.

Bernardi et al. (2006) identified a sample of 490 early-type galaxies in HDEs from the SDSS at redshifts of $z \leq 0.06$. They define the HDEs as those galaxy systems of total luminosity

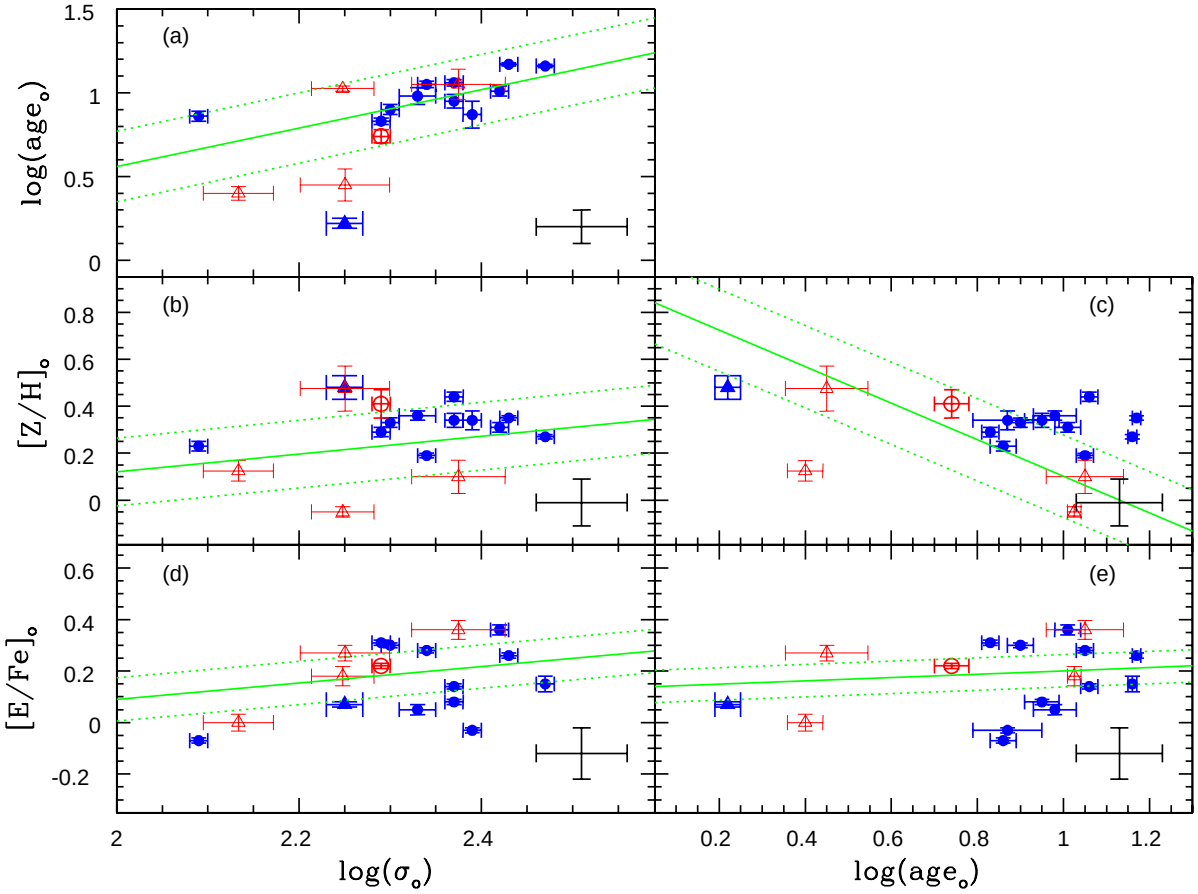

Figure 4.2: Relations between the central age, velocity dispersion (σ_o), total metallicity $[Z/H]_o$ and α-elements abundance $[E/Fe]_o$. Solid lines are correlations from Bernardi et al. (2006) for low redshift ≤ 0.06 galaxies in HDEs, and dotted lines represent their 1σ scatter. In panel (a), isolated galaxies exhibit slightly more scatter towards younger ages for their velocity dispersion than those in dense environments. In panel (b), the $[Z/H]_o$ and velocity dispersion of isolated galaxies follow a similar trend as the HDE galaxies with a tendency to higher metallicities. In panel (c), isolated galaxies follow a similar age-metallicity relation as those in HDE with a tendency to higher metallicities. In panels (d) and (e), isolated galaxies exhibit more scatter towards lower $[E/Fe]_o$ for their velocity dispersion and age than those in HDEs. In all panels, solid symbols are data of the present sample, the solid triangle represents NGC 2865, the open circle is NGC 821 from Proctor et al. (2005) and open triangles are data for galaxies from Denicoló et al. (2005a). We plot data for NGC 1045 from our present study only. Error bars in the bottom right corners are the systematic error of ± 0.1 dex for age, $[Z/H]_o$, $[E/Fe]_o$ and ± 0.05 for $\log(\sigma_o)$.

more than 10 times the luminosity of a typical early-type galaxy. To obtain a high S/N ratio for their spectra, they co-added similar objects by using narrow bins in luminosity, size, velocity dispersion, and redshift (Bernardi et al. 2003d). The 490 galaxies produced 105 composite spectra of S/N$\sim$ 100. Using their published stellar population parameters and correlations between those parameters, we have measured the 1σ scatter of their galaxies about these correlations. In Fig. 4.2, solid lines are the best fit relation from Bernardi et al., and dotted lines represent the 1σ scatter calculated by us. Similar trends to Bernardi et al. were found for galaxies in HDEs by previous studies (e.g. Kuntschner et al. 2002; Mehlert et al. 2003; Collobert et al. 2006; Sánchez-Blázquez et al. 2006b).

For our isolated galaxies, trends between the stellar population parameters in the central regions and the central velocity dispersion (a proxy for mass) are examined in Fig. 4.2 (a),(b) and (d), while panels (c) and (e) show correlations of [Z/H] and [E/Fe] with age. Isolated galaxies follow similar trends to those in HDEs with more massive galaxies being older, more metal-rich and with higher $[E/Fe]_o$ than less massive ones. Isolated galaxies show slightly higher scatter towards younger ages, higher $[Z/H]_o$ and lower $[E/Fe]_o$ for their velocity dispersion than those in HDEs. In panels (d) and (e), the two galaxies NGC 4240 and MCG-01-27-013 are the most deviant galaxy from the correlations with very low $[E/Fe]_o$ for their velocity dispersion and age.

Similarly, comparing galaxies in low density environments with those in Fornax cluster, Kuntschner et al. (2002) found that both samples follow similar $\log(\sigma_o)$-metallicity trends, although galaxies in low density environments show higher metallicities by $\simeq 0.15$ dex.

Panel (c) shows the observed age-metallicity relation for the isolated galaxies. Although the correlated errors of the age and metallicity may be partly responsible for this correlation (e.g. Kuntschner et al. 2001), our isolated galaxies follow a similar correlation to HDE galaxies. While the effect of the correlated errors is expected to reduce the measured metallicity of old galaxies, we note that the oldest three of our galaxies (ESO218-G002, MCG-03-26-030 and NGC 2271) with age $>$ 11 Gyrs, tend to be more metal-rich than the average galaxy. On the other hand, the galaxy NGC 6172 tends to be younger and less metal-rich than the general trend of the correlation. The stellar population of this galaxy is extracted from the emission corrected Lick absorption indices from D05a, which perhaps leads to measuring a younger age.

As a function of central age, panel (e) shows that many of the isolated galaxies have low $[E/Fe]_o$ for their age compared to their counterparts in HDEs. Low values of $[E/Fe]_o$ have been previously reported by Collobert et al. (2006) for their galaxies in low density environments.

In summary, isolated galaxies in our sample span a large range of ages. Scaling relations between central stellar parameters are similar to those for galaxies in higher density environments albeit with a tendency to younger central ages, higher [Z/H] and lower [E/Fe].

4.3.2 Kinematic and stellar population radial profiles

The radial recession profile of the stellar population parameters are fit with a weighted least squares method to measure the gradient for all apertures beyond the seeing limit of $1''$. The linear fits of σ, log(age), [E/Fe] and [Z/H] versus $\log(R/R_e)$ are listed in Table 4.5. We note that our measurements of [Z/H] and [E/Fe] gradients of the galaxy NGC 2865 are comparable to those found by Sánchez-Blázquez et al. (2007), although they found a steeper age gradient of 1.15 ± 0.05. Throughout this paper we use our measurements for this galaxy which is shown in all plots as a solid triangle.

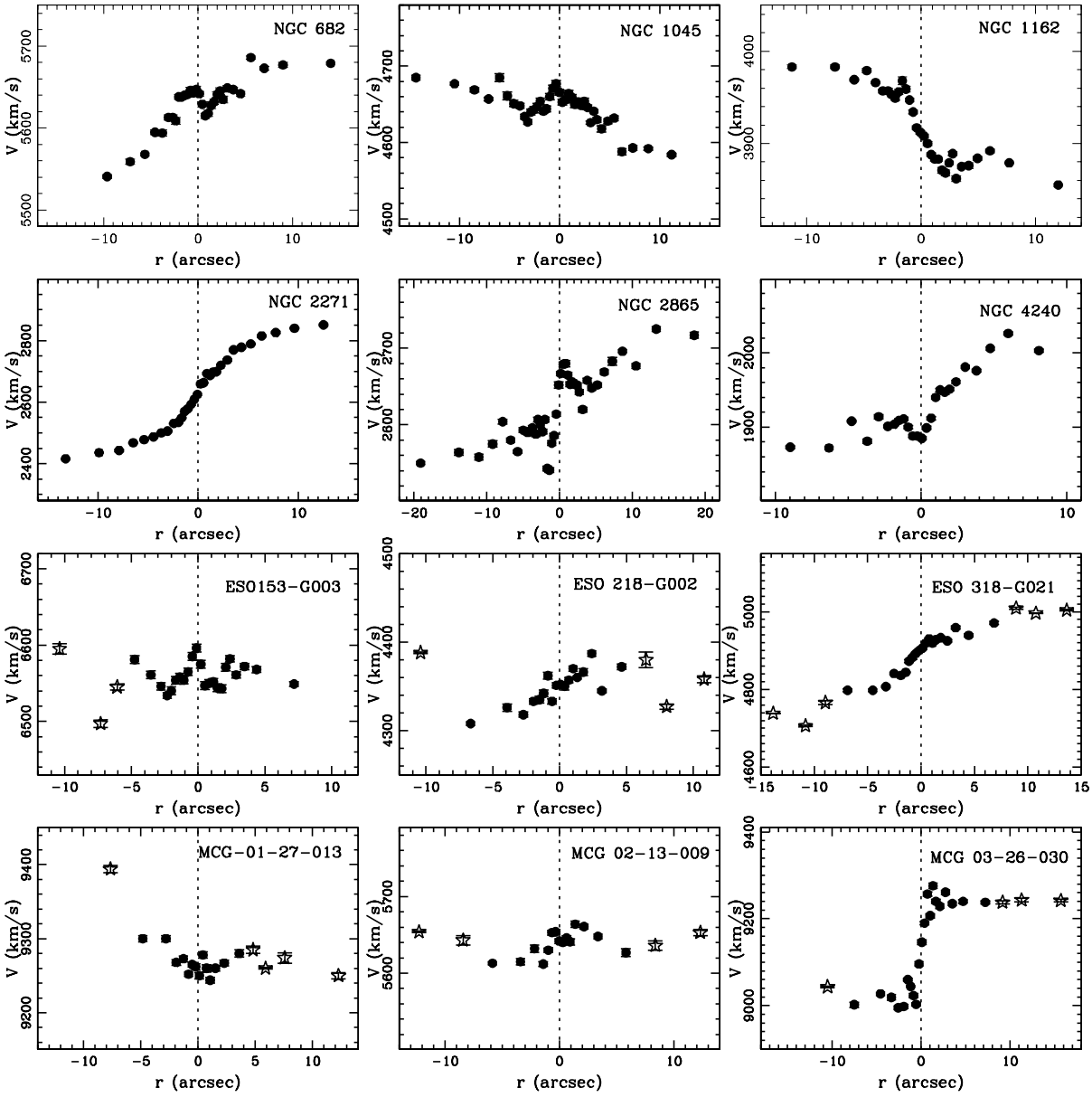

Figure 4.3: Rotational velocity profiles for our sample of isolated galaxies. Stars symbols represent apertures of lower S/N and are not used for the stellar population analysis.

In the following sections we examine the radial profile of each parameter in detail.

Rotation velocity and velocity dispersion profiles

The radial velocity profiles of the galaxies are shown in Fig. 4.3, while those of the velocity dispersion for each galaxy are shown in the top panels of Figures 4.4. The detailed kinematics of our sample of galaxies have been previously studied by HF06. Reproducing the velocity profiles (see Sec 2.3), we confirm their findings of kinematic substructures in some of these galaxies. Rapidly rotating cores are detected in seven galaxies, three reveal fast rotating outer discs, while three galaxies show central peaked velocity dispersion profiles (see HF06

for details).

Age profiles

Although having a wide range of ages, Figures 4.4 show that the majority of our sample of isolated early-type galaxies show statistically insignificant age gradients with an average of 0.04 ± 0.08 dex per dex. Four of these galaxies (NGC 2271, ESO153-G003, ESO218-G002 and MCG03-26-030) have uniform ages older than 10 Gyrs indicating a formation epoch at $z > 2$. Two galaxies, ESO318-G021 and MCG01-27-013, show intermediate ages of 8.9 and 8.0 Gyrs which indicate an extended star formation history to $z \approx 1$.

Although two galaxies, NGC 682 and NGC 4240, show insignificant age gradients, they are composed of both old and relatively younger populations, which suggests a secondary star formation epoch for these two galaxies. NGC 682 shows a global age of $\sim 8.0 \pm 0.6$ Gyrs, with a younger population of about 4.0 ± 0.5 Gyrs in the region around $\log(r/r_e) = -0.5$. The stellar kinematics at the same region and outwards indicates the presence of a rotating disk with a rotational velocity of 150 km/s combined with a low velocity dispersion which declines from about 200 km/s at $r/r_e = 0.15$ reaching 130 km/s at the outer regions. For NGC 4240, despite its statistically insignificant age gradient of $+0.16 \pm 0.12$, it has evidence for younger stars ($\sim 7.4 \pm 0.5$ Gyr) in the central regions at $r/r_e < 0.1$.

Remarkable positive gradients, with the central regions being younger, are seen in two galaxies. The galaxy NGC 1162 shows a gradient of $+0.29 \pm 0.07$ with the central stellar population having an intermediate age of about 6.8 ± 0.4 Gyr for $r/r_e < 0.13$ compared to an age > 10 Gyr in the outer regions. NGC 2865 is the youngest member of our sample with a central stellar population as young as 1.7 Gyr for $r/r_e < 0.2$ and intermediate age stars of ~ 7 Gyr outwards. This galaxy shows the steepest overall age gradient of $+0.63 \pm 0.07$. The kinematics of the central ($r < 4''$) regions of these two galaxies suggest rotationally supported cores (Fig. 4.3; see also HF06).

NGC 1045 and MCG-02-13-009 show negative age gradients of -0.19 ± 0.04 and -0.58 ± 0.27 respectively. The former galaxy has a population of intermediate age stars (~ 7 Gyr) beyond $r/r_e \sim 0.2$. This galaxy also shows asymmetrical rotation and a declining velocity dispersion profile outwards indicating velocity substructure (see also HF06). While the later galaxy shows a steady age decrease outwards, a peaked central velocity dispersion and a slowly rotating body.

We note that in the HDE of the Coma cluster, Mehlert et al. (2003) measured insignificant age gradients for 91 per cent of their galaxies.

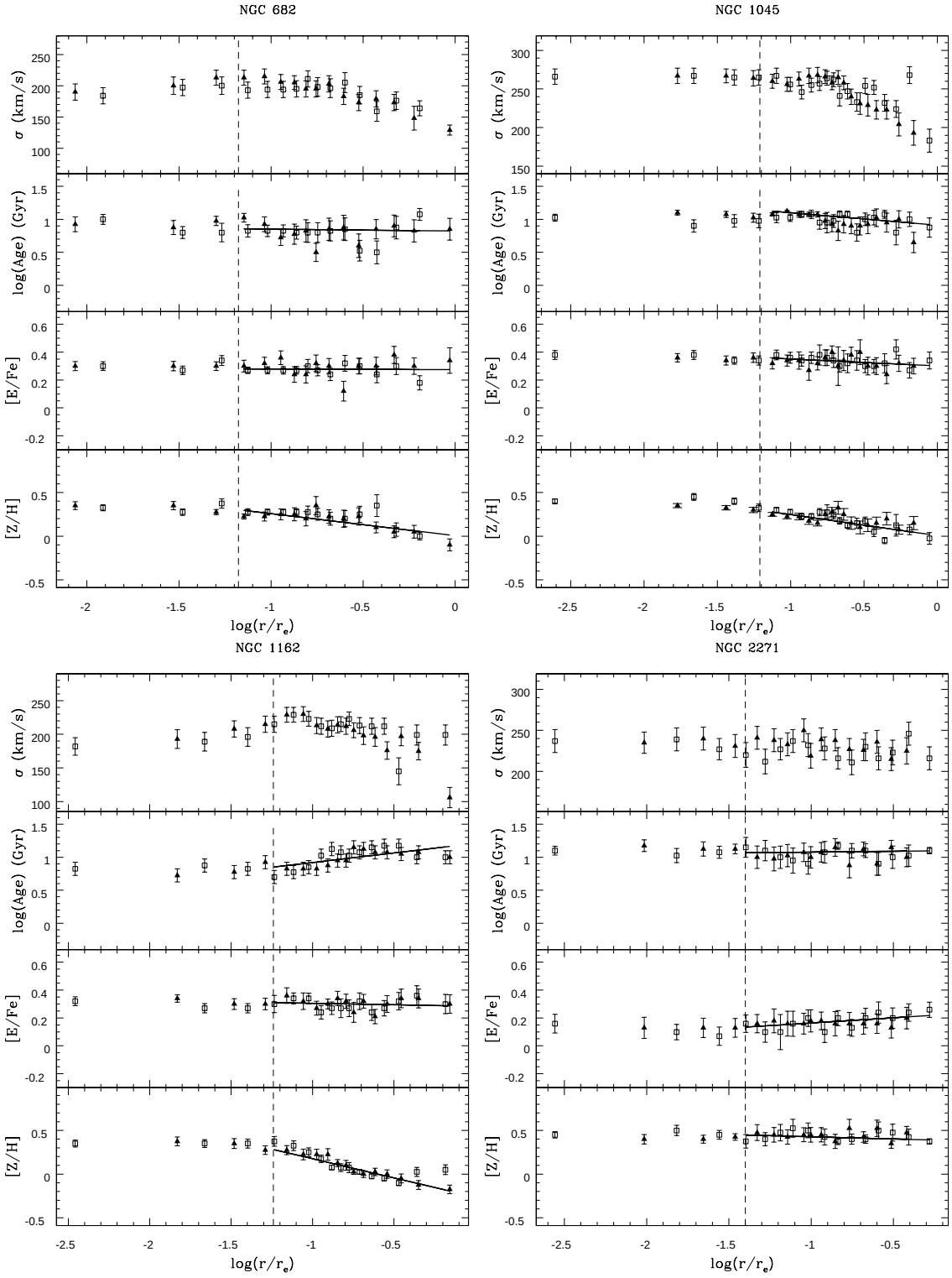

Figure 4.4: The logarithmic radial profile of the velocity dispersion σ, log (age), [E/Fe] and [Z/H] in terms of the effective radius. Squares and triangle symbols represent the apertures on different sides of the galaxy centre. The vertical dashed line represents the seeing limit. The solid line is the weighted linear least square fit to all apertures beyond the seeing limit.

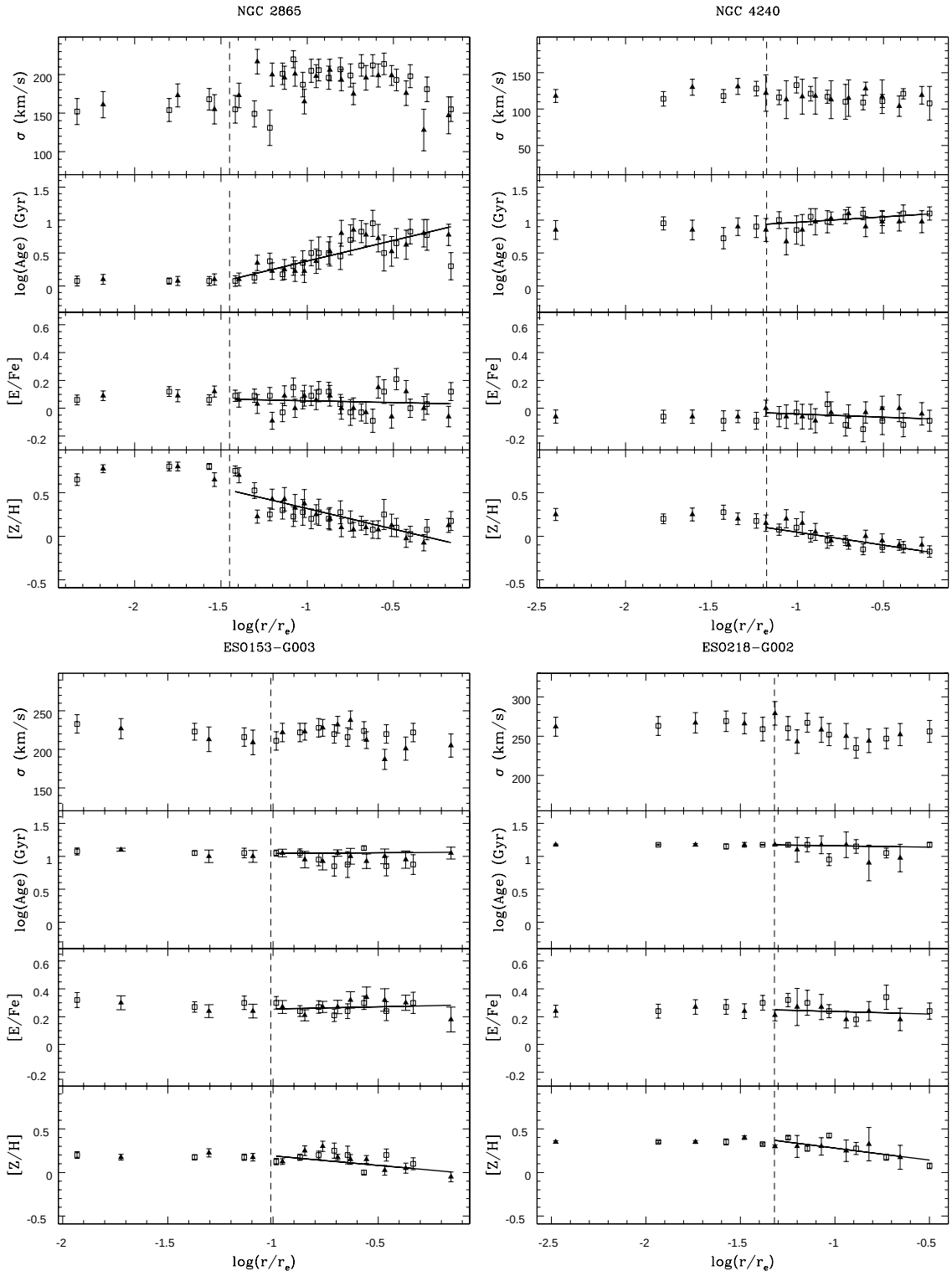

Figure 4.4: (continue).

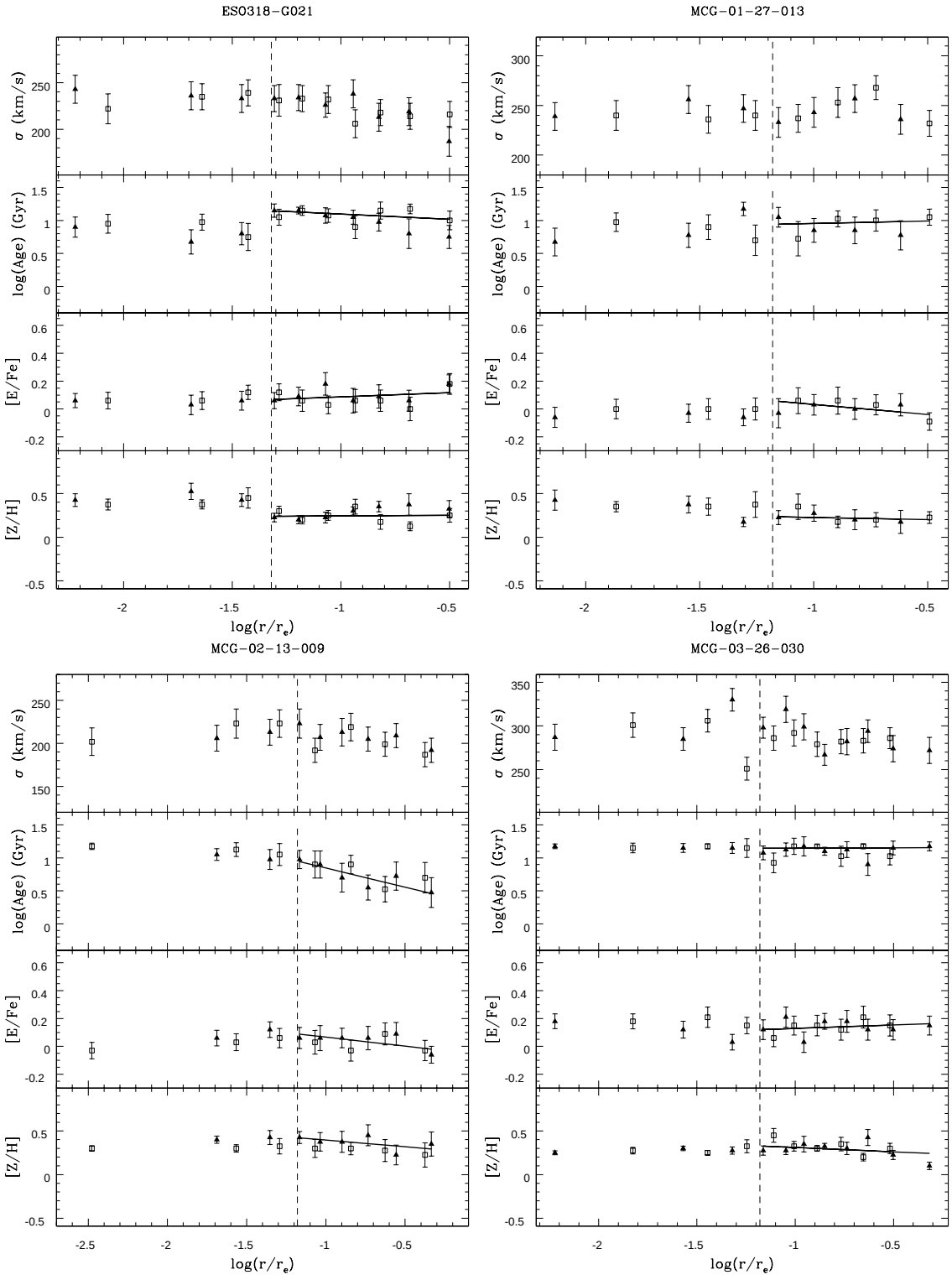

Figure 4.4: (continue).

Table 4.6: The radial gradients of the age, [E/Fe] and [Z/H] parameters.

Galaxy	log(age)	[E/Fe]	[Z/H]
NGC 682	–0.03 ± 0.08	–0.01 ± 0.03	–0.25 ± 0.03
NGC 1045	–0.19 ± 0.04	–0.05 ± 0.03	–0.24 ± 0.03
NGC 1162	0.29 ± 0.07	–0.02 ± 0.04	–0.44 ± 0.03
NGC 2271	0.03 ± 0.07	0.07 ± 0.05	–0.05 ± 0.04
NGC 2865	0.63 ± 0.07	–0.03 ± 0.03	–0.47 ± 0.05
NGC 4240	0.16 ± 0.12	–0.01 ± 0.06	–0.30 ± 0.06
ESO153-G003	0.02 ± 0.08	0.03 ± 0.07	–0.22 ± 0.05
ESO218-G002	–0.04 ± 0.04	–0.04 ± 0.07	–0.28 ± 0.04
ESO318-G021	–0.16 ± 0.11	0.06 ± 0.07	0.01 ± 0.07
MCG-01-27-013	0.07 ± 0.25	–0.14 ± 0.13	–0.05 ± 0.14
MCG-02-13-009	–0.58 ± 0.27	–0.13 ± 0.10	–0.15 ± 0.15
MCG-03-26-030	0.01 ± 0.04	0.05 ± 0.08	–0.10 ± 0.02

Metallicity profiles

The mean metallicity gradient of the 17 isolated galaxies is -0.25 ± 0.05. The two youngest galaxies of the sample NGC 1162 and NGC 2865, both have steep positive age gradients, and show steep metallicity gradients of -0.44 ± 0.03 and -0.47 ± 0.05 respectively. NGC 821 also has a young central stellar population and a very steep [Z/H] gradient of -0.72 ± 0.04 (Proctor et al. 2005).

On the other hand, three galaxies (ESO318-G021, MCG -01-27-013 and MCG-02-13-009) which show statistically insignificant age gradients, also show negligible change of the metallicity between the centre and the outer regions with average radial gradients of -0.06 ± 0.03. The flat metallicity gradient of these three galaxies, can perhaps be due to the short coverage of our spectra, i.e. only to $r_e/3$. While Mehlert et al. (2003) measure on average zero age gradients for galaxies in the Coma cluster, the total metallicity gradient was more pronounced (although with a large scatter) with their galaxies having a mean negative gradient of -0.16 ± 0.12. Sánchez-Blázquez et al. (2007) measure an average [Z/H] gradient of -0.31 ± 0.13 for a sample of galaxies in mostly HDEs.

α-element profiles

Figures 4.4 show that our sample galaxies have insignificant radial gradients of [E/Fe] with an average of -0.03 ± 0.02. Despite the measured flat gradient of [E/Fe] for the galaxy NGC 2865, visual inspection reveals fluctuations between [E/Fe]=–0.1 and 0.1 which may be related to the shell structure of this galaxy. Insignificant radial gradients of [E/Fe] were also found by Mehlert et al. (2003) for the early-type galaxies in the Coma cluster with an average of 0.05 ± 0.05.

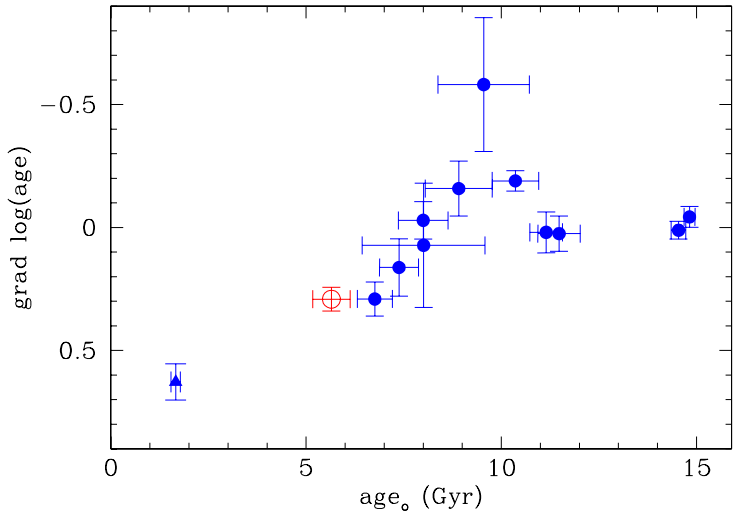

Figure 4.5: The radial gradient of the age shows a strong correlation with central values for galaxies younger than ~ 11 Gyr, while older galaxies show flat age profiles. Symbols as in Fig. 4.2.

Radial gradient correlations

Although most of our galaxies reveal statistically insignificant age gradients, Fig. 4.5 shows that while galaxies older than 11 Gyrs show no age gradients (i.e. uniformally old stellar populations), the age gradients of young galaxies are strongly anti-correlated with the central age. A non-parametric Spearman rank order correlation coefficient gives level of significance lower than 1% (which indicate a probability of correlation of 99%). No significant dependence of the age gradient on the central velocity dispersion, $[Z/H]_o$ or $[E/Fe]_o$ was found. This suggests that galaxy mass and star formation timescale plays little role in establishing age gradients. Thus as a young starburst evolves, the age gradient flattens from positive to almost zero.

Fig. 4.6 panel (a) shows the total metallicity gradient as a function of its central value. The dashed line represents the trend found by Sánchez-Blázquez et al. (2007) for galaxies mostly in HDEs of clusters and groups. Excluding galaxies with flat metallicity gradients (see Sec. 4.4), our galaxies follow the trend. This trend indicates that galaxies with steeper gradients have more metal-enriched inner regions. The galaxy NGC 2271 is the most deviant from the relation with a very shallow gradient for its central metallicity.

A correlation between the metallicity gradient and central age was detected in many previous studies for galaxies in different environments (e.g. Sánchez-Blázquez, Gorgas & Cardiel 2006a; Sánchez-Blázquez et al. 2007). Excluding the three galaxies with flat metallicity gradients (see Sec. 4.4), Fig. 4.6 (b) shows that our galaxies follow similar trends as those found by Sánchez-Blázquez et al. (2007) for galaxies in higher density environments. Galaxies with young central ages tend to have steep metallicity gradients while galaxies with uniform old stellar populations reveal shallower metallicity gradients. Since the galaxies with young

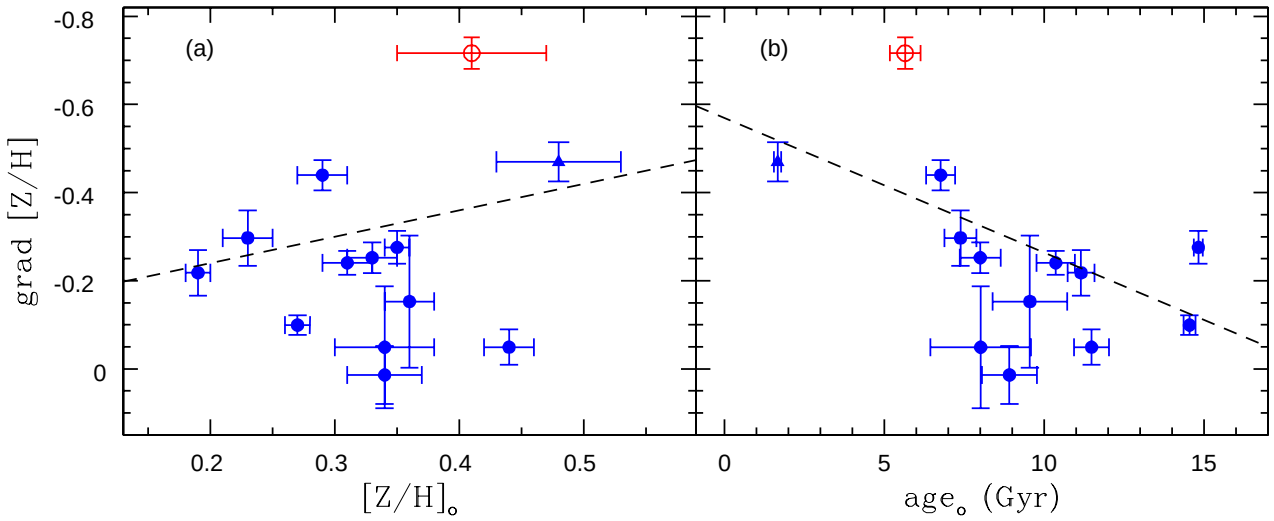

Figure 4.6: The radial gradient of the total metallicity [Z/H] versus (a) the central total metallicity $[Z/H]_o$ and (b) the central age. The dashed line represent the trend found by Sánchez-Blázquez et al. (2007) for HDE galaxies. Excluding galaxies with flat metallicity gradients (see text), our isolated galaxies follow similar trends. Symbols as in Fig. 4.2.

central ages are those with the steepest age gradients (Fig. 4.5), we expect the gradient of the total metallicity and the age gradient to be strongly correlated. Fig. 4.7 shows that galaxies of steep positive age gradients also show steep negative metallicity gradients (a non-parametric Spearman rank order coefficient gives probability of no correlation of 5%, i.e. less than 2σ significance). This implies that the young central stellar populations are also more metal-rich than the old metal-poor stars in the outer regions of the galaxies.

Fig. 4.8 shows that galaxies of smaller mass (lower $\log(\sigma_o)$) tend to reveal steeper metallicity gradients than more massive galaxies (larger $\log(\sigma_o)$). A hint of a similar trend was found by Sánchez-Blázquez et al. (2007) for galaxies of $\log(\sigma_o) \geq 2.2$ ($\sim$ 160 km/s). A change in the trend direction at this velocity dispersion, has been reported in several studies (see Sánchez-Blázquez et al. 2007 and references therein). Thus for galaxies with $\log(\sigma_o) \leq 2.2$, metallicity gradients appear to get shallower for *lower* mass (e.g. Forbes, Sánchez-Blázquez & Proctor 2005). We note that NGC 4240 ($\log(\sigma_o)$= 2.09) is consistent with this suggestion.

Examining the correlation of the metallicity gradient with galaxy dynamical mass $\log(\sigma_o^2 r_e)$ and the absolute magnitude in the K-band (as other proxies of mass) gives similar trends to that of Fig. 4.8.

For a sample of early-type galaxies, Ferreras & Silk (2002) found a correlation between [E/Fe] gradient and its central value. A steep negative gradient for low [E/Fe] galaxies changes to a steep positive gradient for enhanced [E/Fe] galaxies. Using a simple model of star formation and a standard prescription for the rates of supernovae Type II and Ia, Ferreras & Silk found that negative gradients imply inside-out formation which is suggestive of a dissipative collapse formation. On the other hand, a positive gradient is a sign of outside-in formation

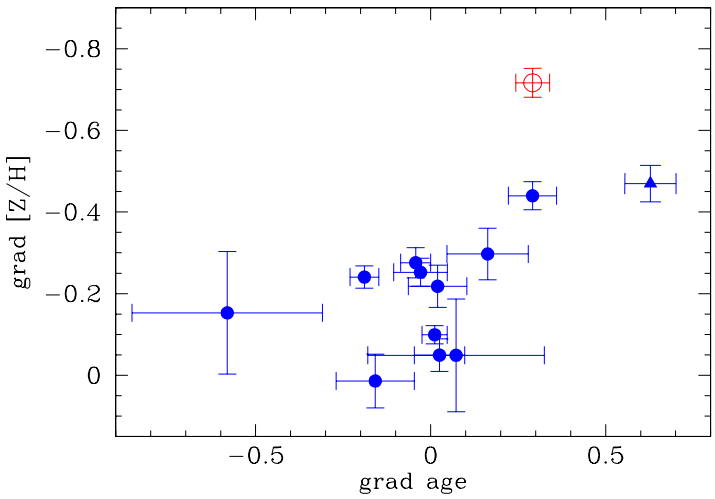

Figure 4.7: The radial gradient of [Z/H] is correlated to the age gradient. Symbols as in Fig. 4.2.

which may be a result of a past merger events which induce central star formation in the merger remnant. For our isolated galaxies, although they show insignificant [E/Fe] gradients on average, Fig. 4.9 shows that there is no obvious correlation between [E/Fe] gradient and its central value or the central age.

4.4 Discussion

Several galaxies in our isolated sample reveal a number of features such as tidal tails, dust, shells, discy and boxy isophotes and highly rotating central discs (Reda et al. 2004; Reda, Forbes & Hau 2005; Hau & Forbes 2006). These structures indicate recent merger/accretion events during the evolutionary history of these galaxies. Measuring the age of the stellar populations of the isolated galaxies reveals that several galaxies have central young stars which also requires a recent gaseous accretion or merger.

If isolated galaxies formed purely by dissipative collapse we would expect uniformly old stellar ages. We find both young central ages and age gradients in some isolated galaxies. Collapse models (e.g. Carlberg 1984; Chiosi & Carraro 2002; Kawata & Gibson 2003) predict steeper metallicity gradients in more massive galaxies. For the bulk of our sample, with velocity dispersions ≥ 160 km/s, we find the opposite behaviour with more massive galaxies have shallower metallicity gradients. A collapse also implies a largely inside-out formation with the inner galaxy regions forming first which predicts a negative [E/Fe] gradient (e.g. Ferreras & Silk 2002). We find isolated galaxies to reveal no overall [E/Fe] gradient. Thus we conclude that pure dissipative collapse can not explain our sample of relatively massive isolated early-type galaxies.

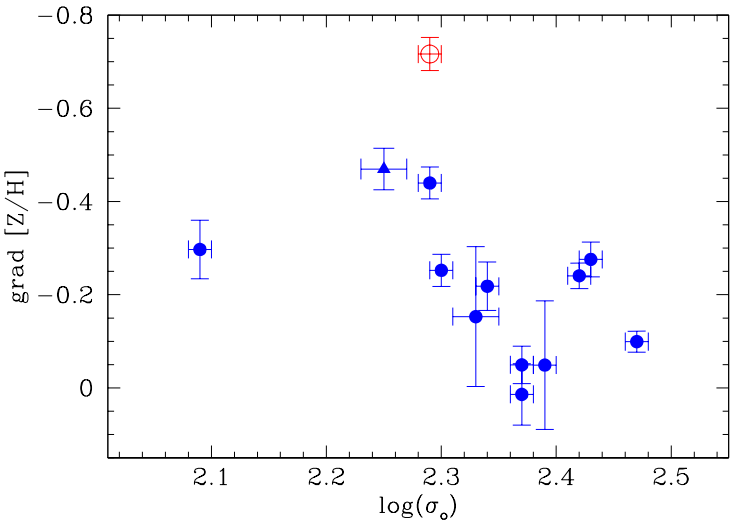

Figure 4.8: The radial gradient of [Z/H] as a function of the central velocity dispersion $\log(\sigma_o)$. An anti-correlation is seen for galaxies with $\log(\sigma_o) \geq 2.2$. Symbols as in Fig. 4.2.

The expectations for stellar population parameters in a hierarchical merger scenario are more varied depending on the gas fraction of the progenitors and their mass ratio (e.g. Kobayashi 2004). Gas-rich mergers are expected to induce central star formation (e.g. Mihos & Hernquist 1996; Springel 2000). The gradients of age and metallicity are predicted to correlate strongly with central young stars that are also metal-rich (Bekki & Shioya 1999). The metallicity gradient is also predicted to be shallower for a merger remnant (e.g. Kobayashi 2004).

The age gradient for the majority of our isolated galaxies (11 out of 13) are found to range from flat to positive. These age gradients are also correlated with the central age which implies that a young burst dominates the luminosity in the central region where it takes place, and thus produces a steep gradient. As these young populations get older and fade, the observed gradient of the luminosity-weighted age becomes shallower. However, two galaxies (NGC 1045 and MCG-02-13-009) show significant negative age gradients. The radial age profile of NGC 1045 reveals a stellar population of intermediate age at $r/r_e \sim 0.2$ and outward, which implies a secondary star formation event induced in the outer regions of the galaxy. That suggests either a late gas accretion or merger with a gas-rich satellite galaxy (Kobayashi 2004). Such accretion may form a star forming ring. Deep imaging of this galaxy reveals strong boxy isophotes and extensive extra tidal light (Reda et al. 2004) which argues in favour of a recent merger. While deep imaging is not available for MCG-02-13-009, its negative age gradient and flat metallicity gradient in the central region is predicted by the simulations of Kobayashi (2004) to be the result of late gas accretion rather than a major merger.

Most of our isolated galaxies (8 out of 13) are found to have negative metallicity gradients, as galaxies with central metal-rich stars tend to have steeper metallicity gradients. The three

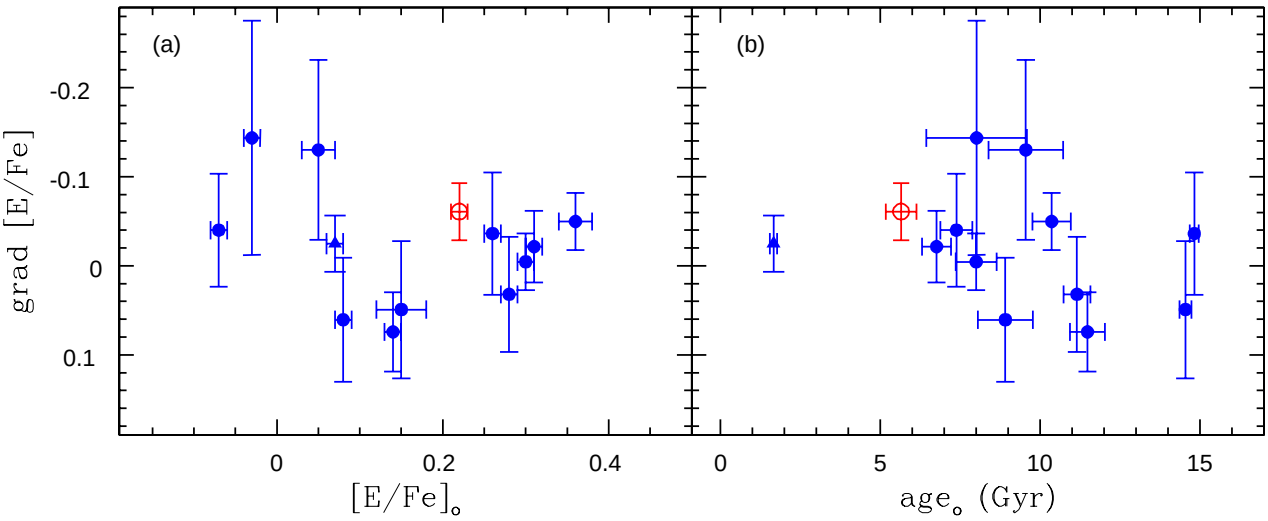

Figure 4.9: The radial gradient of the α-element abundance [E/Fe] versus (a) the central values $[E/Fe]_o$ and (b) the central age. No obvious correlation are found in the two panels. Symbols as in Fig. 4.2.

galaxies NGC 1162, NGC 2865 and NGC 821 have both significant age gradients as well as metallicity gradients, with the young central stellar population also being more metal-rich than the old metal-poor stars in the outer regions.

NGC 1162 has an intermediate central age of 6.8 Gyrs suggesting a secondary star formation event. A major merger of two massive progenitors is expected to produce a more metal-rich stellar population and shallower metallicity gradient than observed. However, a minor merger with a satellite of mass less than 0.2 times that of the primary galaxy is more likely to explain the intermediate central metallicity and the gradient (Kobayashi 2004).

The galaxy NGC 2865 is the youngest (1.7 Gyrs) and most metal-rich ($[Z/H]_o = 0.48$) galaxy of our sample. Its central velocity dispersion of 178 km/s indicates an intermediate mass galaxy. Deep imaging revels a surrounding shell structures (Hau, Carter & Balcells 1999; Reda et al. 2004) and kinematics reveal a kinematically decoupled core in the central 4 arcsec or 6.4 kpc (Hau, Carter & Balcells 1999; Hau & Forbes 2006). The kinematics and stellar population of this galaxy suggest a gas-rich accretion or merger origin for the shell and kinematics structures (Hau, Carter & Balcells 1999). However, the steep metallicity gradient of –0.47 prefer a gas-rich accretion by a metal-rich parent galaxy.

The galaxy NGC 821 has a central stellar population of 5.6 Gyrs old and a high metallicity of $[Z/H]_o = 0.4$, which indicates a secondary star burst. Gas accretion or a minor merger would produce a lower central metallicity, while a major merger would have reduced the very steep metallicity gradient of –0.72. In the detailed study of Proctor et al. (2005), NGC 821 is speculated to consume its own gas to fuel a secondary central burst of star formation.

The metallicity gradient of isolated galaxies are found to be steeper for less massive galaxies.

This result is consistent with a major merger history for the massive galaxies (e.g. Bekki & Shioya 1999). During the merger process, the high metallicity stars in the centre of the galaxy are transported to the outer regions which dilutes the metallicity gradient (Bekki & Shioya 1999). On the other hand, the induced star formation during the merger at the centre of the merger remnant is expected to maintain the metallicity gradient to some extent. The final metallicity gradient of the merger remnant is shallower than the progenitors and the newly formed central stars will also produce relatively steep age gradients for these galaxies (Kobayashi 2004). The gas-rich merger simulation of Bekki & Shioya (1999) predicts a one-to-one correlation between the age gradient and metallicity gradient. However, our isolated galaxies show a correlation of slope 0.6 ± 0.1.

Both isolated galaxies, and those in HDEs, show similar age-mass relations as more massive galaxies are older than smaller ones. That suggests either the less massive galaxies have had successive star formation events (bursts induced by mergers) continuing until recent epochs, while more massive galaxies did not suffer such events. Alternatively, all galaxies started forming their stars in a single burst (similar to a dissipative collapse) at the same epoch which stopped earlier in more massive galaxies, while less massive galaxies continue forming new stars for extended epochs. Several mechanisms have been introduced to suppress the star formation processes in more massive galaxies such as a central active galactic nuclei (e.g. Springel, Di Matteo & Hernquist 2005; De Lucia et al. 2006). The dependence of the star formation efficiency on the circular velocity of the galaxy can also delay the star formation in small galaxies relative to more massive galaxies (e.g. De Lucia, Kauffmann & White 2004).

The old galaxies in our sample (NGC 2271, ESO153-G003, ESO218-G002 and MCG-03-26-030) with central age ≥ 11 Gyrs show flat age gradients which indicates that all stars are formed at same time at $z \geq 2$. They also tend to be the most massive galaxies. This can be a result of a single burst of star formation during a rapid collapse of a single cloud (Larson 1974; 1975; Carlberg 1984). The observed metallicity gradient of these galaxies (< -0.28) is much less than the predicted gradients of the dissipative collapse models. The major merger scenario can explain the shallow metallicity gradients of these galaxies but not their uniform old populations. Another mechanism such as developing central active galactic nuclei (e.g. Springel, Di Matteo & Hernquist 2005; De Lucia et al. 2006 is necessary to stop any further star formation after the merger. The low metallicity of ESO153-G003 ($[\mathrm{Z/H}]_o = 0.19$) suggests progenitors of relatively small size for this galaxy. The galaxy NGC 2271 has the highest metallicity among these galaxies ($[\mathrm{Z/H}]_o = 0.44$) with a flat metallicity gradient of -0.05 ± 0.04. It also shows elongated shape ($\epsilon = 0.3$) and a solid body rotation (Fig. 4.3) with $(V/\sigma_o)^* = 1.45 \pm 0.12$ (Hau & Forbes 2006) which may indicate a massive disk progenitor.

The shallow metallicity gradients of the two galaxies NGC 682 and NGC 4240 indicate past major mergers. On the other hand, their uniform luminosity weighted intermediate ages suggest a very small fraction of induced star formation.

The magnitude of the metallicity gradients are found to correlate to the age gradient. The suggested mechanism causing these gradients is that each star formation event will enrich the ISM, followed by radial inflow, causing the subsequent stellar generations at the galaxy centre to be more metal-rich, as well as younger. A natural result of this process is the observed age-metallicity relation. The dynamical effect of supernova feedback is expected to be relatively weaker in more massive galaxies, consequently the star formation rate is more efficient in these galaxies than in less massive ones. The deep potential well of massive galaxies maintains their gas long enough to perform more complete chemical processes to produce higher metallicities (e.g. Arimoto & Yoshii 1987; Edmunds 1990; Matteucci 1994) resulting in the observed mass-metallicity relation.

Independent of the galaxy mass, or the details of the merging process, the observed correlation between the metallicity gradient and its central value can be reproduced by the gas-rich merger simulations of Bekki & Shioya (1999). The results of these models are also consistent with the observed insignificant gradients of [E/Fe] within 1 effective radius of the isolated galaxies.

The parameter $[E/Fe]_o$ measures the abundance ratio of the α-element to the Fe-peak elements which are predicted to be released to the interstellar medium by supernovae type II and Ia and on different time scales. In that sense, $[E/Fe]_o$ is commonly used to quantify the duration of star formation (Worthey, Faber & Gonzalez 1992; Matteucci 1994; Thomas, Greggio & Bender 1999; Thomas et al. 2005). For the isolated galaxies as well as in HDEs, the lower $[E/Fe]_o$ of the less massive galaxies points to extended star formation for these galaxies. However, the isolated early-type galaxies tend to have younger ages and lower $[E/Fe]_o$ for their central velocity dispersion than their counterparts in HDEs. Furthermore, we also note that isolated galaxies of intermediate ages tend to have lower $[E/Fe]_o$ than the galaxies in HDEs. This is expected if the extended star formation is triggered with recent mergers which have stopped in HDEs at higher redshifts but continue to recent epochs for galaxies in low density environments such as our isolated galaxies.

Chapter 5

Scaling relations of isolated early-type galaxies

This chapter is based upon Reda, Forbes & Hau 2005, MNRAS, 360, 693. The velocity dispersion measurements from Hau & Forbes (2006) are replaced by new measurements by the author from chapter 4.

5.1 Introduction

The effect of local environment on a galaxy's formation history and fundamental parameters has been the motivation for many studies. Environmental effects have been seen in galaxy scaling relations. For example, in a comparison study of early-type galaxies in the field, groups and rich clusters, de Carvalho & Djorgovski (1992) found that field galaxies showed more intrinsic scatter from their FP than those in clusters, especially when stellar population variables were included. In a study of 9000 early-type galaxies from the Sloan Digital Sky Survey, Bernardi et al. (2003b) found that the scatter from the FP correlates weakly with the galaxy local environment. The results of both de Carvalho & Djorgovski (1992) and Bernardi et al. (2003b) suggest a more extended formation epoch for galaxies in the field versus those in clusters. This is supported by studies that measure the luminosity-weighted age of galaxies in different environments (e.g. Terlevich & Forbes 2002; Proctor et al. 2004b). Interestingly, Evstigneeva, Reshetnikov & Sotnikova (2002) have reported no significant difference in the tilt and scatter of the fundamental plane for strongly interacting early-type galaxies.

Previous studies of the FP in different environments have not been extended to the very low densities of truly isolated galaxies. In such extreme low-density environments we can eliminate the effect of many physical processes, such as tidal interactions, ram-pressure stripping, strangulation, high-speed galaxy-galaxy interactions and ongoing mergers, all of which may affect the evolution of galaxies in denser environments.

The main aspect of this chapter is to investigate the FP for isolated galaxies and compare it with that for galaxies in higher density environments. Our photometric and kinematic parameters are supplemented by data from the literature. Based on the results of this study, we briefly discuss the implications for the formation of isolated early-type galaxies.

5.2 Data sources

5.2.1 The photometric parameters

In Chapter 3 (see also Reda et al. 2004 and 2005) the effective radii R_e and mean effective surface brightnesses $< \mu_e >$ are obtained for 18 galaxies of the sample. Additional data are taken from the photometric catalogue by Prugniel & Heraudeau (1998; PH98) which includes total B magnitudes and $< \mu_e >_B$ for 21 galaxies of our total sample. PH98 fit their data using a linear interpolation between the de Vaucouleurs ($R^{1/4}$) and exponential profiles. We calculate r_e for galaxies from PH98 using their B and $< \mu_e >_B$ values as:

$$\log(r_e) = (< \mu_e >_B - B - 5.885)/5 \tag{5.1}$$

To check any systematic differences between our measurements and PH98 for r_e and $< \mu_e >_B$, we have computed the quantity $\log(r_e) - 0.352 < \mu_e >_B$ for the 12 galaxies in common with our observations. This is the edge-on projection of the FP from Jørgensen, Franx & Kjaergaard (1993; JFK93). Fig. 5.1 shows this quantity for the 12 galaxies in common. The inset in Fig. 5.1 shows the distribution of the residuals of our measurements from the one-to-one relation. Our measurements show a slight systematic offset of 0.04 with small scatter of $1\sigma = 0.07$ which indicates good agreement. The final photometric parameters used in the present study are summarized in Table 5.1.

5.2.2 The kinematic parameters

In Chapter 4, the kinematical parameters of 12 galaxies are measured (see also Reda et al. 2007), and the previously detected kinematical substructures in Hau & Forbes (2006; HF06) are confirmed. The central velocity dispersion (σ_o) is obtained as the average of all apertures within 1/8 of the effective radius. The radial profile of the velocity dispersion (see Figures 4.4) show our galaxies to have nearly constant central velocity dispersion and normalization to a fixed physical diameter is not essential.

D05a measured σ_o for 8 early-type galaxies of our isolated sample. The galaxies were observed at the 2.12-m telescope of *The Observatorio Astrofísico Guillermo Haro*, in Cananea, Mexico. On average, they have eight observations for each galaxy in their study. These

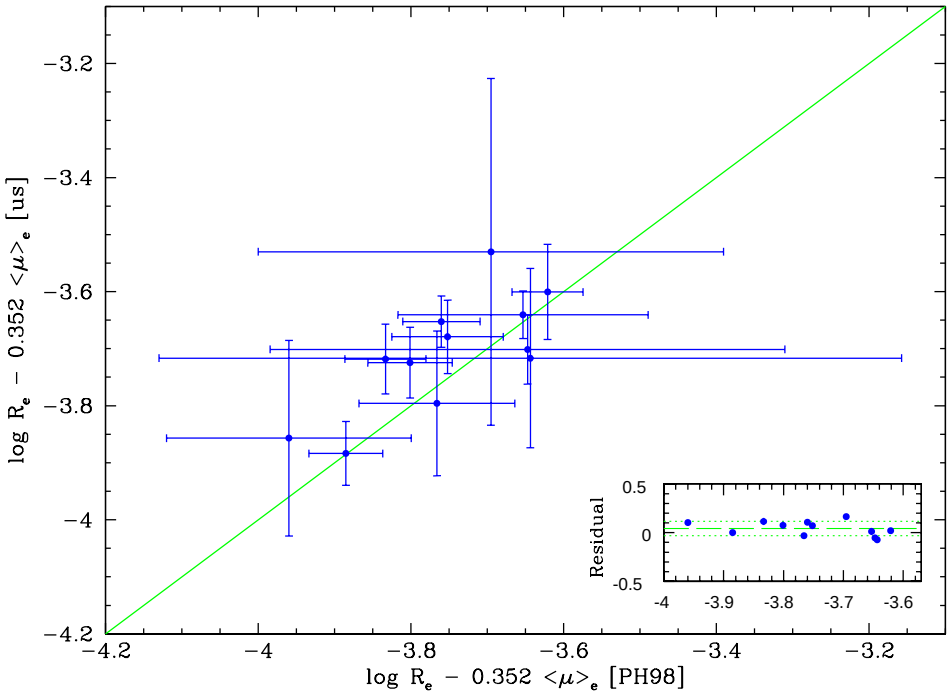

Figure 5.1: Comparison of our measurements of r_e and $< \mu_e >_B$ and those of Prugniel & Heraudeau (1998; PH98), using the edge-on projection of the fundamental plane from Jørgensen, Franx & Kjaergaard (1993). The solid line is the one-to-one relation. The inset shows the distribution of the residuals of our measurements from the one-to-one relation. The long-dashed line is the mean value of the residuals and the dotted lines represent the 1σ dispersion. The common measurements are consistent within the errors.

repeated observations per galaxy, and the deviation from the mean value, give an error on the mean velocity dispersion quoted. Their velocity dispersion (σ_o) measurements were then normalised to a diameter of $3.4''$ for a galaxy at the distance of Coma using the method of Jorgensen, Franx & Kjaergaard (1995; JFK95).

Another source of internal kinematics for our galaxy sample is Prugniel & Simien (1996; PS96). In this catalogue, Prugniel & Simien compiled central velocity dispersions of 1698 galaxies from 3147 measurements. To homogenise the data that they collected from different literature sources, they identified a set of galaxies that have measurements from three or more references with deviations of 20 km/s or less. Using this list of "standard" galaxies, a scale factor was determined for each source and used to scale the velocity dispersion measurements for that source. Then, σ_o values were computed as the mean of the re-scaled measured velocity dispersion, weighted by the inverse of the squared mean error for each source. Errors in the PS96 catalogue are 1σ rms from the mean value.

The σ_o values quoted in PS96 were not normalized to the aperture size as in D05a. In JFK95, they applied the aperture normalization technique to 220 galaxies in a range of environments. Their sample has 35 galaxies in common (after excluding galaxies with low S/N ratio) with the sample of PS96. Using the σ_o measurements of these common galaxies

Table 5.1: Photometric and spectroscopic properties of the sample.

Galaxy	M_B (mag)	$< \mu_e >_B$ (mag/sq.″)	±	log(r_e) (pc)	±	Photo source	log(σ) (km/s)	±	σ source
NGC 0821	-20.5	21.6	0.03	3.70	0.03	PH98	2.33	0.06	D05a
NGC 1045	-20.9	20.8	0.10	3.66	0.10	Ch3	2.42	0.01	T4.4
NGC 1132	-21.8	22.5	0.10	4.12	0.05	Ch3	2.38	0.05	D05a
NGC 1162	-20.7	21.0	0.05	3.62	0.05	PH98	2.29	0.01	T4.4
NGC 2110	-20.0	20.7	0.10	3.59	0.02	Ch3	2.40	0.01	HF06
NGC 2271	-20.0	20.9	0.06	3.47	0.07	PH98	2.37	0.01	T4.4
NGC 2865	-20.7	20.8	0.10	3.68	0.01	Ch3	2.25	0.02	T4.4
NGC 3562	-21.8	21.8	0.09	4.02	0.07	PH98	2.43	0.02	PS96
NGC 6172	-20.4	20.8	0.10	3.61	0.06	Ch3	2.13	0.04	D05a
NGC 6411	-21.2	21.9	0.12	3.90	0.04	PH98	2.25	0.03	D05a
NGC 6653	-21.1	21.6	0.10	3.92	0.02	ESO	2.34	0.04	PS96
NGC 6702	-21.5	22.3	0.05	4.04	0.04	PH98	2.24	0.01	PS96
NGC 6776	-21.7	21.1	0.10	3.90	0.11	ESO	2.32	0.03	PS96
NGC 6799	-21.1	21.3	0.10	3.77	0.02	ESO	2.18	0.02	PS96
NGC 6849	-21.6	22.2	0.10	4.16	0.01	ESO	2.33	0.01	PS96
NGC 7796	-21.0	21.1	0.10	3.71	0.02	ESO	2.41	0.02	PS96
IC 1211	-21.0	21.9	0.03	3.88	0.06	PH98	2.29	0.03	PS96
ESO107-G004	-20.4	21.4	0.20	3.68	0.06	ESO	2.24	0.11	PS96
ESO153-G003	-20.9	20.6	0.10	3.62	0.06	ESO	2.34	0.01	T4.4
ESO194-G021	-19.7	21.0	0.10	3.47	0.02	ESO	-	-	-
ESO218-G002	-20.9	21.5	0.10	3.76	0.11	Ch3	2.43	0.01	T4.4
ESO318-G021	-20.7	21.7	0.04	3.77	0.01	PH98	2.37	0.01	T4.4
ESO462-G015	-22.0	21.3	0.20	3.90	0.02	ESO	2.38	0.09	D05a
MCG-01-27-013	-21.4	22.0	0.10	3.98	0.05	Ch3	2.39	0.01	T4.4
MCG-01-03-018	-21.0	22.3	0.10	3.96	0.01	ESO	2.28	0.03	D05a
MCG-03-26-030	-21.7	21.4	0.10	3.92	0.02	Ch3	2.47	0.01	T4.4

Notes: The adopted data for the fundamental plane study. The sources of the photometric parameters are Tables 3.3 and 3.4 (Ch3) and Prugniel & Heraudeau (1998; PH98). Sources for the velocity dispersion are Table 4.4 (T4.4), Hau & Forbes (2006; HF06) and Prugniel & Simien (1996; PS96). The galaxy ESO194-G021 does not have available velocity dispersion.

from JFK95 ($\sigma_{o[JFK95]}$) and PS96 ($\sigma_{o[PS96]}$), we obtained the transformation:

$$\log(\sigma_{o[JFK95]}) = -0.11 + 1.04 \times \log(\sigma_{o[PS96]}) \tag{5.2}$$

which is used to convert the σ values from PS96 to be consistent with those of D05a. These 35 galaxies cover the redshift range from $cz \approx 750$ km/s to 6500 km/s, which encompasses the range for our isolated galaxy sample. Any redshift-dependent aperture effect on the σ_o values is less than the dispersion of ± 10 km/s about the one-to-one line shown in Fig. 5.2. The inset in Fig. 5.2 shows the distribution of the residuals of the corrected PS96 measurements from the one-to-one relation. The mean value of the residuals show a slight systematic offset of 0.0003 from the one-to-one relation with small scatter of $1\sigma = 0.022$ which indicates good agreement.

The catalogue of PS96 contains velocity dispersions for 18 galaxies of our sample. For the

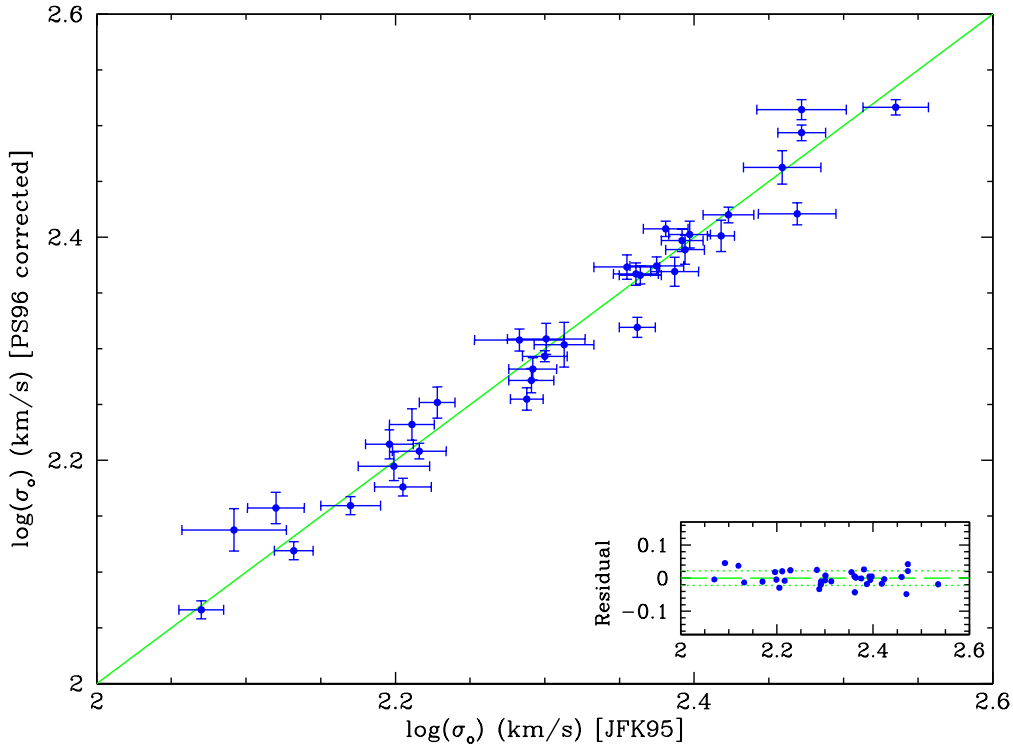

Figure 5.2: Comparison between the velocity dispersion values of 35 galaxies from Prugniel & Simien (1996; PS96) and values from (Jorgensen, Franx & Kjaergaard 1995; JFK95) after applying the transformation $\sigma_{o[JFK95]} = -0.11 + 1.04 \times \sigma_{o[PS96]}$. The solid line is the one-to-one relation. The inset shows the distribution of the residuals as in Fig. 5.1. Good agreement is seen.

common galaxies between PS96 and ours (5 galaxies) and D05a (4 galaxies), we use our values and values from D05a. Fig. 5.3 shows a comparison between our values of σ_o and values from D05a with those from PS96 for the 8 galaxies in common. For the galaxy NGC 2271, we use the velocity dispersion from Koprolin & Zeilinger (2000) who quote a similar value to ours.

The most deviant galaxy in Fig. 5.3 is the galaxy ESO318-G021 which has a velocity dispersion from PS96 ($\log \sigma_o = 2.17$) that is significantly smaller than our measurement ($\log(\sigma_o) = 2.37$) and that of HF06 ($\log(\sigma_o) = 2.39$). We have examined the possible cause for this discrepancy and suggest it is largely due to a mismatch of the template standard star. In the subsequent analysis we adopt our value velocity dispersion for ESO318-G021 (Table 4.4). Considering all 9 galaxies in Fig. 5.3, the inset shows a mean value of the residuals from the one-to-one line of 0.04 with a scatter of $1\sigma = 0.08$.

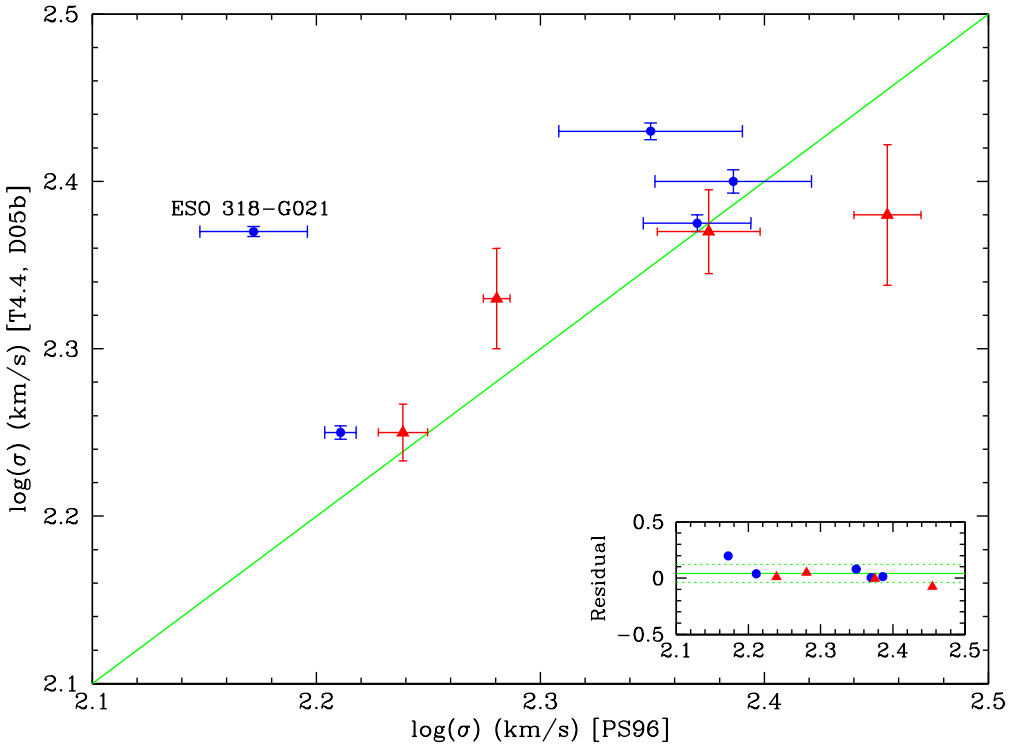

Figure 5.3: Comparison between the velocity dispersion values from Table 4.4 (T4.4) shown as solid circles and Denicoló et al. (2005b; D05b) shown as solid triangles with those of Prugniel & Simien (1996; PS96). For NGC 2271 we use the value quoted in Koprolin & Zeilinger (2000). The solid line is the one-to-one relation. The inset shows the distribution of the residuals as in Fig. 5.1. Reasonable agreement is seen, except for ESO318-G021 (see text for details).

5.3 The fundamental plane in $\log(r_e)$, $< \mu >_e$ and $\log(\sigma)$ space

JFK93 used their imaging observations in the Johnson B and Gunn r-bands, and the central velocity dispersion measurements from Faber et al. (1989) and Dressler (1987), for 33 early-type galaxies in the Coma cluster to compute the FP tilt and scatter. In the B-band, they found a FP of the form:

$$\log(r_e) = 1.203\ \log(\sigma) + 0.352 < \mu >_e - 6.642 \tag{5.3}$$

where r_e values are in pc, and the intrinsic scatter is 0.027 dex. In Fig. 5.4, we show the edge-on projection of the FP for our isolated early-type galaxies using the parameters of JFK93. The solid line is the FP of the Coma cluster galaxies (Eq. 5.3). Considering a typical observational error in our data of 0.05, 0.1 and 0.05 in $\log(r_e)$, $< \mu >_B$ and $\log(\sigma_o)$ respectively and the intrinsic scatter of Coma galaxies, the 1σ scatter of the FP is shown in Fig. 5.4. Our galaxies show a similar tilt and scatter as the Coma cluster galaxies, except for the four galaxies NGC 2865, NGC 6172, NGC 6776 and NGC 6799 which deviate strongly from the FP. The 3 former galaxies are 'young' galaxies of age less than 3.2 Gyrs (Table 4.4;

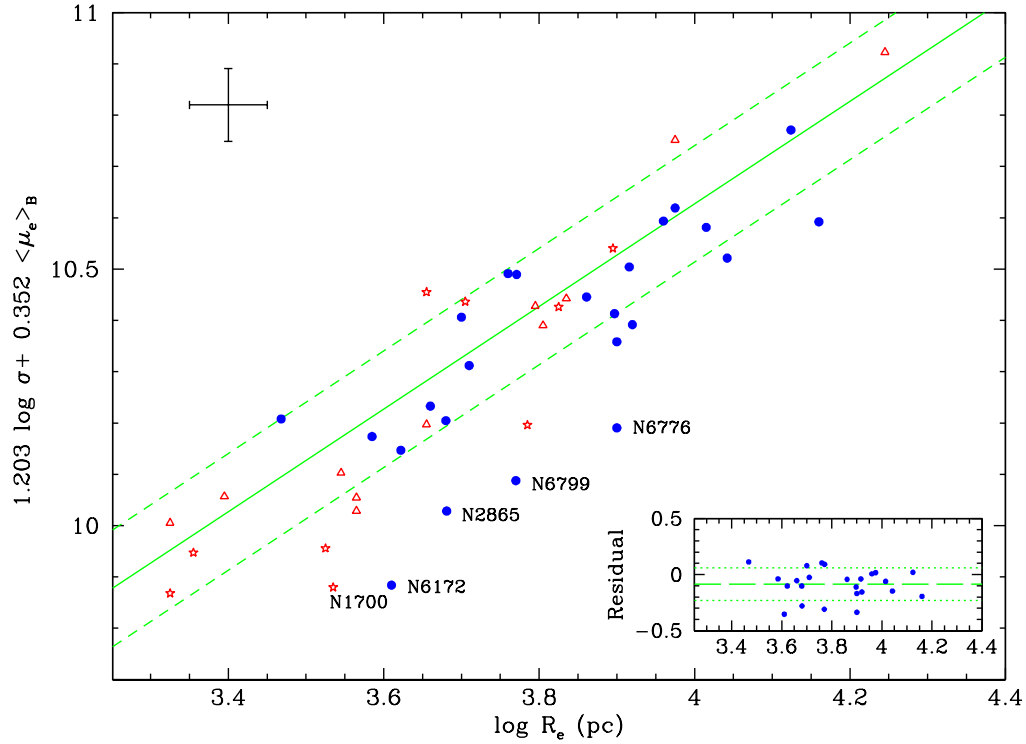

Figure 5.4: The edge-on view of the fundamental plane for the isolated galaxies in Table 4.1. The solid line is the fundamental plane of galaxies in Coma cluster from Jørgensen, Franx & Kjaergaard (1993). The short-dashed lines represent the 1σ dispersion of galaxies in Coma cluster from the same reference. Filled circles are our isolated galaxies in Table 2. Open triangles are galaxies in Hickson Compact Groups and stars are galaxies in the field or loose groups (de la Rosa, de Carvalho & Zepf 2001). Galaxies NGC 2865, NGC 6172, NGC 6776 and NGC 6799 are the most deviant isolated galaxies from the FP and have young ages. The young loose group galaxy NGC 1700 also deviates from the FP. A typical error bar is shown. The inset shows the distribution of the residuals as in Fig. 5.1. The majority (15/23) of our isolated galaxies show negative residuals.

TF02; D05b), while NGC 6799 has no published age. We note that such ages are luminosity-weighted central ages based on Lick absorption lines and single stellar population models to break the age-metallicity degeneracy. Such ages should not be considered absolute but rather relative ages. Several other caveats about the application of Lick-style ages to galaxy populations are discussed in Terlevich & Forbes (2002).

Considering the all 23 isolated galaxies in Fig. 5.4, their residuals from the FP of the Coma cluster show a mean offset of –0.08 and a 1σ dispersion of ~ 0.15 (see inset of Fig. 5.4). About two thirds (15/23) of our isolated galaxies show negative residuals.

From de la Rosa, de Carvalho & Zepf (2001), we take data for 12 elliptical galaxies in Hickson Compact Groups and 7 galaxies in the field or loose groups as a comparison sample. These galaxies cover the same range of r_e, $<\mu>_e$ and σ as our galaxies. We have excluded galaxies with spectra of S/N < 45. We also excluded NGC 4552 which was reported by Caon, Capaccioli & Rampazzo (1990) as a tidally distorted elliptical galaxy with an odd luminosity profile. We find that the sample of de la Rosa et al. also follows a FP similar to that of the Coma cluster ellipticals and the isolated galaxies (Fig. 5.4). The only exception

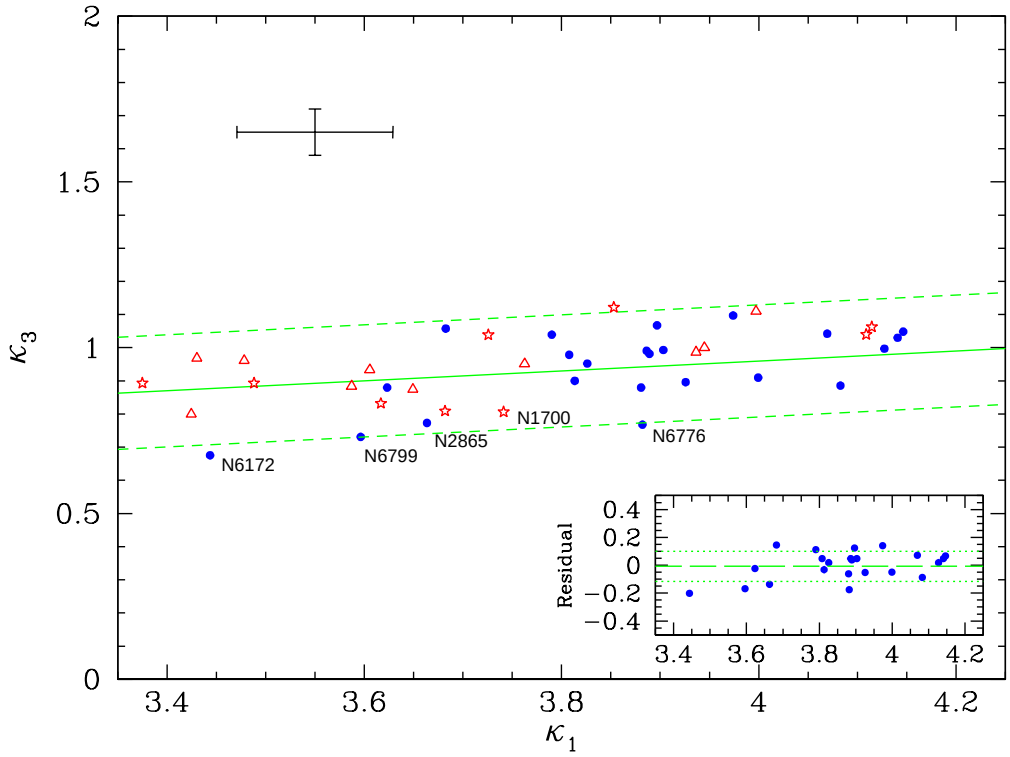

Figure 5.5: The edge-on view of the FP of the isolated galaxies in the κ_1-κ_3 space. Filled circles are our isolated sample. The solid line is the FP for Virgo cluster galaxies from Bender, Burstein & Faber (1992). The short-dashed lines represent the typical observational errors added to the 1σ intrinsic scatter of 0.05 in κ_3 for Virgo cluster galaxies (Nipoti, Londrillo & Ciotti 2003). Solid circles are the isolated galaxies. Open triangles are galaxies in Hickson Compact Groups and stars are galaxies in the field or loose groups (de la Rosa et al. 2001). The highly deviant galaxies from the FP in Fig. 7 show a tendency to have smaller κ_3 values than the average. A typical error bar is shown. The inset shows the distribution of the residuals as in Fig. 5.1.

is NGC 1700 which is also a young galaxy of age ≈ 2 Gyrs (TF02).

5.4 The fundamental plane in κ-space

By a simple orthogonal coordinate transformation (i.e., a rotation), Bender, Burstein & Faber (1992) introduced a different expression for the FP in terms of kappa (κ) space. The axes of this coordinate system are directly proportional to the galaxies physical parameters and defined as.

$$\kappa_1 = \frac{2\ \log(\sigma) + \log(r_e)}{\sqrt{2}} \tag{5.4}$$

$$\kappa_2 = \frac{2\ \log(\sigma) + 2\ \log(I_e) - \log(r_e)}{\sqrt{6}} \tag{5.5}$$

$$\kappa_3 = \frac{2\ \log(\sigma) - \log(I_e) - \log(r_e)}{\sqrt{3}} \tag{5.6}$$

The edge-on view of the FP is represented by κ_1 and κ_3, where κ_1 is a measure of the galaxy mass ($\log(M)$) and κ_3 is related to the M/L ratio.

In Fig. 5.5 we show the distribution of our isolated galaxies in the κ_1-κ_3 space. They show a similar tilt and dispersion to those of Virgo cluster galaxies from Bender, Burstein & Faber (1992). The 5 galaxies that show a strong deviation from the FP in Fig. 5.4, also show a tendency to have smaller κ_3 values i.e. smaller M/L ratio as expected for their young ages. The residuals of the isolated galaxies show a mean value of about –0.01 with 1σ dispersion of ~ 0.11 (see inset of Fig. 5.5) which indicates a good symmetry of our isolated galaxies about the FP of the Coma cluster in the κ space.

5.5 The $< \mu_e >_B$-r_e relation

In Fig. 5.6, we show the projection of the FP in the plane of the mean surface brightness within the effective radius $< \mu_e >_B$ and effective radius r_e in the B-band. The solid line represents the Hamabe & Kormendy (1987) relation

$$\mu_e(V) = 2.94 \log(r_e) + 19.48 \tag{5.7}$$

shifted from V to the B-band assuming typical colours of $B-V = 0.9$. We also transformed the surface brightness (μ_e) at r_e to $< \mu_e >$ using the relation of Graham & Colless (1997). Our isolated galaxies are generally consistent with the Hamabe & Kormendy relation for luminous galaxies. In the figure we also show the galaxies in the field and group sample of de la Rosa et al. (2001) which also show good consistency with the original relation. We note that, while the two galaxies NGC 6172 and NGC 6799 lie on the relation, the two isolated galaxies NGC 2865 and NGC 6776 and the group galaxy NGC 1700 show significant deviations.

In the inset in Fig. 5.6 we show the distribution of the residual of our isolated galaxies from the Hamabe & Kormendy relation. The mean values of the residuals show a slight negative offset of about –0.05 and 1σ dispersion of 0.32.

5.6 Discussion

In Figures 5.4 and 5.5 we have compared the FP for our isolated early-type galaxy sample with that for galaxies in higher density environments. We find that galaxies in a wide range of environments are consistent with the same FP of similar tilt and scatter. In Fig. 5.4, the four galaxies NGC 2865, NGC 6172, NGC 6776 and NGC 6799 of our isolated sample and the group galaxy NGC 1700 of de la Rosa, de Carvalho & Zepf (2001) deviate strongly

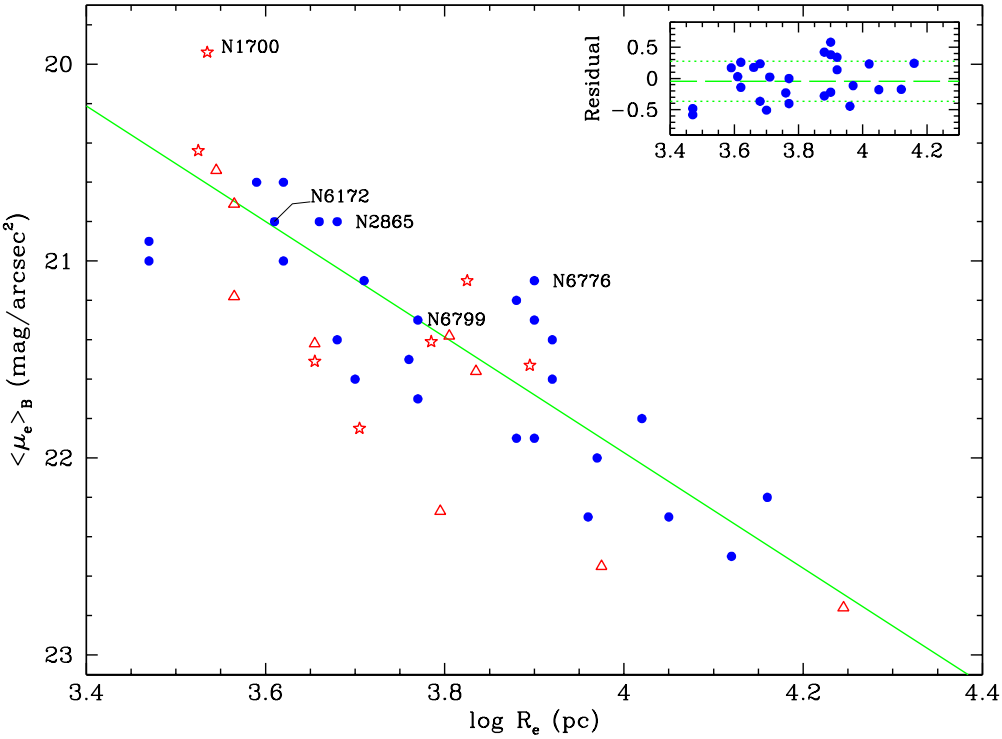

Figure 5.6: The projection of the FP in the plane of the mean surface brightness within the effective radius $< \mu_e >_B$ and effective radius r_e in the B. The solid line represents the Hamabe & Kormendy (1987) relation. The zero-point of the original relation has been shifted from V to the B-band assuming typical colours of $B - V = 0.9$. Symbols as in Fig. 7. The inset shows the distribution of the residuals as in Fig. 5.1. Our isolated galaxies are generally consistent with the Hamabe & Kormendy relation for luminous galaxies.

from the main trend of the FP. In Fig. 5.5, the same five galaxies show a tendency to have smaller κ_3 in the direction of lower M/L ratios which can be explained by the young age of their stellar population.

We note that the isolated galaxies NGC 2865 and NGC 6776 and the group galaxy NGC 1700 also deviate from the $< \mu_e >_B$-r_e relation (Fig. 5.6). This indicates either a relatively large effective radius or high surface brightness. The isolated galaxies NGC 6172 and NGC 6799 lie on the Kormendy relation. The deviation of these two galaxies from the FP can be accounted for by their small velocity dispersions which are about 75 per cent of the expected values for their luminosities (Forbes & Ponman 1999).

The relative mean age of our galaxy sample can be estimated using the values quoted in TF02 and D05b. In their catalogues, the authors used Hβ and [MgFe] absorption line indices to break the age/metalicity degeneracy. These ages reflect the young stars the central regions which were presumably formed during the last gaseous merger event. Therefore, the measured ages of these stellar populations give an estimate of the time elapsed since the last gaseous merger. Twelve galaxies (out of 23) of our sample have available published ages. The mean age of these galaxies is 4.6 $\pm$1.4 Gyr, which is approximately similar to the mean age quoted by Proctor et al. (2004b) for galaxies in small groups and field (5.9 ± 0.7 Gyr)

but younger than galaxies in cluster environments ($> 8.5 \pm 0.7$ Gyr).

In Fig. 5.4, we note that the most deviant galaxies from the FP are the 4 youngest galaxies of our sample with ages $\lesssim 3$ Gyr. NGC 2865 has a relatively blue colour of $B-R = 1.3$ (Table 3.2) and reveals many fine structures such as shells, tidal light, dust and a kinematically distinct core (Chapter 3; Hau, Carter & Balcells 1999) which implies a past merger involving at least one gas-rich progenitor. In Chapter 4 we measured an age of 1.7 Gyr for NGC 2865 which is comparable to that of Hau, Carter & Balcells (1999) who quoted an age estimate of ~ 1.1 Gyr since the last merger, and the < 1.5 Gyr estimated by TF02.

NGC 6776 has a tidal tail, shells and extensive extra tidal light. The tidal tail suggests at least one of the progenitors was a disk galaxy. In a detailed photometric and spectroscopic study of NGC 6776, Sansom, Reid & Boisson (1988) measured a rapid rotation of ≈ 100 km/s and a velocity dispersion of ≈ 200 km/s. They detected no dust or young stars which led them to conclude that the merger occurred $\geqslant 1$ Gyr ago. TF02 measured an age of 3.2 Gyr for its stellar population.

While the residual image of NGC 6172 (Fig. 3.4) did not reveal any obvious features, the unsharp-masking and colour map by Colbert, Mulchaey & Zabludoff (2001) revealed a weak shell and some dust near the centre of the galaxy. Its global blue colour ($B-R = 1.3$; Table 3.2) and the young age of 1.8 Gyr (D05b) suggest a recent starburst induced by a merger.

NGC 6799 has a large dust lane along its eastern edge (Colbert, Mulchaey & Zabludoff 2001). The residuals from the FP, using the method of PS96, is -0.37 which suggests the presence of a young stellar population of age $\lesssim 1.5$ Gyr (Forbes, Ponman & Brown 1998). This evidence supports the suggestion of a merger past for NGC 6799.

Despite the young age of 2.6 and 5.4 Gyr for NGC 1045 (note that we measured 10.4 Gyr in Chapter 5) and ESO462-G015 respectively (D05b), and the tidal tail that was detected in NGC 1045 (Fig. 3.4) indicating a recent merger, they both lie within 1σ of the FP.

The two galaxies NGC 6849 and MCG-01-03-018, have very old ages (TF02; D05b). The old age for their central stellar populations and the absence of fine structures suggests that there has not been a gaseous merger in the recent past for these two galaxies.

The galaxy NGC 1132 reveals an extended group-like X-ray structure. This lead Mulchaey & Zabludoff (1999) to speculate that this galaxy was a remnant of a merged group of galaxies (a fossil). The absence of fine structure and an old central stellar population (D05b) suggests that it formed at early epochs and has not accreted any gas-rich galaxies recently.

Numerical simulations show that dissipational mergers between two disk, star-forming and gas-rich galaxies can produce non-homologous galaxies reproducing the observed tilt and scatter of the FP (Bekki 1998). Dissipationless mergers can also reproduce the FP (Hjorth & Madsen 1995; Capelato, de Carvalho & Carlberg 1995; Levine 1997; Dantas et al. 2003; Nipoti, Londrillo & Ciotti 2003). However, as Nipoti, Londrillo & Ciotti (2003) point out,

dissipationless merging has difficulty explaining other scaling relations such as the colour-magnitude and black hole mass-σ relations. Unlike major mergers, neither accretion of smaller galaxies or a simple monolithic collapse are plausible scenarios to reproduce the FP (Dantas et al. 2003; Nipoti, Londrillo & Ciotti 2003), however more realistic collapse conditions need to be explored.

An equal-mass merger of two massive galaxies would be expected to lie on the Kormendy (1977) relation (Evstigneeva et al. 2004) as we have seen in Fig. 5.6. If the elliptical galaxy was initially located on the $< \mu_e >_B$-r_e relation, then the accretion of small dwarfs will not have a strong effect on its size nor on its overall luminosity.

Chapter 6

Conclusions and future work

6.1 Conclusions

This thesis represents a contribution to the outstanding debate regarding the formation and evolution of elliptical galaxies. The majority of these galaxies are found in high density environments such as groups or clusters. Elliptical galaxies in low density environments are rare but hold important clues about galaxy formation and evolution. We introduce a sample of 36 highly isolated elliptical galaxies as candidates for this study. These galaxies are required to be at least 2 B-band magnitudes brighter than the next brightest galaxy within 0.67 Mpc in the plane of the sky and recession velocity of 700 km s^{-1}.

This study investigates the luminosity, colour, morphology, kinematics and stellar population of subsamples of our isolated elliptical galaxy sample. Satellite galaxies in the field of several galaxies are also detected and used to quantify the environmental effect on the primary galaxy. Results are compared to the predictions of the competing models of galaxy formation and evolution which are discussed to determine the most probable formation scenario of elliptical galaxies.

Here we present wide-field imaging for 20 isolated elliptical galaxies. We also include imaging of four group galaxies and an isolated galaxy pair for comparison. Our images cover a field-of-view of about 30.6×30.6 arcmin, corresponding to an area of hundreds of square kiloparsecs surrounding each galaxy. From our CCD images we confirm the early-type morphology of each of our sample galaxies.

A mean effective colour of $(B–R)_e = 1.54 \pm 0.14$ is measured for our isolated galaxies which is similar to the colour of early-type galaxies in denser environments. Also, they are consistent with the slope and scatter of the colour-magnitude relation for Coma cluster galaxies. This result suggests an early formation epoch for the bulk of stars in our isolated and group galaxies at $z > 2$ (10.3 Gyrs ago in the ΛCDM cosmology). The scatter in this relation is explained as a result of a secondary starburst, resulting from a gaseous merger at a later

epoch.

However, there are also some morphological fine structures indicating recent merger/accretion events. The radial profile of the isophotal parameters, as well as the model-subtracted images reveal some fine structures such as plumes, dust, shells, discy and boxy structures in several isolated galaxies. About 60 per cent (11 galaxies) of our isolated galaxies revealed evidence of past mergers such as shells, dust, plumes, discy and boxy structures. Four of these eleven galaxies are the youngest members of our sample with ages $\lesssim 3$ Gyrs.

The distribution of these different morphological features in our isolated galaxies is similar to that of luminous early-type galaxies in loose groups and clusters, suggesting a similar frequency of mergers and interactions.

We also briefly discuss possible formation scenarios for isolated galaxies. We conclude that the major merger of two massive galaxies could explain several of our sample galaxies. An alternative scenario of a collapsed poor group of a few galaxies is also possible, specifically to explain the observed high central density of dwarfs in the field of the isolated galaxy. The collapse of a large, virialized group does not appear to explain the most of our isolated galaxies. Mergers of many gaseous fragments or the accretion of several dwarfs by a large elliptical galaxy would not give rise to the observed fine structures seen in some of our isolated galaxies.

We also present the fundamental plane for our sample of isolated elliptical galaxies. It shows a similar tilt and scatter to that for galaxies in denser environments. However some galaxies deviate from the relation due to the young age of their stellar populations or lower velocity dispersions. These young galaxies also show a tendency to have smaller mass-to-light ratios in κ-space. The distribution of these galaxies in the $< \mu_e >_B$-R_e projection is consistent with this interpretation.

Elliptical galaxies in such isolated environments show a relatively young mean age which is similar to that of galaxies in the field and small groups, but is younger than that for galaxies in clusters and Hickson Compact Groups. This result is qualitatively consistent with the expectations of hierarchical galaxy formation.

Long slit spectra along the semi-major axis of the galaxy were used to explore the kinematic substructure and spatial distribution of the stellar populations in twelve isolated ellipticals. Highly rotating disks in the core, fast rotating outer parts and centrally peaked velocity dispersion profiles are detected in several galaxies. This evidence suggests a merger event in the past of these galaxies.

Regarding the stellar population parameters, isolated galaxies show a wide range of ages, metallicities and α-elements abundance in their central stellar populations. More massive galaxies tend to be older, more metal-rich and more α-element enhanced than less massive galaxies in the same sense as galaxies in high density environments. Although isolated galaxies tend to be slightly younger, more metal-rich and have lower α-elements abundance

for their mass.

The majority of the isolated galaxies in our sample show insignificant gradients of both age and α-elements abundance. Although a correlation between the age gradient and central age indicates the tendency for the newly formed stars to be located closer to the galaxy centre. The metallicity gradients range from very steep to flat. Metallicity gradients are found to correlate with parameters of the central stellar populations such as central metallicity, age and velocity dispersions. Metallicity gradients also show a remarkable correlation with the age gradients.

From these results we conclude that mergers at different redshifts, of progenitors of different mass ratios and gas fractions, are needed to reproduce the observed properties of these galaxies. However, for other isolated galaxies, which show neither fine structure nor young stellar populations, we speculate that they formed at early epochs and have evolved passively thereafter.

6.2 Future work

This thesis has presented the stellar population, photometric and kinematical properties of a number of isolated elliptical galaxies. These galaxies are a subsample of the original list of 36 galaxies which are identified as highly isolated galaxies in the local Universe. Imaging and spectroscopic observations of the other galaxies of the sample will add more details to our understanding of the formation and evolution of these unique objects and also quantify the environmental effects on the evolution of their counterparts in the environments of higher densities.

In Sec. 3.5.6 we show that for 10 of our isolated ellipticals, the magnitude difference between the isolated galaxy and the second brightest galaxy in its environment is comparable to those of fossil groups ($R_{12} \geq 2$ mag). Our isolated galaxies also have magnitudes which are comparable to the total magnitude of loose groups. These two facts suggest that these isolated galaxies could be a merged remnant of a previous loose group. The presence of an extended X-ray halo around isolated galaxies will be a fossil evidence of the suggested merged group. The number of our isolated ellipticals with available X-ray data is very limited and further observations of the entire sample (e.g. with the XMM satellite) will help to determine the merger history of these galaxies.

Determining the actual number and dynamics of dwarf satellite galaxies in the field of the isolated galaxies are important for at least two reasons. First, these dwarf galaxies provide an observable tracer of the outer regions of the dark matter halo which is hosting the isolated galaxy. The velocity dispersion of these dwarfs is required to determine the mass of the host halo (e.g. Gill et al. 2004). Second, despite the general success of the standard ΛCDM paradigm in explaining many observed features of the Universe, this theory predicts about

two orders of magnitude more satellite galaxies orbiting their host haloes than are observed (e.g. Moore et al. 1999). Therefore, spectroscopic observations of the detected satellites in the field of our isolated ellipticals is essential to identify the genuine dwarf satellites.

In the present work, we detected the satellite galaxies in the field of 10 isolated galaxies of our sample. Due to the importance of these dwarfs in understanding the formation and evolution of the primary galaxy and also the hosting dark matter halo, further wide field imaging for the other galaxies of our sample is required.

Identifying a sample of highly isolated early-type galaxies at high redshift will help determine if these galaxies are the earlier progenitors of our sample, or isolated galaxies in the local Universe were formed by very recent merger/accretion events. Previous attempts to define galaxies in low density environments at high redshift such as those of Bernardi et al. (2003a; 2006) are useful. However, their selection criterion are not strict enough to provide the required isolation condition to match our sample in the local universe. Isolated galaxies are like gems, although rare, worthy of additional mining...

Bibliography

Aars C. E., Marcum P. M., Fanelli M. N., 2001, AJ, 122, 2923
Aceves H., Velázquez H., 2005, MNRAS, 360, L50
Adams M. T., Jensen E. B., Stocke J. T., 1980, AJ, 85, 1010
Aguilar L. A., Merritt D., 1990, ApJ, 354, 33
Amendola L., Di Nella H., Montuori M., Sylos Labini F., 1997, Fractals, 5, 635
Aragon-Salamanca A., Ellis R. S., Couch W. J., Carter D., 1993, MNRAS, 262, 764
Arimoto N., 1988, uglr.work, 43
Arimoto N., Yoshii Y., 1987, A&A, 173, 23
Arnold V. I., Avez A., 1968, Ergodic Problems in Classical Mechanics, New York, Benjamin
Arp H., 1966a, ApJS, 14, 1
Arp H., 1966b, Atlas of peculiar galaxies, California Institute of Technology, Pasadena, California 91109
Arp H. C., Madore B. F., 1987, A Catalogue of Southern Peculiar Galaxies and Associations. Cambridge Univ. Press, Cambridge
Baade W., 1944, ApJ, 100, 137
Balcells M., 1997, ApJ, 486, L87
Balcells M., Quinn P. J., 1990, ApJ, 361, 381
Balogh M. L., Morris S. L., 2000, MNRAS, 318, 703
Barbuy B., Renzini A., Ortolani S., Bica E., Guarnieri M. D., 1999, A&A, 341, 539
Barnes J. E., 1989, Natur, 338, 123
Barnes J. E., 2004, MNRAS, 350, 798
Barnes J. E., Hernquist L., 1992, ARA&A, 30, 705
Baum W. A., 1959, PASP, 71, 106
Bekki K., 1998, ApJ, 496, 713
Bekki K., Shioya Y., 1997, ApJ, 478, L17
Bekki K., Shioya Y., 1999, ApJ, 513, 108
Bender R., 1988, A&A, 193, L7
Bender R., Burstein D., Faber S. M., 1992, ApJ, 399, 462
Bender R., Doebereiner S., Moellenhoff C., 1988, A&AS, 74, 385
Bender R., Moellenhoff C., 1987, A&A, 177, 71
Bender R., Saglia R. P., 1999, ASPC, 182, 113
Bender R., Surma P., Doebereiner S., Moellenhoff C., Madejsky R., 1989, A&A, 217, 35
Bernardi M., Renzini A., da Costa L. N., Wegner G., Alonso M. V., Pellegrini P. S., Rité C., Willmer C. N. A., 1998, ApJ, 508, L143
Bernardi M., et al., 2003a, AJ, 125, 1817
Bernardi M., et al., 2003b, AJ, 125, 1849
Bernardi M., et al., 2003c, AJ, 125, 1866
Bernardi M., et al., 2003d, AJ, 125, 1882
Bernardi M., Nichol R. C., Sheth R. K., Miller C. J., Brinkmann J., 2006, AJ, 131, 1288
Bertin E., Arnouts S., 1996, A&AS, 117, 393

Binette L., Magris C. G., Stasinska G., Bruzual A. G., 1994, A&A, 292, 13
Binney J., 1978, MNRAS, 183, 501
Binney J., Merrifield M., 1998, Galactic astronomy, Princeton University Press, Princeton, NJ
Binney J., Petrou M., 1985, MNRAS, 214, 449
Binney J., Tremaine S., 1987, Galactic Dynamics. Princeton Univ. Press, Princeton, NJ
Blanton M. R., et al., 2001, AJ, 121, 2358
Blanton M. R., et al., 2003, ApJ, 592, 819
Blumenthal G. R., Faber S. M., Primack J. R., Rees M. J., 1984, Natur, 311, 517
Bono G., Caputo F., Cassisi S., Castellani V., Marconi M., 1997, ApJ, 489, 822
Bower R. G., Kodama T., Terlevich A., 1998, MNRAS, 299, 1193
Bower R. G., Lucey J. R., Ellis R. S., 1992, MNRAS, 254, 601
Boylan-Kolchin M., Ma C.-P., Quataert E., 2005, MNRAS, 362, 184
Boylan-Kolchin M., Ma C.-P., Quataert E., 2006, MNRAS, 369, 1081
Brough S., Proctor R.N, Forbes D. A., Couch W. J., Collins C. A., Burke D. J., Mann R. G., 2007, MNRAS, submitted
Bradt H. V., Burke B. F., Canizares C. R., Greenfield P. E., Kelley R. L., McClintock J. E., Koski A. T., van Paradijs J., 1978, ApJ, 226, L111
Bregman J. N., Hogg D. E., Roberts M. S., 1992, ApJ, 387, 484
Bressan A., Chiosi C., Tantalo R., 1996, A&A, 311, 425
Burkert A., Naab T., 2005, MNRAS, 363, 597
Burstein D., Faber S. M., Gaskell C. M., Krumm N., 1984, ApJ, 287, 586
Burstein D., Faber S. M., Gonzalez J. J., 1986, AJ, 91, 1130
Buson L. M., et al., 1993, A&A, 280, 409
Buzzoni A., Gariboldi G., Mantegazza L., 1992, AJ, 103, 1814
Buzzoni A., Mantegazza L., Gariboldi G., 1994, AJ, 107, 513
Caon N., Capaccioli M., Rampazzo R., 1990, A&AS, 86, 429
Caon N., Macchetto D., Pastoriza M., 2000, ApJS, 127, 39
Capaccioli M., Caon N., D'Onofrio M., 1992, MNRAS, 259, 323
Capelato H. V., de Carvalho R. R., Carlberg R. G., 1995, ApJ, 451, 525
Carlberg R. G., 1984, ApJ, 286, 403
Carter D., Thomson R. C., Hau G. K. T., 1998, MNRAS, 294, 182
Carretta E., Cohen J. G., Gratton R. G., Behr B. B., 2001, AJ, 122, 1469
Cassisi S., Castellani V., degl'Innocenti S., Salaris M., Weiss A., 1999, A&AS, 134, 103
Chiosi C., Carraro G., 2002, MNRAS, 335, 335
Christlein D., Zabludoff A. I., 2003, ApJ, 591, 764
Cimatti A., et al., 2004, Natur, 430, 184
Ciotti L., van Albada T. S., 2001, ApJ, 552, L13
Coelho P., Barbuy B., Perrin M.-N., Idiart T., Schiavon R. P., Ortolani S., Bica E., 2001, A&A, 376, 136
Colbert J. W., Mulchaey J. S., Zabludoff A. I., 2001, AJ, 121, 808 (CMZ01)
Colless M., et al., 2001, MNRAS, 328, 1039 (2dFGRS)
Collobert M., Sarzi M., Davies R. L., Kuntschner H., Colless M., 2006, MNRAS, 370, 1213
Cowie L. L., Songaila A., Hu E. M., Cohen J. G., 1996, AJ, 112, 839
Cox T. J., Dutta S. N., Di Matteo T., Hernquist L., Hopkins P. F., Robertson B., Springel V., 2006, ApJ, 650, 791
Croton D. J., et al., 2006, MNRAS, 365, 11
Dantas C. C., Capelato H. V., Ribeiro A. L. B., de Carvalho R. R., 2003, MNRAS, 340, 398
Davies R. L., Efstathiou G., Fall S. M., Illingworth G., Schechter P. L., 1983, ApJ, 266, 41

Davies R. L., Sadler E. M., Peletier R. F., 1993, MNRAS, 262, 650
De Angeli F., Piotto G., Cassisi S., Busso G., Recio-Blanco A., Salaris M., Aparicio A., Rosenberg A., 2005, AJ, 130, 116
de Carvalho R. R., Djorgovski S., 1992, ApJ, 389, L49
de la Rosa I. G., de Carvalho R. R., Zepf S. E., 2001, AJ, 122, 93
De Lucia G., Kauffmann G., White S. D. M., 2004, MNRAS, 349, 1101
De Lucia G., Springel V., White S. D. M., Croton D., Kauffmann G., 2006, MNRAS, 366, 499
Denicoló G., Terlevich R., Terlevich E., Forbes D. A., Terlevich A., Carrasco L., 2005a, MNRAS, 356, 1440 (D05a)
Denicoló G., Terlevich R., Terlevich E., Forbes D. A., Terlevich A., 2005b, MNRAS, 358, 813 (D05b)
de Vaucouleurs G., 1948, AnAp, 11, 247
de Vaucouleurs G., 1961, ApJS, 5, 233
de Vaucouleurs G., Capaccioli M., 1979, ApJS, 40, 699
de Vaucouleurs G., de Vaucouleurs A., Corwin H.G., Buta R.J., Paturel G., Fouqu P., 1991, Third reference catalogue of bright galaxies. Springer, New York
Djorgovski S., Davis M., 1987, ApJ, 313, 59
Djorgovski S., de Carvalho R., Han M.-S., 1988, ASPC, 4, 329
Domínguez M. J., Zandivarez A. A., Martínez H. J., Merchán M. E., Muriel H., Lambas D. G., 2002, MNRAS, 335, 825
Doi M., Fukugita M., Okamura S., 1993, MNRAS, 264, 832
Dressler A., 1980, ApJ, 236, 351
Dressler A., 1984, ApJ, 281, 512
Dressler A., 1987, ApJ, 317, 1
Drory N., Bender R., Feulner G., Hopp U., Maraston C., Snigula J., Hill G. J., 2003, ApJ, 595, 698
Ebneter K., Balick B., 1985, AJ, 90, 183
Ebneter K., Davis M., Djorgovski S., 1988, AJ, 95, 422
Edmunds M. G., 1990, MNRAS, 246, 678
Eggen O. J., Lynden-Bell D., Sandage A. R., 1962, ApJ, 136, 748
Ellis R. S., Smail I., Dressler A., Couch W. J., Oemler A. J., Butcher H., Sharples R. M., 1997, ApJ, 483, 582
Erwin P., Graham A. W., Caon N., 2004, cbhg.symp
Eskridge P. B., Fabbiano G., Kim D.-W., 1995, ApJS, 97, 141
Eskridge P. B., Fabbiano G., Kim D.-W., 1995, ApJ, 442, 523
Evstigneeva E. A., de Carvalho R. R., Ribeiro A. L., Capelato H. V., 2004, MNRAS, 349, 1052
Evstigneeva E. A., Reshetnikov V. P., Sotnikova N. Y., 2002, A&A, 381, 6
Faber S. M., 1973, ApJ, 179, 731
Faber S. M., Friel E. D., Burstein D., Gaskell C. M., 1985, ApJS, 57, 711
Faber S. M., Jackson R. E., 1976, ApJ, 204, 668
Faber S. M., Wegner G., Burstein D., Davies R. L., Dressler A., Lynden-Bell D., Terlevich R. J., 1989, ApJS, 69, 763
Fagotto F., Bressan A., Bertelli G., Chiosi C., 1994, A&AS, 105, 29
Fall S. M., Efstathiou G., 1980, MNRAS, 193, 189
Feltzing S., Gilmore G., 2000, A&A, 355, 949
Ferrari C., Benoist C., Maurogordato S., Cappi A., Slezak E., 2005, A&A, 430, 19
Ferreras I., Charlot S., Silk J., 1999, ApJ, 521, 81

Ferreras I., Silk J., 2002, MNRAS, 336, 1181
Ferrari F., Pastoriza M. G., Macchetto F., Caon N., 1999, A&AS, 136, 269
Ferrini F., Poggianti B. M., 1993, ApJ, 410, 44
Flint K., 2001, PhD thesis, University of California
Flint K., Bolte M., Mendes de Oliveira C., 2003, Ap&SS, 285, 191
Forbes D. A., 1991, MNRAS, 249, 779
Forbes D. A., 1992, PhD thesis, University of Cambridge
Forbes D. A., Ponman T. J., 1999, MNRAS, 309, 623
Forbes D. A., Ponman T. J., Brown R. J. N., 1998, ApJ, 508, L43
Forbes D. A., Sánchez-Blázquez P., Proctor R., 2005, MNRAS, 361, L6
Forbes D. A., Thomson R. C., 1992, MNRAS, 254, 723
Forman W., Jones C., Tucker W., 1985, ApJ, 293, 102
Franx M., Illingworth G. D., 1988, ApJ, 327, L55
Franx M., Illingworth G., Heckman T., 1989, AJ, 98, 538
Fraser C. W., 1972, Obs, 92, 51
Fujita Y., 2004, PASJ, 56, 29
Garcia A. M., 1993, A&AS, 100, 47
Geha M., Guhathakurta P., van der Marel R. P., 2002, AJ, 124, 3073
Gill S. P. D., Knebe A., Gibson B. K., Dopita M. A., 2004, MNRAS, 351, 410
Girardi M., Mardirossian F., Marinoni C., Mezzetti M., Rigoni E., 2003, A&A, 410, 461
Gladders M. D., Lopez-Cruz O., Yee H. K. C., Kodama T., 1998, ApJ, 501, 571
González-García A. C., Balcells M., 2005, MNRAS, 357, 753
González-García A. C., van Albada T. S., 2003, MNRAS, 342, L36
Gorgas J., Faber S. M., Burstein D., Gonzalez J. J., Courteau S., Prosser C., 1993, ApJS, 86, 153
Goto T., Yamauchi C., Fujita Y., Okamura S., Sekiguchi M., Smail I., Bernardi M., Gomez P. L., 2003, MNRAS, 346, 601
Goudfrooij P., de Jong T., 1995, A&A, 298, 784
Goudfrooij P., de Jong T., Hansen L., Norgaard-Nielsen H. U., 1994, MNRAS, 271, 833
Goudfrooij P., Hansen L., Jorgensen H. E., Norgaard-Nielsen H. U., 1994, A&AS, 105, 341
Governato F., Reduzzi L., Rampazzo R., 1993, MNRAS, 261, 379
Graham A., Colless M., 1997, MNRAS, 287, 221
Graham A. W., Erwin P., Caon N., Trujillo I., 2001, ApJ, 563, L11
Graham A. W., Erwin P., Caon N., Trujillo I., 2003, RMxAC, 17, 196
Graham A. W., Driver S. P., 2007, ApJ, 655, 77
Graham A. W., Trujillo I., Caon N., 2001, AJ, 122, 1707
Greggio L., 1997, MNRAS, 285, 151
Greggio L., Renzini A., 1983, A&A, 118, 217
Gunn J. E., Gott J. R. I., 1972, ApJ, 176, 1
Guzman R., Lucey J. R., Carter D., Terlevich R. J., 1992, MNRAS, 257, 187
Haines C. P., Merluzzi P., Mercurio A., Gargiulo A., Krusanova N., Busarello G., La Barbera F., Capaccioli M., 2006, MNRAS, 371, 55
Hamabe M., Kormendy J., 1987, IAUS, 127, 379
Hashimoto M., Iwamoto K., Nomoto K., 1993, ApJ, 414, L105
Hau G. K. T., Carter D., Balcells M., 1999, MNRAS, 306, 437
Hau G. K. T., Forbes D. A., 2006, MNRAS, 371, 633 (HF06)
Hau G. K. T., Thomson R. C., 1994, MNRAS, 270, L23
Hernquist L., Barnes J. E., 1991, Natur, 354, 210
Hernquist L., Spergel D. N., 1992, ApJ, 399, L117

Hernquist L., Weil M. L., 1992, Natur, 358, 734
Hibbard J. E., Mihos J. C., 1995, AJ, 110, 140
Hjorth J., Madsen J., 1995, ApJ, 445, 55
Holden B. P., Stanford S. A., Eisenhardt P., Dickinson M., 2004, AJ, 127, 2484
Hoessel J. G., Oegerle W. R., Schneider D. P., 1987, AJ, 94, 1111
Hubble E., Humason M. L., 1931, ApJ, 74, 43
Illingworth G., 1977, ApJ, 218, L43
Jarrett T. H., Chester T., Cutri R., Schneider S. E., Huchra J. P., 2003, AJ, 125, 525
Jedrzejewski R. I., 1987, MNRAS, 226, 747
Jesseit R., Naab T., Peletier R., Burkert A., 2007, MNRAS, 144
Jones L. R., Ponman T. J., Forbes D. A., 2000, MNRAS, 312, 139
Jones L. R., Ponman T. J., Horton A., Babul A., Ebeling H., Burke D. J., 2003, MNRAS, 343, 627
Jorgensen I., 1997, MNRAS, 288, 161
Jørgensen I., 1999, MNRAS, 306, 607
Jorgensen I., Franx M., Kjaergaard P., 1993, ApJ, 411, 34 (JFK93)
Jorgensen I., Franx M., Kjaergaard P., 1995, MNRAS, 276, 1341 (JFK95)
Karachentseva V.E., 1973, Comm. Spac. Ap. Obs. USSR, 8, 1
Kauffmann G., 1995, MNRAS, 274, 153
Kauffmann G., White S. D. M., Heckman T. M., Ménard B., Brinchmann J., Charlot S., Tremonti C., Brinkmann J., 2004, MNRAS, 353, 713
Kawata D., Gibson B. K., 2003, MNRAS, 346, 135
Kauffmann G., Charlot S., 1998, MNRAS, 294, 705
Kawata D., Gibson B. K., 2003, MNRAS, 346, 135
Kelson D. D., Illingworth G. D., Franx M., van Dokkum P. G., 2006, ApJ, 653, 159
Khochfar S., Burkert A., 2003, ApJ, 597, L117
Khosroshahi H. G., Raychaudhury S., Ponman T. J., Miles T. A., Forbes D. A., 2004, MNRAS, 349, 527
Kim Y.-C., Demarque P., Yi S. K., Alexander D. R., 2002, ApJS, 143, 499
Kirshner R. P., Oke J. B., 1975, ApJ, 200, 574
Knapp G. R., Turner E. L., Cunniffe P. E., 1985, AJ, 90, 454
Kobayashi C., 2004, MNRAS, 347, 740
Kobayashi C., Arimoto N., 1999, ApJ, 527, 573
Kodama T., 2001, Ap&SS, 276, 877
Kodama T., Arimoto N., 1997, A&A, 320, 41
Kodama T., Arimoto N., Barger A. J., Arag'on-Salamanca A., 1998, A&A, 334, 99
Kodama T., Bower R. G., Bell E. F., 1999, MNRAS, 306, 561
Koprolin W., Zeilinger W. W., 2000, A&AS, 145, 71
Kormendy J., 1977, ApJ, 218, 333
Kormendy J., 1982, ApJ, 257, 75
Kormendy J., 1985, ApJ, 295, 73
Kormendy J., Bender R., 1996, ApJ, 464, L119
Korn A. J., Maraston C., Thomas D., 2005, A&A, 438, 685
Kuehn F., Ryden B. S., 2005, ApJ, 634, 1032
Kuntschner H., 2000, MNRAS, 315, 184
Kuntschner H., Lucey J. R., Smith R. J., Hudson M. J., Davies R. L., 2001, MNRAS, 323, 615
Kuntschner H., Smith R. J., Colless M., Davies R. L., Kaldare R., Vazdekis A., 2002, MNRAS, 337, 172

Kurucz R. L., 1979, ApJS, 40, 1
La Barbera F., Busarello G., Merluzzi P., Massarotti M., Capaccioli M., 2003, ApJ, 595, 127
La Barbera F., de Carvalho R. R., Gal R. R., Busarello G., Merluzzi P., Capaccioli M., Djorgovski S. G., 2005, ApJ, 626, L19
Landolt A. U., 1992, AJ, 104, 340
Larson R. B., 1974, MNRAS, 166, 585
Larson R. B., 1975, MNRAS, 173, 671
Larson R. B., Tinsley B. M., 1978, ApJ, 219, 46
Lauberts A., Valentijn E.A., 1989, The surface photometry catalogue of the ESO-Uppsala galaxies. European Southern Observatory (ESO), Garching
Lauer T. R., 1985, MNRAS, 216, 429
Lauer T. R., 1985, ApJ, 292, 104
Lavery R. J., Henry J. P., 1988, ApJ, 330, 596
Lejeune T., Cuisinier F., Buser R., 1997, A&AS, 125, 229
Levine S., 1997, The Nature of Elliptical Galaxies; 2nd Stromlo Symposium. ASP Conference Series; Vol. 116; 1997; ed. Arnaboldi M., Da Costa G.S. and Saha P., p.166
Lynden-Bell D., 1967, MNRAS, 136, 101
Longhetti M., Bressan A., Chiosi C., Rampazzo R., 2000, A&A, 353, 917
Macchetto F., Pastoriza M., Caon N., Sparks W. B., Giavalisco M., Bender R., Capaccioli M., 1996, A&AS, 120, 463
McWilliam A., 1997, ARA&A, 35, 503
Madau P., Ferguson H. C., Dickinson M. E., Giavalisco M., Steidel C. C., Fruchter A., 1996, MNRAS, 283, 1388
Maeder A., Meynet G., 1989, A&A, 210, 155
Majewski S. R., Hawley S. L., Munn J. A., 1996, ASPC, 92, 119
Malin D. F., Carter D., 1983, ApJ, 274, 534
Maraston C., 1998, MNRAS, 300, 872
Maraston C., 2003, egcs.conf, 237
Maraston C., Greggio L., Renzini A., Ortolani S., Saglia R. P., Puzia T. H., Kissler-Patig M., 2003, A&A, 400, 823
Marcum P. M., Aars C. E., Fanelli M. N., 2004, AJ, 127, 3213
Martel A. R., et al., 2004, AJ, 128, 2758
Matteucci F., 1994, A&A, 288, 57
Matteucci F., 2003, Ap&SS, 284, 539
Matteucci F., Brocato E., 1990, ApJ, 365, 539
Matteucci F., Greggio L., 1986, A&A, 154, 279
Matteucci F., Tornambe A., 1987, A&A, 185, 51
McDermid R. M., et al., 2006, MNRAS, 373, 906
McGlynn T. A., 1984, ApJ, 281, 13
Mehlert D., Saglia R. P., Bender R., Wegner G., 1998, A&A, 332, 33
Mehlert D., Thomas D., Saglia R. P., Bender R., Wegner G., 2003, A&A, 407, 423
Merluzzi P., 1998, A&A, 338, 807
Merritt D., 1984, ApJ, 276, 26
Michard R., Prugniel P., 2004, A&A, 423, 833
Mihos J. C., Hernquist L., 1996, ApJ, 464, 641
Miles T. A., Raychaudhury S., Forbes D. A., Goudfrooij P., Ponman T. J., Kozhurina-Platais V., 2004, MNRAS, 355, 785
Milosavljević M., Merritt D., 2001, ApJ, 563, 34
Mo H. J., Mao S., White S. D. M., 1998, MNRAS, 295, 319

Mobasher B., et al., 2003, ApJ, 587, 605
Moore B., Katz N., Lake G., Dressler A., Oemler A., 1996, Natur, 379, 613
Moore B., Lake G., Katz N., 1998, ApJ, 495, 139
Moore B., Lake G., Quinn T., Stadel J., 1999, MNRAS, 304, 465
Moore B., Ghigna S., Governato F., Lake G., Quinn T., Stadel J., Tozzi P., 1999, ApJ, 524, L19
Morganti R., Sadler E. M., Oosterloo T., Pizzella A., Bertola F., 1997, AJ, 113, 937
Morganti R., et al., 2006, MNRAS, 371, 157
Moriondo G., et al., 1999, A&AS, 137, 101
Mulchaey J. S., Zabludoff A. I., 1999, ApJ, 514, 133
Naab T., Burkert A., 2003, ApJ, 597, 893
Naab T., Jesseit R., Burkert A., 2006, MNRAS, 372, 839
Naab T., Khochfar S., Burkert A., 2006, ApJ, 636, L81
Nieto J.-L., Bender R., 1989, A&A, 215, 266
Nipoti C., Londrillo P., Ciotti L., 2003, MNRAS, 342, 501
Nipoti C., Londrillo P., Ciotti L., 2006, MNRAS, 370, 681
Nomoto K., Thielemann F.-K., Yokoi K., 1984, ApJ, 286, 644
O'Connell R. W., 1994, nngl.conf, 255
Okamura S., Kodaira K., Watanabe M., 1984, ApJ, 280, 7
Oemler A. J., 1974, ApJ, 194, 1
Origlia L., Rich R. M., Castro S., 2002, AJ, 123, 1559
O'Sullivan E., Forbes D. A., Ponman T. J., 2001, MNRAS, 328, 461
Pagel B. E. J., 1970, VA, 12, 313
Peebles P. J. E., 1982, ApJ, 263, L1
Peletier R. F., Davies R. L., Illingworth G. D., Davis L. E., Cawson M., 1990, AJ, 100, 1091
Pfefferkorn F., Boller T., Rafanelli P., 2001, A&A, 368, 797
Phillips M. M., Jenkins C. R., Dopita M. A., Sadler E. M., Binette L., 1986, AJ, 91, 1062
Pierfederici F., Rampazzo R., 2004, AN, 325, 359
Ponman T. J., Allan D. J., Jones L. R., Merrifield M., McHardy I. M., Lehto H. J., Luppino G. A., 1994, Natur, 369, 462
Postman M., et al., 2005, ApJ, 623, 721
Pritzl B. J., Venn K. A., Irwin M., 2005, AJ, 130, 2140
Proctor R. N., Forbes D. A., Beasley M. A., 2004a, MNRAS, 355, 1327
Proctor R. N., Forbes D. A., Forestell A., Gebhardt K., 2005, MNRAS, 362, 857
Proctor R. N., Forbes D. A., Hau G. K. T., Beasley M. A., De Silva G. M., Contreras R., Terlevich A. I., 2004b, MNRAS, 349, 1381
Proctor R. N., Sansom A. E., 2002, MNRAS, 333, 517
Prugniel P., Heraudeau P., 1998, A&AS, 128, 299 (PH98)
Prugniel P., Simien F., 1996, A&A, 309, 749 (PS96)
Prugniel P., Simien F., 1997, A&A, 321, 111
Puzia T. H., Saglia R. P., Kissler-Patig M., Maraston C., Greggio L., Renzini A., Ortolani S., 2002, A&A, 395, 45
Raychaudhury S., 1989, Natur, 342, 251
Raychaudhury S., 1990
Reda F. M., Forbes D. A., Beasley M. A., O'Sullivan E. J., Goudfrooij P., 2004, MNRAS, 354, 851 (R04)
Reda F. M., Forbes D. A., Hau G. K. T., 2005, MNRAS, 360, 693 (R05)
Reda F. M., Proctor R. N., Forbes D. A., Hau G. K. T., Larsen S. S., 2007, MNRAS, in press (R07)

Reduzzi L., Longhetti M., Rampazzo R., 1996, MNRAS, 282, 149 (RLR96)
Rees M. J., Ostriker J. P., 1977, MNRAS, 179, 541
Reid N., Boisson C., Sansom E. A., 1994, MNRAS, 269, 713
Renzini A., Fusi Pecci F., 1988, ARA&A, 26, 199
Robertson B., Cox T. J., Hernquist L., Franx M., Hopkins P. F., Martini P., Springel V., 2006, ApJ, 641, 21
Robinson L. B., Wampler E. J., 1972, PASP, 84, 161
Roos N., Aarseth S. J., 1982, A&A, 114, 41
Sadler E. M., Gerhard O. E., 1985, MNRAS, 214, 177
Saglia R. P., Maraston C., Greggio L., Bender R., Ziegler B., 2000, A&A, 360, 911
Salasnich B., Girardi L., Weiss A., Chiosi C., 2000, A&A, 361, 1023
Salpeter E. E., 1955, ApJ, 121, 161
Sandage A., Visvanathan N., 1978, ApJ, 223, 707
Sánchez-Blázquez P., Forbes D. A., Strader J., Brodie J., Proctor R., 2007, astro-ph/0702572
Sánchez-Blázquez P., Gorgas J., Cardiel N., 2006, A&A, 457, 823
Sánchez-Blázquez P., Gorgas J., Cardiel N., González J. J., 2006, A&A, 457, 809
Sansom A. E., Reid I. N., Boisson C., 1988, MNRAS, 234, 247
Saraiva M. F., Ferrari F., Pastoriza M. G., 1999, A&A, 350, 399
Sarzi M., et al., 2007, NewAR, 51, 18
Saucedo-Morales J., Bieging J., 2001, ApSSS, 277, 449
Schechter P., 1976, ApJ, 203, 297
Schlegel D. J., Finkbeiner D. P., Davis M., 1998, ApJ, 500, 525
Schweizer F., Seitzer P., Faber S. M., Burstein D., Dalle Ore C. M., Gonzalez J. J., 1990, ApJ, 364, L33
Schweizer F., 1980, ApJ, 237, 303
Schweizer F., 1982, ApJ, 252, 455
Schweizer F., 1983, IAUS, 100, 319
Schweizer F., 1992 in Structure, Dynamics and Chemical Evolution of Elliptical Galaxies, I.J. Danziger, W.W. Zeiliger, K. Kjr (Eds.) ESO/IPC, p.651
Schweizer F., Seitzer P., 1988, ApJ, 328, 88
Schweizer F., Seitzer P., Faber S. M., Burstein D., Dalle Ore C. M., Gonzalez J. J., 1990, ApJ, 364, L33
Schweizer F., Seitzer P., 1992, AJ, 104, 1039
Seitzer P., Schweizer F., 1990, Dynamics and Interaction of Elliptical Galaxies, ed. R. Wielen (Berlin: Springer-Verlag), 270
Sérsic J. L., 1968, Atlas de Galaxias Australes, Observatorio Astronomico, Cordoba, Argentina
Serra P., Trager S. C., van der Hulst J. M., Oosterloo T. A., Morganti R., van Gorkom J. H., Sadler E. M., 2007, NewAR, 51, 3
Shaver P. A., Wall J. V., Kellermann K. I., Jackson C. A., Hawkins M. R. S., 1996, Natur, 384, 439
Silk J., 1977, ApJ, 214, 152
Smith R. M., Martínez V. J., Graham M. J., 2004, ApJ, 617, 1017 (SMG04)
Soares D. S. L., de Souza R. E., de Carvalho R. R., Couto da Silva T. C., 1995, A&AS, 110, 371
Springel V., 2000, MNRAS, 312, 859
Springel V., Di Matteo T., Hernquist L., 2005, MNRAS, 361, 776
Springel V., Di Matteo T., Hernquist L., 2005, ApJ, 620, L79
Stanford S. A., Eisenhardt P. R. M., Dickinson M., 1995, ApJ, 450, 512

Stanford S. A., Eisenhardt P. R., Dickinson M., 1998, ApJ, 492, 461
Stiavelli M., 1998, ApJ, 495, L91
Stocke J. T., Keeney B. A., Lewis A. D., Epps H. W., Schild R. E., 2004, AJ, 127, 1336
Strom S. E., Strom K. M., Goad J. W., Vrba F. J., Rice W., 1976, ApJ, 204, 684
Tantalo R., Chiosi C., 2004, MNRAS, 353, 405
Tantalo R., Chiosi C., Bressan A., 1998, A&A, 333, 419
Tamura N., Kobayashi C., Arimoto N., Kodama T., Ohta K., 2000, AJ, 119, 2134
Tamura N., Ohta K., 2000, AJ, 120, 533
Tanaka M., Goto T., Okamura S., Shimasaku K., Brinkmann J., 2004, AJ, 128, 2677
Tantalo R., Chiosi C., Bressan A., 1998, A&A, 333, 419
Temi P., Mathews W. G., Brighenti F., Bregman J. D., 2003, ApJ, 585, L121
Terlevich A. I., Forbes D. A., 2002, MNRAS, 330, 547 (TF02)
Thielemann F.-K., Nomoto K., Hashimoto M.-A., 1996, ApJ, 460, 408
Thomas D., Greggio L., Bender R., 1999, MNRAS, 302, 537
Thomas D., Maraston C., Bender R., 2003, MNRAS, 339, 897 (TMB03)
Thomas D., Maraston C., Bender R., Mendes de Oliveira C., 2005, ApJ, 621, 673
Thomas D., Maraston C., Korn A., 2004, MNRAS, 351, L19 (TMK04)
Thomson R. C., 1991, MNRAS, 253, 256
Thomson R. C., Wright A. E., 1990, MNRAS, 247, 122
Toomre A., Toomre J., 1972, ApJ, 178, 623
Trager S. C., Faber S. M., Worthey G., González J. J., 2000, AJ, 119, 1645
Trager S. C., Faber S. M., Worthey G., González J. J., 2000, AJ, 120, 165
Trager S. C., Worthey G., Faber S. M., Burstein D., Gonzalez J. J., 1998, ApJS, 116, 1
Tremaine S., 1999, MNRAS, 307, 877
Tremaine S., Henon M., Lynden-Bell D., 1986, MNRAS, 219, 285
Trentham N., Hodgkin S., 2002, MNRAS, 333, 423
Trentham N., Tully R. B., 2002, MNRAS, 335, 712
Trenti M., Bertin G., van Albada T. S., 2005, A&A, 433, 57
Tripicco M., 1993, ASPC, 48, 432
Tripicco M. J., Bell R. A., 1995, AJ, 110, 3035 (TB95)
Tripicco M. J., Dorman B., Bell R. A., 1993, AJ, 106, 618
Trinchieri G., Goudfrooij P., 2002, A&A, 386, 472
Trujillo I., Burkert A., Bell E. F., 2004, ApJ, 600, L39
Trujillo I., Graham A. W., Caon N., 2001, MNRAS, 326, 869
Valluri M., Vass I. M., Kazantzidis S., Kravtsov A. V., Bohn C. L., 2007, ApJ, 658, 731
van Albada T. S., 1982, MNRAS, 201, 939
VandenBerg D. A., 2000, ApJS, 129, 315
Vass I. M., Valluri M., Kazantzidis S., Kravtsov A. V., Bohn C. L., 2005, AAS, 37, 1297
Vazdekis A., 1999, ApJ, 513, 224
Vazdekis A., Kuntschner H., Davies R. L., Arimoto N., Nakamura O., Peletier R., 2001, ApJ, 551, L127
Vorontsov-Velyaminov B. A., 1959, Atlas and Catalog of Interacting Galaxies, Sternberg Institute, Moscow
Waddington I., et al., 2002, MNRAS, 336, 1342
Westera P., Lejeune T., Buser R., Cuisinier F., Bruzual G., 2002, A&A, 381, 524
White S. D. M., 1980, MNRAS, 191, 1P
White S. D. M., Rees M. J., 1978, MNRAS, 183, 341
Worthey G., 1991, BAAS, 23, 1457
Worthey G., 1998, ASPC, 147, 13

Worthey G., 1999, ASP Conf. Ser. 192: Spectrophotometric Dating of Stars and Galaxies, 192, 283
Worthey G., 1994, ApJS, 95, 107
Worthey G., Collobert M., 2003, ApJ, 586, 17
Worthey G., Faber S. M., Gonzalez J. J., 1992, ApJ, 398, 69
Worthey G., Faber S. M., Gonzalez J. J., Burstein D., 1994, ApJS, 94, 687
Worthey G., Ottaviani D. L., 1997, ApJS, 111, 377
Yi S. K., Kim Y.-C., Demarque P., 2003, ApJS, 144, 259
Zabludoff A. I., Mulchaey J. S., 2000, ApJ, 539, 136
Zepf S. E., Whitmore B. C., 1993, ApJ, 418, 72
Ziegler B. L., Saglia R. P., Bender R., Belloni P., Greggio L., Seitz S., 1999, A&A, 346, 13
Zwicky F. et al., 1957, Catalog of Galaxies & Clusters of Galaxies, Vol. 1-6, California Institute of technology, Pasadena

Appendix A

A list of candidate satellite galaxies in the field of the isolated galaxies

List of the candidate satellite galaxies within a projected radius of $\sim$ 15 arcmins of an isolated galaxy. Column 1 gives the serial number as given by SExtractor. Column 2 and 3 gives the Right Ascension and Declination in J2000 coordinates. Columns 4, 5 and 6 give the R magnitude, object class and the radius A (in arcsecond) of the object as measured by the SExtractor. The R magnitude is corrected for galactic extinction (A_R) assuming same values as that in Table 3.1 for the parent isolated galaxy. Column 7 is the absolute magnitude in the R-band, assuming the object is located at the same distance from the Sun as the parent isolated. Column 8 gives the projected distance (in kpc) on the sky between the candidate satellite galaxy and the parent isolated galaxy.

Table A.1: List of the candidate satellite galaxies in the field of NGC 1045.

Number (1)	RA (J2000) (2)	DEC (J2000) (3)	R (mag) (4)	Class (5)	A (arcsec) (6)	M_R (mag) (7)	Dist (kpc) (8)
147	02 39 53.6	-11 01 34.0	14.02	0.03	7.0	-19.87	303
530	02 40 23.0	-11 21 01.4	15.18	0.00	3.9	-18.71	81
1248	02 41 13.6	-11 13 06.9	15.94	0.03	3.0	-17.95	202
966	02 40 55.6	-11 11 06.7	16.04	0.03	2.1	-17.84	150
752	02 40 36.5	-11 21 15.1	16.06	0.00	2.1	-17.83	88
1018	02 40 58.1	-11 14 12.1	16.11	0.03	1.6	-17.77	133
735	02 40 35.3	-11 18 49.2	16.15	0.02	2.0	-17.74	48
1169	02 41 07.6	-11 12 43.1	16.18	0.03	2.1	-17.70	180
676	02 40 31.0	-11 15 09.0	16.25	0.03	1.8	-17.64	27
1230	02 41 11.8	-11 10 33.0	16.26	0.03	1.8	-17.63	213
695	02 40 31.7	-11 20 57.6	16.30	0.01	1.4	-17.58	77
767	02 40 37.6	-11 15 08.2	16.31	0.03	2.3	-17.57	46
644	02 40 28.8	-11 15 18.7	16.33	0.01	2.0	-17.56	22
572	02 40 25.1	-11 28 13.2	16.39	0.00	2.5	-17.50	204
1112	02 41 03.7	-11 10 16.1	16.41	0.03	1.5	-17.47	186
1064	02 41 01.6	-11 19 33.8	16.42	0.03	1.8	-17.47	150
1296	02 41 38.3	-11 26 25.8	16.47	0.03	1.6	-17.41	344
1438	02 41 24.6	-11 13 19.1	16.51	0.03	1.5	-17.37	247
687	02 40 31.8	-11 23 48.0	16.52	0.01	1.8	-17.37	126
1251	02 41 14.7	-11 14 49.9	16.54	0.02	5.7	-17.35	200
753	02 40 36.2	-11 22 21.4	16.55	0.00	1.3	-17.33	106
613	02 40 26.8	-11 15 33.2	16.56	0.00	2.3	-17.32	19
436	02 40 12.6	-10 58 09.2	16.62	0.08	1.1	-17.26	330
1566	02 41 31.3	-11 13 44.2	16.65	0.02	1.8	-17.23	273
434	02 40 13.2	-11 11 39.0	16.65	0.03	1.4	-17.24	109
175	02 39 54.0	-11 23 43.4	16.67	0.01	1.6	-17.21	194
1157	02 41 05.9	-11 07 43.0	16.68	0.03	1.6	-17.21	223
1259	02 41 28.0	-11 00 49.0	16.68	0.03	1.4	-17.21	375
989	02 40 56.0	-11 14 56.3	16.68	0.02	1.4	-17.20	120
1132	02 41 05.1	-11 16 49.8	16.74	0.02	1.9	-17.14	156
212	02 39 57.0	-11 11 25.5	16.84	0.02	1.6	-17.05	163
765	02 40 36.7	-11 03 59.5	16.86	0.03	1.5	-17.03	223
1354	02 41 25.8	-11 13 10.5	16.88	0.03	1.4	-17.00	252
978	02 40 55.5	-11 17 31.2	16.88	0.02	1.6	-17.01	116
1475	02 41 18.8	-11 11 35.4	16.90	0.05	1.3	-16.99	232
791	02 40 38.8	-11 23 49.1	17.02	0.01	1.2	-16.87	133
1179	02 41 07.4	-11 12 44.5	17.03	0.03	1.5	-16.85	179
1363	02 41 30.6	-11 01 42.8	17.03	0.02	1.5	-16.85	372
1188	02 41 08.4	-11 13 25.5	17.05	0.02	1.7	-16.83	179
1094	02 41 02.2	-11 10 24.5	17.07	0.03	1.3	-16.82	180
24	02 39 38.8	-11 04 02.1	17.08	0.02	1.1	-16.80	306

Table A.1: Candidate satellite galaxies in the field of NGC 1045 (continued).

Number (1)	RA (J2000) (2)	DEC (J2000) (3)	R (mag) (4)	Class (5)	A (arcsec) (6)	M_R (7)	Dist (kpc) (8)
1243	02 41 12.2	-11 18 27.8	17.10	0.04	1.2	-16.79	189
1494	02 41 15.9	-11 09 17.0	17.10	0.01	1.6	-16.78	239
346	02 40 09.1	-10 57 06.7	17.11	0.03	1.6	-16.78	351
455	02 40 14.3	-10 58 42.3	17.14	0.00	1.5	-16.74	319
1177	02 41 07.2	-11 18 57.3	17.17	0.08	1.1	-16.71	170
110	02 39 47.0	-11 17 32.5	17.21	0.00	1.9	-16.68	179
781	02 40 37.7	-11 09 21.6	17.23	0.01	1.3	-16.66	132
355	02 40 10.0	-11 28 20.1	17.25	0.02	1.2	-16.63	220
983	02 40 55.3	-11 08 43.9	17.26	0.01	1.3	-16.62	178
1418	02 41 38.6	-11 15 10.3	17.28	0.01	1.7	-16.61	301
1091	02 41 02.3	-11 18 38.8	17.29	0.02	1.5	-16.60	148
914	02 40 50.9	-11 19 16.0	17.32	0.01	1.4	-16.56	106
1466	02 41 19.7	-11 08 27.4	17.34	0.02	1.3	-16.55	261
1256	02 41 39.3	-11 17 37.0	17.35	0.02	1.2	-16.53	303
603	02 40 26.8	-11 17 12.5	17.35	0.00	2.2	-16.53	13
1054	02 41 00.0	-11 13 01.1	17.37	0.03	1.1	-16.51	148
388	02 40 11.5	-11 25 16.7	17.39	0.02	1.1	-16.50	169
1172	02 41 06.9	-11 14 00.3	17.42	0.03	1.1	-16.47	170
1461	02 41 22.4	-10 58 50.6	17.43	0.01	1.4	-16.46	387
661	02 40 29.1	-11 09 58.3	17.46	0.02	1.2	-16.43	115
1060	02 40 59.9	-10 58 22.5	17.47	0.01	1.4	-16.42	345
1152	02 41 05.2	-11 08 43.3	17.47	0.03	1.3	-16.42	208
526	02 40 20.0	-11 09 16.7	17.47	0.02	1.2	-16.41	133
1127	02 41 04.0	-11 14 26.1	17.48	0.01	1.1	-16.40	156
918	02 40 50.8	-11 14 18.3	17.48	0.04	1.2	-16.40	103
1181	02 41 07.5	-11 14 32.5	17.52	0.01	1.3	-16.36	170
1371	02 41 30.4	-11 15 40.8	17.52	0.00	1.9	-16.37	265
792	02 40 38.9	-11 21 17.6	17.55	0.05	0.8	-16.33	93
835	02 40 43.9	-11 19 35.5	17.55	0.09	1.2	-16.34	83
1339	02 41 33.7	-11 14 23.5	17.56	0.04	1.1	-16.32	281
6	02 39 36.1	-11 04 40.2	17.56	0.00	2.0	-16.33	307
641	02 40 28.0	-11 20 52.3	17.56	0.09	0.9	-16.32	75
288	02 40 03.8	-11 11 19.0	17.58	0.00	1.4	-16.30	141
640	02 40 28.0	-11 00 18.6	17.60	0.00	2.6	-16.29	284
486	02 40 15.7	-10 57 04.5	17.62	0.03	0.7	-16.27	346
1037	02 40 58.4	-11 01 00.3	17.64	0.01	1.2	-16.24	301
539	02 40 21.7	-11 21 21.5	17.64	0.07	1.0	-16.25	88
721	02 40 34.6	-11 13 55.7	17.66	0.04	1.1	-16.23	53
779	02 40 37.3	-11 22 01.8	17.69	0.00	0.8	-16.19	102
1386	02 41 28.8	-11 01 44.8	17.71	0.03	1.0	-16.18	366
972	02 40 54.6	-11 09 30.7	17.72	0.01	1.1	-16.16	166
347	02 40 09.3	-11 25 25.0	17.76	0.01	1.7	-16.12	175
248	02 40 00.3	-11 19 36.3	17.77	0.00	1.8	-16.11	132
1286	02 41 39.6	-11 13 07.1	17.79	0.07	1.0	-16.10	310
1531	02 41 12.6	-11 00 45.9	17.80	0.01	1.7	-16.09	335
1156	02 41 05.2	-11 12 53.2	17.82	0.06	1.0	-16.06	169
797	02 40 39.0	-11 22 43.1	17.83	0.01	0.7	-16.06	116
202	02 39 56.2	-11 21 47.9	17.84	0.04	0.9	-16.04	166
309	02 40 06.2	-11 15 56.2	17.84	0.01	1.3	-16.05	97
451	02 40 14.3	-11 20 59.7	17.85	0.03	1.0	-16.03	98
780	02 40 37.3	-11 21 04.7	17.85	0.03	0.7	-16.04	86
955	02 40 54.1	-11 25 14.4	17.86	0.05	1.0	-16.03	186
982	02 40 55.0	-11 12 49.5	17.89	0.00	1.3	-16.00	130
1126	02 41 04.5	-11 16 13.9	17.91	0.02	1.3	-15.98	154
649	02 40 28.6	-11 24 38.7	17.93	0.00	1.2	-15.95	141
1492	02 41 16.2	-11 21 56.9	17.94	0.03	1.7	-15.95	224
632	02 40 27.6	-11 23 38.4	17.94	0.02	0.9	-15.94	123
635	02 40 27.7	-11 23 52.7	17.95	0.05	0.9	-15.94	127
614	02 40 26.6	-11 24 39.6	17.96	0.03	1.0	-15.92	141
74	02 39 43.3	-11 17 30.6	17.96	0.00	1.5	-15.93	195
719	02 40 32.4	-11 21 17.8	17.97	0.01	0.6	-15.92	83
390	02 40 11.0	-11 21 28.1	18.02	0.00	0.9	-15.87	114
738	02 40 34.4	-11 21 47.0	18.02	0.07	0.7	-15.87	94
1134	02 41 03.9	-11 08 41.3	18.03	0.00	1.2	-15.86	205
789	02 40 38.7	-11 24 44.1	18.03	0.01	0.9	-15.86	148
732	02 40 33.8	-11 21 28.8	18.05	0.03	0.6	-15.84	88
970	02 40 54.7	-11 19 36.8	18.05	0.09	1.0	-15.84	123
1440	02 41 41.8	-11 15 33.6	18.07	0.00	1.0	-15.82	314
1520	02 41 28.6	-11 00 35.4	18.07	0.00	1.1	-15.82	380
876	02 40 47.1	-11 09 32.3	18.07	0.02	1.0	-15.82	146
1309	02 41 35.4	-11 16 20.0	18.09	0.00	1.1	-15.79	286
1043	02 40 59.0	-11 13 06.9	18.10	0.00	1.3	-15.88	143
86	02 39 44.6	-11 08 05.3	18.12	0.00	1.2	-15.77	240
1511	02 41 17.0	-11 05 13.4	18.13	0.00	0.8	-15.75	287
533	02 40 20.4	-11 03 59.2	18.16	0.03	0.7	-15.73	223
537	02 40 21.5	-11 22 13.3	18.16	0.00	0.9	-15.72	103
664	02 40 29.4	-11 23 52.6	18.16	0.02	0.8	-15.73	127
1369	02 41 18.7	-11 02 52.1	18.18	0.00	1.0	-15.70	322
1481	02 41 18.1	-11 17 45.6	18.20	0.01	1.1	-15.68	213
1022	02 40 57.4	-11 12 52.7	18.21	0.02	1.0	-15.68	139
1277	02 41 37.3	-11 11 15.9	18.23	0.07	0.8	-15.65	309
1521	02 41 16.2	-11 28 00.1	18.23	0.09	0.9	-15.65	285
642	02 40 28.1	-11 23 52.1	18.23	0.07	0.8	-15.66	127
203	02 39 55.5	-11 04 21.1	18.24	0.03	0.7	-15.64	257
654	02 40 28.4	-11 22 07.3	18.24	0.01	0.9	-15.65	96
1110	02 41 03.0	-11 22 20.1	18.27	0.09	0.8	-15.61	178
1145	02 41 04.3	-11 03 17.7	18.29	0.06	1.0	-15.59	278
1065	02 41 00.6	-11 19 47.3	18.30	0.04	0.9	-15.58	148
168	02 39 52.9	-11 26 31.8	18.30	0.07	0.8	-15.58	232
1176	02 41 06.8	-11 18 53.0	18.31	0.09	1.0	-15.57	168

Table A.1: Candidate satellite galaxies in the field of NGC 1045 (continued).

Number (1)	RA (J2000) (2)	DEC (J2000) (3)	R (mag) (4)	Class (5)	A (arcsec) (6)	M_R (7)	Dist (kpc) (8)
1298	02 41 36.7	-11 09 07.4	18.33	0.08	1.0	-15.56	319
711	02 40 32.2	-11 26 06.7	18.35	0.02	0.8	-15.54	167
263	02 40 01.5	-11 21 40.1	18.36	0.02	0.7	-15.53	146
32	02 39 39.2	-11 04 07.1	18.36	0.06	0.6	-15.53	304
466	02 40 15.2	-11 10 25.8	18.37	0.00	1.0	-15.51	122
657	02 40 28.8	-11 24 34.2	18.38	0.03	0.7	-15.50	139
222	02 39 56.7	-10 58 12.7	18.42	0.01	0.7	-15.46	349
607	02 40 25.4	-11 03 28.7	18.43	0.01	0.8	-15.45	229
1280	02 41 37.6	-10 58 44.4	18.46	0.04	0.9	-15.43	430
1431	02 41 25.6	-11 22 05.7	18.49	0.08	0.9	-15.39	262
760	02 40 36.6	-11 22 17.2	18.51	0.00	1.0	-15.37	105
870	02 40 46.1	-11 07 09.9	18.51	0.01	0.9	-15.38	181
1569	02 41 22.6	-10 57 55.1	18.52	0.05	0.9	-15.36	400
648	02 40 27.9	-11 10 51.2	18.54	0.02	0.9	-15.35	100
1193	02 41 08.2	-11 25 25.7	18.56	0.07	0.8	-15.32	229
1490	02 41 23.6	-10 59 14.9	18.56	0.01	0.9	-15.32	384
284	02 40 03.3	-11 24 49.9	18.58	0.01	0.8	-15.31	180
1136	02 41 04.2	-11 16 54.6	18.60	0.01	0.9	-15.28	152
1197	02 41 08.0	-11 14 29.1	18.61	0.01	0.7	-15.28	172
1552	02 41 38.8	-11 07 14.8	18.61	0.02	1.2	-15.28	342
900	02 40 48.9	-11 07 53.9	18.61	0.00	1.0	-15.28	175
149	02 39 50.8	-11 18 42.5	18.62	0.09	0.8	-15.27	166
737	02 40 34.3	-11 16 06.2	18.62	0.00	0.8	-15.26	25
863	02 40 45.5	-11 05 19.8	18.62	0.02	0.7	-15.27	209
551	02 40 22.4	-11 22 18.0	18.64	0.07	0.7	-15.24	103
550	02 40 22.5	-11 24 28.5	18.66	0.08	0.7	-15.23	140
934	02 40 52.5	-11 22 57.3	18.66	0.00	0.8	-15.22	151
651	02 40 28.2	-11 22 10.0	18.67	0.01	0.6	-15.21	97
1287	02 41 38.0	-11 02 00.1	18.68	0.00	1.2	-15.21	392
759	02 40 36.3	-11 26 44.9	18.71	0.05	0.5	-15.18	180
1523	02 41 15.7	-11 17 02.7	18.74	0.01	0.8	-15.15	201
589	02 40 24.7	-11 21 09.7	18.75	0.04	0.6	-15.13	81
867	02 40 46.5	-11 24 44.1	18.76	0.00	0.9	-15.13	161
1452	02 41 22.7	-10 58 51.9	18.77	0.06	0.9	-15.11	387
519	02 40 19.5	-11 15 14.8	18.77	0.00	0.8	-15.11	45
1048	02 40 59.3	-11 15 30.2	18.78	0.01	1.0	-15.10	132
629	02 40 27.4	-11 24 27.0	18.78	0.09	0.7	-15.10	137
663	02 40 29.0	-11 23 56.6	18.78	0.09	0.6	-15.11	128
1131	02 41 03.7	-11 11 33.1	18.79	0.02	0.7	-15.10	174
1187	02 41 07.4	-11 15 23.3	18.79	0.08	0.8	-15.09	167
602	02 40 25.8	-11 25 03.7	18.79	0.04	0.7	-15.10	148
669	02 40 29.3	-11 20 43.8	18.81	0.01	0.7	-15.07	72
929	02 40 51.9	-11 14 26.9	18.82	0.04	0.7	-15.07	106
1082	02 41 00.8	-11 06 17.8	18.84	0.09	0.7	-15.05	226
1519	02 41 16.7	-11 26 02.5	18.84	0.01	0.7	-15.05	264
899	02 40 49.4	-11 26 01.1	18.84	0.00	0.8	-15.04	187
947	02 40 53.1	-11 15 17.0	18.84	0.00	1.0	-15.05	107
1154	02 41 04.6	-11 00 55.9	18.85	0.02	0.8	-15.03	314
1092	02 41 01.8	-11 15 52.6	18.86	0.00	1.1	-15.03	142
427	02 40 12.1	-11 15 27.2	18.88	0.01	0.9	-15.00	73
854	02 40 45.0	-11 24 03.6	18.89	0.00	0.7	-15.00	148
1515	02 41 17.2	-11 13 49.5	18.90	0.01	0.8	-14.99	213
345	02 40 08.9	-11 22 24.8	18.90	0.01	0.8	-14.99	132
501	02 40 18.0	-11 24 09.7	18.91	0.05	0.7	-14.97	140
1290	02 41 38.2	-11 06 56.4	18.92	0.07	0.7	-14.97	342
516	02 40 19.4	-11 23 22.7	18.92	0.04	0.6	-14.97	125
866	02 40 45.9	-11 12 57.7	18.94	0.00	0.8	-14.94	97
927	02 40 52.2	-11 25 30.3	18.94	0.01	0.7	-14.95	185
1080	02 41 01.2	-11 21 39.8	18.95	0.08	0.7	-14.94	165
1233	02 41 10.9	-11 14 01.3	18.95	0.00	0.8	-14.94	187
1105	02 41 02.6	-11 26 10.5	18.99	0.00	0.8	-14.90	222
734	02 40 33.7	-11 05 34.8	19.03	0.00	0.9	-14.85	193
78	02 39 43.4	-11 18 03.6	19.03	0.03	0.7	-14.85	195
1186	02 41 07.3	-11 13 08.1	19.04	0.05	0.6	-14.85	176
853	02 40 44.1	-10 59 14.9	19.04	0.08	0.8	-14.85	310
1123	02 41 03.6	-11 18 34.0	19.05	0.08	0.8	-14.84	154
517	02 40 19.2	-11 15 14.0	19.05	0.01	0.7	-14.84	46
15	02 39 37.2	-10 57 37.2	19.06	0.08	0.7	-14.83	398
1088	02 41 01.1	-11 02 46.6	19.07	0.08	0.7	-14.81	279
666	02 40 29.4	-11 25 04.0	19.08	0.02	0.7	-14.80	148
1215	02 41 09.5	-11 13 00.9	19.09	0.08	0.6	-14.80	186
207	02 39 56.1	-11 13 47.3	19.10	0.05	0.6	-14.79	148
1011	02 40 56.6	-11 10 23.2	19.11	0.00	0.8	-14.78	161
1090	02 41 01.5	-11 14 58.1	19.11	0.01	0.7	-14.77	143
1327	02 41 34.0	-11 08 17.6	19.11	0.02	0.6	-14.77	315
855	02 40 45.0	-11 18 37.0	19.11	0.05	0.7	-14.78	78
860	02 40 45.8	-11 20 58.1	19.11	0.01	0.7	-14.78	106
310	02 40 05.8	-11 11 11.8	19.12	0.07	0.7	-14.76	136
694	02 40 30.5	-11 11 07.8	19.12	0.00	0.9	-14.77	95
1561	02 41 26.5	-10 58 24.6	19.14	0.08	0.6	-14.75	403
1285	02 41 42.4	-11 09 27.1	19.15	0.01	0.7	-14.74	340
1542	02 41 14.6	-10 57 36.3	19.15	0.04	0.6	-14.74	386
1532	02 41 43.2	-11 24 45.2	19.16	0.08	0.7	-14.73	350
906	02 40 49.6	-11 21 48.3	19.16	0.00	0.5	-14.73	128
121	02 39 46.8	-11 09 48.9	19.18	0.02	0.7	-14.70	215
45	02 39 40.7	-11 19 45.3	19.19	0.05	0.6	-14.70	213
796	02 40 39.1	-11 23 52.8	19.19	0.03	0.8	-14.69	135
634	02 40 27.7	-11 23 36.7	19.20	0.00	0.9	-14.68	123
1559	02 41 30.7	-10 58 26.0	19.21	0.02	0.7	-14.67	414
990	02 40 55.5	-11 23 38.4	19.21	0.09	0.6	-14.69	168

Table A.1: Candidate satellite galaxies in the field of NGC 1045 (continued).

Number (1)	RA (J2000) (2)	DEC (J2000) (3)	R (mag) (4)	Class (5)	A (arcsec) (6)	M_R (7)	Dist (kpc) (8)
1010	02 40 56.3	-11 06 45.8	19.22	0.02	0.6	-14.67	209
1265	02 41 38.3	-11 14 37.0	19.22	0.05	0.7	-14.66	300
353	02 40 09.0	-11 24 29.0	19.22	0.08	0.5	-14.67	161
1263	02 41 27.7	-11 00 23.0	19.23	0.09	0.6	-14.66	380
1462	02 41 22.8	-11 27 04.1	19.23	0.07	0.8	-14.66	296
376	02 40 09.9	-10 56 59.8	19.25	0.01	1.3	-14.63	352
1008	02 40 56.2	-11 07 25.5	19.26	0.01	0.8	-14.62	199
108	02 39 45.7	-10 58 54.7	19.26	0.00	0.8	-14.63	360
1211	02 41 09.6	-11 26 29.6	19.26	0.01	0.6	-14.63	246
1262	02 41 30.9	-11 22 13.4	19.29	0.05	0.7	-14.60	284
1595	02 41 32.8	-11 05 27.1	19.29	0.08	0.6	-14.59	337
598	02 40 25.6	-11 23 58.7	19.29	0.01	0.7	-14.60	130
1235	02 41 11.1	-11 16 46.5	19.30	0.02	0.6	-14.59	182
1056	02 40 59.7	-11 16 55.1	19.32	0.06	0.7	-14.57	133
122	02 39 47.2	-11 21 34.0	19.32	0.00	0.7	-14.57	197
1450	02 41 21.8	-11 24 17.4	19.32	0.03	0.6	-14.57	264
237	02 39 59.2	-11 14 50.2	19.33	0.04	0.6	-14.55	130
476	02 40 16.0	-11 21 40.5	19.33	0.05	0.4	-14.56	104
1384	02 41 29.0	-11 03 59.3	19.34	0.08	0.7	-14.55	340
681	02 40 30.1	-11 24 05.2	19.35	0.01	0.6	-14.54	131
1439	02 41 41.6	-11 21 56.9	19.36	0.03	0.6	-14.53	326
971	02 40 53.8	-10 58 41.5	19.36	0.02	0.7	-14.52	331
930	02 40 52.4	-11 25 43.1	19.37	0.06	0.6	-14.51	189
568	02 40 22.9	-11 05 00.0	19.40	0.02	0.7	-14.48	204
919	02 40 50.5	-11 10 56.0	19.40	0.01	0.6	-14.48	136
859	02 40 45.5	-11 23 36.7	19.41	0.01	0.8	-14.47	142
541	02 40 21.1	-11 04 54.7	19.42	0.00	0.7	-14.46	206
1405	02 41 29.4	-11 22 38.2	19.43	0.02	0.5	-14.46	281
1408	02 41 27.7	-11 06 50.4	19.48	0.09	0.7	-14.41	305
158	02 39 51.5	-11 18 33.2	19.48	0.07	0.6	-14.41	162
1100	02 41 02.1	-11 19 42.7	19.50	0.02	0.7	-14.39	153
1063	02 40 59.4	-11 00 21.9	19.54	0.04	0.5	-14.35	313
1500	02 41 22.1	-11 23 09.2	19.54	0.06	0.6	-14.35	256
672	02 40 29.5	-11 24 44.7	19.55	0.06	0.5	-14.34	142
445	02 40 13.0	-11 09 50.6	19.56	0.09	0.6	-14.34	135
260	02 40 01.3	-11 25 59.2	19.60	0.03	0.6	-14.29	202
725	02 40 33.0	-11 20 41.0	19.60	0.01	0.6	-14.29	74
813	02 40 41.2	-11 16 55.4	19.65	0.09	0.6	-14.24	54
1159	02 41 05.1	-11 08 22.7	19.66	0.00	0.6	-14.22	212
1072	02 41 00.2	-11 11 24.7	19.71	0.02	0.5	-14.18	162
998	02 40 55.8	-11 12 46.4	19.71	0.00	1.1	-14.18	134

Table A.2: List of the candidate satellite galaxies in the field of NGC 1132.

Number	RA (J2000)	DEC (J2000)	R (mag)	Class	A (arcsec)	M_R (mag)	Dist (kpc)
195	02 52 18.4	-01 17 46.7	13.52	0.03	7.5	-21.28	223
935	02 53 19.8	-01 08 02.5	14.63	0.02	6.4	-20.18	296
279	02 52 24.0	-01 17 14.2	14.72	0.00	8.2	-20.08	184
794	02 53 05.2	-01 25 22.6	14.96	0.03	2.2	-19.85	256
590	02 52 47.7	-01 13 11.5	15.50	0.00	2.9	-19.31	91
465	02 52 37.7	-01 20 56.4	15.85	0.01	1.8	-18.96	150
699	02 52 56.9	-01 17 49.5	15.95	0.03	1.7	-18.85	52
45	02 52 02.3	-01 05 18.6	16.06	0.06	1.2	-18.75	445
351	02 52 29.1	-01 04 22.7	16.14	0.05	1.3	-18.67	357
684	02 52 54.5	-01 04 14.0	16.18	0.00	1.4	-18.62	329
370	02 52 29.1	-01 02 42.7	16.20	0.04	1.3	-18.61	398
698	02 52 55.9	-01 04 09.2	16.40	0.00	1.3	-18.41	332
866	02 53 10.2	-01 15 01.4	16.51	0.00	1.3	-18.30	132
1093	02 53 34.9	-01 17 33.0	16.56	0.00	2.2	-18.25	294
629	02 52 50.0	-01 15 48.3	16.57	0.01	1.0	-18.24	19
718	02 52 57.4	-01 20 53.8	16.59	0.00	0.9	-18.22	125
1222	02 53 37.7	-01 07 54.9	16.64	0.01	1.7	-18.17	387
248	02 52 18.8	-00 58 23.9	16.69	0.00	1.6	-18.12	532
676	02 52 54.0	-01 16 43.9	16.81	0.00	1.1	-17.99	19
466	02 52 37.1	-01 10 10.1	16.97	0.01	1.3	-17.84	194
1082	02 53 33.8	-01 20 44.7	17.02	0.00	1.8	-17.79	307
196	02 52 13.5	-01 02 11.9	17.02	0.02	1.2	-17.79	459
642	02 52 51.1	-01 23 17.3	17.02	0.01	1.2	-17.79	183
407	02 52 33.0	-01 19 06.0	17.03	0.01	1.2	-17.78	141
219	02 52 16.1	-01 08 42.4	17.04	0.03	1.4	-17.77	314
457	02 52 35.7	-01 00 15.2	17.07	0.02	1.2	-17.74	448
1023	02 53 27.1	-01 06 03.4	17.08	0.02	1.4	-17.73	369
1129	02 53 55.5	-00 57 24.4	17.08	0.00	1.5	-17.73	669
802	02 53 04.1	-01 05 04.8	17.10	0.00	1.3	-17.70	317
605	02 52 47.3	-01 15 18.5	17.12	0.00	1.3	-17.69	41
424	02 52 33.9	-01 21 29.5	17.17	0.01	1.1	-17.64	178
610	02 52 47.7	-01 21 07.4	17.21	0.01	1.0	-17.60	127
1058	02 53 31.0	-01 17 04.9	17.22	0.00	1.5	-17.59	267
886	02 53 11.7	-01 19 48.8	17.24	0.02	1.1	-17.57	163
874	02 53 10.5	-01 15 23.4	17.25	0.02	0.9	-17.56	132
402	02 52 32.5	-01 19 37.1	17.28	0.04	1.0	-17.53	152
495	02 52 38.1	-00 58 53.8	17.28	0.01	1.1	-17.53	480
1297	02 53 40.9	-01 14 56.7	17.29	0.00	1.8	-17.52	335
598	02 52 46.7	-01 14 37.5	17.30	0.01	1.5	-17.51	58
889	02 53 12.6	-01 21 07.0	17.30	0.00	1.4	-17.51	189
298	02 52 24.5	-01 04 23.3	17.34	0.01	0.9	-17.47	371
91	02 52 05.4	-01 13 53.5	17.35	0.00	1.4	-17.46	315
818	02 53 05.4	-01 11 31.4	17.37	0.05	1.1	-17.43	163

Table A.2: Candidate satellite galaxies in the field of NGC 1132 (continued).

Number (1)	RA (J2000) (2)	DEC (J2000) (3)	R (mag) (4)	Class (5)	A (arcsec) (6)	M_R (mag) (7)	Dist (kpc) (8)
572	02 52 45.9	-01 20 59.4	17.38	0.08	0.9	-17.43	126
602	02 52 46.9	-01 12 02.2	17.38	0.00	1.3	-17.43	122
695	02 52 55.6	-01 17 14.0	17.39	0.00	1.1	-17.42	35
1039	02 53 28.7	-01 01 36.9	17.44	0.01	1.2	-17.37	471
362	02 52 28.8	-01 08 24.1	17.45	0.01	2.5	-17.36	264
614	02 52 47.3	-01 04 12.5	17.45	0.08	0.8	-17.36	330
1104	02 53 44.7	-01 27 08.3	17.46	0.01	0.9	-17.35	458
651	02 52 52.0	-01 23 44.6	17.50	0.04	1.1	-17.30	195
481	02 52 37.7	-01 21 05.6	17.51	0.06	0.8	-17.30	153
552	02 52 42.9	-01 14 42.3	17.54	0.01	1.1	-17.27	73
1279	02 53 36.4	-01 05 28.1	17.55	0.01	1.0	-17.26	423
915	02 53 15.4	-01 15 31.1	17.56	0.02	1.0	-17.25	164
917	02 53 15.3	-00 59 24.6	17.56	0.03	1.0	-17.25	485
722	02 52 57.2	-01 21 57.9	17.57	0.00	0.7	-17.24	152
586	02 52 45.8	-01 20 48.7	17.62	0.01	0.7	-17.19	122
1107	02 53 49.8	-01 00 28.2	17.65	0.07	0.9	-17.16	582
243	02 52 18.3	-01 04 25.1	17.65	0.02	0.7	-17.16	392
445	02 52 34.7	-01 09 11.3	17.66	0.02	1.1	-17.15	225
988	02 53 23.2	-01 04 55.0	17.67	0.03	0.9	-17.14	377
1312	02 54 00.7	-01 10 44.1	17.70	0.00	1.2	-17.11	490
548	02 52 42.5	-01 20 08.1	17.74	0.02	0.9	-17.07	114
723	02 52 57.2	-01 20 44.8	17.74	0.01	0.5	-17.07	121
462	02 52 36.4	-01 02 27.0	17.75	0.00	1.1	-17.06	389
205	02 52 14.5	-01 14 22.9	17.77	0.00	1.3	-17.04	253
489	02 52 37.8	-01 02 05.8	17.77	0.00	1.0	-17.04	396
1201	02 53 51.1	-01 15 57.4	17.78	0.04	1.0	-17.03	401
453	02 52 35.3	-01 13 58.5	17.78	0.00	1.0	-17.02	126
821	02 53 05.4	-01 08 16.1	17.82	0.00	1.2	-16.98	239
10	02 51 59.6	-01 10 29.9	17.84	0.00	1.2	-16.97	382
765	02 53 00.5	-01 22 45.6	17.84	0.07	0.6	-16.97	179
388	02 52 30.1	-01 04 22.7	17.86	0.02	0.6	-16.95	354
425	02 52 33.3	-01 03 55.4	17.89	0.01	0.8	-16.92	358
80	02 52 04.0	-01 04 02.6	17.91	0.01	0.6	-16.90	460
850	02 53 08.8	-01 23 59.4	17.91	0.00	1.1	-16.90	233
897	02 53 13.0	-01 13 10.0	17.92	0.09	0.8	-16.89	170
1009	02 53 25.0	-01 00 02.8	17.94	0.01	1.2	-16.87	495
517	02 52 40.0	-01 09 13.9	18.01	0.02	1.0	-16.80	208
1187	02 53 56.7	-01 20 34.4	18.02	0.00	1.1	-16.79	452
503	02 52 39.0	-01 11 31.5	18.02	0.00	1.2	-16.79	156
786	02 53 02.9	-01 23 36.8	18.02	0.01	1.0	-16.79	207
430	02 52 33.8	-01 14 43.6	18.05	0.02	0.9	-16.76	126
478	02 52 37.6	-01 21 13.5	18.10	0.05	0.7	-16.71	157
820	02 53 05.4	-01 14 27.4	18.10	0.00	0.9	-16.71	108
1068	02 53 30.8	-01 05 17.5	18.12	0.00	0.9	-16.69	400
499	02 52 38.8	-01 20 10.1	18.12	0.00	1.2	-16.69	130
982	02 53 22.1	-01 04 54.9	18.12	0.00	1.1	-16.69	372
707	02 52 56.0	-01 02 29.4	18.14	0.01	0.6	-16.66	376
914	02 53 15.2	-01 15 48.9	18.14	0.07	0.8	-16.67	161
1321	02 53 59.7	-01 18 06.1	18.15	0.01	1.2	-16.66	461
1017	02 53 26.3	-01 25 48.0	18.16	0.07	0.8	-16.65	343
1314	02 54 01.7	-01 21 27.3	18.17	0.01	0.9	-16.64	491
63	02 52 02.7	-01 03 31.2	18.17	0.01	0.7	-16.64	476
434	02 52 33.9	-01 10 31.3	18.23	0.01	0.9	-16.58	197
549	02 52 42.3	-01 22 54.0	18.24	0.00	0.7	-16.57	182
469	02 52 37.1	-01 16 28.4	18.25	0.09	0.8	-16.56	94
710	02 52 56.7	-01 24 56.6	18.25	0.01	0.8	-16.56	230
828	02 53 05.7	-01 09 45.2	18.26	0.00	1.0	-16.55	204
521	02 52 40.1	-01 21 08.4	18.29	0.09	0.6	-16.52	146
1209	02 53 41.0	-01 26 27.3	18.30	0.00	0.7	-16.51	427
1249	02 53 53.4	-01 24 21.6	18.30	0.01	0.8	-16.51	467
537	02 52 41.6	-01 09 53.4	18.34	0.02	0.8	-16.47	188
972	02 53 20.5	-01 03 23.9	18.34	0.00	0.8	-16.47	402
115	02 52 07.0	-01 23 54.4	18.36	0.05	0.8	-16.45	358
468	02 52 37.1	-01 22 44.5	18.41	0.08	0.7	-16.40	193
484	02 52 37.4	-01 02 03.6	18.42	0.01	0.6	-16.39	398
711	02 52 56.2	-01 01 55.8	18.43	0.02	0.6	-16.38	391
769	02 53 00.6	-01 01 50.4	18.43	0.00	0.9	-16.38	397
1326	02 53 59.0	-00 59 48.9	18.45	0.00	1.1	-16.36	637
1153	02 53 45.3	-01 16 37.7	18.46	0.01	0.9	-16.35	362
1176	02 53 42.1	-01 09 42.6	18.47	0.01	0.7	-16.34	386
558	02 52 43.2	-01 22 24.4	18.47	0.04	0.6	-16.33	168
201	02 52 13.7	-01 09 11.6	18.48	0.01	1.0	-16.33	318
224	02 52 16.6	-01 07 39.6	18.50	0.09	0.8	-16.31	331
825	02 53 05.7	-01 14 13.4	18.50	0.01	0.8	-16.31	113
330	02 52 24.8	-01 17 02.0	18.51	0.04	0.8	-16.30	178
859	02 53 09.3	-01 18 49.5	18.52	0.08	0.7	-16.29	136
855	02 53 08.8	-01 17 47.8	18.54	0.01	0.6	-16.27	122
1346	02 53 33.8	-00 59 15.8	18.56	0.00	1.0	-16.25	543
908	02 53 14.0	-01 15 31.6	18.56	0.03	0.6	-16.25	154
213	02 52 15.1	-01 24 46.9	18.57	0.08	0.8	-16.24	329
237	02 52 17.9	-01 20 59.5	18.57	0.09	0.8	-16.24	255
1076	02 53 32.1	-01 15 10.4	18.59	0.00	1.1	-16.22	276
256	02 52 20.3	-01 24 05.2	18.59	0.01	0.6	-16.22	291
595	02 52 45.8	-00 59 38.0	18.59	0.01	0.7	-16.22	453
959	02 53 19.4	-01 22 02.0	18.59	0.00	0.7	-16.22	240
452	02 52 35.1	-01 15 15.0	18.60	0.07	0.7	-16.21	113
1298	02 53 57.2	-01 00 18.6	18.61	0.01	0.8	-16.20	619
1010	02 53 25.3	-01 21 08.3	18.62	0.00	0.6	-16.19	260
1356	02 54 00.4	-00 57 46.0	18.62	0.01	0.9	-16.19	683
1180	02 53 55.7	-00 59 15.1	18.64	0.03	0.7	-16.16	633

Table A.2: Candidate satellite galaxies in the field of NGC 1132 (continued).

Number (1)	RA (J2000) (2)	DEC (J2000) (3)	R (mag) (4)	Class (5)	A (arcsec) (6)	M_R (mag) (7)	Dist (kpc) (8)
73	02 52 04.1	-01 25 54.0	18.64	0.08	0.6	-16.17	405
907	02 53 14.1	-01 19 53.3	18.65	0.01	0.8	-16.16	178
1088	02 53 33.4	-01 20 45.0	18.66	0.00	0.8	-16.15	305
840	02 53 07.2	-01 00 07.2	18.66	0.08	0.8	-16.15	451
547	02 52 41.6	-01 03 20.0	18.67	0.03	0.7	-16.14	358
851	02 53 08.2	-01 01 05.8	18.67	0.01	0.7	-16.13	428
978	02 53 21.9	-01 21 32.0	18.67	0.04	0.7	-16.14	246
1015	02 53 25.5	-01 04 00.2	18.69	0.00	0.8	-16.12	405
1065	02 53 31.1	-01 21 59.3	18.69	0.03	0.7	-16.12	305
631	02 52 49.3	-01 16 34.4	18.69	0.01	0.7	-16.11	13
1125	02 53 43.8	-01 02 13.0	18.71	0.00	0.8	-16.10	520
419	02 52 32.7	-01 03 27.9	18.72	0.01	0.6	-16.09	371
534	02 52 41.2	-01 11 21.9	18.72	0.00	0.8	-16.09	153
793	02 53 02.9	-01 09 46.0	18.72	0.08	0.5	-16.08	196
788	02 53 03.0	-01 22 45.8	18.73	0.01	0.9	-16.08	186
485	02 52 38.0	-01 21 01.6	18.76	0.00	0.8	-16.05	151
65	02 52 03.1	-01 12 13.3	18.76	0.00	0.7	-16.05	343
714	02 52 56.8	-01 15 41.9	18.76	0.09	0.7	-16.05	42
1089	02 53 33.6	-01 21 34.7	18.77	0.01	0.8	-16.04	315
1277	02 53 56.9	-00 59 56.4	18.77	0.09	0.6	-16.04	625
737	02 52 57.9	-01 10 00.0	18.77	0.09	0.6	-16.04	179
421	02 52 33.2	-00 57 24.1	18.79	0.04	1.0	-16.01	526
88	02 52 04.9	-01 25 11.5	18.80	0.00	0.8	-16.01	389
1171	02 53 43.6	-01 07 49.0	18.81	0.00	0.6	-16.00	420
1342	02 54 00.2	-01 26 56.4	18.81	0.01	0.7	-16.00	541
618	02 52 47.9	-01 22 34.2	18.81	0.01	0.6	-16.00	165
943	02 53 17.7	-01 20 53.2	18.81	0.07	0.6	-16.00	213
1200	02 53 39.4	-00 59 16.6	18.84	0.01	0.6	-15.97	563
604	02 52 46.3	-00 59 51.4	18.84	0.00	0.6	-15.97	447
556	02 52 42.7	-01 20 36.7	18.88	0.00	0.7	-15.93	125
1044	02 53 28.6	-00 59 37.4	18.89	0.00	0.9	-15.92	517
879	02 53 10.4	-01 23 54.4	18.89	0.09	0.7	-15.92	237
1232	02 53 38.0	-01 23 20.8	18.91	0.07	0.6	-15.90	363
241	02 52 18.4	-01 27 01.9	18.92	0.00	0.7	-15.89	359
701	02 52 55.8	-01 09 25.8	18.92	0.01	0.6	-15.89	191
112	02 52 06.1	-01 03 01.8	18.94	0.05	0.6	-15.87	471
1315	02 53 59.9	-00 59 51.1	18.95	0.01	0.8	-15.86	641
100	02 52 05.9	-01 22 33.6	18.96	0.04	0.6	-15.84	345
1144	02 53 50.2	-01 02 30.3	18.96	0.08	0.6	-15.84	545
1165	02 53 44.0	-01 16 38.1	18.98	0.06	0.6	-15.83	353
1238	02 53 39.1	-00 57 45.2	19.03	0.00	0.8	-15.78	596
867	02 53 09.4	-00 59 49.2	19.04	0.01	0.6	-15.77	463
1085	02 53 33.2	-01 23 21.9	19.05	0.02	0.6	-15.76	336
443	02 52 34.7	-01 20 35.9	19.05	0.01	0.7	-15.76	157
659	02 52 52.3	-01 15 24.6	19.05	0.05	0.5	-15.76	29
207	02 52 14.1	-01 06 04.0	19.07	0.02	0.6	-15.74	374
189	02 52 12.4	-01 15 59.3	19.11	0.03	0.5	-15.70	261
444	02 52 34.4	-01 11 00.4	19.11	0.08	0.6	-15.70	185
842	02 53 07.4	-01 04 15.4	19.13	0.02	0.6	-15.68	345
641	02 52 50.5	-01 25 34.2	19.16	0.01	0.7	-15.65	244
551	02 52 42.2	-01 18 29.3	19.18	0.07	0.6	-15.63	81
1278	02 53 36.0	-01 10 10.7	19.19	0.05	0.6	-15.61	344
777	02 53 00.9	-01 01 51.1	19.22	0.02	0.8	-15.58	397
987	02 53 22.9	-01 08 31.0	19.24	0.05	0.6	-15.57	301
772	02 53 01.2	-01 15 32.5	19.25	0.00	1.0	-15.56	71
1181	02 53 40.9	-01 20 03.4	19.26	0.09	0.6	-15.55	346
956	02 53 18.7	-01 17 56.7	19.37	0.09	0.5	-15.44	187
656	02 52 51.6	-01 08 11.6	19.40	0.08	0.5	-15.41	222
583	02 52 45.2	-01 14 46.6	19.42	0.08	0.5	-15.39	61
1338	02 54 03.3	-01 20 01.9	19.47	0.07	0.6	-15.34	492
486	02 52 37.8	-01 20 12.1	19.70	0.07	0.6	-15.11	134

Table A.3: List of the candidate satellite galaxies in the field of NGC 2110.

Number	RA (J2000)	DEC (J2000)	R (mag)	Class	A (arcsec)	M_R (mag)	Dist (kpc)
1819	05 52 07.5	-07 36 12.0	12.51	0.03	9.0	-19.71	73
3276	05 52 34.4	-07 25 40.9	14.15	0.00	5.6	-18.08	49
1656	05 51 58.8	-07 16 41.6	15.41	0.00	4.1	-16.82	90
100	05 51 22.7	-07 33 11.4	15.49	0.00	1.6	-16.74	108
222	05 51 25.5	-07 28 54.6	15.63	0.00	1.4	-16.60	92
1559	05 51 55.3	-07 16 52.0	15.93	0.04	1.4	-16.30	91
7	05 51 19.9	-07 32 44.0	15.96	0.00	1.6	-16.27	112
521	05 51 31.9	-07 32 23.6	16.11	0.00	1.1	-16.11	89
294	05 51 27.3	-07 34 11.4	16.32	0.00	1.6	-15.91	104
4097	05 52 50.7	-07 32 15.6	16.37	0.02	1.5	-15.85	90
409	05 51 30.4	-07 30 16.9	16.38	0.01	1.4	-15.85	85
508	05 51 31.6	-07 32 44.9	16.54	0.00	0.9	-15.68	91
3488	05 52 38.2	-07 25 46.9	16.55	0.02	2.0	-15.68	56
2205	05 52 11.1	-07 27 59.4	16.57	0.02	1.5	-15.66	5
2842	05 52 23.9	-07 24 49.3	16.73	0.02	1.3	-15.50	33
2348	05 52 12.3	-07 20 37.3	16.84	0.02	1.2	-15.39	54
953	05 51 41.5	-07 38 38.9	16.85	0.02	1.2	-15.38	110
216	05 51 24.8	-07 28 43.8	16.86	0.01	0.8	-15.37	94
103	05 51 21.1	-07 28 41.4	16.95	0.00	0.7	-15.28	101
326	05 51 27.3	-07 28 38.3	16.98	0.01	0.7	-15.24	88
136	05 51 22.4	-07 25 51.5	17.02	0.01	1.3	-15.21	98
344	05 51 27.6	-07 28 47.1	17.03	0.02	0.7	-15.19	88
2368	05 52 12.4	-07 26 28.1	17.05	0.00	0.7	-15.18	7

Table A.3: Candidate satellite galaxies in the field of NGC 2110 (continued).

Number (1)	RA (J2000) (2)	DEC (J2000) (3)	R (mag) (4)	Class (5)	A (arcsec) (6)	M_R (mag) (7)	Dist (kpc) (8)
240	05 51 25.5	-07 27 01.4	17.05	0.01	1.2	-15.18	91
729	05 51 36.4	-07 24 40.6	17.16	0.00	2.3	-15.07	73
140	05 51 22.4	-07 33 02.6	17.23	0.00	1.1	-15.00	108
367	05 51 28.6	-07 33 36.0	17.27	0.01	0.7	-14.96	99
2657	05 52 19.0	-07 34 04.3	17.31	0.04	0.9	-14.91	57
2723	05 52 20.3	-07 33 15.0	17.39	0.05	0.8	-14.84	52
795	05 51 37.9	-07 12 18.5	17.42	0.01	1.2	-14.81	139
1709	05 51 58.5	-07 39 03.9	17.44	0.01	1.0	-14.79	99
2851	05 52 24.0	-07 26 08.9	17.45	0.03	1.0	-14.78	28
348	05 51 28.0	-07 27 25.9	17.53	0.00	1.0	-14.70	86
164	05 51 22.9	-07 23 44.8	17.55	0.03	1.0	-14.68	101
2422	05 52 14.2	-07 27 39.8	17.56	0.00	1.2	-14.66	7
579	05 51 32.8	-07 34 02.0	17.56	0.01	0.6	-14.67	94
724	05 51 36.0	-07 33 17.2	17.57	0.00	0.7	-14.66	85
1298	05 51 49.5	-07 32 45.3	17.58	0.01	1.0	-14.64	62
2258	05 52 09.6	-07 28 19.3	17.60	0.01	0.6	-14.62	8
1052	05 51 43.5	-07 15 12.7	17.66	0.00	0.9	-14.57	113
105	05 51 22.1	-07 32 58.9	17.68	0.00	1.1	-14.54	109
1745	05 51 59.5	-07 19 08.5	17.71	0.00	0.9	-14.52	70
2212	05 52 08.6	-07 31 36.2	17.72	0.00	0.8	-14.50	35
2543	05 52 16.6	-07 36 14.4	17.73	0.02	1.0	-14.50	73
4757	05 53 17.0	-07 26 09.9	17.77	0.05	1.1	-14.45	134
3173	05 52 30.5	-07 23 37.1	17.79	0.06	0.9	-14.44	50
2187	05 52 07.8	-07 36 32.3	17.82	0.03	0.6	-14.40	75
141	05 51 22.3	-07 32 58.2	17.84	0.00	1.2	-14.39	108
2544	05 52 16.5	-07 33 35.3	17.88	0.04	0.8	-14.35	52
3449	05 52 36.4	-07 17 25.8	17.92	0.00	0.9	-14.30	95
2673	05 52 18.9	-07 22 51.5	17.96	0.01	0.7	-14.27	39
3213	05 52 31.2	-07 18 12.4	17.96	0.02	0.9	-14.26	85
3345	05 52 34.0	-07 14 34.2	17.96	0.02	0.9	-14.27	114
3975	05 52 47.3	-07 37 16.7	17.97	0.09	0.7	-14.26	110
1601	05 51 55.2	-07 17 41.1	17.99	0.00	0.8	-14.23	84
1333	05 51 50.3	-07 32 57.4	18.01	0.00	0.9	-14.22	62
2157	05 52 07.0	-07 28 13.5	18.02	0.00	0.6	-14.20	10
2982	05 52 26.3	-07 19 18.7	18.02	0.00	1.0	-14.21	72
2579	05 52 17.4	-07 26 28.0	18.08	0.00	1.0	-14.15	15
5030	05 53 01.7	-07 16 45.7	18.08	0.01	0.9	-14.15	134
3838	05 52 44.3	-07 24 44.4	18.10	0.08	0.7	-14.13	70
2485	05 52 15.1	-07 37 08.7	18.11	0.00	0.9	-14.12	80
1372	05 51 51.1	-07 36 26.1	18.12	0.00	0.9	-14.10	84
4547	05 53 24.2	-07 38 18.0	18.13	0.00	1.1	-14.10	173
3872	05 52 44.9	-07 22 06.9	18.14	0.02	1.0	-14.09	80
5089	05 52 56.2	-07 36 41.5	18.16	0.00	1.0	-14.06	119
837	05 51 38.8	-07 33 54.3	18.17	0.00	1.1	-14.05	84
2518	05 52 15.6	-07 15 15.9	18.18	0.08	0.6	-14.05	98
3607	05 52 39.9	-07 31 42.3	18.19	0.00	1.0	-14.04	68
53	05 51 19.6	-07 10 59.9	18.19	0.00	0.9	-14.03	169
3819	05 52 44.2	-07 37 06.8	18.26	0.00	0.9	-13.97	104
1113	05 51 45.3	-07 27 37.6	18.27	0.00	1.1	-13.95	51
1534	05 51 54.0	-07 32 48.7	18.27	0.03	0.9	-13.96	56
133	05 51 21.6	-07 33 19.2	18.28	0.01	0.6	-13.95	111
2178	05 52 07.5	-07 27 34.1	18.28	0.01	0.7	-13.95	7
3563	05 52 38.8	-07 28 07.1	18.29	0.00	0.9	-13.93	57
948	05 51 40.9	-07 34 14.1	18.29	0.00	0.8	-13.94	82
932	05 51 40.1	-07 14 44.3	18.30	0.00	0.8	-13.92	120
1805	05 51 59.8	-07 14 47.1	18.32	0.09	0.6	-13.90	104
2677	05 52 19.0	-07 32 24.0	18.32	0.01	0.5	-13.91	44
5116	05 53 07.7	-07 20 11.2	18.33	0.00	0.7	-13.90	129
1381	05 51 51.2	-07 24 54.4	18.34	0.01	0.9	-13.89	44
2269	05 52 09.8	-07 19 53.8	18.36	0.00	0.7	-13.86	60
363	05 51 28.1	-07 34 10.7	18.36	0.02	0.5	-13.86	103
1804	05 52 00.0	-07 10 41.0	18.37	0.00	0.6	-13.86	137
3331	05 52 33.9	-07 36 51.9	18.37	0.00	0.7	-13.86	91
3502	05 52 37.4	-07 25 05.3	18.37	0.00	0.7	-13.86	56
2645	05 52 18.3	-07 32 00.4	18.39	0.01	0.5	-13.84	41
640	05 51 34.1	-07 29 01.3	18.39	0.09	0.6	-13.84	75
3298	05 52 32.9	-07 17 05.4	18.40	0.07	0.6	-13.82	94
135	05 51 21.6	-07 14 49.7	18.41	0.09	0.6	-13.82	142
349	05 51 27.8	-07 26 52.7	18.41	0.09	0.7	-13.81	87
5483	05 52 58.9	-07 22 22.9	18.42	0.00	1.1	-13.80	105
1213	05 51 47.6	-07 34 22.2	18.43	0.00	1.0	-13.80	74
4183	05 52 51.7	-07 38 02.5	18.43	0.00	0.8	-13.80	120
4938	05 53 11.8	-07 24 36.8	18.43	0.09	0.7	-13.80	125
4427	05 53 22.2	-07 33 02.4	18.44	0.08	0.7	-13.79	152
3967	05 52 47.2	-07 31 35.8	18.45	0.02	0.9	-13.78	81
3110	05 52 29.0	-07 18 39.3	18.47	0.05	0.6	-13.76	79
1242	05 51 47.9	-07 20 24.8	18.48	0.09	0.7	-13.74	73
3075	05 52 28.4	-07 18 30.5	18.48	0.00	0.6	-13.75	80
3194	05 52 30.8	-07 18 08.5	18.48	0.01	0.8	-13.74	85
3810	05 52 43.8	-07 38 44.5	18.48	0.02	0.6	-13.74	114
4260	05 52 53.0	-07 37 30.3	18.48	0.00	0.6	-13.75	119
5388	05 53 00.7	-07 26 07.5	18.48	0.09	0.7	-13.75	101
560	05 51 32.4	-07 33 57.6	18.49	0.00	0.8	-13.74	94
5807	05 53 20.2	-07 32 41.3	18.50	0.00	0.8	-13.72	147
4282	05 52 53.3	-07 23 53.1	18.51	0.00	0.8	-13.71	90
572	05 51 32.6	-07 27 24.7	18.52	0.01	0.6	-13.70	77
3422	05 52 35.8	-07 38 56.5	18.54	0.00	0.7	-13.68	107
2792	05 52 22.8	-07 22 32.5	18.56	0.00	1.6	-13.66	45
2946	05 52 25.7	-07 19 33.0	18.56	0.04	0.6	-13.67	70
2953	05 52 25.5	-07 08 28.2	18.57	0.07	0.5	-13.66	156

Table A.3: Candidate satellite galaxies in the field of NGC 2110 (continued).

Number (1)	RA (J2000) (2)	DEC (J2000) (3)	R (mag) (4)	Class (5)	A (arcsec) (6)	M_R (mag) (7)	Dist (kpc) (8)
3696	05 52 41.1	-07 13 29.9	18.59	0.00	0.6	-13.64	128
1753	05 51 58.9	-07 24 44.7	18.60	0.02	0.6	-13.62	32
3749	05 52 42.0	-07 14 19.1	18.60	0.00	0.8	-13.62	123
504	05 51 31.3	-07 25 50.5	18.60	0.09	0.8	-13.63	80
1133	05 51 45.3	-07 19 03.5	18.62	0.01	0.7	-13.61	85
3540	05 52 38.3	-07 25 40.1	18.62	0.04	0.6	-13.61	57
415	05 51 30.0	-07 30 49.9	18.63	0.00	1.6	-13.59	87
4817	05 53 09.1	-07 20 47.4	18.63	0.04	0.8	-13.59	129
3473	05 52 36.9	-07 34 44.9	18.64	0.09	0.6	-13.59	80
1478	05 51 52.8	-07 11 40.5	18.68	0.05	0.6	-13.54	133
3248	05 52 31.8	-07 18 00.4	18.69	0.05	0.6	-13.54	87
285	05 51 26.0	-07 17 37.8	18.70	0.00	0.8	-13.53	120
539	05 51 31.9	-07 21 03.4	18.70	0.00	0.9	-13.52	94
5448	05 52 59.1	-07 36 42.6	18.70	0.07	0.6	-13.53	124
4242	05 52 52.5	-07 25 52.4	18.71	0.01	0.6	-13.52	85
4435	05 53 20.0	-07 37 16.3	18.71	0.00	0.7	-13.52	162
4152	05 52 51.0	-07 37 19.8	18.75	0.00	0.7	-13.48	115
3662	05 52 40.8	-07 26 34.7	18.77	0.04	0.6	-13.46	61
5277	05 53 04.5	-07 22 39.2	18.77	0.07	0.6	-13.45	115
1327	05 51 49.7	-07 09 50.7	18.78	0.09	0.7	-13.44	149
3894	05 52 45.6	-07 37 45.1	18.78	0.03	0.6	-13.44	110
3883	05 52 45.3	-07 37 23.5	18.81	0.01	0.7	-13.41	108
5074	05 53 08.7	-07 35 37.8	18.81	0.01	1.0	-13.41	135
2969	05 52 26.1	-07 28 40.8	18.82	0.03	0.6	-13.41	32
1886	05 52 01.3	-07 12 46.5	18.84	0.00	0.7	-13.38	120
3686	05 52 40.9	-07 07 44.6	18.84	0.03	0.6	-13.39	171
3601	05 52 39.5	-07 38 07.3	18.85	0.05	0.6	-13.37	105
543	05 51 31.8	-07 37 23.4	18.85	0.06	0.6	-13.37	114
577	05 51 32.7	-07 33 58.8	18.85	0.01	0.8	-13.38	94
197	05 51 23.7	-07 38 02.8	18.86	0.07	0.6	-13.37	129
2085	05 52 05.5	-07 27 20.7	18.88	0.03	0.5	-13.35	10
4969	05 53 11.0	-07 14 47.5	18.90	0.01	0.9	-13.32	159
5126	05 53 07.6	-07 33 35.5	18.91	0.05	0.6	-13.31	126
179	05 51 23.1	-07 33 55.7	18.94	0.01	0.6	-13.29	110
3325	05 52 33.4	-07 19 32.0	18.94	0.03	0.7	-13.29	78
3818	05 52 44.0	-07 38 20.8	18.94	0.01	0.5	-13.29	112
5193	05 53 05.1	-07 38 34.2	18.94	0.08	0.6	-13.29	143
5496	05 52 56.5	-07 30 15.2	18.95	0.07	0.6	-13.27	95
72	05 51 20.1	-07 36 07.7	18.95	0.05	0.6	-13.28	125
2372	05 52 12.3	-07 32 48.5	18.98	0.04	0.5	-13.25	45
708	05 51 35.5	-07 16 40.4	18.98	0.01	0.7	-13.25	112
282	05 51 26.1	-07 22 59.7	18.99	0.00	0.7	-13.24	97
4890	05 53 11.7	-07 25 15.2	19.01	0.01	0.6	-13.21	124
643	05 51 34.2	-07 34 38.7	19.06	0.04	0.5	-13.17	95
1857	05 52 00.7	-07 11 57.6	19.07	0.08	0.6	-13.16	127
2127	05 52 06.5	-07 23 05.6	19.11	0.01	0.8	-13.12	35
1154	05 51 46.0	-07 31 39.4	19.12	0.09	0.5	-13.10	61
732	05 51 36.0	-07 23 46.0	19.13	0.09	0.5	-13.09	76
1030	05 51 42.7	-07 20 43.8	19.14	0.08	0.6	-13.08	78
3569	05 52 38.6	-07 21 40.1	19.14	0.06	0.5	-13.09	72
714	05 51 35.8	-07 37 16.0	19.14	0.08	0.5	-13.09	108
1061	05 51 43.9	-07 38 24.2	19.15	0.07	0.6	-13.08	105
2201	05 52 07.9	-07 24 13.8	19.15	0.03	0.6	-13.08	25
4150	05 52 50.4	-07 19 17.7	19.21	0.00	0.6	-13.01	103
4696	05 53 18.1	-07 28 03.7	19.21	0.01	0.5	-13.01	136
1523	05 51 53.6	-07 33 07.1	19.24	0.08	0.5	-12.98	58
477	05 51 30.5	-07 26 39.9	19.25	0.09	0.5	-12.98	81
562	05 51 32.0	-07 13 21.9	19.25	0.03	0.6	-12.97	138
4500	05 53 08.8	-07 21 22.3	19.28	0.02	0.6	-12.94	127
500	05 51 31.0	-07 23 11.2	19.28	0.01	0.6	-12.94	87
662	05 51 34.6	-07 37 34.9	19.29	0.08	0.6	-12.94	111
4205	05 52 51.4	-07 19 11.9	19.30	0.07	0.5	-12.93	105
3938	05 52 46.0	-07 16 56.1	19.31	0.08	0.6	-12.92	110
1165	05 51 46.2	-07 26 12.0	19.32	0.09	0.5	-12.90	50
3330	05 52 33.8	-07 38 59.1	19.32	0.01	0.6	-12.91	106
271	05 51 25.9	-07 21 52.6	19.34	0.03	0.5	-12.88	101
218	05 51 24.1	-07 11 59.5	19.36	0.02	0.6	-12.86	157
2628	05 52 18.0	-07 36 58.6	19.38	0.09	0.5	-12.85	80
2600	05 52 17.3	-07 20 30.8	19.42	0.06	0.5	-12.81	57
768	05 51 36.7	-07 24 16.4	19.43	0.07	0.5	-12.80	73
199	05 51 23.4	-07 21 05.1	19.45	0.05	0.5	-12.78	108
67	05 51 20.1	-07 28 46.7	19.45	0.02	0.6	-12.77	103

Table A.4: List of the candidate satellite galaxies in the field of NGC 2865.

Number	RA (J2000)	DEC (J2000)	R (mag)	Class	A (arcsec)	M_R (mag)	Dist (kpc)
4284	09 23 56.0	-22 53 42.6	15.78	0.00	4.4	-16.94	174
6933	09 24 20.3	-23 02 56.9	15.96	0.03	3.0	-16.76	137
2595	09 23 24.5	-23 11 07.5	16.05	0.03	2.2	-16.67	19
2641	09 23 25.5	-23 08 06.5	16.08	0.03	2.5	-16.64	18
6741	09 24 25.1	-23 06 26.5	16.10	0.03	2.6	-16.62	134
2300	09 23 19.2	-23 08 16.8	16.32	0.03	2.0	-16.40	28
108	09 22 38.0	-23 20 15.6	16.56	0.02	2.4	-16.16	163
5569	09 24 17.0	-22 53 50.8	16.62	0.01	1.6	-16.10	195
7369	09 24 46.8	-23 18 25.5	16.65	0.02	2.2	-16.07	202
1671	09 23 09.5	-23 19 23.0	16.73	0.02	3.5	-15.99	111
929	09 22 53.1	-22 55 10.5	16.76	0.03	1.4	-15.96	171
6930	09 24 22.9	-23 19 45.6	16.77	0.00	2.8	-15.95	162

Table A.4: Candidate satellite galaxies in the field of NGC 2865 (continued).

Number (1)	RA (J2000) (2)	DEC (J2000) (3)	R (mag) (4)	Class (5)	A (arcsec) (6)	M_R (mag) (7)	Dist (kpc) (8)
4640	09 24 00.1	-22 52 15.4	16.88	0.03	1.6	-15.84	191
2791	09 23 27.7	-23 19 55.6	16.89	0.03	2.5	-15.83	105
1955	09 23 12.6	-22 53 15.9	16.90	0.03	1.4	-15.82	172
3716	09 23 44.9	-23 08 47.9	16.90	0.01	2.0	-15.82	36
1072	09 22 56.1	-23 02 20.5	17.02	0.00	2.3	-15.70	108
5716	09 24 45.5	-22 57 27.8	17.09	0.03	1.4	-15.63	217
3394	09 23 37.7	-23 10 10.8	17.10	0.02	1.6	-15.62	19
2904	09 23 29.6	-23 11 35.6	17.19	0.02	3.1	-15.53	20
2016	09 23 13.4	-23 12 35.6	17.24	0.03	1.5	-15.48	49
1553	09 23 05.1	-22 54 17.3	17.31	0.01	2.0	-15.41	167
3954	09 23 48.7	-23 03 47.1	17.36	0.02	2.2	-15.36	74
3094	09 23 34.1	-23 18 42.8	17.42	0.00	2.5	-15.30	93
7080	09 24 19.7	-23 13 55.2	17.43	0.00	2.0	-15.29	125
5866	09 24 42.1	-23 00 00.6	17.45	0.00	2.0	-15.27	196
55	09 22 36.6	-23 19 26.7	17.49	0.00	2.0	-15.23	160
3240	09 23 34.4	-22 56 08.3	17.54	0.03	1.2	-15.18	138
3245	09 23 35.1	-23 06 00.2	17.56	0.02	2.0	-15.16	39
7281	09 24 45.5	-23 05 11.8	17.62	0.06	1.1	-15.10	183
809	09 22 50.7	-23 11 57.4	17.68	0.03	1.4	-15.04	95
2812	09 23 26.9	-23 08 21.0	17.69	0.01	1.0	-15.03	14
2290	09 23 18.5	-23 16 51.7	17.70	0.02	1.6	-15.02	79
2704	09 23 25.4	-23 07 04.2	17.72	0.03	1.6	-15.00	28
7188	09 24 17.6	-22 54 08.5	17.77	0.00	0.8	-14.95	194
3801	09 23 45.5	-23 09 05.8	17.79	0.03	1.0	-14.93	37
4110	09 23 50.1	-22 58 30.1	17.87	0.01	1.4	-14.85	123
6150	09 24 38.2	-22 53 20.0	17.87	0.02	1.3	-14.85	231
3934	09 23 47.9	-23 19 10.5	17.88	0.00	2.0	-14.84	106
3339	09 23 36.1	-23 10 03.3	17.90	0.06	1.0	-14.82	15
3851	09 23 46.6	-23 14 48.3	17.91	0.03	1.2	-14.81	66
6898	09 24 19.5	-22 54 38.4	17.91	0.00	0.8	-14.81	192
847	09 22 51.2	-23 07 37.3	17.91	0.02	2.0	-14.81	93
6529	09 24 29.3	-23 07 00.4	17.93	0.05	1.0	-14.79	142
3855	09 23 46.3	-22 53 29.3	17.95	0.02	1.3	-14.77	169
5686	09 24 49.4	-23 16 34.6	17.96	0.04	1.0	-14.76	200
6018	09 24 38.0	-22 53 38.9	17.97	0.00	2.0	-14.75	229
4327	09 23 53.9	-22 56 28.0	17.99	0.05	1.0	-14.73	146
4337	09 23 54.3	-23 16 14.8	17.99	0.01	2.0	-14.73	89
715	09 22 48.9	-23 02 14.9	18.01	0.01	1.6	-14.71	122
2568	09 23 23.3	-23 10 20.5	18.02	0.01	2.0	-14.70	17
3362	09 23 36.6	-23 08 17.3	18.03	0.04	1.1	-14.69	21
403	09 22 42.6	-23 06 34.4	18.04	0.03	1.3	-14.68	115
5653	09 24 21.4	-22 52 51.3	18.04	0.00	0.8	-14.68	209
3323	09 23 36.5	-23 17 30.6	18.05	0.00	1.5	-14.67	82
2063	09 23 14.0	-23 07 00.4	18.06	0.00	1.2	-14.66	45
411	09 22 42.9	-23 17 56.0	18.06	0.01	2.0	-14.66	139
6302	09 24 32.8	-22 53 45.5	18.06	0.01	1.0	-14.66	220
1182	09 22 57.4	-22 55 07.1	18.10	0.01	1.3	-14.62	166
3972	09 23 48.1	-23 09 58.7	18.10	0.05	1.0	-14.62	43
1877	09 23 10.7	-23 20 59.4	18.12	0.04	0.9	-14.60	125
5628	09 24 48.3	-23 07 58.9	18.12	0.01	1.1	-14.60	185
3173	09 23 33.5	-23 11 40.5	18.17	0.03	1.0	-14.55	23
1024	09 22 54.6	-23 16 18.0	18.18	0.02	1.4	-14.54	107
7064	09 24 19.3	-22 53 04.6	18.21	0.00	0.9	-14.51	205
7309	09 24 42.0	-23 00 09.9	18.21	0.04	1.1	-14.51	195
4822	09 24 03.8	-23 18 20.4	18.22	0.01	1.5	-14.50	120
3742	09 23 44.2	-23 13 03.3	18.24	0.00	1.4	-14.48	49
5443	09 24 14.7	-23 20 12.4	18.27	0.01	1.2	-14.45	151
5382	09 24 13.4	-23 13 21.9	18.28	0.01	1.2	-14.44	109
3184	09 23 33.4	-23 02 18.4	18.29	0.03	1.0	-14.43	75
7146	09 24 18.0	-22 53 10.0	18.33	0.00	0.7	-14.39	202
1141	09 22 56.7	-23 20 24.8	18.34	0.01	1.1	-14.38	135
3682	09 23 42.9	-23 03 45.7	18.35	0.02	2.0	-14.37	67
1592	09 23 05.2	-23 02 37.1	18.36	0.01	1.2	-14.36	92
2667	09 23 24.0	-23 09 54.5	18.36	0.03	0.9	-14.36	14
7119	09 24 18.3	-23 20 52.7	18.36	0.00	1.2	-14.36	162
5157	09 24 09.4	-23 10 59.0	18.37	0.06	1.0	-14.35	94
5965	09 24 28.1	-22 52 14.4	18.38	0.05	1.0	-14.34	224
6339	09 24 31.4	-23 07 05.3	18.39	0.01	1.4	-14.33	147
7379	09 24 47.0	-23 02 17.4	18.39	0.03	2.0	-14.33	196
625	09 22 46.7	-22 50 50.6	18.41	0.02	1.0	-14.31	217
21	09 22 34.6	-23 11 47.4	18.43	0.01	1.3	-14.29	131
3861	09 23 46.1	-23 09 16.4	18.44	0.04	0.9	-14.28	38
5196	09 24 10.1	-23 16 03.1	18.44	0.05	0.9	-14.28	115
3295	09 23 35.8	-23 18 59.6	18.45	0.02	1.1	-14.27	97
2974	09 23 29.3	-23 10 44.0	18.46	0.00	0.6	-14.26	11
3299	09 23 35.1	-23 09 59.1	18.46	0.00	0.7	-14.26	13
5901	09 24 42.8	-23 10 50.5	18.46	0.05	0.9	-14.26	172
6826	09 24 46.7	-23 02 51.8	18.46	0.08	1.0	-14.26	193
6624	09 24 28.3	-22 59 32.5	18.47	0.03	1.0	-14.25	172
1339	09 23 00.8	-22 54 38.4	18.48	0.01	1.3	-14.24	167
3537	09 23 39.4	-23 09 08.2	18.48	0.01	1.0	-14.24	23
4338	09 23 54.3	-23 20 44.4	18.48	0.02	1.2	-14.24	127
3080	09 23 31.7	-23 07 23.3	18.49	0.01	1.0	-14.23	23
573	09 22 45.7	-22 52 34.3	18.49	0.00	1.0	-14.23	203
6103	09 24 37.5	-22 55 40.1	18.49	0.06	0.9	-14.23	214
936	09 22 52.7	-23 06 05.6	18.51	0.02	1.0	-14.21	94
4504	09 23 57.2	-23 04 17.1	18.53	0.01	1.2	-14.19	84
884	09 22 52.4	-23 08 13.4	18.55	0.00	2.0	-14.17	88
1170	09 22 57.7	-22 55 38.2	18.57	0.00	1.2	-14.15	161
2703	09 23 24.5	-23 03 22.2	18.57	0.06	0.8	-14.15	65

Table A.4: Candidate satellite galaxies in the field of NGC 2865 (continued).

Number (1)	RA (J2000) (2)	DEC (J2000) (3)	R (mag) (4)	Class (5)	A (arcsec) (6)	M_R (mag) (7)	Dist (kpc) (8)
2106	09 23 14.6	-22 56 06.0	18.58	0.01	1.0	-14.14	143
2111	09 23 14.9	-23 19 55.6	18.60	0.00	1.3	-14.12	111
2762	09 23 25.5	-23 05 15.7	18.60	0.00	0.6	-14.12	45
1814	09 23 09.1	-22 59 03.7	18.62	0.00	1.2	-14.10	118
3061	09 23 31.4	-23 04 19.0	18.63	0.01	1.1	-14.09	54
3253	09 23 34.7	-23 16 28.1	18.64	0.01	1.1	-14.08	71
2409	09 23 20.0	-23 18 09.8	18.65	0.01	1.0	-14.07	90
3047	09 23 30.9	-22 57 01.4	18.65	0.07	0.9	-14.07	129
4265	09 23 52.3	-22 54 44.2	18.65	0.07	1.0	-14.07	161
6419	09 24 31.5	-23 12 34.6	18.66	0.02	0.9	-14.06	148
3834	09 23 45.9	-23 07 56.0	18.67	0.05	0.9	-14.05	41
4756	09 24 02.4	-22 50 52.0	18.67	0.00	2.0	-14.05	206
3084	09 23 32.1	-23 08 45.7	18.69	0.00	1.1	-14.03	10
3130	09 23 32.4	-22 53 33.7	18.69	0.02	1.1	-14.03	164
2794	09 23 26.0	-23 08 17.4	18.70	0.00	0.6	-14.02	16
289	09 22 40.2	-23 04 32.5	18.72	0.01	1.3	-14.00	127
1381	09 23 01.0	-23 17 43.8	18.73	0.04	0.8	-13.99	107
3685	09 23 43.0	-23 07 57.0	18.73	0.01	1.3	-13.99	35
40	09 22 35.3	-23 03 49.0	18.73	0.01	1.0	-13.99	141
6027	09 24 38.2	-22 53 27.9	18.73	0.07	1.0	-13.99	230
2049	09 23 13.4	-23 08 41.2	18.74	0.01	0.8	-13.98	39
2830	09 23 27.4	-23 04 18.6	18.74	0.01	1.3	-13.98	54
3550	09 23 39.6	-23 08 53.0	18.75	0.07	0.9	-13.97	24
6135	09 24 36.5	-23 03 22.2	18.76	0.01	0.9	-13.96	169
2090	09 23 14.2	-23 09 55.7	18.77	0.01	1.1	-13.95	36
677	09 22 47.6	-23 08 20.2	18.77	0.01	0.9	-13.95	100
1845	09 23 10.0	-23 04 08.6	18.78	0.00	1.1	-13.94	73
3182	09 23 33.6	-23 20 07.3	18.78	0.01	0.9	-13.94	108
4020	09 23 48.5	-23 10 06.8	18.79	0.04	0.8	-13.93	44
1618	09 23 05.2	-22 53 23.5	18.80	0.01	1.0	-13.92	176
5309	09 24 11.2	-22 50 07.6	18.80	0.01	1.0	-13.92	222
569	09 22 45.4	-22 52 12.9	18.80	0.03	0.9	-13.92	206
6691	09 24 22.3	-23 11 23.1	18.80	0.01	1.0	-13.92	125
3012	09 23 31.3	-23 08 39.9	18.81	0.00	0.8	-13.91	10
6607	09 24 23.8	-22 56 16.9	18.82	0.00	0.6	-13.90	186
2953	09 23 29.0	-23 01 09.9	18.83	0.03	0.9	-13.89	86
5830	09 24 43.7	-23 00 04.3	18.83	0.02	0.9	-13.89	199
6181	09 24 35.8	-22 51 36.1	18.83	0.01	1.2	-13.89	241
3015	09 23 30.5	-23 12 08.2	18.84	0.01	1.0	-13.88	26
2874	09 23 29.7	-23 08 25.6	18.85	0.01	0.5	-13.87	12
3949	09 23 47.5	-23 09 29.3	18.85	0.03	0.8	-13.87	42
2238	09 23 16.5	-23 06 39.7	18.86	0.03	1.0	-13.86	43
4866	09 24 03.5	-23 00 41.4	18.86	0.02	1.0	-13.86	121
2147	09 23 15.3	-23 07 10.3	18.89	0.00	1.3	-13.83	42
3503	09 23 39.1	-23 17 17.2	18.89	0.00	1.5	-13.83	81
6726	09 24 26.1	-23 06 09.7	18.89	0.01	0.9	-13.83	137
4331	09 23 54.2	-23 15 24.0	18.90	0.00	1.0	-13.82	82
1224	09 22 57.5	-22 53 08.9	18.92	0.00	0.8	-13.80	184
5289	09 24 11.2	-23 06 42.1	18.94	0.01	1.0	-13.78	102
2707	09 23 25.3	-23 09 15.6	18.95	0.00	0.9	-13.77	11
2800	09 23 26.2	-23 04 34.7	18.95	0.00	0.7	-13.77	52
4329	09 23 53.8	-22 56 03.8	18.95	0.01	1.0	-13.77	149
6227	09 24 35.9	-23 07 35.2	18.95	0.03	0.8	-13.77	157
6600	09 24 27.5	-22 55 56.9	18.95	0.01	0.7	-13.77	194
6965	09 24 20.3	-22 55 24.2	18.95	0.06	0.5	-13.77	187
6119	09 24 38.1	-22 58 48.9	18.96	0.01	0.9	-13.76	195
5698	09 24 46.0	-23 05 14.6	18.97	0.03	0.9	-13.75	184
7377	09 24 46.9	-23 04 53.7	18.97	0.04	1.1	-13.75	187
2930	09 23 28.7	-23 07 54.5	18.99	0.06	0.8	-13.73	17
4551	09 23 57.9	-23 10 45.4	18.99	0.05	0.8	-13.73	67
7284	09 24 47.2	-23 20 43.6	18.99	0.00	1.5	-13.73	214
172	09 22 37.7	-22 59 30.8	19.02	0.05	0.8	-13.70	160
2753	09 23 25.2	-22 50 50.5	19.02	0.01	1.0	-13.70	192
3520	09 23 39.0	-23 02 45.0	19.02	0.05	0.9	-13.70	73
1489	09 23 03.6	-23 02 36.7	19.03	0.00	1.5	-13.69	94
2983	09 23 30.0	-23 16 26.7	19.03	0.00	1.0	-13.69	70
5969	09 24 40.5	-23 06 46.9	19.03	0.01	1.0	-13.69	169
2820	09 23 26.5	-23 00 51.7	19.04	0.01	1.1	-13.68	90
4240	09 23 52.3	-23 15 49.0	19.04	0.01	0.9	-13.68	82
1478	09 23 03.0	-23 07 21.1	19.05	0.01	0.9	-13.67	67
6443	09 24 31.5	-22 59 39.5	19.05	0.00	1.3	-13.67	177
6788	09 24 21.0	-22 52 28.8	19.05	0.06	0.5	-13.67	212
684	09 22 47.7	-23 08 15.2	19.05	0.01	0.8	-13.67	100
6925	09 24 22.7	-23 06 33.4	19.05	0.00	1.0	-13.67	128
3592	09 23 40.5	-23 11 52.1	19.06	0.01	1.1	-13.66	34
3788	09 23 45.3	-23 07 56.6	19.06	0.08	0.8	-13.66	40
4626	09 23 59.2	-23 12 40.1	19.06	0.03	1.0	-13.66	76
2237	09 23 16.9	-23 11 53.2	19.07	0.02	1.0	-13.65	38
3906	09 23 46.7	-23 08 49.5	19.08	0.06	0.9	-13.64	40
4987	09 24 06.0	-23 12 40.0	19.08	0.07	0.9	-13.64	91
1589	09 23 04.7	-22 58 57.2	19.10	0.02	0.8	-13.62	124
2500	09 23 21.4	-23 09 18.7	19.10	0.02	0.8	-13.62	20
7245	09 24 29.9	-23 18 35.2	19.11	0.00	1.0	-13.61	168
3101	09 23 32.5	-23 02 45.9	19.12	0.00	2.0	-13.60	70
2427	09 23 20.2	-23 04 06.0	19.13	0.04	0.7	-13.59	60
489	09 22 44.2	-23 20 01.2	19.13	0.01	0.8	-13.59	151
332	09 22 41.1	-22 58 35.5	19.14	0.00	0.8	-13.58	161
682	09 22 47.5	-22 52 30.4	19.14	0.00	1.2	-13.58	201
6695	09 24 27.1	-23 11 57.7	19.18	0.00	1.3	-13.54	136
7042	09 24 21.1	-23 16 46.1	19.18	0.01	0.9	-13.54	141

Table A.4: Candidate satellite galaxies in the field of NGC 2865 (continued).

Number (1)	RA (J2000) (2)	DEC (J2000) (3)	R (mag) (4)	Class (5)	A (arcsec) (6)	M_R (mag) (7)	Dist (kpc) (8)
2519	09 23 21.4	-23 05 33.4	19.19	0.04	0.9	-13.53	46
1615	09 23 05.5	-23 17 58.6	19.20	0.00	1.1	-13.52	103
3604	09 23 40.2	-22 50 12.5	19.20	0.01	0.9	-13.52	100
4094	09 23 49.6	-23 04 35.2	19.20	0.02	0.8	-13.52	69
6290	09 24 31.9	-22 55 11.3	19.20	0.01	0.5	-13.52	207
2396	09 23 19.6	-23 12 32.8	19.21	0.01	0.9	-13.51	38
6191	09 24 35.6	-23 12 05.5	19.21	0.01	0.8	-13.51	157
1284	09 22 58.8	-22 53 49.6	19.23	0.01	0.7	-13.49	177
3153	09 23 32.6	-23 11 41.0	19.23	0.02	0.8	-13.49	22
4064	09 23 49.3	-23 12 23.0	19.23	0.01	0.9	-13.49	54
6534	09 24 47.6	-23 00 50.0	19.24	0.02	0.7	-13.48	203
1144	09 22 56.4	-23 04 37.2	19.26	0.02	0.9	-13.46	93
1155	09 22 56.3	-22 53 22.9	19.26	0.08	0.7	-13.46	183
1101	09 22 55.3	-22 52 40.9	19.27	0.00	0.8	-13.45	191
1270	09 22 58.7	-23 09 16.5	19.27	0.00	0.9	-13.45	73
1513	09 23 03.5	-22 57 15.2	19.28	0.01	1.0	-13.44	140
3411	09 23 37.3	-23 18 38.5	19.28	0.04	0.8	-13.44	93
4204	09 23 51.2	-23 06 23.2	19.28	0.07	0.7	-13.44	60
5927	09 24 27.5	-23 14 07.6	19.28	0.06	0.7	-13.44	143
2640	09 23 23.1	-22 51 12.1	19.29	0.06	0.7	-13.43	188
320	09 22 40.9	-23 12 31.0	19.29	0.01	0.8	-13.43	118
6644	09 24 29.1	-23 07 03.0	19.30	0.00	1.1	-13.42	142
2942	09 23 29.5	-23 13 53.0	19.31	0.04	1.1	-13.41	44
3899	09 23 46.6	-23 07 14.2	19.31	0.00	0.9	-13.41	46
5048	09 24 07.1	-23 12 25.2	19.31	0.05	0.8	-13.41	92
6710	09 24 26.1	-23 09 42.5	19.31	0.00	1.1	-13.41	132
2583	09 23 22.9	-23 05 18.6	19.33	0.01	0.9	-13.39	47
3848	09 23 46.0	-23 12 42.9	19.33	0.00	0.8	-13.39	49
4185	09 23 50.9	-23 08 56.2	19.33	0.03	0.8	-13.39	50
5264	09 24 10.7	-22 55 01.8	19.33	0.00	0.8	-13.39	177
6612	09 24 27.7	-22 53 00.1	19.33	0.01	0.8	-13.39	217
1663	09 23 06.2	-23 02 46.6	19.34	0.00	1.2	-13.38	89
2252	09 23 16.5	-22 51 40.0	19.34	0.06	0.7	-13.38	186
2241	09 23 16.4	-23 06 23.3	19.35	0.07	1.0	-13.37	45
2473	09 23 20.6	-23 01 06.5	19.35	0.06	0.7	-13.37	89
1764	09 23 07.9	-23 05 25.9	19.36	0.09	0.7	-13.36	66
249	09 22 39.5	-22 50 18.7	19.36	0.01	0.9	-13.36	230
2569	09 23 21.9	-23 04 29.4	19.36	0.03	0.5	-13.36	55
2643	09 23 23.2	-22 51 21.7	19.36	0.05	0.8	-13.36	187
3516	09 23 38.6	-22 54 10.0	19.36	0.00	1.0	-13.36	159
4498	09 23 56.9	-23 05 33.5	19.36	0.01	1.0	-13.36	76
6258	09 24 30.5	-23 18 21.5	19.36	0.00	0.8	-13.36	168
2177	09 23 15.5	-23 07 01.4	19.37	0.07	0.6	-13.35	42
2388	09 23 19.2	-23 04 55.0	19.37	0.05	0.7	-13.35	54
3006	09 23 30.0	-23 01 47.4	19.38	0.00	0.8	-13.34	80
5373	09 24 12.9	-23 12 41.8	19.38	0.01	1.0	-13.34	106
202	09 22 38.7	-23 21 28.0	19.39	0.09	0.8	-13.33	170
3833	09 23 45.5	-23 04 04.4	19.40	0.04	0.8	-13.32	67
4448	09 23 56.3	-23 06 52.0	19.40	0.00	1.2	-13.32	68
2961	09 23 29.4	-23 19 43.6	19.41	0.05	0.8	-13.31	103
2295	09 23 17.7	-23 07 06.3	19.42	0.02	0.7	-13.30	38
3175	09 23 33.0	-23 07 57.0	19.42	0.02	0.9	-13.30	18
6468	09 24 29.9	-23 06 42.2	19.42	0.01	0.9	-13.30	144
3626	09 23 41.4	-23 16 36.6	19.43	0.00	1.3	-13.29	76
5791	09 24 43.6	-23 06 22.2	19.43	0.00	0.9	-13.29	176
2168	09 23 15.3	-22 54 06.9	19.45	0.02	0.8	-13.27	162
6193	09 24 37.4	-23 12 55.8	19.45	0.00	1.0	-13.27	162
1785	09 23 08.0	-22 59 41.1	19.46	0.00	0.6	-13.26	113
2119	09 23 14.5	-23 07 12.2	19.46	0.09	0.6	-13.26	43
2940	09 23 28.5	-23 08 05.5	19.46	0.01	0.5	-13.26	15
2885	09 23 27.9	-23 06 20.6	19.47	0.01	0.8	-13.25	33
3725	09 23 43.5	-23 04 17.8	19.47	0.01	0.8	-13.25	63
561	09 22 45.3	-23 10 56.1	19.48	0.02	0.8	-13.24	105
6047	09 24 39.0	-23 00 00.4	19.48	0.00	0.8	-13.24	190
4170	09 23 50.5	-22 58 38.3	19.49	0.00	0.7	-13.23	122
680	09 22 47.5	-23 11 47.4	19.49	0.04	0.7	-13.23	101
1923	09 23 11.1	-23 00 49.7	19.50	0.01	1.0	-13.22	100
2627	09 23 23.2	-23 01 26.5	19.50	0.00	1.1	-13.22	85
4849	09 24 03.3	-23 04 21.9	19.50	0.07	0.8	-13.22	95
5070	09 24 07.2	-22 54 32.1	19.51	0.00	1.1	-13.21	177
6331	09 24 32.9	-23 17 04.9	19.51	0.03	0.9	-13.21	167
1933	09 23 11.7	-23 21 13.4	19.52	0.00	0.8	-13.20	126
3701	09 23 43.0	-22 57 38.4	19.52	0.00	1.3	-13.20	126
4976	09 24 05.6	-23 14 33.6	19.53	0.04	0.8	-13.19	98
6005	09 24 37.4	-23 03 20.5	19.53	0.04	0.7	-13.19	171
6463	09 24 31.9	-23 17 52.9	19.53	0.00	1.1	-13.19	169
7154	09 24 26.1	-23 15 08.4	19.54	0.02	0.8	-13.18	144
5859	09 24 43.3	-23 13 07.0	19.55	0.00	1.0	-13.17	176
7298	09 24 33.1	-23 01 19.8	19.55	0.00	0.8	-13.17	171
2967	09 23 29.5	-23 14 17.1	19.56	0.00	0.9	-13.16	48
3373	09 23 36.4	-23 09 14.2	19.56	0.01	0.6	-13.16	15
3838	09 23 45.6	-23 06 19.0	19.56	0.01	0.7	-13.16	50
5177	09 24 09.3	-23 08 28.0	19.56	0.01	0.8	-13.16	93
6616	09 24 28.3	-23 19 59.3	19.56	0.06	0.7	-13.16	173
3795	09 23 44.7	-23 04 48.5	19.57	0.04	0.9	-13.15	60
4356	09 23 54.4	-23 16 23.2	19.57	0.08	0.7	-13.15	90
6743	09 24 26.4	-23 06 16.8	19.58	0.09	0.7	-13.14	137
1439	09 23 02.0	-23 19 14.2	19.59	0.00	1.4	-13.13	118
41	09 22 35.0	-23 00 56.1	19.59	0.00	0.6	-13.13	156
4892	09 24 04.0	-23 14 31.5	19.59	0.00	0.7	-13.13	94

Table A.4: Candidate satellite galaxies in the field of NGC 2865 (continued).

Number (1)	RA (J2000) (2)	DEC (J2000) (3)	R (mag) (4)	Class (5)	A (arcsec) (6)	M_R (mag) (7)	Dist (kpc) (8)
7161	09 24 18.0	-22 55 57.6	19.59	0.01	0.6	-13.13	179
2363	09 23 18.5	-22 52 42.0	19.60	0.00	0.7	-13.12	174
3354	09 23 35.8	-22 52 14.9	19.60	0.09	0.7	-13.12	178
3905	09 23 46.8	-23 16 35.5	19.60	0.07	0.7	-13.12	81
6970	09 24 22.4	-23 13 52.6	19.60	0.00	1.1	-13.12	131
4399	09 23 55.6	-23 20 31.3	19.61	0.00	0.9	-13.11	127
6024	09 24 35.9	-22 53 18.6	19.61	0.00	0.7	-13.11	227
3206	09 23 33.4	-23 10 56.8	19.62	0.08	0.5	-13.10	16
3583	09 23 40.2	-23 21 20.0	19.62	0.07	0.7	-13.10	122
1959	09 23 11.9	-23 18 23.7	19.63	0.08	0.8	-13.09	99
4258	09 23 52.3	-23 09 47.6	19.63	0.08	0.6	-13.09	53
1547	09 23 04.1	-23 16 10.7	19.64	0.05	0.7	-13.08	90
1972	09 23 12.1	-23 20 52.7	19.64	0.04	0.7	-13.08	122
2055	09 23 13.2	-22 53 21.6	19.64	0.01	0.7	-13.08	170
2531	09 23 21.7	-22 55 40.0	19.64	0.00	1.0	-13.08	144
5288	09 24 11.2	-23 12 58.0	19.64	0.01	0.8	-13.08	103
7166	09 24 18.0	-23 13 52.0	19.64	0.09	0.7	-13.08	121
2245	09 23 16.5	-22 59 01.2	19.65	0.00	0.6	-13.07	112
2715	09 23 24.4	-23 04 12.7	19.65	0.07	0.5	-13.07	56
1481	09 23 02.7	-22 59 06.5	19.66	0.04	0.6	-13.06	124
290	09 22 39.9	-22 50 28.0	19.66	0.01	0.7	-13.06	228
4195	09 23 51.1	-23 11 24.9	19.66	0.00	0.7	-13.06	53
6058	09 24 37.9	-22 58 52.5	19.67	0.00	0.8	-13.05	194
1556	09 23 04.4	-23 16 11.2	19.68	0.06	0.8	-13.04	90
2243	09 23 16.3	-22 52 50.1	19.68	0.00	0.7	-13.04	174
712	09 22 48.0	-23 15 47.7	19.68	0.00	0.5	-13.04	116
808	09 22 49.9	-23 08 55.8	19.68	0.06	0.7	-13.04	93
3055	09 23 30.8	-23 02 04.3	19.69	0.03	0.7	-13.03	77
3457	09 23 37.9	-23 16 12.8	19.69	0.01	0.9	-13.03	70
1233	09 22 57.7	-23 18 45.8	19.70	0.03	0.5	-13.02	120
1321	09 22 59.7	-23 19 41.0	19.70	0.00	0.7	-13.02	124
2638	09 23 23.5	-23 01 22.2	19.70	0.00	1.2	-13.02	85
5371	09 24 12.6	-23 11 57.5	19.70	0.00	0.7	-13.02	103
906	09 22 51.9	-23 18 04.9	19.70	0.00	0.7	-13.02	124
307	09 22 40.6	-23 14 14.2	19.71	0.01	0.7	-13.01	124
5187	09 24 09.5	-23 07 17.9	19.71	0.04	0.7	-13.01	96
395	09 22 42.1	-23 04 00.3	19.72	0.00	0.8	-13.00	126
6614	09 24 19.5	-22 55 51.6	19.72	0.03	0.5	-13.00	182
6668	09 24 47.4	-22 50 58.9	19.72	0.08	0.7	-13.00	263
6754	09 24 26.3	-23 11 06.1	19.72	0.04	0.9	-13.00	134
1533	09 23 03.6	-22 58 10.8	19.73	0.02	0.7	-12.99	132
2833	09 23 26.6	-22 54 53.9	19.73	0.02	1.0	-12.99	151
6409	09 24 32.4	-22 56 53.1	19.73	0.01	0.6	-12.99	196
2346	09 23 18.4	-23 01 12.7	19.74	0.08	0.6	-12.98	89
3145	09 23 32.6	-23 18 45.7	19.74	0.03	0.7	-12.98	93
3595	09 23 40.2	-23 10 48.3	19.74	0.05	0.7	-12.98	27
6604	09 24 19.7	-23 21 22.7	19.74	0.01	0.6	-12.98	168
1577	09 23 04.1	-22 50 55.4	19.75	0.02	0.6	-12.97	200
2353	09 23 18.8	-23 20 07.4	19.75	0.03	0.7	-12.97	110
3582	09 23 40.2	-23 15 17.9	19.75	0.09	0.7	-12.97	63
2325	09 23 18.2	-23 07 20.9	19.76	0.00	0.7	-12.96	35
244	09 22 39.4	-23 11 41.1	19.76	0.00	0.7	-12.96	120
4073	09 23 49.1	-23 03 57.0	19.76	0.00	1.0	-12.96	73
4394	09 23 54.8	-22 54 29.8	19.76	0.07	0.7	-12.96	165
7256	09 24 35.0	-23 08 12.9	19.76	0.05	1.0	-12.96	154
850	09 22 50.6	-22 52 42.4	19.76	0.00	0.7	-12.96	195
2533	09 23 21.4	-23 01 50.4	19.77	0.09	0.6	-12.95	81
3343	09 23 35.8	-23 11 18.5	19.77	0.01	0.6	-12.95	22
4161	09 23 50.6	-23 16 14.2	19.78	0.00	0.7	-12.94	83
6633	09 24 28.7	-23 06 07.5	19.78	0.00	0.6	-12.94	143
4544	09 23 57.8	-23 20 19.0	19.79	0.00	0.5	-12.93	127
5632	09 24 47.5	-22 59 34.7	19.79	0.02	0.8	-12.93	209
1566	09 23 04.2	-23 15 51.0	19.80	0.00	0.6	-12.92	87
7139	09 24 18.0	-22 55 29.9	19.81	0.01	0.4	-12.91	183
1410	09 23 01.3	-23 12 51.9	19.82	0.08	0.6	-12.90	74
1001	09 22 53.7	-22 59 03.8	19.83	0.01	0.8	-12.89	137
2212	09 23 16.2	-23 18 48.4	19.83	0.08	0.6	-12.89	99
3443	09 23 37.9	-23 14 38.2	19.83	0.00	0.7	-12.89	54
4875	09 24 03.9	-23 17 09.6	19.83	0.00	0.8	-12.89	111
5591	09 24 16.4	-22 55 46.2	19.83	0.04	0.5	-12.89	179
1506	09 23 03.3	-22 56 00.4	19.84	0.02	0.9	-12.88	152
2776	09 23 25.5	-23 04 17.4	19.84	0.00	0.5	-12.88	55
3103	09 23 31.6	-23 08 16.8	19.84	0.07	0.5	-12.88	14
3359	09 23 36.3	-23 16 39.1	19.84	0.05	0.6	-12.88	73
1672	09 23 06.4	-23 10 53.1	19.85	0.05	0.6	-12.87	56
1979	09 23 11.7	-22 58 36.2	19.85	0.00	0.6	-12.87	120
5973	09 24 38.8	-23 17 27.8	19.85	0.00	0.9	-12.87	181
2061	09 23 13.4	-23 09 30.8	19.86	0.04	0.5	-12.86	38
365	09 22 41.4	-22 57 27.4	19.86	0.01	0.6	-12.86	168
3300	09 23 35.2	-23 18 46.4	19.87	0.08	0.6	-12.85	94
3820	09 23 45.3	-23 12 17.5	19.87	0.01	0.6	-12.85	45
3607	09 23 40.5	-23 07 00.1	19.88	0.08	0.8	-12.84	37
4319	09 23 53.5	-23 08 38.8	19.88	0.08	0.6	-12.84	56
6244	09 24 33.5	-23 01 43.1	19.88	0.06	0.7	-12.84	170
7244	09 24 48.5	-23 03 42.3	19.88	0.00	0.7	-12.84	194
4030	09 23 48.3	-23 04 29.6	19.89	0.05	0.6	-12.83	68
6380	09 24 32.8	-23 17 03.2	19.89	0.03	0.8	-12.83	166
7076	09 24 20.3	-23 14 18.4	19.89	0.01	0.8	-12.83	128
4168	09 23 50.6	-23 06 04.6	19.90	0.00	0.6	-12.82	60
6627	09 24 18.5	-23 07 23.9	19.90	0.05	0.6	-12.82	116

Table A.4: Candidate satellite galaxies in the field of NGC 2865 (continued).

Number (1)	RA (J2000) (2)	DEC (J2000) (3)	R (mag) (4)	Class (5)	A (arcsec) (6)	M_R (mag) (7)	Dist (kpc) (8)
1038	09 22 53.9	-22 54 05.8	19.91	0.02	0.6	-12.81	179
6768	09 24 24.2	-23 02 54.4	19.91	0.08	0.6	-12.81	145
7109	09 24 20.2	-23 21 08.4	19.91	0.01	0.7	-12.81	167
5145	09 24 08.8	-23 07 21.6	19.92	0.00	0.8	-12.80	94
6631	09 24 18.4	-22 59 17.6	19.92	0.02	0.8	-12.80	155
2817	09 23 26.1	-22 50 44.5	19.93	0.01	0.5	-12.79	193
4137	09 23 50.1	-23 09 43.1	19.93	0.04	0.6	-12.79	47
2188	09 23 15.8	-23 14 26.9	19.94	0.03	0.7	-12.78	59
37	09 22 34.9	-22 51 53.9	19.94	0.00	0.8	-12.78	222
3718	09 23 43.2	-23 10 48.1	19.94	0.00	0.8	-12.78	34
3845	09 23 45.9	-23 16 43.6	19.94	0.09	0.6	-12.78	81
402	09 22 42.4	-23 18 05.1	19.94	0.02	0.8	-12.78	141
5657	09 24 29.5	-23 08 16.2	19.94	0.01	0.7	-12.78	140
6061	09 24 37.7	-22 56 00.7	19.94	0.00	0.8	-12.78	212
6332	09 24 33.0	-23 02 07.6	19.94	0.01	0.8	-12.78	167
1418	09 23 01.4	-23 13 27.1	19.95	0.06	0.6	-12.77	77
2378	09 23 18.7	-23 05 55.5	19.95	0.08	0.7	-12.77	45
3358	09 23 35.9	-22 56 42.6	19.95	0.02	0.7	-12.77	132
5136	09 24 08.8	-23 16 04.8	19.95	0.00	0.7	-12.77	112
5305	09 24 11.0	-22 59 49.9	19.95	0.04	0.7	-12.77	139
2326	09 23 18.3	-23 16 32.1	19.96	0.07	0.6	-12.76	75
4932	09 24 04.9	-23 20 38.0	19.96	0.04	0.6	-12.76	139
5138	09 24 08.6	-23 08 37.0	19.96	0.00	0.7	-12.76	91
5586	09 24 16.6	-23 06 02.5	19.97	0.00	0.8	-12.75	116
2514	09 23 21.2	-23 06 07.7	19.98	0.00	0.5	-12.74	40
2945	09 23 28.8	-23 16 38.3	19.98	0.01	0.6	-12.74	71
3611	09 23 40.4	-23 15 59.8	19.98	0.08	0.6	-12.74	69
703	09 22 47.9	-23 00 55.8	19.98	0.01	0.7	-12.74	132
3784	09 23 44.6	-23 10 51.6	20.00	0.04	0.6	-12.72	37
451	09 22 43.2	-23 02 41.0	20.00	0.03	0.6	-12.72	130
6028	09 24 37.9	-22 51 34.6	20.00	0.00	0.7	-12.72	244
954	09 22 52.6	-22 56 14.0	20.00	0.05	0.6	-12.72	162
1245	09 22 58.1	-23 20 25.5	20.01	0.00	0.6	-12.71	133
2266	09 23 16.8	-22 55 38.6	20.01	0.08	0.7	-12.71	146
7183	09 24 16.9	-22 50 00.2	20.01	0.07	0.8	-12.71	229
2108	09 23 14.2	-23 08 15.9	20.02	0.01	0.5	-12.70	39
2549	09 23 21.9	-23 05 08.4	20.02	0.00	0.7	-12.70	49
2864	09 23 27.6	-23 18 17.0	20.02	0.05	0.6	-12.70	88
3745	09 23 43.8	-23 09 30.1	20.03	0.04	0.6	-12.69	33
6351	09 24 33.1	-23 06 32.0	20.03	0.01	0.6	-12.69	152
7346	09 24 47.4	-23 02 02.3	20.03	0.06	0.7	-12.69	198
1837	09 23 09.4	-23 20 43.9	20.04	0.00	0.8	-12.68	123
6827	09 24 23.3	-23 15 11.4	20.04	0.01	0.5	-12.68	137
6880	09 24 21.9	-23 03 01.5	20.04	0.06	0.8	-12.68	140
735	09 22 48.5	-23 13 55.5	20.04	0.00	0.6	-12.68	106
93	09 22 36.2	-23 04 44.8	20.04	0.01	0.6	-12.68	135
3097	09 23 31.7	-23 14 50.2	20.05	0.09	0.7	-12.67	53
3568	09 23 39.5	-23 05 24.5	20.05	0.09	0.7	-12.67	48
3309	09 23 35.2	-23 11 19.0	20.06	0.08	0.6	-12.66	21
5512	09 24 15.0	-23 04 31.5	20.06	0.08	0.6	-12.66	118
6457	09 24 30.6	-23 03 58.5	20.06	0.07	0.6	-12.66	154
6908	09 24 27.4	-22 56 59.9	20.06	0.02	0.5	-12.66	187
923	09 22 51.9	-22 53 29.5	20.06	0.08	0.6	-12.66	187
4366	09 23 54.6	-23 21 03.3	20.07	0.00	0.7	-12.65	130
3981	09 23 47.8	-23 08 58.5	20.08	0.06	0.6	-12.64	42
835	09 22 50.5	-23 13 23.8	20.08	0.01	0.6	-12.64	100
2691	09 23 24.2	-23 20 37.0	20.09	0.05	0.7	-12.63	113
3395	09 23 37.0	-23 18 59.3	20.09	0.00	0.7	-12.63	97
3875	09 23 46.1	-23 11 49.5	20.09	0.00	0.6	-12.63	44
797	09 22 49.8	-23 13 26.7	20.09	0.01	0.6	-12.63	101
3183	09 23 33.2	-23 17 11.4	20.10	0.08	0.6	-12.62	77
1830	09 23 08.9	-22 51 16.1	20.11	0.00	0.6	-12.61	193
2445	09 23 20.0	-23 04 36.3	20.11	0.01	0.5	-12.61	56
2867	09 23 27.6	-23 13 26.3	20.11	0.09	0.6	-12.61	39
3188	09 23 33.3	-23 18 19.8	20.11	0.00	0.8	-12.61	89
3461	09 23 38.1	-23 19 34.5	20.11	0.01	0.6	-12.61	103
3965	09 23 47.4	-23 09 57.1	20.11	0.07	0.5	-12.61	41
5624	09 24 48.8	-23 18 21.4	20.11	0.00	0.7	-12.61	206
11	09 22 35.0	-23 17 24.0	20.12	0.00	0.8	-12.60	151
3126	09 23 32.0	-23 06 30.9	20.12	0.09	0.5	-12.60	32
3334	09 23 35.9	-23 18 15.3	20.12	0.00	0.7	-12.60	89
3574	09 23 39.7	-23 05 57.6	20.12	0.01	0.5	-12.60	44
943	09 22 52.3	-23 11 41.4	20.12	0.00	0.5	-12.60	90
1603	09 23 04.8	-23 02 27.5	20.13	0.06	0.5	-12.59	93
3937	09 23 46.8	-23 05 01.6	20.13	0.00	0.7	-12.59	61
4435	09 23 55.5	-23 08 24.1	20.13	0.00	0.7	-12.59	61
6000	09 24 28.2	-23 00 57.2	20.13	0.00	0.6	-12.59	163
7138	09 24 26.1	-23 11 56.9	20.13	0.00	0.7	-12.59	134
7374	09 24 43.7	-22 58 38.6	20.13	0.01	0.6	-12.59	206
1150	09 22 56.4	-23 18 57.9	20.14	0.07	0.5	-12.58	123
1617	09 23 04.9	-22 59 41.7	20.14	0.01	0.6	-12.58	117
2180	09 23 15.1	-22 51 40.3	20.14	0.04	0.6	-12.58	186
510	09 22 44.1	-23 07 38.2	20.14	0.00	0.8	-12.58	109
2521	09 23 21.3	-23 02 40.2	20.15	0.01	0.6	-12.57	73
5553	09 24 15.6	-22 54 24.0	20.15	0.01	0.7	-12.57	189
144	09 22 37.1	-23 01 26.5	20.16	0.09	0.5	-12.56	149
1440	09 23 01.8	-23 08 57.9	20.17	0.01	0.6	-12.55	66
4517	09 23 57.8	-23 14 17.6	20.17	0.01	0.6	-12.55	81
2186	09 23 15.4	-22 55 55.2	20.18	0.08	0.7	-12.54	144
2504	09 23 20.8	-22 50 33.9	20.18	0.05	0.6	-12.54	195

Table A.4: Candidate satellite galaxies in the field of NGC 2865 (continued).

Number (1)	RA (J2000) (2)	DEC (J2000) (3)	R (mag) (4)	Class (5)	A (arcsec) (6)	M_R (mag) (7)	Dist (kpc) (8)
2705	09 23 24.6	-23 20 32.1	20.18	0.09	0.6	-12.54	112
7009	09 24 19.5	-23 10 51.4	20.18	0.00	0.8	-12.54	117
1648	09 23 05.6	-23 01 58.9	20.19	0.00	0.5	-12.53	96
1878	09 23 09.9	-22 52 46.1	20.19	0.07	0.6	-12.53	178
5556	09 24 16.1	-23 14 28.0	20.19	0.00	0.6	-12.53	119
6068	09 24 38.2	-23 05 29.0	20.19	0.01	0.8	-12.53	166
3366	09 23 36.4	-23 18 00.0	20.2	0.07	0.6	-12.52	87
1593	09 23 04.6	-23 03 15.7	20.20	0.06	0.6	-12.52	87
2684	09 23 24.1	-23 18 08.4	20.20	0.00	0.7	-12.52	88
2729	09 23 24.6	-23 00 30.4	20.20	0.08	0.5	-12.52	93
5620	09 24 49.3	-23 19 59.4	20.20	0.07	0.6	-12.52	214
6566	09 24 29.1	-22 59 12.4	20.20	0.07	0.6	-12.52	175
6951	09 24 22.0	-23 16 05.5	20.20	0.04	0.5	-12.52	139
1398	09 23 00.8	-23 12 53.4	20.21	0.08	0.5	-12.51	75
1825	09 23 09.3	-23 21 21.1	20.22	0.09	0.6	-12.50	129
2469	09 23 20.6	-23 15 29.5	20.22	0.04	0.5	-12.50	63
3475	09 23 38.0	-23 09 17.3	20.22	0.05	0.5	-12.50	19
3924	09 23 46.8	-23 14 07.7	20.22	0.09	0.6	-12.50	61
5731	09 24 44.7	-23 10 30.8	20.22	0.01	0.5	-12.50	176
4138	09 23 50.9	-23 11 25.6	20.23	0.03	0.5	-12.49	52
4666	09 23 59.8	-22 58 30.9	20.23	0.04	0.8	-12.49	133
5808	09 24 43.8	-23 10 25.6	20.23	0.02	0.7	-12.49	174
6844	09 24 22.1	-23 20 45.4	20.23	0.09	0.6	-12.49	167
7323	09 24 48.1	-23 15 49.6	20.23	0.00	0.6	-12.49	194
2743	09 23 25.2	-23 13 25.8	20.24	0.00	0.7	-12.48	40
3091	09 23 31.5	-23 06 51.6	20.24	0.00	0.8	-12.48	28
4131	09 23 49.7	-22 57 09.3	20.24	0.00	0.5	-12.48	135
5380	09 24 12.8	-23 16 17.9	20.25	0.00	0.7	-12.47	122
6277	09 24 41.0	-23 07 57.9	20.25	0.00	0.7	-12.47	168
1901	09 23 10.7	-23 18 58.7	20.26	0.00	0.7	-12.46	105
2602	09 23 22.8	-23 20 32.2	20.26	0.09	0.6	-12.46	112
3637	09 23 40.8	-22 51 36.7	20.26	0.00	0.9	-12.46	185
719	09 22 48.0	-22 51 15.2	20.26	0.01	0.6	-12.46	211
872	09 22 51.3	-23 20 13.1	20.26	0.01	0.6	-12.46	141
1517	09 23 03.6	-23 17 56.0	20.27	0.03	0.6	-12.45	104
4282	09 23 52.8	-23 17 19.6	20.27	0.08	0.5	-12.45	95
4415	09 23 55.2	-23 07 00.3	20.27	0.06	0.5	-12.45	65
1448	09 23 02.2	-23 17 34.0	20.28	0.05	0.5	-12.44	104
218	09 22 38.5	-22 54 16.6	20.28	0.00	0.6	-12.44	197
3646	09 23 41.3	-23 21 21.3	20.28	0.03	0.6	-12.44	123
6617	09 24 27.9	-23 13 16.2	20.28	0.07	0.5	-12.44	141
6839	09 24 23.7	-23 05 51.9	20.28	0.03	0.5	-12.44	132
325	09 22 40.6	-22 50 28.4	20.29	0.00	0.7	-12.43	227
5239	09 24 09.8	-22 54 31.5	20.29	0.00	0.5	-12.43	180
5268	09 24 10.6	-23 08 37.4	20.29	0.05	0.6	-12.43	96
5379	09 24 12.7	-23 16 19.5	20.29	0.01	0.7	-12.43	121
6029	09 24 38.3	-23 10 23.4	20.29	0.04	0.6	-12.43	161
7272	09 24 49.4	-23 07 12.1	20.3	0.08	0.5	-12.42	188
1676	09 23 06.2	-22 58 18.8	20.30	0.09	0.5	-12.42	128
3110	09 23 31.9	-23 19 37.8	20.30	0.06	0.5	-12.42	102
4046	09 23 48.9	-23 12 26.8	20.30	0.01	0.7	-12.42	53
6986	09 24 47.1	-22 51 29.3	20.30	0.00	0.6	-12.42	259
830	09 22 50.1	-22 50 28.2	20.30	0.09	0.7	-12.42	216
3915	09 23 46.9	-23 14 50.9	20.31	0.06	0.6	-12.41	66
4653	09 23 59.4	-22 57 27.8	20.31	0.01	0.6	-12.41	142
4928	09 24 04.3	-23 02 16.7	20.31	0.01	0.5	-12.41	110
6042	09 24 40.0	-23 08 32.3	20.31	0.00	0.6	-12.41	165
6963	09 24 20.6	-22 50 54.5	20.31	0.07	0.8	-12.41	225
1714	09 23 07.2	-23 20 12.0	20.32	0.01	0.6	-12.40	120
3322	09 23 35.1	-22 51 38.1	20.32	0.05	0.5	-12.40	184
3627	09 23 40.5	-23 03 29.9	20.32	0.06	0.6	-12.40	67
6322	09 24 33.4	-23 05 50.6	20.32	0.00	0.5	-12.40	154
1157	09 22 56.5	-23 19 03.0	20.33	0.01	0.5	-12.39	124
2555	09 23 21.7	-23 03 54.7	20.33	0.00	0.6	-12.39	61
2695	09 23 24.3	-23 19 21.8	20.33	0.00	0.7	-12.39	100
4134	09 23 50.0	-23 07 42.6	20.33	0.01	0.6	-12.39	51
3476	09 23 38.0	-23 08 48.3	20.34	0.06	0.6	-12.38	21
4850	09 24 03.3	-23 15 03.1	20.34	0.07	0.6	-12.38	96
5298	09 24 11.3	-23 20 06.3	20.34	0.00	0.6	-12.38	144
1584	09 23 04.5	-23 12 45.8	20.35	0.01	0.6	-12.37	67
2958	09 23 28.8	-23 03 32.6	20.35	0.00	0.6	-12.37	62
3019	09 23 30.3	-23 12 27.0	20.35	0.07	0.5	-12.37	29
5215	09 24 09.9	-23 11 17.4	20.35	0.06	0.6	-12.37	95
91	09 22 36.0	-22 50 17.4	20.35	0.04	0.8	-12.37	234
706	09 22 48.0	-23 17 44.5	20.36	0.05	0.5	-12.36	128
1272	09 22 58.5	-23 15 30.1	20.37	0.03	0.6	-12.35	94
3135	09 23 32.1	-23 07 20.0	20.37	0.06	0.5	-12.35	23
4385	09 23 54.9	-23 14 11.8	20.37	0.00	0.6	-12.35	75
4880	09 24 03.8	-23 17 12.4	20.37	0.00	0.6	-12.35	111
6281	09 24 34.7	-23 04 56.5	20.37	0.06	0.6	-12.35	159
2781	09 23 25.9	-23 18 01.3	20.38	0.01	0.4	-12.34	86
2989	09 23 29.5	-23 01 54.6	20.38	0.09	0.6	-12.34	78
3222	09 23 33.5	-23 08 27.1	20.38	0.01	0.6	-12.34	14
4944	09 24 04.7	-23 07 21.8	20.38	0.09	0.5	-12.34	85
1571	09 23 03.9	-22 54 55.8	20.39	0.01	0.6	-12.33	161
3536	09 23 39.0	-23 06 52.2	20.39	0.06	0.6	-12.33	35
372	09 22 41.6	-23 07 39.0	20.39	0.00	0.7	-12.33	115
1581	09 23 04.4	-23 14 34.2	20.4	0.00	0.7	-12.32	78
4009	09 23 48.1	-23 15 20.3	20.40	0.07	0.5	-12.32	72
4525	09 23 57.2	-23 17 20.2	20.40	0.09	0.6	-12.32	101

Table A.4: Candidate satellite galaxies in the field of NGC 2865 (continued).

Number (1)	RA (J2000) (2)	DEC (J2000) (3)	R (mag) (4)	Class (5)	A (arcsec) (6)	M_R (mag) (7)	Dist (kpc) (8)
5001	09 24 05.8	-23 11 47.3	20.40	0.01	0.6	-12.32	87
591	09 22 45.6	-23 11 28.3	20.40	0.01	0.7	-12.32	105
74	09 22 35.8	-23 18 34.1	20.40	0.00	0.7	-12.32	156
5719	09 24 47.0	-23 20 42.6	20.41	0.07	0.8	-12.31	213
1600	09 23 04.9	-23 16 14.0	20.42	0.01	0.5	-12.30	89
4120	09 23 49.9	-23 14 53.2	20.42	0.05	0.5	-12.30	71
6204	09 24 35.8	-23 03 43.2	20.42	0.09	0.5	-12.30	166
7319	09 24 44.4	-23 12 14.4	20.42	0.07	0.6	-12.30	177
3333	09 23 35.5	-23 08 49.7	20.43	0.07	0.4	-12.29	15
4325	09 23 53.3	-23 01 37.3	20.43	0.04	0.5	-12.29	98
5040	09 24 06.7	-23 01 56.4	20.43	0.00	0.7	-12.29	117
5365	09 24 11.8	-22 52 00.2	20.43	0.01	0.7	-12.29	205
6107	09 24 38.8	-22 54 33.5	20.43	0.01	0.5	-12.29	223
700	09 22 47.7	-23 13 56.3	20.43	0.09	0.5	-12.29	108
1476	09 23 02.8	-23 19 35.4	20.44	0.00	0.6	-12.28	120
2722	09 23 24.5	-23 07 33.4	20.44	0.08	0.5	-12.28	24
3741	09 23 43.7	-23 09 45.6	20.44	0.00	0.6	-12.28	32
6527	09 24 29.6	-22 50 50.5	20.44	0.06	0.6	-12.28	238
1898	09 23 10.6	-23 16 31.9	20.45	0.00	0.5	-12.27	83
2219	09 23 16.2	-23 20 15.6	20.45	0.01	0.7	-12.27	113
230	09 22 38.9	-23 13 59.0	20.45	0.03	0.6	-12.27	127
3846	09 23 45.8	-23 18 50.2	20.45	0.02	0.5	-12.27	101
4638	09 23 59.4	-23 17 05.3	20.45	0.08	0.5	-12.27	103
1132	09 22 55.7	-22 50 50.1	20.46	0.07	0.5	-12.26	208
4647	09 23 59.4	-23 06 18.8	20.46	0.01	0.6	-12.26	77
5004	09 24 05.9	-23 10 05.9	20.46	0.00	0.5	-12.26	85
5129	09 24 08.1	-22 58 40.8	20.46	0.01	0.5	-12.26	143
5603	09 24 49.6	-23 02 03.6	20.46	0.05	0.6	-12.26	202
6252	09 24 34.2	-23 02 01.7	20.46	0.02	0.5	-12.26	170
17	09 22 34.8	-23 11 36.7	20.47	0.04	0.6	-12.25	130
3507	09 23 38.6	-23 06 18.9	20.47	0.03	0.5	-12.25	39
5820	09 24 42.9	-23 09 35.2	20.47	0.05	0.6	-12.25	171
878	09 22 50.9	-22 54 07.6	20.47	0.09	0.5	-12.25	182
2181	09 23 15.4	-23 04 33.4	20.48	0.00	0.7	-12.24	61
3147	09 23 32.1	-22 53 34.3	20.48	0.09	0.7	-12.24	164
3721	09 23 43.2	-23 10 08.8	20.48	0.06	0.5	-12.24	32
814	09 22 49.9	-23 08 57.7	20.48	0.02	0.6	-12.24	93
1895	09 23 10.2	-22 50 23.3	20.49	0.09	0.5	-12.23	201
6239	09 24 35.0	-23 00 01.5	20.49	0.02	0.5	-12.23	182
6480	09 24 39.0	-22 50 07.0	20.49	0.08	0.5	-12.23	257
3415	09 23 36.9	-23 06 21.6	20.50	0.00	0.6	-12.22	37
112	09 22 36.7	-23 19 20.0	20.51	0.08	0.5	-12.21	159
1559	09 23 04.0	-23 12 43.2	20.51	0.08	0.5	-12.21	68
2234	09 23 16.5	-23 21 18.0	20.51	0.06	0.4	-12.21	123
3462	09 23 37.8	-23 13 59.7	20.51	0.03	0.5	-12.21	48
1070	09 22 54.5	-22 58 37.7	20.52	0.01	0.6	-12.20	139
2385	09 23 19.1	-23 11 06.8	20.52	0.04	0.6	-12.20	29
5454	09 24 14.1	-23 18 56.1	20.52	0.01	0.5	-12.20	141
5567	09 24 16.1	-23 10 03.0	20.52	0.00	0.5	-12.20	109
3018	09 23 30.1	-23 11 31.7	20.54	0.08	0.5	-12.18	19
4189	09 23 51.0	-23 20 49.1	20.54	0.03	0.5	-12.18	124
1162	09 22 56.4	-23 07 54.5	20.55	0.04	0.5	-12.17	80
155	09 22 37.2	-23 09 08.4	20.55	0.03	0.4	-12.17	123
1849	09 23 09.6	-23 14 39.4	20.55	0.09	0.4	-12.17	70
3400	09 23 36.7	-23 10 05.3	20.55	0.04	0.5	-12.17	17
2698	09 23 24.0	-23 03 52.9	20.56	0.02	0.5	-12.16	60
4045	09 23 48.5	-23 03 24.2	20.56	0.03	0.5	-12.16	77
2775	09 23 25.3	-23 02 36.0	20.58	0.01	0.6	-12.14	72
3396	09 23 36.7	-23 10 07.3	20.58	0.01	0.5	-12.14	17
874	09 22 50.8	-22 50 33.8	20.58	0.07	0.6	-12.14	215
1023	09 22 53.5	-22 55 35.5	20.59	0.02	0.5	-12.13	166
1098	09 22 55.1	-23 02 16.0	20.59	0.04	0.5	-12.13	110
1437	09 23 01.9	-23 21 02.9	20.59	0.02	0.5	-12.13	133
2231	09 23 16.2	-23 04 16.9	20.59	0.03	0.6	-12.13	63
5682	09 24 46.8	-22 51 37.8	20.59	0.08	0.5	-12.13	258
2660	09 23 23.2	-22 57 00.1	20.60	0.01	0.4	-12.12	129
7066	09 24 27.1	-23 16 04.1	20.60	0.02	0.5	-12.12	150
6650	09 24 28.2	-23 17 18.1	20.61	0.02	0.5	-12.11	158
3986	09 23 47.5	-23 05 00.6	20.62	0.05	0.5	-12.10	62
4467	09 23 56.1	-23 08 06.1	20.63	0.05	0.5	-12.09	63
3014	09 23 29.9	-23 03 07.3	20.65	0.07	0.5	-12.07	66
5467	09 24 13.6	-22 51 22.2	20.65	0.00	0.6	-12.07	213
3382	09 23 36.3	-23 01 53.1	20.66	0.09	0.5	-12.06	80
3546	09 23 39.0	-23 09 03.0	20.66	0.05	0.5	-12.06	22
7090	09 24 20.2	-23 07 31.0	20.66	0.05	0.5	-12.06	120
1841	09 23 09.1	-22 54 51.6	20.67	0.02	0.5	-12.05	158
4515	09 23 56.6	-22 56 52.7	20.67	0.00	0.5	-12.05	144
5203	09 24 09.5	-23 06 45.6	20.67	0.09	0.4	-12.05	97
1041	09 22 54.1	-23 06 58.7	20.68	0.00	0.5	-12.04	88
3532	09 23 39.0	-23 17 35.5	20.68	0.08	0.5	-12.04	84
6101	09 24 38.4	-23 04 43.5	20.69	0.07	0.5	-12.03	168
3262	09 23 34.0	-23 08 07.7	20.71	0.06	0.5	-12.01	18
5164	09 24 09.2	-23 20 09.7	20.71	0.09	0.4	-12.01	142
1528	09 23 03.4	-23 07 04.2	20.73	0.04	0.5	-11.99	67
4458	09 23 55.8	-23 01 24.5	20.73	0.01	0.5	-11.99	103
6295	09 24 33.6	-22 56 45.8	20.73	0.05	0.5	-11.99	199
3125	09 23 32.0	-23 19 20.9	20.75	0.01	0.4	-11.97	99
3771	09 23 43.8	-22 50 27.2	20.75	0.01	0.5	-11.97	198
6553	09 24 19.9	-23 08 39.9	20.75	0.04	0.5	-11.97	118
425	09 22 42.4	-22 57 42.5	20.76	0.03	0.4	-11.96	165

Table A.4: Candidate satellite galaxies in the field of NGC 2865 (continued).

Number (1)	RA (J2000) (2)	DEC (J2000) (3)	R (mag) (4)	Class (5)	A (arcsec) (6)	M_R (mag) (7)	Dist (kpc) (8)
3141	09 23 32.2	-23 13 17.3	20.77	0.04	0.5	-11.95	38
3328	09 23 35.5	-23 17 31.6	20.77	0.04	0.4	-11.95	82
4212	09 23 51.3	-23 10 06.4	20.78	0.06	0.5	-11.94	50
4312	09 23 53.2	-23 13 07.6	20.78	0.09	0.5	-11.94	65
4326	09 23 53.5	-23 17 32.9	20.78	0.07	0.4	-11.94	98
1189	09 22 56.8	-23 01 37.4	20.79	0.05	0.5	-11.93	112
1355	09 22 59.6	-22 55 34.3	20.79	0.05	0.4	-11.93	160
1565	09 23 04.0	-23 11 03.1	20.79	0.01	0.5	-11.93	62
2988	09 23 29.1	-23 02 55.3	20.79	0.05	0.4	-11.93	68
4346	09 23 53.7	-23 01 43.0	20.79	0.01	0.4	-11.93	98
5320	09 24 11.2	-23 07 18.4	20.79	0.06	0.4	-11.93	100
6615	09 24 27.0	-23 09 18.7	20.80	0.09	0.5	-11.92	134
4360	09 23 54.0	-23 00 21.7	20.81	0.07	0.4	-11.91	110
895	09 22 51.3	-23 02 16.0	20.81	0.04	0.5	-11.91	117
3303	09 23 34.7	-22 57 12.0	20.82	0.03	0.5	-11.90	127
188	09 22 38.0	-23 19 54.3	20.83	0.02	0.4	-11.89	160
412	09 22 42.3	-23 03 32.4	20.83	0.02	0.5	-11.89	127
3294	09 23 34.8	-23 02 10.0	20.84	0.08	0.5	-11.88	77
3928	09 23 46.9	-23 17 07.9	20.86	0.01	0.4	-11.86	86
83	09 22 35.8	-23 04 45.4	20.86	0.01	0.5	-11.86	136
1737	09 23 07.1	-23 02 42.2	20.87	0.02	0.4	-11.85	88
68	09 22 35.5	-23 08 49.8	20.93	0.04	0.4	-11.79	127
304	09 22 40.2	-23 16 09.8	20.94	0.03	0.4	-11.78	134
422	09 22 42.4	-22 57 59.7	21.00	0.01	0.5	-11.72	162
772	09 22 49.0	-23 08 16.9	21.13	0.08	0.4	-11.59	96
3557	09 23 39.2	-23 09 06.4	21.15	0.09	0.4	-11.57	22
3628	09 23 40.8	-23 20 51.1	21.15	0.09	0.4	-11.57	117
3662	09 23 40.9	-23 02 14.3	21.26	0.09	0.3	-11.46	79
3057	09 23 30.6	-22 57 41.7	23.01	0.01	0.7	-9.71	121

Table A.5: List of the candidate satellite galaxies in the field of NGC 4240.

Number	RA (J2000)	DEC (J2000)	R (mag)	Class	A (arcsec)	M_R (mag)	Dist (kpc)
931	12 17 26.0	-09 58 06.9	15.25	0.00	4.4	-17.05	9
413	12 16 54.3	-09 52 23.6	15.94	0.03	2.9	-16.36	73
44	12 16 36.2	-09 55 49.7	16.17	0.00	3.4	-16.13	100
257	12 16 45.5	-09 40 00.4	16.27	0.03	2.2	-16.04	165
763	12 17 13.0	-10 05 16.5	16.28	0.02	4.2	-16.03	73
1006	12 17 26.5	-10 01 58.0	16.53	0.02	2.6	-15.77	41
1100	12 17 31.9	-09 59 10.3	16.81	0.02	2.5	-15.49	24
1941	12 18 26.1	-10 05 58.9	16.88	0.01	3.5	-15.42	149
490	12 16 57.6	-09 38 54.2	16.93	0.03	1.6	-15.37	163
1480	12 17 52.5	-10 08 33.5	17.09	0.02	2.0	-15.21	113
916	12 17 20.8	-09 41 49.5	17.14	0.03	1.6	-15.16	129
186	12 16 41.7	-10 05 55.2	17.18	0.03	1.8	-15.12	115
1463	12 17 50.8	-10 03 30.6	17.20	0.00	1.5	-15.11	77
632	12 17 05.0	-09 48 02.0	17.25	0.01	2.0	-15.05	86
690	12 17 08.7	-09 59 57.5	17.26	0.02	1.8	-15.04	40
64	12 16 34.7	-10 02 13.9	17.41	0.04	1.2	-14.89	111
491	12 16 57.5	-09 39 35.3	17.44	0.03	1.6	-14.86	158
1310	12 17 42.7	-09 43 06.6	17.51	0.01	1.0	-14.79	124
2374	12 18 32.5	-09 40 47.9	17.55	0.02	1.5	-14.76	198
7	12 16 32.9	-09 38 59.9	17.55	0.02	1.9	-14.75	186
385	12 16 50.6	-09 42 32.5	17.56	0.04	1.3	-14.74	141
1243	12 17 40.6	-10 05 27.0	17.60	0.03	1.4	-14.70	78
372	12 16 50.1	-09 44 25.9	17.60	0.03	1.3	-14.71	128
1363	12 17 45.7	-09 54 51.8	17.66	0.02	1.4	-14.64	48
163	12 16 40.4	-09 58 11.0	17.66	0.04	1.2	-14.64	91
1384	12 17 46.4	-09 43 58.3	17.67	0.02	1.2	-14.63	120
975	12 17 24.1	-09 40 39.5	17.69	0.02	1.7	-14.61	138
454	12 16 55.9	-09 56 19.3	17.72	0.01	2.0	-14.58	59
301	12 16 46.4	-09 39 38.7	17.75	0.04	1.2	-14.55	167
2276	12 18 33.5	-10 08 30.9	17.79	0.02	1.3	-14.52	174
582	12 17 03.5	-10 01 26.7	17.81	0.00	2.5	-14.49	56
40	12 16 33.1	-10 03 42.3	17.86	0.00	1.0	-14.44	120
1059	12 17 29.0	-10 05 01.4	17.88	0.01	1.4	-14.42	68
1217	12 17 38.1	-09 49 09.5	17.89	0.04	1.3	-14.42	73
985	12 17 25.3	-09 58 16.1	17.89	0.00	4.3	-14.41	10
341	12 16 48.1	-09 44 53.5	17.91	0.04	1.2	-14.39	127
165	12 16 40.2	-09 38 53.9	17.93	0.01	1.4	-14.37	179
621	12 17 04.7	-10 08 19.6	17.98	0.02	1.3	-14.33	103
819	12 17 14.8	-09 57 13.7	17.98	0.01	1.8	-14.32	19
2286	12 18 16.8	-09 55 42.2	18.01	0.00	1.5	-14.29	110
119	12 16 37.1	-09 49 30.9	18.03	0.02	1.1	-14.27	117
59	12 16 34.3	-10 04 24.1	18.03	0.01	1.0	-14.27	120
43	12 16 33.2	-10 02 54.7	18.04	0.01	0.7	-14.27	117
185	12 16 40.9	-10 02 22.2	18.08	0.00	0.9	-14.22	100
2065	12 18 18.3	-09 56 50.4	18.14	0.01	1.5	-14.16	113
555	12 17 01.4	-10 06 04.0	18.17	0.03	1.2	-14.13	89
2249	12 18 30.4	-09 43 42.7	18.19	0.05	1.2	-14.11	178
764	12 17 11.7	-09 59 46.0	18.19	0.02	1.1	-14.11	34
229	12 16 43.1	-09 43 59.1	18.22	0.04	1.1	-14.08	139
1271	12 17 40.7	-09 43 27.3	18.24	0.01	0.8	-14.07	120
1051	12 17 28.1	-09 55 42.6	18.25	0.02	1.2	-14.05	14
1187	12 17 36.5	-09 47 47.9	18.26	0.01	1.2	-14.05	82
845	12 17 16.9	-09 56 48.6	18.26	0.01	1.7	-14.04	15
360	12 16 49.3	-10 04 55.6	18.29	0.01	1.3	-14.02	98
507	12 16 57.7	-09 39 33.0	18.30	0.02	1.2	-14.01	158

Table A.5: Candidate satellite galaxies in the field of NCG 4240(continued).

Number (1)	RA (J2000) (2)	DEC (J2000) (3)	R (mag) (4)	Class (5)	A (arcsec) (6)	M_R (mag) (7)	Dist (kpc) (8)
572	12 17 02.5	-10 08 29.2	18.30	0.03	1.1	-14.00	106
156	12 16 39.6	-09 50 41.3	18.31	0.01	1.3	-13.99	107
774	12 17 12.5	-10 05 42.8	18.31	0.02	1.2	-13.99	77
2332	12 18 30.4	-09 43 26.1	18.32	0.00	1.4	-13.98	180
639	12 17 05.0	-09 48 44.4	18.32	0.01	1.2	-13.98	80
531	12 16 58.9	-09 39 57.8	18.33	0.01	1.8	-13.98	154
1932	12 18 26.7	-09 47 20.3	18.36	0.01	1.2	-13.95	154
704	12 17 08.4	-09 38 15.7	18.36	0.01	1.3	-13.94	162
1756	12 18 05.7	-09 44 43.9	18.40	0.01	1.1	-13.90	135
66	12 16 34.3	-10 02 11.8	18.41	0.01	0.7	-13.90	112
881	12 17 18.3	-09 59 54.9	18.41	0.00	1.5	-13.89	26
617	12 17 04.7	-09 48 52.5	18.42	0.00	2.0	-13.88	80
1299	12 17 42.0	-09 43 20.5	18.45	0.00	0.7	-13.85	122
664	12 17 06.2	-09 38 28.5	18.45	0.01	1.4	-13.85	161
2234	12 18 10.5	-09 54 14.5	18.46	0.09	1.0	-13.84	99
293	12 16 46.4	-09 50 09.6	18.46	0.00	1.4	-13.84	97
1076	12 17 29.2	-09 40 06.8	18.47	0.09	1.0	-13.83	143
321	12 16 47.5	-09 46 25.3	18.48	0.01	1.3	-13.82	118
1077	12 17 29.3	-09 43 33.1	18.49	0.00	1.4	-13.81	115
1128	12 17 32.6	-09 57 39.9	18.49	0.00	1.6	-13.81	18
1562	12 17 55.1	-09 50 01.2	18.49	0.00	1.3	-13.81	88
623	12 17 04.3	-09 48 00.4	18.49	0.01	1.2	-13.81	87
546	12 17 00.3	-10 04 07.1	18.51	0.01	1.2	-13.79	77
1215	12 17 37.3	-09 43 14.4	18.52	0.00	0.7	-13.78	120
495	12 16 57.1	-09 37 29.4	18.52	0.03	1.0	-13.78	175
1250	12 17 40.5	-09 56 25.8	18.53	0.02	1.1	-13.77	34
132	12 16 38.1	-10 05 33.8	18.53	0.06	1.0	-13.78	119
765	12 17 11.6	-09 41 47.7	18.54	0.09	1.1	-13.77	131
189	12 16 40.9	-09 40 36.8	18.55	0.03	1.0	-13.75	165
786	12 17 13.3	-10 05 41.0	18.55	0.01	1.2	-13.76	76
359	12 16 49.1	-09 43 19.5	18.59	0.01	1.2	-13.71	137
530	12 16 58.9	-10 02 50.4	18.59	0.01	1.1	-13.71	71
264	12 16 44.3	-09 38 41.0	18.60	0.01	1.2	-13.70	176
219	12 16 42.7	-09 39 38.1	18.61	0.02	1.2	-13.69	170
952	12 17 22.5	-10 03 21.0	18.61	0.06	1.0	-13.69	53
1038	12 17 26.9	-09 50 08.3	18.62	0.03	0.9	-13.68	59
1505	12 17 52.1	-10 05 18.8	18.63	0.00	1.0	-13.67	90
757	12 17 10.9	-09 38 59.2	18.63	0.08	0.9	-13.67	155
1333	12 17 44.2	-10 06 09.3	18.66	0.00	1.2	-13.64	87
1371	12 17 47.8	-10 04 28.4	18.66	0.01	1.3	-13.64	79
1696	12 18 02.3	-09 40 25.0	18.66	0.02	1.2	-13.65	162
218	12 16 43.1	-09 55 17.5	18.66	0.00	1.5	-13.65	86
945	12 17 21.8	-09 38 02.2	18.66	0.03	0.8	-13.64	161
2055	12 18 17.1	-09 52 51.1	18.67	0.02	1.1	-13.63	116
1870	12 18 11.4	-10 04 18.1	18.68	0.05	1.0	-13.62	116
649	12 17 05.6	-10 08 11.0	18.70	0.06	1.0	-13.60	101
744	12 17 10.4	-09 57 21.5	18.70	0.01	1.1	-13.60	28
157	12 16 39.6	-09 55 11.2	18.71	0.06	0.9	-13.59	94
968	12 17 23.5	-09 53 49.0	18.71	0.04	1.1	-13.60	27
2272	12 18 32.9	-09 41 36.2	18.72	0.00	1.1	-13.59	194
830	12 17 15.4	-09 47 51.3	18.78	0.08	1.0	-13.52	80
1840	12 18 13.3	-10 01 32.9	18.81	0.00	1.5	-13.49	109
1159	12 17 33.9	-10 06 32.2	18.82	0.01	1.1	-13.48	82
1783	12 18 07.2	-09 49 51.3	18.83	0.08	1.0	-13.47	108
478	12 16 56.1	-09 39 05.4	18.83	0.01	0.9	-13.47	163
893	12 17 18.8	-10 05 17.9	18.83	0.08	0.9	-13.47	70
1033	12 17 26.7	-09 39 23.6	18.88	0.06	0.9	-13.42	149
140	12 16 38.3	-09 41 06.4	18.88	0.07	0.9	-13.42	165
1607	12 17 57.9	-10 06 56.5	18.88	0.01	1.0	-13.42	109
382	12 16 50.3	-10 02 40.3	18.88	0.00	0.9	-13.42	84
2007	12 18 22.7	-09 57 44.3	18.89	0.01	1.1	-13.41	122
697	12 17 07.8	-09 52 01.4	18.89	0.01	1.4	-13.42	54
2057	12 18 18.4	-09 47 22.8	18.91	0.00	1.1	-13.39	139
34	12 16 32.4	-09 44 31.0	18.91	0.02	0.8	-13.39	151
437	12 16 53.6	-09 41 20.1	18.94	0.00	0.9	-13.36	147
836	12 17 15.8	-09 50 17.8	18.94	0.00	1.0	-13.36	59
1022	12 17 26.7	-10 06 32.0	18.96	0.00	0.9	-13.34	80
674	12 17 06.6	-09 38 10.8	18.96	0.06	1.0	-13.34	164
1451	12 17 50.1	-10 08 46.2	18.97	0.03	1.0	-13.33	112
2115	12 18 15.9	-09 45 31.6	18.97	0.01	1.4	-13.33	145
2060	12 18 32.8	-09 40 51.6	18.98	0.02	1.1	-13.33	198
2364	12 18 33.0	-09 40 08.8	18.98	0.02	1.0	-13.33	202
117	12 16 37.0	-09 45 38.8	18.99	0.00	1.4	-13.31	137
2150	12 18 14.8	-09 56 06.8	19.00	0.03	0.9	-13.30	106
1302	12 17 42.1	-09 44 39.8	19.01	0.00	0.7	-13.29	111
1560	12 17 55.1	-10 00 00.8	19.01	0.00	1.1	-13.30	69
571	12 17 02.2	-10 04 15.7	19.01	0.05	0.9	-13.29	76
876	12 17 17.8	-10 06 25.4	19.01	0.03	0.9	-13.29	80
895	12 17 18.5	-09 43 58.0	19.02	0.00	1.0	-13.29	111
1387	12 17 46.4	-10 05 35.0	19.03	0.03	1.0	-13.27	85
462	12 16 55.2	-09 39 57.9	19.03	0.01	1.0	-13.27	156
593	12 17 02.7	-09 53 29.9	19.03	0.09	0.9	-13.27	53
1400	12 17 46.6	-09 44 08.4	19.05	0.00	0.8	-13.25	119
2325	12 18 08.7	-09 41 36.9	19.05	0.02	0.9	-13.25	160
1495	12 17 51.4	-09 55 52.3	19.06	0.01	0.9	-13.24	57
324	12 16 47.5	-09 59 46.9	19.07	0.00	0.9	-13.23	79
1441	12 17 49.0	-09 49 06.0	19.08	0.00	1.2	-13.22	85
1586	12 17 56.6	-10 06 46.4	19.10	0.01	1.1	-13.20	106
20	12 16 31.6	-09 41 36.5	19.11	0.02	1.4	-13.19	170
1547	12 17 54.1	-10 00 26.6	19.14	0.07	0.9	-13.16	68

Table A.5: Candidate satellite galaxies in the field of NCG 4240(continued).

Number (1)	RA (J2000) (2)	DEC (J2000) (3)	R (mag) (4)	Class (5)	A (arcsec) (6)	M_R (mag) (7)	Dist (kpc) (8)
2110	12 18 15.9	-09 45 34.7	19.14	0.05	1.0	-13.16	145
247	12 16 43.4	-09 39 39.2	19.15	0.07	0.8	-13.15	170
295	12 16 45.7	-09 37 32.2	19.17	0.07	1.0	-13.13	183
188	12 16 40.9	-09 58 55.9	19.18	0.07	1.0	-13.12	91
1611	12 17 58.0	-10 08 21.5	19.19	0.03	0.8	-13.11	118
698	12 17 07.7	-09 45 01.7	19.19	0.01	0.8	-13.11	107
137	12 16 38.0	-09 39 52.3	19.21	0.06	0.9	-13.09	174
2231	12 18 11.0	-09 38 47.5	19.21	0.01	0.9	-13.09	183
665	12 17 05.9	-09 47 32.1	19.21	0.07	1.1	-13.09	89
833	12 17 15.3	-09 37 46.6	19.21	0.00	0.8	-13.09	164
2259	12 18 07.9	-10 04 18.4	19.22	0.01	0.7	-13.08	110
396	12 16 51.2	-09 47 13.3	19.22	0.00	1.0	-13.08	107
1185	12 17 36.4	-10 02 03.1	19.23	0.01	0.9	-13.07	49
1949	12 18 26.1	-09 54 26.3	19.23	0.00	1.2	-13.07	131
2086	12 18 15.1	-09 58 43.7	19.25	0.04	1.0	-13.05	107
1674	12 18 01.1	-09 59 18.2	19.26	0.04	0.8	-13.05	79
1178	12 17 35.8	-09 42 08.0	19.27	0.00	1.0	-13.03	128
443	12 16 54.2	-09 50 53.4	19.28	0.01	0.9	-13.02	81
1704	12 18 02.7	-09 53 25.5	19.30	0.01	0.9	-13.00	86
1511	12 17 52.1	-09 59 09.9	19.31	0.00	1.1	-12.99	60
1577	12 17 55.3	-09 37 58.1	19.32	0.08	0.8	-12.98	174
1623	12 17 58.5	-09 37 21.8	19.32	0.01	1.3	-12.98	181
1873	12 18 09.0	-09 37 38.5	19.33	0.09	0.9	-12.97	189
562	12 17 01.7	-10 05 40.6	19.33	0.00	1.0	-12.97	86
567	12 17 01.3	-09 40 46.8	19.35	0.00	0.9	-12.96	145
564	12 17 01.6	-10 06 15.2	19.38	0.05	0.7	-12.93	90
1442	12 17 48.9	-09 55 47.4	19.39	0.00	1.0	-12.91	52
1473	12 17 50.9	-09 56 52.5	19.39	0.00	1.1	-12.91	55
2270	12 18 28.4	-09 59 01.8	19.39	0.01	0.9	-12.91	135
448	12 16 54.3	-09 38 32.5	19.39	0.01	0.8	-12.91	168
835	12 17 15.4	-09 38 43.9	19.40	0.06	0.8	-12.91	156
869	12 17 17.2	-09 43 12.9	19.40	0.00	0.9	-12.90	118
342	12 16 47.9	-09 41 51.5	19.41	0.07	0.9	-12.89	149
80	12 16 35.1	-09 47 41.6	19.41	0.03	0.9	-12.89	129
275	12 16 44.7	-09 38 48.2	19.45	0.05	0.8	-12.85	175
2121	12 18 17.0	-09 42 07.9	19.46	0.06	0.6	-12.84	167
911	12 17 19.7	-09 49 26.8	19.46	0.05	0.7	-12.84	65
984	12 17 24.2	-10 04 44.2	19.47	0.00	1.0	-12.83	64
1326	12 17 43.6	-10 03 48.8	19.48	0.09	0.7	-12.82	70
2019	12 18 21.5	-09 49 57.5	19.48	0.07	0.8	-12.82	134
2125	12 18 14.9	-09 51 07.6	19.48	0.00	1.0	-12.82	117
121	12 16 36.8	-09 50 52.2	19.49	0.00	0.8	-12.81	111
206	12 16 41.8	-10 04 51.2	19.49	0.01	0.7	-12.81	110
1512	12 17 52.0	-09 58 56.2	19.50	0.01	0.8	-12.80	60
970	12 17 23.6	-10 04 42.8	19.50	0.00	0.7	-12.80	64
325	12 16 47.0	-09 39 36.0	19.52	0.09	0.8	-12.78	166
2088	12 18 09.1	-09 48 42.1	19.53	0.00	0.8	-12.77	117
1001	12 17 25.0	-09 45 50.7	19.54	0.01	0.7	-12.76	95
1656	12 18 00.1	-10 07 17.2	19.54	0.05	0.7	-12.76	114
887	12 17 18.2	-09 48 22.7	19.54	0.01	0.8	-12.76	74
877	12 17 17.8	-10 05 39.4	19.56	0.05	0.8	-12.74	73
917	12 17 20.6	-10 06 22.0	19.56	0.00	0.9	-12.74	79
1191	12 17 36.7	-09 57 28.8	19.57	0.01	1.0	-12.73	26
1550	12 17 54.1	-10 07 27.4	19.58	0.01	0.8	-12.72	107
2264	12 18 07.5	-09 50 13.7	19.58	0.03	0.7	-12.72	107
352	12 16 48.2	-09 42 18.6	19.60	0.00	0.9	-12.70	145
1354	12 17 44.2	-09 38 26.3	19.62	0.01	0.8	-12.68	163
577	12 17 02.0	-09 47 00.2	19.62	0.09	0.7	-12.69	96
914	12 17 19.8	-09 41 31.0	19.62	0.09	0.8	-12.68	132
2031	12 18 32.3	-09 51 36.2	19.63	0.09	0.7	-12.67	149
2199	12 18 12.7	-09 50 42.0	19.63	0.00	0.8	-12.67	114
133	12 16 38.5	-10 05 32.6	19.64	0.00	1.1	-12.66	119
1556	12 17 54.2	-09 41 08.9	19.64	0.09	0.7	-12.66	148
2118	12 18 17.1	-09 39 34.9	19.64	0.00	0.9	-12.66	184
327	12 16 47.2	-09 56 21.1	19.64	0.07	0.7	-12.66	77
2392	12 18 33.4	-09 59 08.9	19.65	0.08	0.7	-12.65	145
50	12 16 33.3	-09 48 39.9	19.65	0.01	0.7	-12.65	127
138	12 16 38.3	-10 02 13.5	19.66	0.01	0.9	-12.64	104
2138	12 18 15.6	-09 50 06.7	19.66	0.01	0.7	-12.65	122
1241	12 17 39.6	-09 59 30.5	19.67	0.01	0.8	-12.63	38
2326	12 18 32.0	-10 06 07.4	19.68	0.06	0.7	-12.62	161
1209	12 17 37.1	-09 44 12.5	19.69	0.02	0.6	-12.62	112
1554	12 17 54.1	-09 40 26.9	19.69	0.01	0.6	-12.61	154
2045	12 18 36.9	-09 43 57.7	19.72	0.01	0.8	-12.58	188
896	12 17 18.6	-10 02 53.7	19.72	0.01	0.7	-12.58	50
2299	12 18 30.7	-09 47 08.3	19.73	0.03	0.8	-12.57	162
578	12 17 02.0	-09 39 15.2	19.74	0.02	1.0	-12.56	157
1830	12 18 35.4	-10 07 16.6	19.75	0.09	0.7	-12.55	171
222	12 16 42.4	-09 45 24.8	19.75	0.02	0.7	-12.55	131
2390	12 18 32.6	-09 48 19.5	19.75	0.01	0.8	-12.55	160
800	12 17 13.2	-09 42 56.9	19.75	0.01	0.7	-12.55	121
958	12 17 22.9	-10 07 37.1	19.75	0.00	1.0	-12.55	89
1924	12 18 32.6	-09 53 15.2	19.76	0.06	0.7	-12.54	146
2213	12 18 10.2	-09 38 24.6	19.76	0.02	0.7	-12.54	184
2239	12 18 09.9	-10 02 36.2	19.77	0.04	0.7	-12.53	106
1413	12 17 47.4	-09 40 35.9	19.79	0.03	0.6	-12.51	147
809	12 17 13.6	-09 51 00.5	19.79	0.01	0.8	-12.51	55
962	12 17 22.7	-09 38 59.0	19.81	0.04	0.7	-12.49	153
1612	12 17 57.8	-09 52 12.4	19.82	0.00	0.8	-12.49	81
1101	12 17 30.5	-09 39 15.8	19.83	0.02	0.8	-12.47	151

Table A.5: Candidate satellite galaxies in the field of NCG 4240(continued).

Number (1)	RA (J2000) (2)	DEC (J2000) (3)	R (mag) (4)	Class (5)	A (arcsec) (6)	M_R (mag) (7)	Dist (kpc) (8)
2376	12 18 29.6	-10 07 48.7	19.83	0.06	0.7	-12.47	164
2385	12 18 33.7	-09 50 12.7	19.83	0.03	0.6	-12.47	156
498	12 16 57.1	-09 52 11.9	19.84	0.06	0.7	-12.46	69
1822	12 18 35.5	-09 46 55.4	19.85	0.02	0.6	-12.45	171
410	12 16 51.8	-09 46 37.8	19.85	0.08	0.6	-12.45	111
527	12 16 58.6	-10 05 19.3	19.86	0.01	0.6	-12.44	87
1247	12 17 39.8	-09 47 57.3	19.88	0.02	0.8	-12.42	83
811	12 17 13.8	-10 01 15.2	19.89	0.01	0.7	-12.41	41
2149	12 18 13.1	-09 44 14.2	19.91	0.05	0.6	-12.40	149
180	12 16 40.5	-10 01 14.5	19.92	0.04	0.6	-12.38	97
591	12 17 02.6	-10 05 57.2	19.92	0.06	0.6	-12.38	87
1404	12 17 46.7	-09 48 41.3	19.93	0.08	0.6	-12.37	85
1654	12 17 59.8	-09 54 29.3	19.94	0.05	0.6	-12.37	77
1319	12 17 43.0	-09 46 56.9	19.95	0.00	0.7	-12.35	94
1883	12 18 30.4	-10 07 33.0	19.95	0.08	0.7	-12.35	164
2154	12 18 19.6	-10 07 40.1	19.95	0.06	0.6	-12.35	146
1048	12 17 27.1	-09 37 50.2	19.97	0.01	0.7	-12.34	163
2344	12 18 14.4	-09 46 19.6	19.97	0.07	0.6	-12.33	138
2379	12 18 34.4	-10 07 11.1	19.98	0.01	0.7	-12.32	169
1940	12 18 26.6	-10 06 05.9	19.99	0.01	0.7	-12.32	151
1843	12 18 15.3	-09 40 11.3	20.00	0.08	0.7	-12.30	178
671	12 17 06.6	-10 08 36.6	20.01	0.01	0.6	-12.30	104
430	12 16 53.2	-10 08 11.2	20.02	0.08	0.6	-12.28	114
2230	12 18 11.0	-09 51 09.4	20.03	0.03	0.6	-12.27	109
1889	12 18 20.2	-10 01 26.1	20.05	0.01	0.7	-12.25	122
1208	12 17 37.5	-10 06 00.9	20.09	0.06	0.7	-12.21	80
2051	12 18 20.3	-09 44 35.3	20.09	0.02	0.6	-12.21	157
1375	12 17 45.1	-09 38 07.8	20.13	0.01	0.8	-12.17	166
2063	12 18 20.5	-09 41 59.4	20.13	0.08	0.7	-12.18	173
1259	12 17 40.4	-10 06 01.7	20.19	0.02	0.6	-12.12	83
1842	12 18 15.0	-09 58 40.8	20.19	0.03	0.6	-12.12	106
2001	12 18 23.4	-10 03 32.2	20.19	0.04	0.6	-12.11	135
2389	12 18 26.5	-09 47 20.2	20.19	0.08	0.6	-12.12	154
650	12 17 05.1	-09 54 13.2	20.19	0.07	0.6	-12.11	46
515	12 16 57.8	-09 51 16.1	20.21	0.05	0.6	-12.09	73
2288	12 18 18.5	-09 54 33.2	20.23	0.05	0.6	-12.07	115

Table A.6: List of the candidate satellite galaxies in the field of NGC 6172.

Number	RA (J2000)	DEC (J2000)	R (mag)	Class	A (arcsec)	M_R (mag)	Dist (kpc)
2301	16 22 15.7	-01 22 54.2	14.23	0.03	9.1	-19.89	158
2153	16 22 11.3	-01 33 27.0	15.04	0.00	3.6	-19.08	50
2639	16 22 17.1	-01 21 58.1	15.06	0.03	3.0	-19.06	177
696	16 21 36.5	-01 29 30.2	15.50	0.03	2.6	-18.62	165
11	16 21 18.9	-01 34 28.9	16.26	0.03	1.6	-17.86	258
4755	16 23 10.3	-01 11 56.7	16.32	0.03	2.0	-17.80	474
506	16 21 30.9	-01 13 07.2	16.38	0.03	2.0	-17.74	395
1979	16 22 01.8	-01 28 54.4	16.45	0.00	2.4	-17.67	54
1742	16 21 57.1	-01 31 21.4	16.46	0.00	3.2	-17.66	62
747	16 21 36.9	-01 29 41.3	16.49	0.03	2.0	-17.63	162
2330	16 22 09.7	-01 30 29.5	16.60	0.03	2.0	-17.53	7
603	16 21 33.5	-01 24 40.5	16.61	0.02	2.0	-17.51	214
427	16 21 28.9	-01 36 51.6	16.68	0.03	2.0	-17.44	231
5	16 21 19.8	-01 31 33.2	16.68	0.00	2.5	-17.44	245
428	16 21 28.9	-01 30 10.0	16.77	0.03	1.4	-17.35	200
2520	16 22 12.8	-01 22 51.7	16.83	0.00	2.0	-17.29	157
762	16 21 36.7	-01 30 21.2	16.98	0.03	1.2	-17.14	162
735	16 21 36.3	-01 34 10.3	17.01	0.02	1.4	-17.11	176
5628	16 23 19.9	-01 27 37.3	17.06	0.00	2.0	-17.06	348
1371	16 21 47.8	-01 12 10.9	17.17	0.01	2.2	-16.95	381
419	16 21 30.5	-01 15 25.8	17.22	0.00	1.2	-16.90	357
3919	16 22 44.2	-01 36 03.1	17.23	0.03	1.2	-16.89	196
1078	16 21 42.1	-01 21 16.7	17.25	0.03	1.4	-16.87	231
5568	16 23 21.7	-01 26 35.9	17.25	0.00	2.0	-16.87	361
800	16 21 37.6	-01 41 03.5	17.28	0.03	1.1	-16.84	254
1297	16 21 46.9	-01 29 46.6	17.33	0.04	1.2	-16.79	114
4473	16 22 54.6	-01 13 42.9	17.42	0.03	1.1	-16.70	400
5405	16 23 20.9	-01 19 37.1	17.43	0.00	2.2	-16.69	411
2942	16 22 22.7	-01 23 34.8	17.46	0.00	1.3	-16.66	156
5683	16 23 19.1	-01 17 58.2	17.47	0.02	1.1	-16.65	422
740	16 21 35.7	-01 13 58.9	17.65	0.01	2.0	-16.47	370
251	16 21 24.8	-01 16 29.1	17.67	0.02	1.3	-16.45	357
5570	16 23 22.0	-01 36 53.4	17.69	0.04	1.1	-16.43	372
4928	16 23 06.4	-01 27 26.6	17.73	0.01	1.1	-16.39	284
5689	16 23 19.0	-01 30 43.5	17.81	0.01	1.2	-16.31	338
5127	16 22 59.6	-01 30 09.3	17.85	0.07	1.0	-16.27	243
1200	16 21 44.7	-01 39 24.4	17.86	0.03	1.1	-16.26	207
1487	16 21 54.1	-01 22 31.4	17.86	0.00	2.0	-16.26	180
951	16 21 39.9	-01 37 06.5	17.87	0.03	1.0	-16.25	190
738	16 21 36.2	-01 32 18.3	17.89	0.00	1.3	-16.23	166
909	16 21 39.4	-01 30 03.8	17.89	0.04	1.0	-16.23	149
2346	16 22 08.9	-01 36 54.5	17.90	0.02	1.1	-16.22	118
4925	16 23 03.3	-01 37 58.9	17.91	0.01	1.5	-16.21	296
2809	16 22 18.9	-01 26 20.1	17.94	0.01	1.3	-16.18	99
5481	16 22 53.6	-01 35 47.6	17.94	0.03	1.0	-16.18	234
3154	16 22 27.0	-01 31 55.9	17.96	0.01	1.1	-16.16	86
1122	16 21 42.8	-01 27 41.7	18.03	0.06	0.9	-16.09	145
1257	16 21 45.8	-01 20 52.5	18.06	0.01	1.1	-16.06	228

Table A.6: Candidate satellite galaxies in the field of NCG 6172(continued).

Number (1)	RA (J2000) (2)	DEC (J2000) (3)	R (mag) (4)	Class (5)	A (arcsec) (6)	M_R (mag) (7)	Dist (kpc) (8)
828	16 21 37.9	-01 33 20.9	18.07	0.00	1.6	-16.05	163
1844	16 21 58.0	-01 32 19.3	18.09	0.02	1.0	-16.03	64
887	16 21 39.1	-01 42 18.0	18.11	0.00	1.4	-16.01	269
2949	16 22 22.6	-01 22 43.2	18.13	0.07	1.0	-15.99	171
587	16 21 32.8	-01 40 47.0	18.15	0.01	1.2	-15.97	265
3740	16 22 40.8	-01 37 20.4	18.17	0.00	1.0	-15.95	197
1551	16 21 52.5	-01 31 35.0	18.19	0.06	0.9	-15.93	85
2127	16 22 04.1	-01 16 50.3	18.19	0.00	1.4	-15.93	275
844	16 21 38.0	-01 30 03.4	18.20	0.00	1.1	-15.92	156
2980	16 22 23.2	-01 15 57.8	18.22	0.01	1.0	-15.90	298
2642	16 22 14.9	-01 23 11.0	18.24	0.00	1.5	-15.88	152
745	16 21 36.0	-01 32 35.0	18.24	0.03	0.9	-15.88	168
460	16 21 29.4	-01 28 33.2	18.25	0.01	1.1	-15.87	202
4591	16 23 12.9	-01 23 53.3	18.28	0.03	1.0	-15.84	337
4968	16 23 04.6	-01 15 38.5	18.28	0.00	1.2	-15.84	400
3562	16 22 35.4	-01 16 02.1	18.34	0.02	0.9	-15.78	316
2090	16 22 03.6	-01 33 27.8	18.35	0.00	1.0	-15.77	59
3983	16 22 45.4	-01 29 44.5	18.36	0.01	0.9	-15.76	175
5529	16 23 22.2	-01 34 53.7	18.36	0.01	1.0	-15.76	362
1150	16 21 43.3	-01 20 51.6	18.38	0.03	0.9	-15.74	234
455	16 21 28.6	-01 15 21.9	18.38	0.02	0.7	-15.74	364
1027	16 21 41.2	-01 31 52.7	18.39	0.05	0.8	-15.73	141
3555	16 22 37.2	-01 28 08.2	18.40	0.04	1.0	-15.72	144
447	16 21 28.7	-01 12 30.5	18.40	0.01	1.1	-15.72	411
2556	16 22 12.8	-01 23 04.3	18.44	0.01	0.9	-15.68	153
635	16 21 33.5	-01 30 19.1	18.44	0.00	1.1	-15.68	177
3878	16 22 43.2	-01 35 37.9	18.45	0.08	0.8	-15.67	188
1218	16 21 45.1	-01 41 30.6	18.50	0.05	0.9	-15.62	240
4738	16 23 10.3	-01 33 29.6	18.51	0.03	0.9	-15.61	300
4437	16 23 17.0	-01 30 44.4	18.53	0.00	0.9	-15.59	328
959	16 21 40.0	-01 19 50.9	18.53	0.02	1.1	-15.59	260
3475	16 22 33.1	-01 12 19.8	18.57	0.00	1.0	-15.55	380
3476	16 22 33.6	-01 38 26.7	18.57	0.02	0.9	-15.55	188
4464	16 23 04.4	-01 25 12.7	18.6	0.01	0.9	-15.53	288
1069	16 21 41.9	-01 29 09.7	18.60	0.02	0.8	-15.52	140
4048	16 22 47.4	-01 28 45.6	18.61	0.00	1.2	-15.51	188
2083	16 22 03.2	-01 38 45.8	18.62	0.01	0.9	-15.50	157
2085	16 22 03.2	-01 34 03.5	18.63	0.04	0.8	-15.49	70
1823	16 21 57.1	-01 18 30.6	18.64	0.00	0.9	-15.48	249
5109	16 23 02.8	-01 15 39.9	18.64	0.02	1.0	-15.48	394
1967	16 22 00.1	-01 17 56.5	18.65	0.00	0.9	-15.47	257
4930	16 23 07.3	-01 21 39.2	18.68	0.00	1.0	-15.44	334
3846	16 22 42.4	-01 29 05.6	18.69	0.00	1.0	-15.43	163
4974	16 23 06.0	-01 37 49.1	18.69	0.00	1.0	-15.43	306
3177	16 22 27.1	-01 16 29.0	18.72	0.06	0.8	-15.40	293
465	16 21 28.7	-01 14 36.9	18.73	0.06	0.6	-15.39	376
739	16 21 36.0	-01 38 47.4	18.76	0.02	1.0	-15.36	226
3343	16 22 31.0	-01 13 08.2	18.77	0.04	1.0	-15.35	362
4064	16 22 47.4	-01 30 01.4	18.77	0.00	0.9	-15.35	184
4630	16 23 19.9	-01 11 45.2	18.77	0.06	0.8	-15.35	507
4788	16 23 10.2	-01 14 47.0	18.78	0.00	1.0	-15.34	431
2267	16 22 07.1	-01 32 16.7	18.81	0.02	1.0	-15.31	30
3879	16 22 42.7	-01 14 31.2	18.81	0.02	0.9	-15.31	358
4180	16 22 50.2	-01 26 20.5	18.82	0.01	1.2	-15.30	216
2476	16 22 10.9	-01 13 30.3	18.83	0.00	0.9	-15.29	339
4739	16 23 09.6	-01 24 18.6	18.83	0.00	1.1	-15.29	319
3625	16 22 36.8	-01 35 39.1	18.85	0.09	0.7	-15.27	162
5450	16 22 54.5	-01 11 20.4	18.85	0.01	0.8	-15.27	440
4892	16 23 07.8	-01 36 08.1	18.86	0.01	1.0	-15.26	301
5604	16 23 18.3	-01 26 16.0	18.89	0.09	0.8	-15.23	346
2443	16 22 10.4	-01 29 25.9	18.90	0.01	1.0	-15.22	28
5352	16 22 57.7	-01 30 25.4	18.90	0.00	0.8	-15.22	234
1134	16 21 42.9	-01 23 25.9	18.91	0.01	0.9	-15.21	196
1147	16 21 43.6	-01 21 35.0	18.92	0.00	1.3	-15.20	222
4751	16 23 09.7	-01 11 25.3	18.94	0.03	0.8	-15.18	480
5694	16 23 19.6	-01 24 35.1	18.95	0.05	0.9	-15.17	362
2062	16 22 02.7	-01 28 37.6	18.96	0.02	0.9	-15.16	55
404	16 21 27.9	-01 20 17.9	18.96	0.02	1.0	-15.16	290
1324	16 21 47.1	-01 39 43.9	18.97	0.04	0.7	-15.15	205
1369	16 21 47.6	-01 22 29.6	18.97	0.06	0.8	-15.15	196
3675	16 22 38.4	-01 40 20.3	18.97	0.00	1.0	-15.15	232
1620	16 21 54.0	-01 40 27.7	18.98	0.00	1.0	-15.14	202
1943	16 21 59.9	-01 32 54.2	19.00	0.00	1.0	-15.12	62
2494	16 22 11.3	-01 17 38.7	19.00	0.05	0.7	-15.12	258
1192	16 21 43.9	-01 13 44.3	19.02	0.04	0.9	-15.10	358
2963	16 22 23.1	-01 38 04.3	19.02	0.00	0.9	-15.10	155
1955	16 22 00.0	-01 32 43.3	19.03	0.02	0.8	-15.09	59
812	16 21 37.0	-01 28 53.3	19.03	0.00	1.0	-15.09	165
4021	16 22 46.0	-01 12 16.4	19.04	0.05	0.7	-15.08	404
5589	16 22 54.1	-01 24 54.2	19.05	0.05	0.8	-15.07	246
1284	16 21 46.2	-01 36 36.0	19.06	0.00	0.9	-15.06	160
5232	16 23 16.7	-01 42 06.4	19.06	0.00	0.8	-15.06	394
5594	16 23 21.6	-01 34 59.9	19.06	0.01	0.7	-15.06	360
4208	16 22 50.0	-01 20 36.0	19.07	0.00	0.7	-15.05	281
4637	16 23 13.1	-01 23 24.1	19.07	0.02	0.8	-15.05	342
1383	16 21 47.8	-01 18 40.9	19.08	0.05	0.8	-15.04	261
1762	16 21 55.7	-01 16 16.8	19.08	0.00	0.7	-15.04	293
3696	16 22 38.6	-01 19 12.2	19.08	0.00	1.0	-15.04	268
719	16 21 35.4	-01 41 08.0	19.08	0.00	0.8	-15.05	262
811	16 21 37.2	-01 37 51.0	19.08	0.07	0.8	-15.04	209

Table A.6: Candidate satellite galaxies in the field of NCG 6172(continued).

Number (1)	RA (J2000) (2)	DEC (J2000) (3)	R (mag) (4)	Class (5)	A (arcsec) (6)	M_R (mag) (7)	Dist (kpc) (8)
5028	16 23 04.7	-01 31 34.5	19.09	0.04	0.8	-15.03	268
4707	16 22 58.6	-01 21 51.4	19.17	0.00	0.8	-14.95	296
5382	16 23 21.1	-01 28 33.2	19.18	0.00	1.1	-14.94	351
2096	16 22 03.3	-01 35 07.2	19.19	0.00	0.8	-14.93	88
4223	16 22 50.6	-01 40 26.5	19.19	0.02	0.8	-14.93	273
5026	16 23 02.0	-01 35 16.0	19.19	0.09	0.8	-14.93	269
5037	16 23 15.8	-01 29 48.6	19.19	0.00	0.9	-14.93	323
1933	16 21 59.4	-01 28 52.2	19.20	0.00	0.7	-14.92	64
1972	16 22 00.3	-01 31 13.6	19.22	0.01	0.9	-14.90	46
2325	16 22 08.2	-01 38 34.0	19.22	0.01	0.9	-14.90	150
2155	16 22 04.4	-01 33 49.1	19.23	0.06	0.7	-14.89	63
340	16 21 26.1	-01 21 50.9	19.24	0.00	0.8	-14.88	277
832	16 21 37.1	-01 14 28.2	19.24	0.01	0.7	-14.88	358
1374	16 21 47.9	-01 39 33.9	19.28	0.02	0.7	-14.84	201
2571	16 22 13.2	-01 33 39.0	19.28	0.04	0.7	-14.84	56
5051	16 23 04.0	-01 30 59.0	19.28	0.05	0.6	-14.84	264
698	16 21 34.6	-01 33 43.2	19.28	0.00	0.8	-14.84	180
1475	16 21 50.2	-01 38 16.3	19.30	0.02	0.6	-14.82	173
2692	16 22 15.7	-01 22 16.5	19.32	0.06	0.7	-14.80	170
274	16 21 25.0	-01 42 33.3	19.32	0.01	0.6	-14.80	316
3203	16 22 28.0	-01 38 20.3	19.32	0.09	0.7	-14.80	171
4976	16 23 06.2	-01 30 36.2	19.33	0.02	0.6	-14.79	275
5080	16 23 02.1	-01 30 26.5	19.33	0.00	0.8	-14.79	256
3780	16 22 40.2	-01 24 37.6	19.34	0.00	0.9	-14.78	192
64	16 21 19.7	-01 32 58.5	19.35	0.04	0.8	-14.77	248
1189	16 21 44.0	-01 36 22.2	19.36	0.06	0.7	-14.76	165
5537	16 23 20.8	-01 13 23.5	19.36	0.01	0.6	-14.76	487
1812	16 21 57.0	-01 24 29.2	19.37	0.01	0.7	-14.75	139
2411	16 22 09.6	-01 32 18.0	19.37	0.00	0.8	-14.75	27
3226	16 22 28.1	-01 16 31.2	19.37	0.05	0.7	-14.75	294
5530	16 23 15.7	-01 36 34.2	19.37	0.01	0.7	-14.75	341
2868	16 22 19.5	-01 22 09.6	19.38	0.06	0.7	-14.74	176
4274	16 22 51.8	-01 28 54.5	19.38	0.05	0.6	-14.74	208
1636	16 21 53.9	-01 36 51.8	19.39	0.01	0.5	-14.73	140
1759	16 21 55.8	-01 28 38.8	19.39	0.07	0.7	-14.73	80
5553	16 23 18.4	-01 42 26.2	19.39	0.02	0.8	-14.73	404
2106	16 22 03.2	-01 14 51.7	19.40	0.08	0.6	-14.72	314
3393	16 22 32.0	-01 35 20.4	19.41	0.01	0.7	-14.71	139
1786	16 21 56.3	-01 19 13.0	19.42	0.00	0.7	-14.70	237
3200	16 22 27.4	-01 11 18.6	19.43	0.00	0.8	-14.69	392
2616	16 22 13.9	-01 31 34.3	19.44	0.06	0.6	-14.68	24
1986	16 22 00.5	-01 27 17.9	19.45	0.00	0.6	-14.67	83
1327	16 21 46.9	-01 31 02.3	19.46	0.00	0.6	-14.66	111
1898	16 21 58.8	-01 27 56.6	19.46	0.09	0.7	-14.66	78
2519	16 22 11.9	-01 37 08.3	19.46	0.01	0.5	-14.66	123
2604	16 22 13.9	-01 42 31.0	19.46	0.07	0.7	-14.66	228
5340	16 22 58.5	-01 33 34.0	19.46	0.00	0.7	-14.66	243
225	16 21 23.6	-01 32 14.2	19.48	0.05	0.6	-14.64	227
2502	16 22 11.3	-01 19 27.2	19.48	0.00	0.8	-14.64	223
3770	16 22 40.3	-01 31 07.6	19.48	0.00	0.7	-14.64	149
5618	16 23 18.3	-01 29 35.1	19.48	0.06	0.6	-14.64	336
2687	16 22 15.7	-01 22 09.9	19.50	0.06	0.7	-14.62	172
3097	16 22 25.6	-01 40 06.9	19.50	0.00	0.6	-14.62	196
2965	16 22 23.0	-01 39 49.0	19.51	0.00	0.7	-14.61	186
5039	16 23 04.4	-01 31 01.1	19.52	0.00	0.6	-14.60	267
1157	16 21 43.3	-01 19 50.5	19.54	0.00	0.6	-14.58	251
604	16 21 32.6	-01 41 24.7	19.54	0.00	0.7	-14.58	274
213	16 21 23.3	-01 38 17.0	19.55	0.01	0.7	-14.57	269
2629	16 22 14.3	-01 17 44.1	19.55	0.02	0.7	-14.57	257
5386	16 22 55.0	-01 11 31.1	19.56	0.01	0.5	-14.56	438
2466	16 22 10.8	-01 32 55.6	19.57	0.07	0.6	-14.56	40
3786	16 22 40.8	-01 40 20.5	19.57	0.05	0.6	-14.55	239
1118	16 21 42.4	-01 18 36.2	19.59	0.00	0.7	-14.53	274
649	16 21 33.5	-01 35 08.5	19.59	0.06	0.6	-14.53	196
2426	16 22 09.8	-01 33 07.3	19.61	0.06	0.6	-14.51	44
4546	16 23 13.0	-01 17 42.6	19.61	0.02	0.6	-14.51	402
4996	16 23 05.9	-01 32 08.8	19.63	0.00	0.6	-14.49	275
1072	16 21 41.7	-01 27 16.8	19.64	0.04	0.8	-14.48	154
2865	16 22 19.2	-01 20 54.2	19.64	0.01	0.8	-14.48	200
813	16 21 36.8	-01 15 32.6	19.64	0.08	0.7	-14.48	340
1164	16 21 43.3	-01 12 49.4	19.66	0.05	0.7	-14.46	376
3986	16 22 45.2	-01 27 14.7	19.66	0.06	0.6	-14.46	186
4121	16 22 48.5	-01 36 17.5	19.66	0.01	0.7	-14.46	217
3821	16 22 41.0	-01 11 14.0	19.68	0.01	0.6	-14.44	413
3028	16 22 23.8	-01 26 26.4	19.69	0.01	0.6	-14.43	110
4330	16 23 15.4	-01 19 46.3	19.69	0.01	0.6	-14.43	387
1540	16 21 51.9	-01 36 27.8	19.70	0.03	0.5	-14.42	140
3636	16 22 36.8	-01 24 17.4	19.70	0.03	0.6	-14.42	184
1755	16 21 55.7	-01 29 29.4	19.72	0.03	0.6	-14.40	73
2251	16 22 06.3	-01 30 45.8	19.72	0.05	0.6	-14.40	17
3110	16 22 26.0	-01 20 17.1	19.72	0.06	0.6	-14.40	221
3189	16 22 27.3	-01 16 15.4	19.72	0.03	0.6	-14.40	298
3519	16 22 34.1	-01 27 34.4	19.73	0.05	0.5	-14.39	135
4310	16 23 23.2	-01 42 00.9	19.73	0.04	0.8	-14.39	420
264	16 21 24.3	-01 16 50.6	19.75	0.01	0.6	-14.37	353
3320	16 22 30.4	-01 25 34.5	19.75	0.01	0.6	-14.37	144
5326	16 22 57.8	-01 29 35.1	19.75	0.09	0.6	-14.37	236
1476	16 21 50.3	-01 39 00.3	19.76	0.06	0.6	-14.36	185
2310	16 22 07.6	-01 21 27.5	19.77	0.01	0.5	-14.35	184
1539	16 21 52.0	-01 41 24.7	19.79	0.03	0.7	-14.33	223

Table A.6: Candidate satellite galaxies in the field of NCG 6172(continued).

Number (1)	RA (J2000) (2)	DEC (J2000) (3)	R (mag) (4)	Class (5)	A (arcsec) (6)	M_R (mag) (7)	Dist (kpc) (8)
328	16 21 25.9	-01 31 00.9	19.79	0.05	0.5	-14.33	214
5031	16 23 02.6	-01 28 51.8	19.79	0.02	0.7	-14.33	261
532	16 21 30.4	-01 14 18.6	19.80	0.01	0.7	-14.32	376
904	16 21 38.7	-01 20 00.3	19.80	0.01	0.7	-14.32	261
395	16 21 27.6	-01 35 12.8	19.81	0.03	0.5	-14.31	223
23	16 21 18.5	-01 20 17.6	19.83	0.00	0.7	-14.29	325
2028	16 22 01.3	-01 22 29.8	19.84	0.04	0.5	-14.28	168
4006	16 22 45.6	-01 25 33.9	19.84	0.01	0.6	-14.28	203
795	16 21 36.9	-01 39 56.6	19.84	0.04	0.6	-14.29	239
2975	16 22 23.0	-01 41 20.4	19.85	0.06	0.5	-14.27	214
2353	16 22 08.2	-01 21 44.2	19.86	0.04	0.5	-14.26	178
3317	16 22 30.4	-01 40 50.7	19.86	0.01	0.5	-14.26	219
895	16 21 38.8	-01 40 24.2	19.86	0.02	0.6	-14.26	240
1105	16 21 42.3	-01 27 09.4	19.87	0.05	0.6	-14.25	152
4202	16 22 50.0	-01 24 33.3	19.87	0.00	0.6	-14.25	232
5392	16 23 17.0	-01 42 00.2	19.87	0.02	0.6	-14.25	394
3017	16 22 23.7	-01 33 51.6	19.89	0.01	0.6	-14.23	89
3754	16 22 39.4	-01 16 06.5	19.90	0.05	0.5	-14.22	323
2021	16 22 01.4	-01 28 25.9	19.91	0.04	0.6	-14.21	62
1360	16 21 47.7	-01 41 14.7	19.92	0.00	0.6	-14.20	229
2088	16 22 03.1	-01 33 46.2	19.92	0.00	0.6	-14.20	65
1052	16 21 41.2	-01 24 31.6	19.93	0.02	0.6	-14.19	186
3477	16 22 33.5	-01 42 27.8	19.93	0.03	0.6	-14.19	254
5104	16 23 00.7	-01 34 00.8	19.93	0.09	0.5	-14.20	256
1474	16 21 50.1	-01 27 03.0	19.96	0.07	0.7	-14.16	121
3598	16 22 36.3	-01 38 05.9	19.96	0.01	0.7	-14.16	191
399	16 21 27.6	-01 39 04.7	19.97	0.08	0.7	-14.15	261
2871	16 22 19.2	-01 16 11.3	19.98	0.02	0.6	-14.14	290
5509	16 22 54.5	-01 23 49.5	19.99	0.05	0.6	-14.13	258
446	16 21 28.2	-01 12 20.1	20.03	0.08	0.5	-14.09	415
5666	16 23 20.4	-01 25 53.8	20.03	0.05	0.6	-14.09	358
120	16 21 20.9	-01 38 25.1	20.06	0.06	0.5	-14.06	280
4098	16 22 47.5	-01 17 30.0	20.11	0.06	0.5	-14.01	319
4167	16 22 49.3	-01 36 48.5	20.13	0.08	0.5	-13.99	225
1625	16 21 53.8	-01 41 39.9	20.16	0.08	0.5	-13.96	225
5476	16 23 18.8	-01 36 46.0	20.17	0.08	0.5	-13.95	356
176	16 21 22.2	-01 40 14.3	20.22	0.02	0.6	-13.90	296
5391	16 22 57.1	-01 41 56.3	20.22	0.09	0.5	-13.90	316
665	16 21 33.6	-01 30 58.8	20.25	0.08	0.5	-13.87	176
1761	16 21 55.5	-01 18 03.6	20.28	0.08	0.7	-13.84	260

Table A.7: List of the candidate satellite galaxies in the field of ESO 218-G002.

Number	RA (J2000)	DEC (J2000)	R (mag)	Class	A (arcsec)	M_R (mag)	Dist (kpc)
7190	12 20 47.7	-52 20 10.0	15.18	0.03	3.3	-18.48	241
14489	12 21 35.4	-52 43 57.6	16.24	0.03	2.4	-17.42	153
10974	12 21 08.4	-52 41 41.3	16.31	0.03	2.0	-17.35	103
10663	12 21 04.8	-52 28 37.9	16.43	0.03	1.4	-17.23	102
6029	12 20 31.0	-52 46 31.3	16.46	0.09	2.0	-17.20	199
22354	12 22 45.7	-52 23 52.2	16.53	0.05	1.5	-17.13	294
25709	12 22 22.8	-52 23 31.4	16.56	0.03	2.0	-17.10	256
10019	12 21 00.4	-52 27 20.1	16.60	0.00	4.0	-17.06	124
6547	12 20 34.1	-52 46 11.8	16.61	0.04	1.5	-17.05	192
3973	12 20 15.3	-52 15 38.8	16.63	0.03	2.0	-17.03	332
4267	12 20 18.7	-52 46 20.8	16.71	0.08	2.4	-16.95	212
5729	12 20 29.0	-52 38 41.4	16.71	0.03	1.6	-16.95	108
6096	12 20 32.6	-52 37 31.1	16.72	0.04	1.3	-16.94	92
22327	12 22 49.9	-52 32 39.9	16.73	0.01	2.4	-16.93	247
11418	12 21 09.7	-52 43 30.5	16.74	0.03	1.4	-16.92	131
20247	12 22 18.3	-52 24 48.8	16.76	0.04	3.0	-16.90	234
19621	12 22 12.0	-52 45 11.1	16.86	0.08	1.2	-16.80	220
15943	12 21 45.6	-52 29 42.4	16.87	0.06	2.0	-16.79	124
10107	12 21 00.6	-52 29 29.9	16.88	0.00	3.0	-16.78	90
6572	12 20 35.8	-52 39 25.4	16.91	0.00	3.0	-16.75	102
13647	12 21 27.4	-52 28 43.0	16.93	0.03	2.4	-16.73	111
23000	12 23 04.6	-52 41 48.1	16.94	0.03	3.0	-16.72	298
7029	12 20 37.8	-52 21 29.6	16.99	0.01	2.5	-16.67	227
8438	12 20 48.6	-52 24 24.9	17.01	0.02	2.1	-16.65	175
25375	12 22 25.9	-52 32 47.1	17.02	0.04	2.0	-16.64	190
6634	12 20 35.2	-52 44 41.5	17.02	0.02	3.0	-16.64	169
10502	12 21 04.5	-52 35 49.8	17.04	0.00	2.4	-16.62	13
15031	12 21 38.7	-52 33 42.1	17.13	0.07	1.3	-16.53	77
27345	12 22 51.4	-52 22 56.7	17.15	0.00	3.1	-16.51	314
10898	12 21 06.6	-52 33 50.3	17.20	0.03	1.4	-16.46	20
7023	12 20 38.1	-52 43 50.2	17.21	0.03	1.3	-16.45	154
8313	12 20 47.2	-52 40 20.0	17.21	0.08	1.1	-16.45	95
5690	12 20 28.6	-52 38 49.7	17.22	0.02	1.3	-16.44	110
16139	12 21 52.9	-52 16 35.2	17.25	0.00	4.6	-16.41	311
392	12 19 48.6	-52 21 59.7	17.27	0.01	2.3	-16.39	281
20823	12 23 08.7	-52 36 33.6	17.28	0.03	1.2	-16.38	290
21763	12 22 57.7	-52 42 12.4	17.30	0.01	2.0	-16.36	285
14532	12 21 34.7	-52 33 42.4	17.31	0.04	1.1	-16.35	67
19161	12 22 08.1	-52 15 42.6	17.35	0.02	1.5	-16.31	338
26626	12 22 55.7	-52 22 53.9	17.35	0.00	3.0	-16.31	322
8476	12 20 48.6	-52 39 43.5	17.37	0.00	2.0	-16.29	85
11610	12 21 10.9	-52 27 39.7	17.38	0.00	3.0	-16.28	118
18116	12 22 01.5	-52 44 51.3	17.46	0.04	1.2	-16.20	199
4454	12 20 18.3	-52 45 30.9	17.51	0.04	1.2	-16.15	201

Table A.7: Candidate satellite galaxies in the field of ESO 218-G002 (continued).

Number (1)	RA (J2000) (2)	DEC (J2000) (3)	R (mag) (4)	Class (5)	A (arcsec) (6)	M_R (mag) (7)	Dist (kpc) (8)
15958	12 21 45.2	-52 34 24.0	17.52	0.01	2.0	-16.14	90
1817	12 19 58.1	-52 44 48.7	17.55	0.04	1.1	-16.11	226
25296	12 22 27.8	-52 15 56.3	17.59	0.02	1.3	-16.07	358
16287	12 21 46.5	-52 26 49.0	17.61	0.00	0.9	-16.05	160
24537	12 22 34.6	-52 46 00.2	17.66	0.08	1.1	-16.00	268
7082	12 20 38.9	-52 45 38.8	17.67	0.01	2.0	-15.99	179
21115	12 22 58.0	-52 37 24.4	17.69	0.00	1.4	-15.97	265
6058	12 20 30.4	-52 45 10.0	17.69	0.05	1.4	-15.97	181
3700	12 20 13.4	-52 28 42.3	17.70	0.00	1.6	-15.96	165
15764	12 21 43.3	-52 46 43.1	17.72	0.02	1.1	-15.94	201
21695	12 22 53.2	-52 19 03.4	17.73	0.01	0.7	-15.93	358
21729	12 22 56.8	-52 42 32.7	17.73	0.06	1.4	-15.93	285
21877	12 22 53.4	-52 24 47.5	17.73	0.01	1.0	-15.93	301
21435	12 22 56.5	-52 24 56.6	17.74	0.00	1.0	-15.92	305
2296	12 20 01.8	-52 27 27.8	17.74	0.00	2.0	-15.92	199
21532	12 22 55.5	-52 25 02.8	17.75	0.09	1.0	-15.91	303
5373	12 20 26.1	-52 46 50.4	17.76	0.01	1.5	-15.90	209
11266	12 21 09.5	-52 23 04.7	17.79	0.01	1.5	-15.87	190
20807	12 23 04.7	-52 44 04.0	17.81	0.01	3.0	-15.85	312
16473	12 21 48.0	-52 24 33.3	17.83	0.03	1.5	-15.83	192
25197	12 22 30.4	-52 46 47.3	17.86	0.01	3.0	-15.80	269
4405	12 20 17.6	-52 25 06.0	17.87	0.02	2.0	-15.79	199
564	12 19 48.7	-52 29 28.8	17.87	0.03	1.3	-15.79	210
25571	12 22 25.4	-52 20 36.2	17.89	0.00	1.2	-15.77	295
15161	12 21 38.5	-52 28 20.8	17.90	0.07	1.0	-15.76	129
17210	12 21 54.9	-52 43 05.6	17.90	0.01	2.0	-15.76	168
24968	12 22 30.2	-52 18 09.2	17.94	0.06	0.8	-15.72	332
22514	12 22 47.1	-52 19 45.1	17.95	0.06	0.8	-15.71	339
13309	12 21 24.2	-52 38 12.1	17.96	0.00	2.0	-15.70	61
23947	12 22 33.3	-52 18 45.0	17.99	0.00	0.7	-15.67	329
17957	12 22 01.9	-52 46 35.2	18.02	0.06	1.1	-15.64	221
2982	12 20 06.7	-52 39 37.8	18.04	0.01	1.1	-15.62	162
5050	12 20 22.6	-52 27 26.7	18.04	0.09	0.9	-15.62	163
6143	12 20 31.3	-52 34 44.7	18.04	0.01	2.0	-15.62	87
5613	12 20 27.3	-52 46 50.6	18.06	0.00	2.0	-15.60	208
2950	12 20 06.6	-52 40 25.1	18.07	0.09	1.1	-15.59	168
11363	12 21 09.2	-52 38 51.9	18.08	0.00	1.3	-15.58	58
14976	12 21 37.8	-52 45 07.9	18.11	0.04	1.2	-15.55	172
21128	12 22 56.1	-52 17 06.7	18.11	0.07	0.6	-15.55	385
21434	12 22 56.7	-52 17 05.1	18.11	0.02	0.7	-15.55	386
5915	12 20 29.3	-52 39 34.0	18.11	0.01	1.3	-15.55	115
23453	12 22 41.2	-52 15 29.6	18.12	0.06	1.2	-15.54	382
6955	12 20 36.6	-52 32 41.7	18.13	0.04	1.1	-15.53	84
24792	12 22 29.6	-52 40 10.9	18.15	0.06	1.1	-15.51	210
27068	12 23 04.7	-52 37 57.7	18.15	0.00	1.1	-15.51	282
774	12 19 50.7	-52 42 49.8	18.15	0.00	2.0	-15.51	221
15736	12 21 43.2	-52 26 46.6	18.19	0.04	1.2	-15.47	156
25359	12 22 27.6	-52 42 32.9	18.19	0.01	1.0	-15.47	223
3493	12 20 11.0	-52 21 07.7	18.19	0.08	1.1	-15.47	259
12146	12 21 14.5	-52 26 31.1	18.20	0.07	0.8	-15.46	136
27029	12 22 58.0	-52 31 23.4	18.20	0.05	1.2	-15.46	270
11307	12 21 08.6	-52 39 17.8	18.21	0.00	1.2	-15.45	65
18099	12 22 01.0	-52 32 51.9	18.21	0.00	1.3	-15.45	131
20332	12 22 16.8	-52 46 14.5	18.22	0.01	1.1	-15.44	240
837	12 19 50.6	-52 42 54.1	18.23	0.06	1.2	-15.43	221
8337	12 20 47.9	-52 20 21.0	18.24	0.00	2.5	-15.42	238
16050	12 21 45.1	-52 37 27.6	18.26	0.03	1.0	-15.40	96
22325	12 22 48.2	-52 19 43.6	18.26	0.06	0.6	-15.40	342
17702	12 21 56.9	-52 20 54.8	18.27	0.08	1.0	-15.39	253
8893	12 20 51.7	-52 42 40.7	18.27	0.02	1.2	-15.39	124
11646	12 21 10.8	-52 36 13.4	18.28	0.04	0.8	-15.38	18
26230	12 22 21.6	-52 41 25.2	18.28	0.04	1.0	-15.38	201
21420	12 22 55.5	-52 18 44.2	18.30	0.01	0.6	-15.36	365
25653	12 22 21.2	-52 15 33.6	18.30	0.09	0.8	-15.36	355
658	12 19 49.5	-52 21 45.5	18.30	0.01	1.1	-15.36	282
1097	12 19 52.7	-52 24 12.5	18.33	0.00	1.2	-15.33	249
23769	12 22 36.7	-52 16 14.4	18.33	0.00	0.8	-15.33	366
20244	12 22 15.3	-52 23 00.2	18.34	0.00	1.1	-15.32	250
9495	12 20 55.1	-52 33 20.1	18.34	0.05	0.9	-15.32	41
5606	12 20 27.2	-52 46 45.1	18.35	0.07	1.3	-15.31	207
7937	12 20 43.7	-52 22 23.2	18.36	0.02	1.0	-15.30	209
26163	12 22 23.6	-52 39 15.3	18.37	0.08	0.6	-15.29	192
1380	12 19 54.8	-52 35 39.7	18.39	0.00	1.1	-15.27	175
62	12 19 45.1	-52 29 03.0	18.40	0.06	1.1	-15.26	220
506	12 19 48.0	-52 45 21.3	18.41	0.02	1.0	-15.25	249
5577	12 20 26.7	-52 35 38.2	18.41	0.05	1.0	-15.25	99
21969	12 22 53.1	-52 16 32.4	18.42	0.09	1.0	-15.24	387
10632	12 21 02.9	-52 34 51.1	18.43	0.03	0.6	-15.23	12
14038	12 21 30.3	-52 29 57.8	18.44	0.08	0.8	-15.22	97
11387	12 21 08.6	-52 31 51.0	18.45	0.01	1.2	-15.21	51
13206	12 21 22.8	-52 40 33.8	18.46	0.09	1.0	-15.20	92
16438	12 21 47.1	-52 25 20.5	18.50	0.01	0.6	-15.16	180
21354	12 22 56.5	-52 19 23.7	18.50	0.07	0.8	-15.16	359
4724	12 20 20.2	-52 40 19.8	18.50	0.01	1.1	-15.16	140
13729	12 21 28.6	-52 43 49.8	18.51	0.01	1.2	-15.15	145
23106	12 22 43.7	-52 46 34.9	18.53	0.02	1.0	-15.13	291
9699	12 20 56.3	-52 31 48.8	18.53	0.02	1.0	-15.13	59
21672	12 22 53.6	-52 22 22.3	18.54	0.03	0.9	-15.12	323
21828	12 22 55.9	-52 24 50.6	18.54	0.08	0.6	-15.12	305
22587	12 22 46.1	-52 29 13.0	18.55	0.03	2.0	-15.11	253

Table A.7: Candidate satellite galaxies in the field of ESO 218-G002 (continued).

Number (1)	RA (J2000) (2)	DEC (J2000) (3)	R (mag) (4)	Class (5)	A (arcsec) (6)	M_R (mag) (7)	Dist (kpc) (8)
7833	12 20 42.5	-52 19 44.3	18.56	0.08	0.8	-15.10	250
20087	12 22 14.7	-52 37 04.1	18.58	0.00	1.1	-15.08	162
7353	12 20 39.2	-52 27 53.0	18.58	0.03	0.8	-15.08	133
22523	12 22 43.0	-52 26 29.6	18.59	0.07	0.6	-15.07	265
25246	12 22 29.1	-52 39 59.2	18.59	0.00	1.1	-15.07	208
331	12 19 46.6	-52 27 11.6	18.59	0.03	0.8	-15.07	231
24367	12 22 33.7	-52 18 54.0	18.61	0.02	0.6	-15.05	328
19404	12 22 10.0	-52 36 36.0	18.62	0.00	1.2	-15.04	150
26393	12 22 18.7	-52 18 28.3	18.64	0.01	0.9	-15.02	313
2834	12 20 05.2	-52 42 53.1	18.64	0.04	0.9	-15.02	193
2998	12 20 06.4	-52 31 30.2	18.64	0.07	0.8	-15.02	158
25005	12 22 38.6	-52 41 33.6	18.65	0.07	0.9	-15.01	239
5581	12 20 26.8	-52 42 05.2	18.65	0.02	1.0	-15.01	147
15796	12 21 42.4	-52 19 23.3	18.67	0.05	0.8	-14.99	261
11023	12 21 05.8	-52 28 49.1	18.70	0.00	1.0	-14.96	99
26611	12 23 04.8	-52 22 34.0	18.70	0.00	1.2	-14.96	343
18670	12 22 04.3	-52 31 59.8	18.71	0.07	1.0	-14.95	143
15417	12 21 40.3	-52 45 30.5	18.72	0.05	0.6	-14.94	180
25650	12 22 26.8	-52 39 11.8	18.72	0.02	0.6	-14.94	199
4920	12 20 21.5	-52 44 51.6	18.72	0.01	1.0	-14.94	189
10785	12 21 04.6	-52 35 41.6	18.75	0.00	0.9	-14.91	11
27174	12 23 01.7	-52 33 22.9	18.75	0.09	0.5	-14.91	273
24322	12 22 34.0	-52 19 25.0	18.76	0.01	0.5	-14.90	322
6434	12 20 32.8	-52 46 25.9	18.76	0.01	0.9	-14.90	196
16483	12 21 48.2	-52 34 23.5	18.77	0.02	1.3	-14.89	97
7427	12 20 40.0	-52 36 23.9	18.78	0.06	0.9	-14.88	69
3159	12 20 07.7	-52 26 51.6	18.79	0.09	0.8	-14.87	194
7364	12 20 39.9	-52 46 50.7	18.79	0.07	1.0	-14.87	196
750	12 19 49.8	-52 17 09.0	18.79	0.01	1.0	-14.87	340
13416	12 21 24.1	-52 41 16.5	18.80	0.08	0.8	-14.86	104
25533	12 22 25.4	-52 18 29.5	18.80	0.01	0.8	-14.86	321
26234	12 22 19.6	-52 19 01.6	18.80	0.00	0.8	-14.86	306
11225	12 21 07.7	-52 34 15.9	18.81	0.05	1.0	-14.85	13
14657	12 21 34.5	-52 26 06.6	18.81	0.01	0.8	-14.85	155
16706	12 21 49.3	-52 18 55.4	18.81	0.00	1.0	-14.85	274
9430	12 20 54.6	-52 40 55.9	18.81	0.00	1.0	-14.85	96
17299	12 21 54.3	-52 32 06.8	18.82	0.04	1.0	-14.84	120
27132	12 23 02.8	-52 44 50.6	18.82	0.02	0.6	-14.84	314
4801	12 20 20.9	-52 46 31.4	18.82	0.02	1.1	-14.84	211
25477	12 22 27.6	-52 26 54.2	18.83	0.05	0.7	-14.83	230
19323	12 22 08.7	-52 21 47.8	18.84	0.00	1.2	-14.82	256
3404	12 20 09.5	-52 41 05.2	18.84	0.05	0.7	-14.82	168
8931	12 20 51.2	-52 42 45.1	18.84	0.00	1.0	-14.82	126
4939	12 20 21.6	-52 45 22.0	18.85	0.08	0.9	-14.81	195
9108	12 20 52.3	-52 15 53.8	18.85	0.08	1.0	-14.81	305
10388	12 21 01.2	-52 24 38.0	18.86	0.02	1.0	-14.80	166
15812	12 21 42.7	-52 27 21.3	18.86	0.00	0.7	-14.80	148
3942	12 20 14.0	-52 44 03.9	18.87	0.00	1.0	-14.79	190
10543	12 21 02.7	-52 41 03.0	18.89	0.05	0.9	-14.77	93
12108	12 21 14.4	-52 42 49.2	18.89	0.09	0.7	-14.77	122
16819	12 21 50.7	-52 36 55.0	18.89	0.00	0.9	-14.77	106
462	12 19 47.3	-52 44 48.7	18.89	0.01	0.9	-14.77	245
5370	12 20 25.1	-52 35 42.2	18.89	0.09	0.8	-14.77	103
13063	12 21 21.4	-52 46 06.2	18.90	0.00	0.8	-14.76	175
15675	12 21 41.9	-52 46 26.4	18.90	0.01	0.5	-14.76	195
598	12 19 48.6	-52 35 57.5	18.90	0.03	0.8	-14.76	190
19236	12 22 07.4	-52 16 25.8	18.91	0.00	1.0	-14.75	327
1730	12 19 57.3	-52 18 55.0	18.92	0.00	1.0	-14.74	307
5070	12 20 23.0	-52 37 16.8	18.93	0.01	1.2	-14.73	112
8431	12 20 47.0	-52 21 19.7	18.93	0.00	0.7	-14.73	223
8875	12 20 51.3	-52 31 51.0	18.93	0.02	1.4	-14.73	65
14298	12 21 33.4	-52 41 13.6	18.94	0.00	1.6	-14.72	113
20643	12 22 18.1	-52 28 29.1	18.94	0.00	0.9	-14.72	198
6597	12 20 33.8	-52 20 21.3	18.94	0.03	0.8	-14.72	247
1597	12 19 56.0	-52 29 04.6	18.95	0.00	0.9	-14.71	197
2134	12 20 00.2	-52 23 39.1	18.95	0.04	0.8	-14.71	243
3430	12 20 10.3	-52 28 34.4	18.95	0.00	1.1	-14.71	172
10666	12 21 04.0	-52 37 08.5	18.96	0.00	1.3	-14.70	32
11945	12 21 12.6	-52 29 31.1	18.96	0.04	1.0	-14.70	89
2320	12 20 01.4	-52 44 22.9	18.96	0.00	0.8	-14.70	215
12310	12 21 15.4	-52 18 02.6	18.97	0.07	0.8	-14.69	270
8173	12 20 45.7	-52 45 05.9	18.97	0.07	0.8	-14.69	165
20324	12 22 16.3	-52 41 30.7	18.98	0.01	0.8	-14.68	191
11174	12 21 06.9	-52 34 16.6	18.99	0.00	0.7	-14.67	13
17509	12 21 55.5	-52 30 00.0	18.99	0.03	0.9	-14.67	139
21074	12 23 00.1	-52 17 40.1	18.99	0.00	0.9	-14.67	385
21164	12 22 57.2	-52 28 40.8	18.99	0.07	0.6	-14.67	281
10875	12 21 05.1	-52 35 43.6	19.00	0.01	0.8	-14.66	11
1821	12 19 57.9	-52 36 42.2	19.00	0.00	1.1	-14.66	169
9628	12 20 55.5	-52 28 15.8	19.00	0.03	0.6	-14.66	112
13395	12 21 23.6	-52 20 19.1	19.01	0.01	1.0	-14.65	236
4675	12 20 19.4	-52 46 46.5	19.01	0.01	1.0	-14.65	216
18769	12 22 03.9	-52 17 02.8	19.02	0.06	0.7	-14.64	315
3064	12 20 07.0	-52 44 09.3	19.02	0.00	0.9	-14.64	203
19235	12 22 08.4	-52 37 12.3	19.04	0.03	0.8	-14.62	148
23402	12 22 41.7	-52 24 49.3	19.04	0.06	0.8	-14.62	277
3937	12 20 14.2	-52 17 53.6	19.06	0.00	1.2	-14.60	301
22464	12 22 49.3	-52 44 19.6	19.08	0.05	0.8	-14.58	282
8234	12 20 45.4	-52 20 18.9	19.08	0.09	0.6	-14.58	239
15069	12 21 37.7	-52 45 40.0	19.09	0.04	0.5	-14.57	180

Table A.7: Candidate satellite galaxies in the field of ESO 218-G002 (continued).

Number (1)	RA (J2000) (2)	DEC (J2000) (3)	R (mag) (4)	Class (5)	A (arcsec) (6)	M_R (mag) (7)	Dist (kpc) (8)
27089	12 23 02.0	-52 29 01.6	19.09	0.06	0.7	-14.57	289
5533	12 20 26.0	-52 41 17.3	19.09	0.01	0.9	-14.57	139
16479	12 21 47.2	-52 17 13.6	19.10	0.03	0.8	-14.56	297
20061	12 22 13.5	-52 22 59.8	19.10	0.08	0.7	-14.56	247
26909	12 23 05.1	-52 41 12.4	19.10	0.01	1.1	-14.56	296
3987	12 20 14.0	-52 17 45.1	19.10	0.01	0.8	-14.56	303
6463	12 20 32.4	-52 26 51.9	19.10	0.03	0.7	-14.56	155
7539	12 20 40.8	-52 46 15.9	19.10	0.00	1.0	-14.56	186
10127	12 20 59.4	-52 40 47.6	19.11	0.05	0.8	-14.55	91
9110	12 20 52.4	-52 41 05.4	19.12	0.02	0.9	-14.54	100
8458	12 20 47.0	-52 16 55.2	19.13	0.00	0.7	-14.53	291
9761	12 20 56.3	-52 17 11.7	19.13	0.05	0.6	-14.53	284
2252	12 20 00.8	-52 42 34.1	19.14	0.04	0.9	-14.52	198
2781	12 20 04.6	-52 28 26.8	19.14	0.01	0.8	-14.52	184
10238	12 21 00.0	-52 41 29.5	19.15	0.02	0.8	-14.51	101
12019	12 21 13.5	-52 34 25.7	19.15	0.00	0.6	-14.51	17
10762	12 21 04.1	-52 36 20.7	19.17	0.07	0.8	-14.49	21
20023	12 22 12.9	-52 18 36.8	19.17	0.02	0.8	-14.49	303
15110	12 21 37.6	-52 26 54.0	19.18	0.00	0.6	-14.48	148
15323	12 21 39.5	-52 44 46.1	19.18	0.07	0.6	-14.48	169
23239	12 23 01.6	-52 33 06.2	19.18	0.03	0.5	-14.48	274
5846	12 20 28.5	-52 24 31.3	19.18	0.04	0.8	-14.48	192
1277	12 19 53.6	-52 22 35.9	19.19	0.07	0.8	-14.47	266
25566	12 22 25.9	-52 37 44.2	19.20	0.03	0.7	-14.46	191
5796	12 20 28.0	-52 44 46.8	19.20	0.02	0.7	-14.46	179
14110	12 21 30.4	-52 21 03.1	19.21	0.00	0.9	-14.45	228
9458	12 20 54.7	-52 38 14.2	19.21	0.00	0.9	-14.45	58
26688	12 23 03.7	-52 36 12.3	19.22	0.00	0.7	-14.44	277
7708	12 20 41.9	-52 39 53.0	19.23	0.07	0.8	-14.43	97
15530	12 21 40.3	-52 27 30.8	19.24	0.06	0.6	-14.42	143
5262	12 20 24.2	-52 46 28.7	19.24	0.09	0.8	-14.42	207
8738	12 20 49.3	-52 24 16.9	19.25	0.01	0.9	-14.41	177
12853	12 21 19.7	-52 29 56.3	19.27	0.04	1.0	-14.39	86
6968	12 20 36.5	-52 43 58.0	19.27	0.01	0.7	-14.39	158
16634	12 21 48.7	-52 15 34.9	19.28	0.03	0.9	-14.38	323
11046	12 21 05.5	-52 17 43.7	19.29	0.02	0.8	-14.37	274
25367	12 22 24.6	-52 18 32.0	19.29	0.01	0.6	-14.37	320
16786	12 21 49.9	-52 24 14.8	19.30	0.01	0.7	-14.36	199
25507	12 22 27.1	-52 41 32.1	19.30	0.01	1.0	-14.36	214
26740	12 22 36.4	-52 36 10.1	19.30	0.03	0.7	-14.36	212
27048	12 22 21.2	-52 32 03.9	19.30	0.00	0.6	-14.36	182
26384	12 22 18.8	-52 22 32.6	19.31	0.02	0.9	-14.35	261
5948	12 20 29.0	-52 23 42.4	19.31	0.00	0.7	-14.35	203
9219	12 20 52.9	-52 36 50.4	19.31	0.09	0.7	-14.35	44
7760	12 20 42.0	-52 42 48.9	19.32	0.00	0.8	-14.34	135
5724	12 20 27.2	-52 46 22.5	19.33	0.01	0.5	-14.33	202
3748	12 20 12.4	-52 39 28.9	19.34	0.01	0.8	-14.32	149
7857	12 20 42.8	-52 44 31.4	19.34	0.05	0.9	-14.32	159
22563	12 22 48.3	-52 27 27.5	19.35	0.02	0.5	-14.31	269
311	12 19 46.0	-52 44 52.3	19.35	0.07	0.7	-14.31	248
5776	12 20 27.9	-52 45 56.5	19.35	0.02	0.6	-14.31	195
2321	12 20 00.9	-52 42 44.3	19.36	0.00	1.0	-14.30	200
8721	12 20 49.1	-52 34 07.7	19.36	0.00	0.8	-14.30	47
10433	12 21 01.5	-52 44 12.8	19.38	0.01	0.7	-14.28	143
394	12 19 46.8	-52 42 48.1	19.41	0.03	0.8	-14.25	228
3967	12 20 13.7	-52 45 59.0	19.41	0.00	0.6	-14.25	214
15419	12 21 39.5	-52 25 39.2	19.42	0.02	0.5	-14.24	167
6351	12 20 31.7	-52 28 11.8	19.42	0.09	0.6	-14.24	139
24264	12 22 32.4	-52 41 15.4	19.43	0.01	0.6	-14.23	223
25009	12 22 29.9	-52 17 59.0	19.43	0.05	0.8	-14.23	334
2561	12 20 03.0	-52 20 18.5	19.43	0.09	0.7	-14.23	281
8338	12 20 46.4	-52 22 10.7	19.43	0.01	0.8	-14.23	210
8448	12 20 47.2	-52 44 19.9	19.44	0.01	0.6	-14.22	153
12724	12 21 18.9	-52 46 01.2	19.45	0.00	0.8	-14.21	173
12976	12 21 20.1	-52 17 04.7	19.45	0.05	0.9	-14.21	286
368	12 19 46.5	-52 30 14.6	19.45	0.01	0.8	-14.21	209
11245	12 21 07.1	-52 40 30.9	19.46	0.09	0.6	-14.20	84
19074	12 22 06.7	-52 29 29.8	19.46	0.00	0.7	-14.20	166
4568	12 20 18.3	-52 22 59.9	19.46	0.02	0.7	-14.20	225
7477	12 20 40.3	-52 46 01.4	19.46	0.06	0.8	-14.20	183
6811	12 20 35.3	-52 29 24.1	19.47	0.06	0.8	-14.19	119
8254	12 20 45.4	-52 20 02.6	19.47	0.05	0.5	-14.19	244
12926	12 21 19.9	-52 29 12.3	19.48	0.00	0.7	-14.18	97
17593	12 21 55.8	-52 25 06.4	19.48	0.02	1.0	-14.18	195
21736	12 22 56.1	-52 45 04.2	19.48	0.01	0.6	-14.18	302
21191	12 22 56.6	-52 24 44.1	19.50	0.07	0.7	-14.16	308
10964	12 21 05.2	-52 35 53.6	19.51	0.01	1.2	-14.15	13
411	12 19 47.0	-52 41 41.5	19.51	0.02	0.8	-14.15	219
8305	12 20 46.2	-52 34 11.3	19.51	0.00	0.6	-14.15	54
25691	12 22 24.2	-52 22 11.1	19.52	0.02	0.6	-14.14	274
14123	12 21 30.9	-52 34 25.6	19.53	0.09	0.9	-14.13	56
16639	12 21 49.2	-52 34 44.1	19.53	0.01	0.6	-14.13	98
3410	12 20 09.5	-52 45 19.1	19.53	0.04	0.8	-14.13	212
18651	12 22 04.5	-52 43 02.1	19.54	0.09	0.8	-14.12	183
19755	12 22 12.0	-52 44 29.7	19.54	0.06	0.6	-14.12	212
15934	12 21 44.1	-52 40 01.1	19.55	0.09	0.8	-14.11	115
17244	12 21 53.0	-52 20 45.1	19.55	0.07	0.7	-14.11	251
254	12 19 45.4	-52 45 36.0	19.55	0.06	0.5	-14.11	257
11534	12 21 09.5	-52 36 03.0	19.57	0.00	0.7	-14.09	14
14313	12 21 32.9	-52 38 37.2	19.57	0.09	0.8	-14.09	80

Table A.7: Candidate satellite galaxies in the field of ESO 218-G002 (continued).

Number (1)	RA (J2000) (2)	DEC (J2000) (3)	R (mag) (4)	Class (5)	A (arcsec) (6)	M_R (mag) (7)	Dist (kpc) (8)
7283	12 20 38.4	-52 20 50.8	19.57	0.00	0.7	-14.09	236
6343	12 20 31.9	-52 46 19.1	19.58	0.00	0.6	-14.08	196
16335	12 21 46.4	-52 25 23.0	19.59	0.01	0.7	-14.07	179
20291	12 22 15.6	-52 32 30.8	19.59	0.01	0.8	-14.07	167
21716	12 22 57.4	-52 43 53.2	19.59	0.02	0.7	-14.07	295
6503	12 20 32.7	-52 19 38.6	19.59	0.09	0.6	-14.07	258
14951	12 21 36.0	-52 26 01.9	19.60	0.06	0.6	-14.06	158
12936	12 21 19.6	-52 20 37.2	19.61	0.00	0.9	-14.05	230
1360	12 19 54.1	-52 18 59.4	19.61	0.06	0.6	-14.05	310
21214	12 22 56.4	-52 17 24.7	19.62	0.02	0.7	-14.04	382
25198	12 22 28.8	-52 19 49.4	19.62	0.01	0.4	-14.04	309
25951	12 22 23.1	-52 39 24.6	19.62	0.02	0.7	-14.04	192
6241	12 20 31.3	-52 45 24.8	19.62	0.05	1.0	-14.04	184
11297	12 21 07.9	-52 24 04.6	19.63	0.08	0.9	-14.03	174
22801	12 22 47.6	-52 36 32.5	19.63	0.03	0.5	-14.03	239
21836	12 22 54.9	-52 24 39.9	19.64	0.01	0.8	-14.02	305
25595	12 22 23.9	-52 27 51.1	19.64	0.00	1.1	-14.02	215
6227	12 20 30.7	-52 44 04.0	19.64	0.05	0.5	-14.02	166
9443	12 20 54.7	-52 42 39.5	19.64	0.08	0.8	-14.02	122
10426	12 21 01.4	-52 32 17.7	19.66	0.05	0.8	-14.00	47
17911	12 21 58.7	-52 34 44.6	19.66	0.00	0.8	-14.00	121
19887	12 22 12.6	-52 36 54.1	19.66	0.09	0.6	-14.00	157
27161	12 23 03.4	-52 43 10.2	19.66	0.02	0.6	-14.00	303
27342	12 22 58.2	-52 44 10.3	19.66	0.02	0.8	-14.00	299
13245	12 21 22.6	-52 39 57.1	19.67	0.01	0.9	-13.99	83
18668	12 22 03.4	-52 19 48.2	19.67	0.01	0.7	-13.99	276
16828	12 21 50.6	-52 38 35.3	19.68	0.00	0.6	-13.98	115
25149	12 22 24.6	-52 45 51.5	19.68	0.02	0.6	-13.98	249
8404	12 20 46.7	-52 44 29.8	19.68	0.07	0.5	-13.98	155
4849	12 20 20.5	-52 22 57.7	19.69	0.01	0.8	-13.97	223
1634	12 19 55.7	-52 43 37.3	19.70	0.01	0.6	-13.96	218
16956	12 21 51.7	-52 35 26.8	19.70	0.02	0.8	-13.96	104
17224	12 21 53.8	-52 43 23.6	19.70	0.07	0.6	-13.96	170
15995	12 21 44.5	-52 38 53.6	19.71	0.09	0.7	-13.95	105
13701	12 21 27.6	-52 27 50.3	19.72	0.00	0.7	-13.94	124
27263	12 23 02.4	-52 27 18.8	19.72	0.00	0.7	-13.94	300
20224	12 22 14.0	-52 16 10.9	19.73	0.01	0.5	-13.93	338
2497	12 20 02.4	-52 41 58.2	19.73	0.01	0.6	-13.93	190
7206	12 20 38.1	-52 34 29.2	19.73	0.09	0.7	-13.93	72
7263	12 20 38.2	-52 20 03.5	19.73	0.05	0.6	-13.93	248
11956	12 21 12.9	-52 40 09.0	19.74	0.05	0.8	-13.92	79
15697	12 21 42.3	-52 46 42.7	19.74	0.00	0.7	-13.92	200
20062	12 22 13.9	-52 34 06.9	19.74	0.02	0.9	-13.92	158
11775	12 21 10.9	-52 37 48.1	19.76	0.01	0.7	-13.90	42
8048	12 20 44.3	-52 24 02.4	19.76	0.07	0.8	-13.90	184
5771	12 20 27.7	-52 45 05.5	19.77	0.01	0.5	-13.89	183
12092	12 21 14.0	-52 39 51.0	19.79	0.00	0.6	-13.87	75
19722	12 22 10.6	-52 19 25.7	19.79	0.03	0.6	-13.87	289
3205	12 20 07.6	-52 17 22.4	19.79	0.01	0.5	-13.87	315
3513	12 20 10.0	-52 41 16.0	19.80	0.03	0.5	-13.86	168
10478	12 21 02.0	-52 43 04.1	19.81	0.01	0.7	-13.85	125
22821	12 22 46.0	-52 27 02.8	19.81	0.04	0.6	-13.85	267
24564	12 22 32.8	-52 19 08.0	19.81	0.07	0.6	-13.85	324
8994	12 20 51.1	-52 30 15.5	19.82	0.06	0.6	-13.84	86
10026	12 20 58.7	-52 22 18.1	19.83	0.01	1.0	-13.83	203
13220	12 21 21.4	-52 20 10.7	19.83	0.09	0.4	-13.83	238
18773	12 22 05.1	-52 42 57.4	19.84	0.04	0.6	-13.82	183
22384	12 22 50.2	-52 36 36.9	19.84	0.01	0.6	-13.82	245
25837	12 22 20.0	-52 16 59.0	19.84	0.00	0.9	-13.82	334
6639	12 20 34.1	-52 36 24.1	19.84	0.06	0.6	-13.82	83
941	12 19 51.0	-52 25 30.6	19.84	0.00	0.7	-13.82	239
24415	12 22 34.0	-52 17 17.6	19.86	0.09	0.6	-13.80	349
5893	12 20 28.6	-52 46 00.3	19.86	0.05	0.6	-13.80	195
6416	12 20 32.2	-52 42 08.4	19.86	0.04	0.7	-13.80	139
9016	12 20 51.0	-52 19 10.9	19.87	0.00	0.7	-13.79	254
2786	12 20 04.7	-52 26 58.6	19.88	0.08	0.8	-13.78	198
1934	12 19 58.5	-52 24 39.9	19.89	0.03	0.7	-13.77	234
9389	12 20 53.7	-52 30 50.1	19.89	0.01	0.6	-13.77	75
1263	12 19 53.0	-52 44 09.3	19.91	0.01	0.6	-13.75	228
17181	12 21 52.8	-52 25 07.1	19.91	0.03	0.7	-13.75	191
9493	12 20 54.6	-52 36 15.9	19.91	0.01	0.6	-13.75	36
13042	12 21 20.7	-52 36 38.8	19.93	0.01	0.6	-13.73	38
26581	12 23 08.7	-52 40 33.4	19.94	0.04	0.6	-13.72	301
6618	12 20 33.8	-52 38 51.3	19.95	0.01	0.5	-13.71	100
16033	12 21 43.8	-52 17 32.6	19.96	0.06	0.7	-13.70	290
16315	12 21 45.9	-52 16 24.2	19.96	0.04	0.5	-13.70	309
1981	12 19 58.3	-52 44 35.5	19.96	0.03	0.4	-13.70	223
3083	12 20 07.1	-52 24 29.2	19.96	0.02	0.8	-13.70	222
8214	12 20 45.2	-52 20 23.8	19.96	0.01	0.6	-13.70	238
21770	12 22 52.8	-52 28 33.2	19.97	0.01	0.7	-13.69	272
11825	12 21 11.1	-52 18 34.7	19.98	0.00	0.8	-13.68	261
18570	12 22 03.0	-52 26 11.3	19.98	0.01	0.8	-13.68	193
23039	12 22 44.0	-52 26 00.2	20.00	0.00	0.5	-13.66	271
4735	12 20 19.5	-52 27 02.4	20.00	0.06	0.6	-13.66	172
6215	12 20 30.7	-52 22 49.3	20.01	0.07	0.6	-13.65	213
26174	12 22 22.5	-52 44 44.7	20.02	0.05	0.5	-13.64	233
26864	12 22 38.6	-52 44 31.8	20.02	0.07	0.5	-13.64	262
7228	12 20 38.1	-52 34 43.9	20.02	0.04	0.5	-13.64	71
21059	12 22 58.2	-52 36 00.5	20.04	0.04	0.5	-13.62	264
26338	12 23 05.4	-52 23 17.5	20.04	0.02	0.6	-13.62	338

Table A.7: Candidate satellite galaxies in the field of ESO 218-G002 (continued).

Number (1)	RA (J2000) (2)	DEC (J2000) (3)	R (mag) (4)	Class (5)	A (arcsec) (6)	M_R (mag) (7)	Dist (kpc) (8)
4679	12 20 19.1	-52 21 49.9	20.04	0.03	0.6	-13.62	240
7490	12 20 40.2	-52 45 09.0	20.04	0.00	0.6	-13.62	171
12475	12 21 16.1	-52 19 27.3	20.05	0.02	0.5	-13.61	248
8416	12 20 46.7	-52 21 49.6	20.06	0.01	0.8	-13.60	216
27228	12 22 34.5	-52 45 16.3	20.07	0.09	0.6	-13.59	261
8912	12 20 50.5	-52 28 10.4	20.07	0.07	0.7	-13.59	117
9722	12 20 55.8	-52 22 58.5	20.08	0.00	0.5	-13.58	194
579	12 19 47.8	-52 38 26.2	20.10	0.09	0.5	-13.56	198
4190	12 20 15.3	-52 40 50.0	20.11	0.01	0.5	-13.55	154
15620	12 21 40.9	-52 26 42.5	20.12	0.03	0.5	-13.54	154
14215	12 21 31.3	-52 37 28.0	20.14	0.03	0.7	-13.52	66
17632	12 21 56.6	-52 42 34.1	20.14	0.01	0.5	-13.52	165
1924	12 19 58.2	-52 44 39.1	20.14	0.05	0.6	-13.52	224
23709	12 22 39.3	-52 19 32.2	20.15	0.06	0.6	-13.51	329
5120	12 20 22.7	-52 44 15.3	20.15	0.08	0.5	-13.51	179
7049	12 20 36.9	-52 37 53.5	20.15	0.05	0.7	-13.51	85
1099	12 19 51.6	-52 46 15.3	20.16	0.03	0.5	-13.50	253
16915	12 21 50.6	-52 26 20.0	20.16	0.02	0.5	-13.50	172
22952	12 22 45.2	-52 24 08.1	20.17	0.06	0.6	-13.49	290
7449	12 20 39.6	-52 33 00.6	20.18	0.01	0.6	-13.48	75
21537	12 22 57.6	-52 25 42.7	20.20	0.09	0.5	-13.46	302
14541	12 21 33.3	-52 26 06.8	20.21	0.03	0.5	-13.45	154
553	12 19 47.7	-52 38 56.2	20.23	0.01	0.6	-13.43	201
3736	12 20 11.8	-52 38 05.4	20.28	0.02	0.5	-13.38	142
20443	12 22 15.9	-52 27 22.7	20.36	0.08	0.5	-13.30	203
18483	12 22 02.6	-52 33 20.5	20.39	0.06	0.5	-13.27	133
14728	12 21 34.2	-52 20 03.7	20.41	0.01	0.5	-13.25	245
14037	12 21 29.4	-52 18 54.2	20.45	0.05	0.5	-13.21	261
3380	12 20 08.7	-52 37 52.1	20.71	0.07	0.4	-12.95	148

Table A.8: List of the candidate satellite galaxies in the field of ESO318-G021.

Number	RA (J2000)	DEC (J2000)	R (mag)	Class	A (arcsec)	M_R (mag)	Dist (kpc)
6703	10 54 26.5	-40 07 08.9	15.67	0.01	3.6	-18.29	361
3001	10 53 07.2	-40 11 06.9	15.72	0.03	2.5	-18.23	156
1822	10 52 38.9	-40 06 03.1	16.21	0.00	2.5	-17.74	264
5547	10 54 17.0	-40 18 06.4	16.34	0.04	1.5	-17.62	249
3569	10 53 21.5	-40 03 32.9	16.42	0.02	3.3	-17.53	298
6148	10 54 07.3	-40 13 13.4	16.72	0.00	1.8	-17.23	244
6462	10 54 01.8	-40 22 06.8	16.96	0.03	1.5	-16.99	199
3933	10 53 28.9	-40 23 32.4	16.98	0.03	1.4	-16.97	106
3728	10 53 24.4	-40 22 00.9	17.12	0.01	2.1	-16.84	77
3257	10 53 12.2	-40 12 25.7	17.15	0.01	1.4	-16.80	135
3996	10 53 30.2	-40 17 28.5	17.16	0.00	1.9	-16.79	95
2197	10 52 47.0	-40 30 20.5	17.18	0.00	1.4	-16.77	202
5334	10 54 29.5	-40 10 22.7	17.19	0.03	1.3	-16.76	336
1056	10 52 20.0	-40 13 41.0	17.29	0.04	1.4	-16.66	191
4249	10 53 35.6	-40 18 33.6	17.38	0.00	1.0	-16.57	106
1344	10 52 27.3	-40 09 33.2	17.59	0.00	1.7	-16.36	227
4542	10 53 42.5	-40 20 22.9	17.73	0.00	1.2	-16.22	128
5908	10 54 14.2	-40 02 25.5	17.74	0.04	1.3	-16.21	394
6000	10 54 10.6	-40 04 44.7	17.76	0.09	1.0	-16.19	353
1153	10 52 22.7	-40 04 53.5	17.85	0.00	1.9	-16.10	307
6052	10 54 09.7	-40 13 06.0	17.85	0.00	0.7	-16.11	253
6089	10 54 10.6	-40 14 38.7	17.92	0.07	1.1	-16.03	243
1022	10 52 19.0	-40 18 48.3	17.96	0.02	1.0	-15.99	161
6038	10 54 11.5	-40 11 57.5	18.10	0.04	0.7	-15.85	268
3496	10 53 18.1	-40 10 48.6	18.13	0.00	1.6	-15.82	168
1639	10 52 33.5	-40 20 09.0	18.14	0.00	1.0	-15.81	110
2873	10 53 02.8	-40 31 16.7	18.15	0.00	1.1	-15.80	209
4554	10 53 41.7	-40 03 24.5	18.16	0.00	1.2	-15.79	321
2146	10 52 45.4	-40 32 33.0	18.17	0.01	1.0	-15.78	241
4134	10 53 32.8	-40 22 25.0	18.19	0.00	1.2	-15.77	106
6358	10 54 03.7	-40 14 06.0	18.19	0.01	1.2	-15.76	226
3095	10 53 07.3	-40 19 21.9	18.31	0.02	0.6	-15.64	9
1000	10 52 18.3	-40 07 12.0	18.41	0.00	0.8	-15.54	279
3010	10 53 05.3	-40 12 38.8	18.42	0.00	1.4	-15.54	129
4060	10 53 30.6	-40 06 47.1	18.43	0.04	0.9	-15.52	250
3754	10 53 24.0	-40 22 45.7	18.45	0.00	1.0	-15.50	84
5750	10 54 18.7	-40 15 52.1	18.48	0.01	1.2	-15.47	262
902	10 52 15.4	-40 32 14.8	18.49	0.01	0.7	-15.47	284
6250	10 54 04.8	-40 29 04.9	18.51	0.08	0.8	-15.44	265
4904	10 53 50.9	-40 27 34.1	18.66	0.00	0.7	-15.29	211
5985	10 54 12.9	-40 28 03.7	18.69	0.00	1.0	-15.26	277
5272	10 54 29.1	-40 25 25.5	18.70	0.04	0.9	-15.25	307
1978	10 52 41.4	-40 33 07.7	18.74	0.02	0.8	-15.21	256
5492	10 54 25.5	-40 05 55.9	18.74	0.00	1.2	-15.22	373
342	10 52 02.0	-40 07 43.0	18.75	0.01	0.9	-15.20	309
465	10 52 05.1	-40 32 26.2	18.76	0.01	0.8	-15.19	309
5622	10 54 20.0	-40 04 03.4	18.77	0.00	1.0	-15.18	384
1802	10 52 37.2	-40 32 41.7	18.80	0.06	0.8	-15.15	253
2530	10 52 54.3	-40 02 59.1	18.81	0.08	0.8	-15.14	306
3566	10 53 18.9	-40 06 00.0	18.82	0.00	1.0	-15.13	253
5465	10 54 23.1	-40 18 17.6	18.85	0.02	1.1	-15.10	269
3084	10 53 09.1	-40 16 29.2	18.87	0.09	0.9	-15.08	60
525	10 52 06.5	-40 08 19.9	18.88	0.00	0.9	-15.07	290
1951	10 52 40.3	-40 08 47.5	18.89	0.01	0.9	-15.06	216
2567	10 52 55.5	-40 29 24.5	18.89	0.03	0.7	-15.06	178

Table A.8: Candidate satellite galaxies in the field of ESO318-G021 (continued).

Number (1)	RA (J2000) (2)	DEC (J2000) (3)	R (mag) (4)	Class (5)	A (arcsec) (6)	M_R (mag) (7)	Dist (kpc) (8)
2366	10 52 51.1	-40 28 38.5	18.90	0.09	0.8	-15.06	168
959	10 52 17.2	-40 18 03.3	18.90	0.01	0.8	-15.05	169
850	10 52 13.8	-40 20 28.3	18.92	0.01	0.7	-15.03	178
957	10 52 16.9	-40 14 26.2	18.95	0.02	0.7	-15.00	193
1215	10 52 23.2	-40 04 49.6	18.96	0.02	0.8	-14.99	307
2418	10 52 52.0	-40 18 06.5	18.96	0.09	0.7	-14.99	55
4125	10 53 32.1	-40 13 07.9	18.98	0.00	1.0	-14.98	151
5998	10 54 05.0	-40 13 11.0	19.03	0.00	0.8	-14.93	238
2493	10 52 53.6	-40 30 26.1	19.06	0.01	0.6	-14.89	198
3768	10 53 23.5	-40 04 24.2	19.06	0.00	0.9	-14.89	285
1514	10 52 30.4	-40 22 06.7	19.08	0.00	1.1	-14.87	128
309	10 52 00.9	-40 10 35.6	19.08	0.00	0.8	-14.88	278
4710	10 53 45.2	-40 02 57.4	19.08	0.04	0.8	-14.87	334
472	10 52 05.0	-40 32 31.2	19.08	0.00	0.7	-14.88	311
2294	10 52 48.5	-40 02 15.2	19.10	0.00	0.8	-14.85	322
3547	10 53 18.4	-40 13 14.4	19.10	0.00	1.0	-14.86	126
1027	10 52 18.8	-40 19 57.3	19.11	0.01	1.0	-14.85	160
2354	10 52 50.7	-40 28 12.0	19.13	0.09	0.8	-14.83	161
1385	10 52 27.3	-40 21 43.3	19.14	0.00	0.7	-14.81	136
423	10 52 03.7	-40 06 29.7	19.14	0.02	0.8	-14.81	321
2333	10 52 49.9	-40 27 47.5	19.15	0.02	0.6	-14.80	155
3120	10 53 08.0	-40 23 43.5	19.15	0.01	0.7	-14.81	72
3944	10 53 28.0	-40 19 16.7	19.16	0.04	0.8	-14.80	78
1603	10 52 31.9	-40 02 49.5	19.17	0.09	0.7	-14.78	327
1992	10 52 41.2	-40 26 07.9	19.17	0.01	1.1	-14.78	142
4631	10 53 43.6	-40 06 05.6	19.17	0.09	0.7	-14.78	280
427	10 52 03.6	-40 20 50.8	19.18	0.09	0.5	-14.77	214
2289	10 52 48.8	-40 24 38.8	19.19	0.04	0.8	-14.76	105
2870	10 53 01.8	-40 19 56.0	19.20	0.01	0.5	-14.75	13
3993	10 53 29.2	-40 21 58.2	19.20	0.08	0.6	-14.75	91
1373	10 52 26.9	-40 11 44.2	19.21	0.01	0.7	-14.74	197
4888	10 53 50.3	-40 24 03.1	19.21	0.01	0.7	-14.74	173
6612	10 54 33.2	-40 06 45.7	19.21	0.00	0.8	-14.74	384
1311	10 52 25.8	-40 17 15.3	19.23	0.08	0.7	-14.72	144
1856	10 52 37.9	-40 24 27.6	19.23	0.01	0.6	-14.72	127
4150	10 53 32.9	-40 16 19.8	19.23	0.03	0.8	-14.72	113
3761	10 53 23.7	-40 18 07.4	19.25	0.07	0.9	-14.71	70
614	10 52 08.3	-40 28 57.2	19.26	0.00	0.8	-14.69	258
6526	10 54 35.3	-40 07 34.1	19.26	0.09	0.8	-14.69	381
4014	10 53 29.3	-40 11 22.3	19.28	0.00	0.7	-14.67	173
4180	10 53 33.8	-40 22 24.5	19.28	0.00	0.6	-14.68	109
1728	10 52 35.1	-40 24 16.6	19.30	0.01	1.0	-14.65	132
2395	10 52 51.4	-40 19 09.1	19.30	0.09	0.7	-14.65	49
2980	10 53 04.3	-40 08 34.4	19.30	0.06	0.6	-14.65	202
1055	10 52 19.2	-40 20 12.7	19.32	0.02	0.6	-14.63	159
3945	10 53 28.4	-40 31 23.5	19.33	0.08	0.6	-14.62	225
360	10 52 02.5	-40 04 40.0	19.35	0.08	0.7	-14.60	349
5489	10 54 23.7	-40 04 14.2	19.35	0.08	0.6	-14.60	390
86	10 51 55.5	-40 23 43.8	19.35	0.00	0.6	-14.60	251
657	10 52 09.3	-40 20 34.5	19.37	0.01	0.6	-14.58	194
2719	10 52 59.2	-40 27 02.1	19.39	0.07	0.7	-14.56	133
3805	10 53 24.6	-40 09 33.6	19.39	0.00	0.7	-14.56	196
5753	10 54 19.6	-40 13 03.9	19.39	0.05	0.6	-14.57	283
6690	10 54 13.3	-40 16 51.0	19.41	0.01	0.8	-14.54	240
6382	10 54 01.6	-40 11 13.6	19.42	0.05	0.7	-14.54	248
5583	10 54 22.2	-40 22 10.7	19.44	0.00	0.7	-14.51	268
562	10 52 07.0	-40 06 29.8	19.44	0.01	0.7	-14.52	313
4951	10 53 50.9	-40 03 23.2	19.46	0.07	0.6	-14.50	335
5644	10 54 20.6	-40 24 27.5	19.48	0.09	0.7	-14.47	273
3215	10 53 09.9	-40 03 22.8	19.49	0.01	0.6	-14.47	297
5847	10 54 16.0	-40 17 26.3	19.49	0.07	0.7	-14.46	247
2475	10 52 53.1	-40 28 46.9	19.50	0.01	0.6	-14.45	169
6223	10 54 06.8	-40 20 55.6	19.52	0.01	0.6	-14.43	213
239	10 51 59.5	-40 27 14.9	19.54	0.04	0.6	-14.41	264
1647	10 52 33.2	-40 20 08.9	19.55	0.01	0.8	-14.41	111
5097	10 53 54.7	-40 22 20.5	19.55	0.03	0.5	-14.41	176
3991	10 53 29.2	-40 19 28.5	19.57	0.01	0.8	-14.38	82
802	10 52 12.7	-40 21 31.3	19.58	0.03	0.5	-14.38	184
4730	10 53 45.9	-40 08 47.4	19.59	0.05	0.7	-14.36	243
1457	10 52 29.1	-40 26 23.5	19.62	0.04	0.6	-14.33	173
3802	10 53 24.6	-40 18 18.3	19.63	0.06	0.6	-14.32	71
508	10 52 05.8	-40 11 02.4	19.63	0.06	0.7	-14.32	259
6663	10 53 57.2	-40 21 04.1	19.63	0.04	0.6	-14.33	180
1927	10 52 39.3	-40 05 13.8	19.64	0.02	0.7	-14.32	278
5304	10 54 27.6	-40 21 46.6	19.64	0.06	0.6	-14.31	286
1449	10 52 28.8	-40 14 32.6	19.65	0.05	0.7	-14.31	157
1776	10 52 36.2	-40 15 19.6	19.66	0.01	0.7	-14.29	129
5490	10 54 03.9	-40 30 45.5	19.69	0.01	0.6	-14.26	283
3694	10 53 22.3	-40 21 42.2	19.70	0.00	0.6	-14.25	68
786	10 52 12.4	-40 18 24.7	19.71	0.09	0.6	-14.24	184
3253	10 53 11.2	-40 31 28.8	19.72	0.09	0.6	-14.24	213
3311	10 53 12.0	-40 09 00.4	19.73	0.01	0.5	-14.22	196
250	10 51 59.7	-40 14 51.7	19.74	0.01	0.8	-14.21	243
6746	10 54 33.9	-40 18 25.2	19.76	0.04	0.6	-14.19	306
64	10 51 55.0	-40 11 47.2	19.77	0.01	0.6	-14.18	283
6770	10 54 32.2	-40 16 25.3	19.77	0.00	0.7	-14.18	306
4369	10 53 37.5	-40 06 50.7	19.78	0.05	0.6	-14.17	259
207	10 51 58.6	-40 33 31.9	19.79	0.01	0.6	-14.16	339
5598	10 54 20.8	-40 03 53.5	19.80	0.01	0.7	-14.16	388
5661	10 54 18.9	-40 25 30.3	19.81	0.00	1.1	-14.14	274

Table A.8: Candidate satellite galaxies in the field of ESO318-G021 (continued).

Number (1)	RA (J2000) (2)	DEC (J2000) (3)	R (mag) (4)	Class (5)	A (arcsec) (6)	M_R (mag) (7)	Dist (kpc) (8)
930	10 52 16.1	-40 25 28.8	19.82	0.03	0.6	-14.13	199
745	10 52 11.2	-40 16 35.2	19.87	0.01	0.8	-14.08	195
1028	10 52 18.4	-40 06 25.4	19.93	0.06	0.7	-14.02	291
1668	10 52 33.7	-40 15 36.9	20.02	0.03	0.6	-13.94	132
1770	10 52 36.0	-40 23 13.9	20.24	0.07	0.5	-13.71	119
3822	10 53 24.5	-40 03 22.9	20.38	0.08	0.4	-13.57	303
3003	10 53 05.0	-40 09 45.8	22.83	0.01	1.1	-11.12	181
4764	10 53 49.8	-40 25 33.4	98.78	0.02	2.5	64.81	185
4780	10 53 49.8	-40 25 48.1	98.78	0.03	2.4	64.818	188

Table A.9: List of the candidate satellite galaxies in the field of MCG-01-27-013.

Number	RA (J2000)	DEC (J2000)	R (mag)	Class	A (arcsec)	M_R (mag)	Dist (kpc)
300	10 31 32.6	-09 17 50.5	14.85	0.03	8.0	-20.55	364
3120	10 33 14.4	-09 20 39.5	15.33	0.03	5.2	-20.08	588
2938	10 32 55.5	-09 19 47.2	15.82	0.03	2.7	-19.59	425
3690	10 33 04.5	-09 12 18.2	16.12	0.03	2.2	-19.29	463
3854	10 32 57.7	-09 04 26.2	16.16	0.03	4.5	-19.25	530
2735	10 32 49.7	-09 08 47.5	16.26	0.03	2.3	-19.14	383
1224	10 32 00.0	-09 17 39.6	16.39	0.03	3.5	-19.01	156
1729	10 32 16.3	-09 00 31.5	16.62	0.03	1.8	-18.79	489
3416	10 33 20.3	-08 56 10.4	16.84	0.03	2.2	-18.57	875
3644	10 33 04.7	-09 00 31.5	16.86	0.02	2.5	-18.54	670
1845	10 32 20.5	-09 01 36.5	16.89	0.01	2.1	-18.51	455
3645	10 33 03.9	-09 10 55.9	16.93	0.03	1.5	-18.47	468
2595	10 32 45.4	-09 10 39.1	16.95	0.03	1.9	-18.45	319
2255	10 32 34.1	-09 24 15.5	17.13	0.02	2.6	-18.28	400
633	10 31 42.2	-09 23 09.1	17.13	0.02	2.2	-18.27	405
2888	10 32 53.0	-09 15 43.9	17.17	0.03	1.4	-18.23	361
3253	10 33 15.7	-08 54 38.6	17.19	0.03	1.5	-18.21	890
1825	10 32 18.9	-08 59 44.4	17.21	0.09	1.5	-18.19	519
3092	10 33 19.1	-09 08 59.6	17.21	0.03	1.8	-18.20	615
736	10 31 44.4	-09 02 59.3	17.21	0.02	2.1	-18.19	467
3763	10 33 02.1	-09 12 09.7	17.25	0.03	1.9	-18.16	444
2451	10 32 41.8	-09 24 26.0	17.29	0.04	1.3	-18.11	441
2151	10 32 30.9	-09 25 22.4	17.30	0.03	1.5	-18.10	423
231	10 31 29.1	-09 22 30.1	17.30	0.03	1.6	-18.10	471
1956	10 32 24.2	-09 04 44.2	17.31	0.02	1.9	-18.10	355
3522	10 33 07.0	-08 55 39.5	17.31	0.03	1.5	-18.09	816
3558	10 32 57.6	-09 14 02.5	17.34	0.02	2.4	-18.07	397
379	10 31 34.0	-09 03 19.8	17.38	0.03	1.6	-18.02	510
1660	10 32 13.9	-09 23 13.0	17.43	0.02	1.6	-17.97	314
2243	10 32 33.7	-09 23 45.0	17.43	0.03	1.8	-17.98	382
2209	10 32 32.5	-09 22 33.7	17.47	0.03	1.5	-17.94	341
2721	10 32 48.3	-08 58 53.9	17.47	0.06	1.3	-17.93	630
2223	10 32 33.1	-09 08 23.9	17.49	0.03	1.7	-17.92	279
646	10 31 41.3	-09 22 24.2	17.49	0.02	2.4	-17.91	390
389	10 31 34.1	-09 02 11.3	17.51	0.02	1.5	-17.90	541
864	10 31 48.6	-08 58 33.0	17.54	0.01	1.2	-17.87	593
2005	10 32 26.1	-09 01 40.6	17.55	0.03	1.5	-17.85	463
1561	10 32 09.5	-09 15 56.1	17.57	0.04	1.4	-17.83	60
939	10 31 50.5	-09 08 44.6	17.60	0.02	1.5	-17.80	271
827	10 31 46.7	-09 01 19.9	17.61	0.04	1.3	-17.79	509
2259	10 32 34.2	-08 55 05.9	17.62	0.01	1.8	-17.79	706
686	10 31 42.9	-08 58 59.3	17.64	0.03	1.5	-17.77	598
2781	10 32 49.9	-09 10 55.1	17.66	0.02	1.9	-17.75	352
515	10 31 38.0	-09 04 21.8	17.69	0.01	2.0	-17.72	459
2956	10 32 54.5	-08 58 33.8	17.77	0.05	1.2	-17.64	669
3292	10 33 15.2	-09 20 08.3	17.77	0.04	1.4	-17.63	588
1023	10 31 52.0	-08 59 05.1	17.84	0.00	1.8	-17.56	566
1593	10 32 10.4	-09 14 53.6	17.9	0.00	0.9	-17.46	23
3194	10 33 17.7	-09 09 46.2	17.92	0.02	1.4	-17.49	595
322	10 31 32.6	-09 23 33.5	17.92	0.01	1.9	-17.48	472
70	10 31 22.6	-09 13 32.7	17.93	0.05	1.1	-17.47	430
1410	10 32 04.3	-09 21 24.0	17.95	0.04	1.2	-17.45	258
1904	10 32 21.0	-09 09 38.5	17.98	0.01	2.3	-17.42	183
692	10 31 43.2	-09 10 04.4	17.98	0.01	1.3	-17.42	292
2013	10 32 26.5	-09 12 45.9	18.01	0.03	1.5	-17.40	138
3271	10 33 15.3	-09 19 12.9	18.05	0.02	1.9	-17.35	578
45	10 31 22.1	-09 12 49.5	18.05	0.01	1.4	-17.35	437
535	10 31 38.1	-09 02 12.3	18.05	0.02	1.5	-17.35	519
918	10 31 49.0	-08 58 17.9	18.05	0.03	0.7	-17.35	600
1000	10 31 51.7	-08 58 37.7	18.06	0.08	1.1	-17.34	582
1399	10 32 04.0	-09 13 11.9	18.11	0.01	1.9	-17.30	79
2	10 31 20.4	-09 01 39.3	18.12	0.01	1.3	-17.28	634
2504	10 32 43.0	-09 15 41.5	18.13	0.01	1.3	-17.27	275
2692	10 32 47.4	-09 11 38.3	18.17	0.00	2.0	-17.23	323
1855	10 32 20.0	-09 06 11.1	18.18	0.01	1.3	-17.22	296
394	10 31 34.3	-09 13 00.7	18.18	0.02	1.3	-17.23	331
245	10 31 29.3	-09 23 02.9	18.19	0.02	1.3	-17.21	482
3664	10 33 01.5	-08 57 29.7	18.24	0.06	1.3	-17.16	735
1999	10 32 25.9	-09 21 59.9	18.28	0.01	1.8	-17.12	296
1818	10 32 18.9	-09 25 06.9	18.29	0.03	1.2	-17.12	385
1096	10 31 53.9	-09 00 12.8	18.31	0.08	1.0	-17.10	522
2084	10 32 28.4	-09 15 56.1	18.31	0.01	1.8	-17.09	154
1045	10 31 52.6	-08 59 05.7	18.34	0.04	1.3	-17.06	564
3213	10 33 20.4	-08 55 21.4	18.34	0.08	1.2	-17.06	897
2925	10 32 53.9	-08 56 22.9	18.37	0.05	1.7	-17.04	732

Table A.9: Candidate satellite galaxies in the field of MCG-01-27-013 (continued).

Number (1)	RA (J2000) (2)	DEC (J2000) (3)	R (mag) (4)	Class (5)	A (arcsec) (6)	M_R (mag) (7)	Dist (kpc) (8)
959	10 31 50.8	-09 08 34.4	18.37	0.05	1.4	-17.03	274
2800	10 32 49.9	-09 05 38.6	18.39	0.04	1.1	-17.01	451
1541	10 32 09.2	-09 04 34.4	18.40	0.01	1.4	-17.00	345
2932	10 32 53.6	-09 03 16.5	18.42	0.00	1.3	-16.98	533
590	10 31 40.4	-09 25 57.6	18.42	0.00	1.6	-16.98	493
1759	10 32 16.6	-09 13 52.4	18.43	0.05	1.1	-16.98	44
1849	10 32 19.4	-09 06 25.1	18.45	0.01	1.8	-16.95	287
3094	10 33 19.0	-09 22 42.9	18.45	0.00	1.1	-16.96	655
3677	10 33 03.1	-09 11 01.3	18.46	0.07	1.1	-16.95	461
1028	10 31 52.3	-09 09 49.6	18.48	0.01	1.5	-16.92	233
932	10 31 53.2	-09 16 57.9	18.49	0.01	1.4	-16.91	187
408	10 31 34.4	-09 16 55.2	18.50	0.01	1.4	-16.91	339
564	10 31 39.0	-09 23 29.1	18.51	0.04	1.0	-16.89	432
1750	10 32 16.3	-09 13 31.2	18.52	0.01	1.1	-16.89	47
1523	10 32 08.3	-09 12 08.2	18.54	0.01	1.2	-16.86	83
2846	10 32 51.2	-09 20 27.6	18.56	0.00	1.6	-16.84	405
1952	10 32 23.9	-09 09 42.8	18.58	0.00	1.2	-16.83	193
281	10 31 30.4	-08 59 40.2	18.58	0.03	1.1	-16.82	631
803	10 31 46.3	-09 22 46.8	18.58	0.00	1.4	-16.83	372
294	10 31 31.4	-09 21 08.6	18.59	0.01	1.5	-16.81	427
3274	10 33 16.4	-09 19 54.1	18.60	0.01	1.0	-16.80	595
1700	10 32 14.6	-09 13 11.5	18.61	0.00	1.1	-16.79	46
743	10 31 45.3	-08 58 26.4	18.61	0.01	0.8	-16.80	607
2075	10 32 27.8	-09 02 57.5	18.62	0.02	1.3	-16.79	425
3494	10 33 23.4	-09 16 59.0	18.64	0.01	1.1	-16.77	629
3775	10 32 56.2	-09 05 01.7	18.64	0.00	1.1	-16.76	506
3998	10 33 19.7	-09 22 16.8	18.64	0.01	1.0	-16.76	654
995	10 31 51.5	-09 18 41.0	18.64	0.04	0.9	-16.76	235
3249	10 33 14.7	-09 00 00.4	18.67	0.01	1.3	-16.73	745
1740	10 32 15.9	-09 19 08.1	18.69	0.01	1.0	-16.71	172
3757	10 32 58.9	-09 11 31.9	18.69	0.02	1.1	-16.72	421
985	10 31 51.3	-09 09 19.8	18.7	0.01	1.1	-16.67	251
2239	10 32 33.4	-09 25 46.8	18.70	0.01	1.2	-16.70	445
3972	10 33 24.9	-09 23 45.8	18.70	0.06	0.9	-16.70	717
324	10 31 32.0	-09 22 58.7	18.71	0.02	1.1	-16.69	462
3956	10 33 19.6	-09 12 15.2	18.72	0.01	1.2	-16.69	594
994	10 31 51.5	-08 58 33.7	18.72	0.01	1.2	-16.68	584
168	10 31 26.3	-09 24 26.4	18.73	0.00	1.2	-16.68	534
887	10 31 48.6	-09 12 09.6	18.74	0.03	1.0	-16.67	217
745	10 31 44.0	-09 06 37.5	18.76	0.00	1.9	-16.65	365
1622	10 32 12.3	-09 13 39.0	18.79	0.00	1.2	-16.61	24
3710	10 33 03.9	-08 56 46.3	18.79	0.01	1.6	-16.61	768
341	10 31 32.2	-09 09 08.5	18.81	0.02	0.9	-16.59	392
2177	10 32 30.8	-09 00 37.0	18.82	0.00	1.2	-16.59	511
1651	10 32 12.8	-09 15 08.1	18.87	0.00	1.2	-16.54	29
3239	10 33 17.3	-09 14 37.2	18.88	0.01	1.3	-16.52	569
3597	10 33 06.4	-09 11 10.7	18.88	0.02	0.9	-16.52	487
3968	10 33 17.9	-09 24 17.9	18.90	0.01	0.9	-16.50	674
3793	10 33 00.5	-09 04 54.8	18.91	0.01	1.0	-16.50	538
2431	10 32 41.0	-09 19 28.5	18.92	0.02	1.4	-16.49	311
3152	10 33 14.0	-08 56 32.2	18.95	0.01	1.2	-16.45	829
3505	10 33 24.9	-09 08 31.3	18.96	0.04	1.0	-16.44	668
313	10 31 31.3	-09 04 10.7	18.97	0.01	1.0	-16.43	504
688	10 31 42.6	-09 09 25.1	18.97	0.01	1.1	-16.44	309
1342	10 32 01.1	-08 57 05.2	18.98	0.01	0.9	-16.42	616
763	10 31 44.7	-09 21 31.9	18.98	0.00	1.4	-16.43	347
1248	10 31 58.0	-08 57 03.4	18.99	0.01	0.7	-16.42	622
1712	10 32 14.5	-08 56 43.0	19.00	0.00	0.9	-16.40	622
2048	10 32 26.5	-08 57 22.9	19.02	0.03	1.0	-16.39	612
2224	10 32 32.7	-09 06 59.4	19.03	0.00	1.2	-16.37	316
1955	10 32 24.1	-09 09 34.0	19.04	0.02	1.1	-16.36	199
2682	10 32 47.4	-09 25 25.3	19.04	0.01	1.2	-16.37	498
1161	10 31 55.9	-08 57 38.1	19.05	0.00	0.9	-16.35	606
2669	10 32 46.3	-09 09 01.9	19.05	0.01	1.5	-16.36	353
2401	10 32 39.2	-09 12 39.8	19.06	0.05	0.9	-16.34	245
1801	10 32 17.8	-09 19 11.2	19.08	0.00	0.7	-16.32	178
378	10 31 33.3	-09 13 41.1	19.08	0.01	1.0	-16.32	337
503	10 31 36.6	-09 05 09.9	19.09	0.00	1.0	-16.31	447
1394	10 32 03.2	-08 59 59.3	19.10	0.00	1.4	-16.31	512
1447	10 32 05.1	-09 08 12.4	19.10	0.02	1.1	-16.30	224
2211	10 32 32.1	-09 23 02.5	19.10	0.04	1.0	-16.30	354
2499	10 32 42.5	-09 11 51.3	19.11	0.00	1.1	-16.29	280
3465	10 33 08.8	-09 07 56.4	19.11	0.09	0.9	-16.29	544
1790	10 32 17.3	-09 06 41.8	19.12	0.02	1.1	-16.29	273
1908	10 32 21.1	-09 16 39.1	19.12	0.03	1.0	-16.28	114
2574	10 32 44.3	-09 18 50.9	19.12	0.02	1.0	-16.28	323
1554	10 32 08.8	-08 59 19.0	19.13	0.02	1.0	-16.27	531
3800	10 32 59.9	-09 22 46.5	19.13	0.05	1.2	-16.27	513
502	10 31 36.7	-09 01 03.4	19.14	0.00	1.3	-16.27	560
1566	10 32 09.3	-09 10 04.7	19.15	0.04	1.0	-16.26	152
2175	10 32 30.7	-09 16 01.6	19.16	0.09	0.7	-16.24	174
3096	10 33 15.4	-09 01 03.3	19.16	0.00	0.7	-16.25	725
2838	10 32 50.8	-09 06 37.9	19.17	0.00	1.2	-16.24	434
1575	10 32 09.5	-09 18 28.1	19.18	0.09	0.8	-16.22	147
883	10 31 48.2	-09 13 13.1	19.18	0.07	0.8	-16.23	210
1519	10 32 07.5	-09 07 57.5	19.19	0.00	1.6	-16.22	228
1172	10 31 56.0	-08 59 23.6	19.20	0.01	1.0	-16.20	545
1387	10 32 03.2	-09 02 40.5	19.21	0.00	1.3	-16.19	418
3241	10 33 21.3	-09 16 58.1	19.21	0.00	1.0	-16.19	611
365	10 31 32.7	-09 03 12.0	19.21	0.08	0.8	-16.19	521

Table A.9: Candidate satellite galaxies in the field of MCG-01-27-013 (continued).

Number (1)	RA (J2000) (2)	DEC (J2000) (3)	R (mag) (4)	Class (5)	A (arcsec) (6)	M_R (mag) (7)	Dist (kpc) (8)
1305	10 31 59.8	-09 10 03.1	19.23	0.02	1.1	-16.17	184
1505	10 32 07.3	-09 14 00.1	19.23	0.01	0.9	-16.17	42
1532	10 32 08.2	-09 01 18.2	19.23	0.00	0.9	-16.18	461
1768	10 32 16.7	-09 13 07.4	19.24	0.02	0.8	-16.17	59
1489	10 32 06.8	-09 23 04.0	19.25	0.05	0.8	-16.16	311
1005	10 31 51.4	-08 58 31.2	19.26	0.01	1.1	-16.14	586
1770	10 32 16.8	-09 19 02.5	19.26	0.06	0.9	-16.15	171
3346	10 33 10.0	-08 55 56.5	19.26	0.09	0.9	-16.14	823
1074	10 31 53.1	-09 14 05.1	19.27	0.01	0.9	-16.14	164
3083	10 33 20.2	-09 18 53.6	19.27	0.05	0.9	-16.13	616
2217	10 32 32.3	-09 17 27.0	19.28	0.01	0.9	-16.12	208
910	10 31 49.1	-09 13 44.0	19.29	0.02	0.8	-16.12	199
1122	10 31 54.2	-09 00 25.1	19.30	0.00	0.8	-16.10	515
675	10 31 42.3	-09 25 27.5	19.30	0.00	1.0	-16.11	470
8	10 31 19.9	-09 15 08.9	19.30	0.00	1.0	-16.10	454
250	10 31 29.2	-09 13 18.9	19.31	0.05	0.9	-16.09	374
1335	10 32 01.2	-09 22 27.1	19.32	0.07	0.8	-16.09	301
3669	10 33 05.2	-09 01 04.1	19.32	0.00	0.9	-16.08	659
2844	10 32 50.6	-09 12 47.0	19.33	0.02	1.1	-16.07	341
3244	10 33 13.2	-09 05 13.6	19.33	0.05	1.0	-16.08	623
94	10 31 23.1	-09 17 41.9	19.34	0.02	0.9	-16.06	441
3065	10 33 23.8	-09 26 00.4	19.35	0.01	0.9	-16.05	749
1166	10 31 56.4	-09 23 54.5	19.37	0.00	0.8	-16.04	364
1796	10 32 17.8	-09 15 26.9	19.37	0.04	0.8	-16.03	64
2627	10 32 45.5	-09 16 12.8	19.37	0.00	0.9	-16.03	300
385	10 31 33.5	-09 17 31.8	19.37	0.01	0.8	-16.03	353
3340	10 33 10.4	-09 20 30.9	19.39	0.01	0.8	-16.01	554
1588	10 32 10.2	-09 10 02.2	19.40	0.00	1.0	-16.00	152
2349	10 32 37.4	-09 05 44.4	19.40	0.09	0.8	-16.00	376
1571	10 32 09.4	-09 12 58.6	19.41	0.02	0.8	-16.00	52
2997	10 32 55.1	-09 20 13.7	19.41	0.03	0.8	-15.99	429
2623	10 32 45.6	-09 21 13.3	19.42	0.02	0.9	-15.98	381
3501	10 33 09.4	-09 08 12.2	19.44	0.09	0.7	-15.97	545
1454	10 32 05.5	-09 17 37.6	19.45	0.02	1.1	-15.95	129
3856	10 33 22.5	-09 25 29.1	19.45	0.09	0.8	-15.95	729
3575	10 33 07.1	-09 00 30.7	19.46	0.08	0.9	-15.94	685
1606	10 32 10.8	-09 19 32.0	19.48	0.01	0.9	-15.92	183
2831	10 32 50.5	-09 11 24.3	19.48	0.01	1.0	-15.93	352
660	10 31 41.1	-09 02 53.1	19.48	0.00	0.8	-15.92	485
2225	10 32 32.4	-09 14 45.1	19.49	0.00	0.8	-15.91	178
2631	10 32 45.5	-09 08 28.8	19.49	0.00	0.8	-15.92	358
2333	10 32 37.1	-09 20 25.8	19.50	0.00	0.8	-15.90	307
2178	10 32 30.6	-08 57 52.4	19.51	0.07	0.8	-15.89	603
1163	10 31 56.2	-09 16 29.8	19.52	0.01	0.9	-15.88	157
1214	10 31 57.4	-09 00 09.3	19.52	0.00	0.6	-15.88	516
1798	10 32 17.8	-09 17 24.7	19.52	0.00	0.8	-15.89	119
2091	10 32 28.1	-09 07 00.2	19.52	0.00	1.3	-15.89	294
2169	10 32 30.2	-08 55 13.5	19.53	0.00	1.1	-15.87	693
748	10 31 44.3	-09 23 13.7	19.53	0.03	0.8	-15.88	395
206	10 31 27.5	-09 21 38.9	19.54	0.00	0.8	-15.87	465
1928	10 32 21.9	-09 22 22.9	19.56	0.02	0.8	-15.84	297
410	10 31 33.7	-09 02 16.3	19.56	0.04	0.6	-15.84	541
297	10 31 31.0	-09 19 31.9	19.57	0.00	1.1	-15.83	400
265	10 31 29.9	-09 25 29.9	19.58	0.00	0.8	-15.82	538
2308	10 32 35.8	-09 04 28.6	19.59	0.09	0.8	-15.82	405
3829	10 32 59.9	-09 13 32.5	19.60	0.01	1.2	-15.80	419
898	10 31 48.9	-09 22 05.6	19.60	0.00	0.7	-15.81	339
2016	10 32 25.6	-09 01 43.6	19.61	0.00	0.8	-15.80	460
2391	10 32 38.7	-09 07 18.0	19.61	0.07	0.7	-15.80	341
1480	10 32 06.0	-09 14 37.4	19.62	0.00	0.7	-15.79	52
1600	10 32 11.0	-09 25 28.4	19.62	0.03	0.8	-15.79	393
2011	10 32 25.5	-09 07 04.2	19.62	0.01	0.6	-15.79	282
1264	10 31 58.6	-09 04 00.1	19.63	0.00	1.3	-15.78	382
1902	10 32 20.9	-09 12 40.7	19.63	0.00	0.8	-15.77	97
2849	10 32 51.0	-09 23 39.2	19.64	0.00	0.8	-15.76	473
3529	10 33 08.2	-08 59 54.2	19.64	0.01	0.7	-15.76	707
630	10 31 40.3	-09 02 13.3	19.64	0.07	0.8	-15.77	509
1283	10 31 59.4	-09 23 04.4	19.65	0.00	0.8	-15.75	327
2073	10 32 27.4	-09 15 30.4	19.65	0.00	0.8	-15.75	141
272	10 31 29.7	-09 02 54.7	19.65	0.00	0.9	-15.75	546
978	10 31 50.8	-09 03 03.8	19.65	0.05	0.8	-15.76	438
2749	10 32 48.4	-09 11 36.8	19.67	0.09	0.6	-15.74	332
3568	10 33 01.8	-09 16 38.5	19.67	0.00	1.0	-15.73	441
1188	10 31 56.9	-09 24 11.2	19.70	0.00	0.8	-15.71	371
1896	10 32 20.3	-08 59 57.9	19.70	0.09	0.9	-15.70	512
1004	10 31 51.3	-09 04 15.2	19.71	0.04	0.8	-15.69	399
2029	10 32 26.2	-09 12 56.5	19.71	0.06	0.7	-15.69	133
253	10 31 29.3	-09 15 21.8	19.71	0.08	0.7	-15.69	373
2448	10 32 40.8	-09 07 39.7	19.72	0.00	1.1	-15.68	344
1725	10 32 14.9	-09 06 02.9	19.73	0.01	0.7	-15.67	293
2960	10 32 54.1	-09 10 44.2	19.73	0.00	0.7	-15.67	388
3602	10 33 06.4	-08 57 32.0	19.73	0.08	0.9	-15.68	759
869	10 31 47.4	-08 58 51.3	19.73	0.02	0.7	-15.67	587
829	10 31 48.2	-08 58 36.0	19.74	0.01	1.2	-15.66	593
2412	10 32 39.3	-09 13 43.1	19.75	0.00	0.6	-15.65	239
2730	10 32 47.8	-09 00 51.8	19.75	0.01	0.9	-15.66	569
3773	10 33 02.1	-09 12 23.1	19.76	0.00	0.8	-15.64	442
600	10 31 39.3	-09 03 52.3	19.76	0.01	0.8	-15.65	466
1413	10 32 03.8	-09 20 43.3	19.77	0.00	0.7	-15.64	236
3487	10 33 10.0	-09 18 40.6	19.77	0.07	0.9	-15.63	528

Table A.9: Candidate satellite galaxies in the field of MCG-01-27-013 (continued).

Number (1)	RA (J2000) (2)	DEC (J2000) (3)	R (mag) (4)	Class (5)	A (arcsec) (6)	M_R (mag) (7)	Dist (kpc) (8)
3786	10 33 17.4	-09 20 23.0	19.78	0.02	0.6	-15.63	609
865	10 31 47.4	-09 00 47.8	19.78	0.08	0.6	-15.62	523
2614	10 32 45.1	-09 04 00.9	19.79	0.01	0.8	-15.61	465
1271	10 31 58.6	-08 58 38.9	19.81	0.08	0.6	-15.60	566
3009	10 33 20.4	-09 02 35.0	19.81	0.00	0.8	-15.59	727
3410	10 33 12.7	-09 06 36.9	19.81	0.09	0.7	-15.60	595
2249	10 32 33.3	-09 20 18.3	19.82	0.09	0.8	-15.59	281
2465	10 32 41.1	-08 59 14.0	19.84	0.09	0.8	-15.56	591
2988	10 32 54.5	-09 02 11.9	19.85	0.00	0.8	-15.56	566
3861	10 32 56.1	-09 06 46.4	19.85	0.00	1.0	-15.55	468
1177	10 31 56.4	-09 24 05.5	19.87	0.09	0.6	-15.54	370
3008	10 32 55.1	-08 56 17.5	19.87	0.01	0.9	-15.53	740
1301	10 31 59.7	-09 11 11.9	19.88	0.02	0.7	-15.52	153
140	10 31 24.6	-09 13 54.5	19.88	0.02	0.8	-15.53	412
2208	10 32 31.7	-09 14 22.2	19.88	0.00	0.7	-15.52	172
3206	10 33 20.7	-09 04 45.8	19.89	0.08	0.7	-15.52	688
3262	10 33 04.9	-09 04 47.8	19.90	0.08	0.8	-15.50	571
3307	10 33 13.7	-09 03 10.6	19.90	0.00	0.8	-15.50	667
4	10 31 20.2	-09 20 04.7	19.90	0.01	0.8	-15.51	494
2732	10 32 47.9	-08 55 52.6	19.91	0.09	0.9	-15.50	723
3073	10 33 22.4	-09 02 46.8	19.91	0.00	0.7	-15.50	737
1704	10 32 14.3	-09 19 01.5	19.92	0.06	0.6	-15.48	166
2292	10 32 35.1	-08 59 03.7	19.92	0.01	0.8	-15.48	576
1218	10 31 57.7	-09 05 11.3	19.94	0.09	0.8	-15.46	346
1266	10 31 58.7	-09 09 10.4	19.94	0.06	0.7	-15.46	215
2100	10 32 27.9	-09 02 45.6	19.95	0.05	0.7	-15.46	431
2745	10 32 48.6	-09 22 12.2	19.96	0.01	1.0	-15.45	423
3590	10 33 07.4	-09 00 04.1	19.97	0.00	0.6	-15.43	698
1900	10 32 20.7	-09 09 19.4	19.98	0.03	0.7	-15.42	192
2874	10 32 52.0	-09 24 29.5	19.98	0.00	0.8	-15.43	500
3731	10 33 01.3	-09 07 16.1	19.98	0.00	0.7	-15.42	497
1771	10 32 16.9	-09 26 03.7	19.99	0.01	0.8	-15.41	416
3951	10 33 24.9	-09 14 44.6	19.99	0.00	0.9	-15.41	636
2991	10 32 54.7	-09 09 05.9	20.00	0.03	0.7	-15.40	416
1202	10 31 56.8	-09 02 05.0	20.01	0.05	0.6	-15.39	452
1883	10 32 20.3	-09 24 48.1	20.02	0.02	0.6	-15.39	376
2634	10 32 45.8	-09 20 23.2	20.02	0.00	0.8	-15.38	364
3068	10 33 23.0	-09 09 25.2	20.02	0.06	0.7	-15.39	643
1130	10 31 54.8	-09 23 38.5	20.03	0.09	0.8	-15.37	361
1385	10 32 02.7	-09 09 52.7	20.03	0.00	0.9	-15.37	176
2543	10 32 43.4	-09 19 21.2	20.03	0.00	0.7	-15.37	326
3525	10 32 57.4	-08 59 19.6	20.03	0.08	0.7	-15.37	662
3053	10 33 24.0	-09 12 26.0	20.04	0.08	0.8	-15.36	631
1835	10 32 19.0	-09 22 16.0	20.05	0.00	0.6	-15.36	286
2341	10 32 37.3	-09 23 33.9	20.06	0.00	0.6	-15.34	394
2571	10 32 44.3	-09 26 02.2	20.06	0.08	0.8	-15.34	500
812	10 31 45.7	-09 11 26.9	20.06	0.07	0.6	-15.35	249
1092	10 31 53.6	-09 13 59.0	20.07	0.05	0.7	-15.34	159
349	10 31 32.3	-09 20 57.0	20.08	0.00	0.6	-15.33	416
3641	10 32 59.7	-09 21 09.3	20.08	0.06	0.8	-15.32	481
1329	10 32 00.8	-09 21 29.5	20.09	0.05	0.6	-15.32	270
1985	10 32 24.9	-09 19 16.4	20.09	0.00	0.6	-15.31	207
481	10 31 35.7	-09 09 07.1	20.09	0.05	0.7	-15.31	365
1646	10 32 12.4	-09 00 25.5	20.10	0.07	0.7	-15.30	491
643	10 31 40.3	-09 01 51.2	20.10	0.02	0.6	-15.30	520
2275	10 32 34.2	-09 11 17.9	20.11	0.03	0.6	-15.29	221
304	10 31 30.7	-09 22 55.9	20.11	0.01	0.6	-15.29	470
765	10 31 44.7	-09 21 17.8	20.11	0.01	0.7	-15.30	341
2274	10 32 34.0	-08 59 10.7	20.12	0.00	0.6	-15.28	568
1025	10 31 51.7	-09 11 04.5	20.14	0.03	0.6	-15.27	210
1162	10 31 55.9	-09 11 35.3	20.16	0.08	0.5	-15.24	170
1393	10 32 02.9	-09 01 23.6	20.16	0.00	0.5	-15.24	463
2160	10 32 30.1	-09 22 57.6	20.16	0.00	0.7	-15.25	343
684	10 31 41.9	-09 01 48.2	20.17	0.09	0.5	-15.23	514
3422	10 33 21.5	-09 04 39.3	20.19	0.05	0.6	-15.22	696
3456	10 33 09.1	-09 11 32.5	20.19	0.06	0.7	-15.22	507
25	10 31 20.6	-09 22 32.6	20.20	0.08	0.6	-15.21	533
2788	10 32 49.4	-09 13 24.5	20.21	0.00	0.6	-15.19	327
566	10 31 38.5	-09 16 58.1	20.21	0.02	0.6	-15.19	305
3001	10 32 54.8	-09 07 18.6	20.22	0.02	0.7	-15.19	448
3646	10 32 58.6	-09 12 11.5	20.22	0.01	0.7	-15.19	414
1198	10 31 56.7	-09 11 11.1	20.23	0.04	0.6	-15.18	172
1813	10 32 18.0	-09 03 07.5	20.23	0.01	0.7	-15.17	399
3640	10 32 59.1	-09 14 26.8	20.23	0.09	0.6	-15.17	411
2413	10 32 39.4	-09 15 42.7	20.24	0.01	0.6	-15.16	244
2477	10 32 41.8	-09 17 41.2	20.24	0.04	0.7	-15.16	285
3163	10 33 13.3	-09 10 27.0	20.24	0.07	0.8	-15.17	552
418	10 31 34.2	-09 18 01.4	20.24	0.08	0.5	-15.17	353
605	10 31 39.5	-09 11 22.4	20.24	0.01	0.7	-15.17	301
787	10 31 45.2	-09 25 36.3	20.24	0.08	0.5	-15.16	461
884	10 31 48.2	-08 58 16.9	20.25	0.01	1.4	-15.15	603
2530	10 32 42.8	-09 01 50.9	20.26	0.09	0.6	-15.14	516
2919	10 32 52.8	-09 11 05.6	20.26	0.09	0.8	-15.15	374
3119	10 33 15.2	-09 11 28.7	20.26	0.06	0.6	-15.15	560
246	10 31 28.5	-08 58 56.0	20.27	0.01	0.6	-15.14	662
581	10 31 38.9	-09 21 13.1	20.27	0.03	0.6	-15.14	376
2618	10 32 45.3	-09 20 04.4	20.28	0.09	0.5	-15.13	354
4000	10 33 23.5	-09 23 39.2	20.28	0.03	0.7	-15.13	705
1040	10 31 52.1	-09 18 47.7	20.29	0.08	0.5	-15.12	233
1355	10 32 01.4	-09 04 30.8	20.29	0.01	0.6	-15.12	358

Table A.9: Candidate satellite galaxies in the field of MCG-01-27-013 (continued).

Number (1)	RA (J2000) (2)	DEC (J2000) (3)	R (mag) (4)	Class (5)	A (arcsec) (6)	M_R (mag) (7)	Dist (kpc) (8)
16	10 31 20.3	-09 15 02.2	20.29	0.06	0.5	-15.12	450
1829	10 32 18.5	-09 14 06.9	20.30	0.01	0.6	-15.10	57
2551	10 32 43.3	-09 03 51.9	20.30	0.09	0.7	-15.11	460
1602	10 32 10.3	-09 12 04.9	20.31	0.07	0.6	-15.09	80
3574	10 33 07.2	-09 00 30.9	20.31	0.06	0.8	-15.09	686
2835	10 32 50.5	-09 19 08.4	20.32	0.09	0.6	-15.08	376
2893	10 32 52.1	-08 59 48.9	20.32	0.09	0.7	-15.09	620
3801	10 33 00.2	-09 12 57.6	20.32	0.01	0.7	-15.08	423
3925	10 32 55.9	-09 12 08.5	20.32	0.07	0.6	-15.09	390
988	10 31 51.0	-09 24 13.4	20.32	0.06	0.6	-15.09	393
1679	10 32 13.6	-09 09 52.8	20.33	0.00	0.7	-15.08	158
3013	10 33 24.6	-08 58 14.4	20.33	0.01	1.1	-15.07	851
1705	10 32 14.1	-09 07 05.1	20.34	0.08	0.6	-15.06	256
3026	10 33 24.5	-09 09 17.8	20.34	0.01	0.6	-15.06	657
819	10 31 45.9	-09 15 24.9	20.36	0.02	0.5	-15.04	229
2546	10 32 43.6	-09 18 05.7	20.37	0.00	0.6	-15.03	306
2740	10 32 48.0	-09 01 19.3	20.37	0.00	0.6	-15.03	556
2869	10 32 51.6	-09 14 46.9	20.37	0.02	0.6	-15.03	346
3433	10 33 21.9	-09 06 34.1	20.37	0.05	0.5	-15.04	668
838	10 31 46.4	-09 03 16.8	20.37	0.03	0.5	-15.03	449
1932	10 32 21.7	-09 07 54.9	20.38	0.06	0.6	-15.02	242
23	10 31 20.2	-09 00 09.4	20.38	0.03	0.7	-15.02	673
2942	10 32 53.8	-09 25 27.4	20.38	0.06	0.7	-15.03	535
2633	10 32 45.5	-09 23 13.5	20.39	0.00	0.7	-15.01	429
3725	10 33 00.4	-09 16 15.6	20.39	0.07	0.5	-15.02	427
816	10 31 46.0	-09 25 14.9	20.39	0.04	0.6	-15.01	446
969	10 31 50.2	-09 03 29.1	20.41	0.05	0.6	-15.00	427
413	10 31 34.0	-09 17 30.7	20.42	0.08	0.5	-14.98	349
3500	10 33 20.8	-09 13 54.8	20.43	0.01	0.6	-14.98	600
1189	10 31 56.6	-09 11 06.3	20.44	0.03	0.6	-14.96	175
386	10 31 33.3	-09 15 08.8	20.44	0.04	0.5	-14.96	338
632	10 31 40.3	-09 19 29.6	20.47	0.06	0.4	-14.94	330
1121	10 31 54.3	-09 22 20.0	20.48	0.01	0.6	-14.92	321
3401	10 33 25.7	-09 17 03.0	20.48	0.01	0.6	-14.92	649
3403	10 33 11.3	-09 04 44.6	20.48	0.00	0.5	-14.92	618
3535	10 33 09.5	-09 20 26.7	20.48	0.04	0.5	-14.93	545
1056	10 31 52.5	-09 17 09.4	20.49	0.02	0.6	-14.92	196
3897	10 32 56.5	-09 22 58.1	20.49	0.00	0.6	-14.91	494
2461	10 32 41.1	-09 18 39.6	20.50	0.09	0.5	-14.91	296
2533	10 32 43.0	-09 07 23.0	20.50	0.08	0.6	-14.91	365
750	10 31 43.7	-09 11 48.5	20.54	0.07	0.6	-14.86	261
3362	10 33 12.2	-09 09 55.0	20.55	0.01	0.5	-14.86	548
668	10 31 41.3	-09 06 58.4	20.55	0.03	0.5	-14.85	372
2709	10 32 47.5	-09 17 50.5	20.59	0.02	0.6	-14.81	333
1682	10 32 13.7	-09 25 26.2	20.64	0.01	0.5	-14.77	392
6	10 31 20.0	-09 14 06.2	20.67	0.09	0.6	-14.73	452
173	10 31 25.8	-09 23 29.6	20.69	0.02	0.5	-14.71	515
2729	10 32 47.6	-09 05 02.2	20.71	0.05	0.5	-14.69	452
1093	10 31 53.4	-09 12 24.3	20.73	0.08	0.5	-14.67	174
1777	10 32 16.7	-09 11 02.5	20.82	0.03	0.6	-14.59	123
1614	10 32 10.7	-08 57 31.4	20.84	0.07	0.4	-14.57	93
2152	10 32 29.3	-08 56 38.7	20.90	0.06	0.5	-14.51	642
2718	10 32 47.2	-08 58 04.0	20.92	0.03	0.5	-14.48	651

Table A.10: List of the candidate satellite galaxies in the field of MCG-03-26-030.

Number	RA (J2000)	DEC (J2000)	R (mag)	Class	A (arcsec)	M_R (mag)	Dist (kpc)
1124	10 11 05.0	-17 11 39.3	13.88	0.03	5.455	-21.49	111
2929	10 11 53.9	-17 04 43.2	14.29	0.03	4.506	-21.07	394
433	10 10 41.0	-17 04 50.0	15.23	0.03	3.013	-20.14	402
288	10 10 39.0	-16 56 28.4	15.28	0.03	3.812	-20.09	637
3135	10 11 57.7	-17 12 11.8	15.30	0.03	2.703	-20.07	327
1138	10 11 01.1	-17 11 17.5	15.35	0.01	4.385	-20.02	145
3207	10 12 00.6	-17 07 04.1	15.41	0.01	4.762	-19.95	395
738	10 10 48.6	-17 11 38.7	15.76	0.03	2.420	-19.61	246
365	10 10 38.1	-16 54 11.6	15.78	0.03	2.151	-19.59	709
1842	10 11 22.6	-17 15 20.4	15.81	0.03	3.242	-19.56	113
254	10 10 34.4	-17 04 28.3	15.85	0.03	2.694	-19.51	453
4349	10 12 06.4	-16 58 50.7	15.88	0.03	2.523	-19.49	613
83	10 10 29.0	-17 14 22.8	15.96	0.02	4.187	-19.41	414
230	10 10 33.6	-16 55 32.5	15.98	0.03	2.367	-19.39	688
3855	10 12 17.5	-17 04 40.5	16.03	0.03	3.224	-19.34	557
1846	10 11 19.7	-17 22 48.2	16.07	0.03	2.002	-19.30	367
3966	10 12 14.9	-17 02 13.8	16.11	0.00	4.546	-19.26	585
1856	10 11 20.1	-17 03 08.1	16.14	0.03	3.158	-19.23	316
2406	10 11 37.1	-17 11 35.6	16.15	0.03	1.997	-19.21	158
3508	10 12 30.3	-17 06 08.0	16.42	0.00	4.018	-18.95	634
47	10 10 26.7	-16 56 56.6	16.49	0.03	2.044	-18.88	682
2473	10 11 38.6	-17 10 27.6	16.52	0.03	2.521	-18.85	180
1302	10 11 03.2	-16 57 13.5	16.64	0.00	2.402	-18.73	536
3089	10 11 54.8	-16 54 20.3	16.67	0.03	1.753	-18.70	692
997	10 10 54.8	-17 05 17.7	16.72	0.03	2.078	-18.65	309
836	10 10 50.5	-16 57 27.7	16.73	0.00	1.464	-18.64	562
2171	10 11 28.4	-17 13 14.8	16.82	0.03	1.754	-18.55	91
190	10 10 30.9	-16 55 18.3	16.95	0.03	1.753	-18.42	707
3451	10 12 34.7	-17 18 16.3	16.95	0.03	2.555	-18.42	668
3274	10 11 59.5	-17 00 41.9	16.97	0.06	1.556	-18.40	527
1339	10 11 04.4	-17 17 50.3	17.01	0.03	1.432	-18.36	225

Table A.10: Candidate satellite galaxies in the field of MCG-03-26-030 (continued).

Number (1)	RA (J2000) (2)	DEC (J2000) (3)	R (mag) (4)	Class (5)	A (arcsec) (6)	M_R (mag) (7)	Dist (kpc) (8)
4095	10 12 25.7	-17 10 52.2	17.12	0.00	3.001	-18.24	561
504	10 10 41.0	-17 07 08.2	17.12	0.01	1.910	-18.25	356
1314	10 11 04.5	-16 56 59.0	17.13	0.00	1.926	-18.23	542
4102	10 12 31.7	-17 05 24.6	17.16	0.01	2.191	-18.20	654
735	10 10 47.5	-17 02 10.0	17.16	0.00	3.202	-18.20	432
3816	10 12 22.1	-17 06 35.9	17.19	0.03	1.416	-18.18	565
1211	10 11 01.5	-17 14 24.4	17.20	0.04	1.600	-18.17	158
2260	10 11 31.8	-16 55 53.8	17.24	0.02	2.125	-18.12	578
837	10 10 49.9	-16 53 45.8	17.25	0.02	2.399	-18.12	683
3234	10 11 59.3	-17 13 38.1	17.29	0.00	2.358	-18.08	343
402	10 10 37.8	-16 58 46.8	17.29	0.03	1.800	-18.08	575
1825	10 11 18.5	-17 19 57.7	17.30	0.03	1.315	-18.07	268
946	10 10 52.6	-16 58 08.5	17.31	0.00	1.491	-18.06	534
2209	10 11 28.5	-16 58 05.6	17.33	0.03	2.151	-18.04	498
1255	10 11 02.7	-16 54 45.0	17.34	0.00	1.511	-18.03	621
3492	10 12 32.5	-16 53 56.8	17.35	0.03	1.474	-18.02	885
2476	10 11 38.4	-16 59 47.3	17.36	0.00	2.260	-18.01	463
917	10 10 52.0	-16 59 05.5	17.44	0.03	1.446	-17.92	505
3822	10 12 14.8	-17 05 22.4	17.45	0.03	1.501	-17.91	526
1477	10 11 07.8	-17 21 19.7	17.46	0.03	1.785	-17.91	327
4360	10 12 06.8	-17 09 05.4	17.46	0.00	3.037	-17.91	417
33	10 10 25.6	-16 58 00.9	17.52	0.03	1.669	-17.85	659
1544	10 11 09.7	-17 10 12.0	17.53	0.04	1.580	-17.84	100
3167	10 11 57.0	-17 17 02.0	17.53	0.03	1.502	-17.84	362
730	10 10 47.0	-16 58 33.8	17.53	0.02	1.477	-17.84	541
1611	10 11 12.2	-17 11 05.1	17.54	0.01	1.544	-17.83	64
3268	10 11 59.7	-17 04 09.7	17.56	0.05	1.363	-17.80	444
1594	10 11 11.3	-17 07 54.1	17.59	0.04	1.163	-17.77	161
2962	10 11 50.9	-16 54 45.4	17.59	0.04	1.321	-17.78	665
1106	10 10 58.9	-17 20 41.3	17.61	0.00	2.037	-17.76	334
789	10 10 49.4	-17 23 55.3	17.65	0.02	1.883	-17.72	471
10	10 10 24.8	-17 14 08.1	17.66	0.01	1.834	-17.71	448
2303	10 11 32.9	-17 13 44.6	17.66	0.03	1.449	-17.71	132
503	10 10 40.2	-16 55 32.4	17.67	0.08	1.156	-17.70	660
797	10 10 49.7	-16 57 31.9	17.69	0.04	1.068	-17.68	563
2445	10 11 37.0	-17 03 22.2	17.72	0.05	1.200	-17.65	345
2954	10 11 50.8	-16 52 59.8	17.72	0.01	1.718	-17.65	721
3371	10 12 02.5	-17 20 10.7	17.72	0.04	1.399	-17.65	459
1118	10 10 58.7	-17 17 31.4	17.73	0.00	1.723	-17.64	244
2176	10 11 27.6	-16 52 51.2	17.74	0.01	1.634	-17.63	677
1806	10 11 17.7	-17 19 56.5	17.75	0.03	1.156	-17.62	267
1351	10 11 04.6	-17 20 13.9	17.77	0.03	1.338	-17.59	300
1520	10 11 08.3	-17 02 34.8	17.81	0.02	1.400	-17.56	345
2488	10 11 38.2	-16 58 19.5	17.85	0.02	1.469	-17.51	510
226	10 10 32.4	-17 07 28.3	17.86	0.02	1.373	-17.51	415
1192	10 11 00.4	-17 09 12.5	17.87	0.03	1.229	-17.50	181
331	10 10 35.4	-16 59 51.6	17.87	0.05	1.186	-17.50	558
4279	10 12 08.2	-16 55 19.4	17.87	0.01	2.011	-17.50	719
4553	10 12 31.7	-17 05 05.7	17.88	0.03	1.457	-17.49	658
876	10 10 50.7	-16 59 24.9	17.88	0.06	1.160	-17.49	500
1047	10 10 56.1	-16 58 06.9	17.89	0.00	1.080	-17.48	523
2349	10 11 34.4	-16 52 44.1	17.90	0.01	1.783	-17.47	690
2577	10 11 41.4	-16 53 04.7	17.91	0.01	2.242	-17.46	692
340	10 10 35.7	-16 57 15.0	17.91	0.07	1.260	-17.46	629
933	10 10 52.2	-16 58 00.5	17.94	0.00	1.021	-17.42	539
4342	10 12 28.1	-17 18 25.0	17.95	0.05	1.169	-17.42	617
2776	10 11 46.3	-17 14 56.0	17.96	0.03	1.335	-17.41	251
2273	10 11 31.8	-17 20 02.1	17.98	0.03	1.150	-17.39	293
2382	10 11 37.3	-17 02 35.0	17.98	0.01	1.816	-17.39	370
938	10 10 52.4	-16 58 30.7	17.99	0.01	1.215	-17.38	523
4199	10 12 09.5	-17 04 14.8	18.00	0.01	1.640	-17.37	508
280	10 10 33.8	-17 02 55.2	18.02	0.02	1.430	-17.34	490
1201	10 11 01.0	-17 20 49.6	18.04	0.01	1.625	-17.33	331
1355	10 11 04.6	-17 20 07.8	18.04	0.03	1.200	-17.33	296
2864	10 11 48.6	-17 07 53.9	18.04	0.02	1.257	-17.33	293
102	10 10 27.7	-16 53 02.8	18.05	0.05	1.204	-17.32	788
1453	10 11 06.4	-17 11 49.0	18.05	0.00	1.016	-17.32	99
3856	10 12 20.2	-17 11 09.4	18.05	0.05	1.220	-17.32	515
200	10 10 31.1	-16 57 56.6	18.06	0.06	1.090	-17.31	632
3710	10 12 22.6	-17 07 05.4	18.07	0.00	1.385	-17.30	563
635	10 10 43.9	-17 00 50.9	18.07	0.00	2.208	-17.30	487
2450	10 11 36.9	-17 01 54.3	18.08	0.04	1.346	-17.29	391
2860	10 11 48.1	-16 55 52.7	18.09	0.02	1.395	-17.28	620
3801	10 12 04.1	-17 18 39.2	18.11	0.01	1.630	-17.25	441
1132	10 10 58.5	-16 58 06.6	18.12	0.02	0.991	-17.25	517
817	10 10 49.4	-16 56 29.0	18.13	0.00	0.742	-17.24	597
1069	10 10 57.2	-17 19 25.8	18.14	0.02	1.131	-17.23	304
2903	10 11 49.4	-17 01 20.9	18.14	0.08	1.167	-17.23	458
3867	10 12 21.1	-17 06 27.6	18.15	0.01	1.267	-17.22	558
821	10 10 49.8	-16 56 45.5	18.16	0.08	0.770	-17.20	587
3875	10 12 25.6	-17 17 19.2	18.18	0.00	1.585	-17.19	586
1092	10 10 57.2	-16 54 16.6	18.20	0.03	0.887	-17.16	648
1383	10 11 05.0	-16 54 35.5	18.23	0.00	1.323	-17.14	622
2261	10 11 31.2	-16 56 59.7	18.23	0.01	1.847	-17.14	540
3744	10 12 22.3	-16 53 45.8	18.23	0.03	1.171	-17.14	833
1074	10 10 56.7	-16 57 46.8	18.26	0.09	0.921	-17.10	533
894	10 10 51.3	-17 01 35.0	18.26	0.00	1.641	-17.11	432
1179	10 10 59.6	-16 58 03.8	18.27	0.00	0.790	-17.09	516
4570	10 12 30.4	-16 59 50.2	18.28	0.05	1.038	-17.09	737
1738	10 11 16.1	-17 23 10.7	18.29	0.02	1.474	-17.08	380

Table A.10: Candidate satellite galaxies in the field of MCG-03-26-030 (continued).

Number (1)	RA (J2000) (2)	DEC (J2000) (3)	R (mag) (4)	Class (5)	A (arcsec) (6)	M_R (mag) (7)	Dist (kpc) (8)
2773	10 11 48.7	-17 01 02.8	18.29	0.01	2.410	-17.08	463
4220	10 12 09.5	-16 53 39.6	18.29	0.00	1.434	-17.08	773
1017	10 10 54.9	-16 54 20.1	18.30	0.00	0.773	-17.06	651
972	10 10 53.2	-16 57 49.8	18.32	0.00	0.776	-17.05	542
1527	10 11 08.3	-16 58 12.9	18.33	0.01	1.230	-17.04	494
239	10 10 32.1	-16 54 27.8	18.34	0.02	1.612	-17.03	726
3853	10 12 18.3	-17 03 13.3	18.34	0.04	1.063	-17.03	589
1024	10 10 55.4	-16 58 22.8	18.37	0.09	0.860	-17.00	517
1159	10 10 59.0	-16 58 12.3	18.37	0.00	0.881	-17.00	512
2391	10 11 35.2	-17 03 17.7	18.37	0.02	1.094	-17.00	341
1485	10 11 07.4	-17 19 55.3	18.38	0.04	1.139	-16.98	281
1794	10 11 17.1	-17 06 55.3	18.42	0.07	1.204	-16.95	184
2064	10 11 24.6	-17 14 02.3	18.42	0.00	1.172	-16.95	81
2544	10 11 39.6	-17 07 27.6	18.42	0.02	1.156	-16.95	242
1406	10 11 05.0	-16 58 33.5	18.43	0.01	1.008	-16.93	487
3797	10 12 23.1	-17 18 54.4	18.43	0.01	1.305	-16.94	585
401	10 10 37.3	-17 11 51.1	18.43	0.06	1.087	-16.94	339
1627	10 11 12.3	-17 04 08.3	18.44	0.05	1.444	-16.93	285
409	10 10 37.6	-16 58 50.0	18.44	0.02	1.331	-16.93	575
1220	10 11 00.6	-17 00 03.2	18.46	0.01	0.705	-16.91	447
4293	10 12 08.7	-17 17 53.9	18.46	0.02	1.069	-16.91	462
3501	10 12 31.9	-16 57 39.8	18.47	0.01	1.202	-16.90	794
1404	10 11 05.4	-17 10 27.3	18.48	0.01	1.135	-16.89	123
1067	10 10 57.2	-17 05 16.0	18.51	0.02	1.277	-16.86	298
1615	10 11 11.8	-17 09 26.1	18.51	0.01	1.200	-16.86	110
3008	10 11 51.9	-17 17 49.1	18.51	0.09	1.069	-16.86	340
1361	10 11 04.0	-16 58 46.7	18.53	0.00	0.948	-16.83	482
2157	10 11 26.9	-17 03 11.2	18.53	0.02	1.132	-16.84	322
4104	10 12 14.4	-17 17 49.5	18.53	0.00	1.299	-16.83	504
1526	10 11 08.5	-17 08 47.9	18.57	0.01	1.307	-16.79	143
2363	10 11 35.1	-17 17 52.5	18.57	0.01	1.781	-16.80	241
1086	10 10 57.4	-17 05 39.8	18.59	0.01	1.479	-16.78	286
2198	10 11 28.0	-17 15 10.7	18.61	0.01	1.114	-16.75	130
3575	10 12 25.4	-17 10 54.2	18.63	0.02	1.049	-16.74	559
4583	10 12 24.2	-17 08 22.1	18.63	0.01	1.388	-16.73	564
949	10 10 52.9	-17 05 24.3	18.64	0.01	1.155	-16.72	317
2227	10 11 28.8	-17 06 09.1	18.65	0.00	1.672	-16.72	228
308	10 10 34.4	-17 07 59.4	18.65	0.01	1.095	-16.72	392
905	10 10 51.5	-17 11 57.3	18.65	0.02	0.981	-16.72	222
17	10 10 24.7	-16 52 42.3	18.68	0.02	0.983	-16.69	811
898	10 10 51.8	-16 57 23.2	18.69	0.00	1.142	-16.68	560
610	10 10 43.0	-16 55 17.3	18.70	0.05	0.878	-16.67	657
111	10 10 27.5	-16 56 19.6	18.71	0.02	1.164	-16.65	695
2727	10 11 44.9	-17 17 13.5	18.72	0.01	1.341	-16.64	280
3036	10 11 52.5	-17 12 40.4	18.72	0.01	1.414	-16.65	285
3364	10 12 02.0	-17 15 39.8	18.72	0.01	1.154	-16.65	381
2647	10 11 42.5	-16 58 12.0	18.73	0.01	1.319	-16.64	527
2833	10 11 47.4	-17 04 19.2	18.75	0.03	0.960	-16.62	366
4156	10 12 10.9	-17 08 01.6	18.75	0.03	1.032	-16.62	461
175	10 10 30.0	-16 58 14.5	18.76	0.00	1.268	-16.60	629
217	10 10 31.7	-16 56 54.9	18.77	0.01	1.122	-16.60	657
3499	10 12 32.4	-16 54 00.0	18.77	0.03	1.334	-16.60	883
3903	10 12 19.9	-16 58 12.4	18.77	0.01	1.216	-16.59	707
4135	10 12 13.4	-17 06 54.4	18.79	0.03	0.971	-16.58	493
1464	10 11 06.6	-17 12 14.1	18.80	0.01	0.933	-16.56	96
3353	10 12 01.5	-17 07 36.9	18.80	0.03	1.156	-16.57	393
3332	10 12 00.9	-16 54 22.5	18.81	0.02	1.079	-16.56	714
3670	10 12 25.0	-17 03 29.3	18.81	0.01	1.025	-16.56	632
606	10 10 42.9	-16 57 55.7	18.81	0.00	0.917	-16.56	577
155	10 10 29.4	-17 20 58.9	18.82	0.00	1.062	-16.55	506
3163	10 11 56.2	-17 08 51.2	18.82	0.00	1.234	-16.54	336
4438	10 12 04.7	-17 11 03.5	18.82	0.01	1.713	-16.55	387
1224	10 11 01.1	-17 16 51.3	18.83	0.00	1.106	-16.54	214
223	10 10 31.6	-17 01 27.3	18.84	0.01	1.148	-16.53	538
2549	10 11 39.7	-17 22 18.5	18.84	0.08	1.010	-16.53	392
641	10 10 43.7	-16 58 24.9	18.84	0.00	0.962	-16.52	559
1438	10 11 05.6	-16 57 01.4	18.85	0.02	0.774	-16.52	538
2504	10 11 38.4	-16 58 23.6	18.85	0.01	1.098	-16.52	509
2291	10 11 32.2	-17 18 20.0	18.86	0.00	1.066	-16.51	241
4532	10 12 29.3	-17 01 35.3	18.86	0.02	1.142	-16.51	696
507	10 10 40.1	-17 08 34.7	18.86	0.04	0.947	-16.51	341
29	10 10 25.6	-16 53 19.3	18.88	0.00	1.256	-16.48	789
629	10 10 43.8	-17 09 28.0	18.88	0.01	1.164	-16.49	301
1221	10 11 00.5	-16 59 31.5	18.89	0.03	0.760	-16.48	465
1296	10 11 02.3	-16 54 16.9	18.89	0.00	0.749	-16.48	637
1413	10 11 05.6	-17 02 38.2	18.89	0.01	1.334	-16.48	349
2728	10 11 44.3	-17 05 59.1	18.90	0.07	0.889	-16.47	306
3873	10 12 19.2	-17 20 52.3	18.90	0.01	1.187	-16.47	588
1311	10 11 02.8	-16 54 08.1	18.91	0.00	0.951	-16.46	641
3962	10 12 15.7	-17 14 09.2	18.92	0.01	1.343	-16.45	481
4216	10 12 11.8	-17 23 26.8	18.92	0.03	0.893	-16.44	590
4506	10 12 34.6	-17 09 57.5	18.92	0.01	1.363	-16.45	639
1928	10 11 20.4	-17 13 28.2	18.93	0.01	1.131	-16.44	46
3648	10 12 24.2	-17 11 12.0	18.93	0.05	0.854	-16.44	548
3646	10 12 25.1	-17 07 23.0	18.94	0.00	0.645	-16.42	579
3841	10 12 21.1	-17 12 41.9	18.94	0.01	1.049	-16.42	522
901	10 10 51.2	-17 19 07.3	18.95	0.01	1.088	-16.41	327
3192	10 11 58.3	-16 59 38.9	18.96	0.01	1.282	-16.41	549
100	10 10 27.4	-17 11 38.2	18.98	0.01	1.049	-16.39	422
192	10 10 30.4	-16 57 58.7	18.98	0.00	0.973	-16.38	635

Table A.10: Candidate satellite galaxies in the field of MCG-03-26-030 (continued).

Number (1)	RA (J2000) (2)	DEC (J2000) (3)	R (mag) (4)	Class (5)	A (arcsec) (6)	M_R (mag) (7)	Dist (kpc) (8)
369	10 10 36.4	-17 00 45.7	18.99	0.02	0.931	-16.38	528
3555	10 12 10.7	-17 00 00.1	19.00	0.02	1.261	-16.37	608
973	10 10 53.7	-17 22 58.0	19.00	0.06	0.935	-16.37	424
4289	10 12 06.7	-17 09 04.1	19.01	0.00	2.097	-16.35	416
3248	10 11 58.8	-16 57 44.4	19.02	0.00	1.487	-16.35	605
75	10 10 26.7	-16 59 10.8	19.02	0.00	1.221	-16.35	623
1337	10 11 03.4	-17 11 49.1	19.03	0.04	0.575	-16.34	123
1969	10 11 21.7	-17 06 30.4	19.03	0.03	1.019	-16.34	201
1325	10 11 03.7	-17 20 16.8	19.05	0.02	1.056	-16.32	304
1472	10 11 06.2	-16 56 23.1	19.05	0.02	0.610	-16.31	559
2531	10 11 39.0	-16 59 38.8	19.05	0.01	1.161	-16.32	470
3636	10 12 09.4	-17 10 32.7	19.06	0.01	1.231	-16.31	428
1752	10 11 16.1	-17 23 47.8	19.07	0.05	0.858	-16.30	402
2940	10 11 50.2	-17 07 07.0	19.07	0.04	1.072	-16.29	319
1388	10 11 04.3	-16 57 04.4	19.08	0.06	0.577	-16.29	539
4469	10 12 26.5	-17 17 25.7	19.08	0.00	0.893	-16.29	594
3655	10 12 07.9	-17 01 10.3	19.09	0.00	1.461	-16.28	563
3840	10 12 23.7	-17 05 37.4	19.09	0.01	1.021	-16.28	589
1269	10 11 01.5	-16 58 37.6	19.10	0.00	0.734	-16.27	492
1332	10 11 03.2	-16 54 17.6	19.10	0.00	0.721	-16.27	635
1380	10 11 04.6	-17 01 40.7	19.10	0.01	1.103	-16.26	383
3600	10 12 19.4	-17 06 34.1	19.10	0.03	0.882	-16.26	544
3979	10 12 29.3	-17 15 28.6	19.10	0.02	0.893	-16.27	599
3756	10 12 33.7	-17 06 15.5	19.11	0.01	1.061	-16.26	659
4309	10 12 27.6	-17 08 29.9	19.11	0.00	0.723	-16.26	590
1005	10 10 55.3	-17 08 28.9	19.12	0.00	1.690	-16.25	230
1839	10 11 18.3	-17 22 49.6	19.12	0.02	0.921	-16.25	368
895	10 10 51.1	-17 17 25.8	19.12	0.00	1.098	-16.25	288
1754	10 11 15.8	-17 04 03.2	19.13	0.07	1.008	-16.24	285
1071	10 10 56.9	-17 17 20.9	19.14	0.07	0.843	-16.23	250
1441	10 11 06.0	-16 56 14.1	19.14	0.01	1.008	-16.23	565
689	10 10 45.0	-16 57 07.9	19.14	0.02	0.602	-16.23	592
56	10 10 26.1	-16 52 36.8	19.15	0.03	1.018	-16.22	807
1475	10 11 06.8	-17 20 44.2	19.16	0.00	1.167	-16.21	310
1708	10 11 14.9	-17 14 16.7	19.16	0.01	1.031	-16.21	76
2285	10 11 31.6	-17 07 49.1	19.16	0.08	0.938	-16.20	189
3202	10 11 57.3	-16 54 49.7	19.16	0.00	1.158	-16.20	686
1498	10 11 07.5	-17 11 34.6	19.17	0.02	0.946	-16.19	92
4112	10 12 14.3	-17 07 29.3	19.19	0.05	0.933	-16.18	493
1800	10 11 17.1	-17 07 24.3	19.20	0.05	0.867	-16.17	168
4117	10 12 14.3	-17 19 31.8	19.20	0.01	1.204	-16.17	529
754	10 10 47.0	-17 00 05.4	19.20	0.00	0.975	-16.17	495
887	10 10 50.9	-17 00 33.2	19.20	0.02	0.987	-16.17	465
1720	10 11 15.4	-16 54 46.3	19.21	0.00	1.451	-16.16	607
3357	10 12 01.7	-17 23 47.4	19.21	0.00	0.994	-16.16	539
3630	10 12 25.8	-17 13 19.5	19.22	0.04	1.112	-16.15	561
4275	10 12 08.5	-16 55 02.7	19.22	0.00	1.014	-16.15	728
2417	10 11 35.7	-17 19 21.1	19.25	0.00	0.661	-16.12	286
3890	10 12 20.4	-16 52 43.8	19.25	0.00	1.612	-16.12	852
3657	10 12 04.4	-16 56 19.3	19.26	0.00	0.778	-16.10	672
2430	10 11 36.1	-17 02 31.9	19.29	0.02	0.840	-16.08	368
2970	10 11 50.7	-17 02 01.9	19.29	0.00	1.075	-16.08	445
1336	10 11 03.8	-17 23 34.4	19.30	0.00	1.307	-16.07	411
1349	10 11 03.6	-16 57 40.1	19.31	0.09	0.655	-16.06	520
656	10 10 43.8	-16 56 39.9	19.32	0.05	0.588	-16.05	611
1154	10 10 58.7	-16 54 22.8	19.33	0.01	0.676	-16.04	641
1432	10 11 06.0	-17 14 36.9	19.33	0.04	0.915	-16.04	131
1723	10 11 15.4	-17 21 00.0	19.33	0.05	0.922	-16.03	305
466	10 10 39.3	-17 08 40.8	19.33	0.00	1.412	-16.04	345
1944	10 11 21.1	-17 13 30.9	19.34	0.01	1.015	-16.02	50
3017	10 11 51.7	-17 01 57.0	19.34	0.01	0.855	-16.03	452
235	10 10 31.8	-17 00 10.5	19.35	0.00	0.849	-16.02	569
719	10 10 45.9	-16 54 56.5	19.35	0.00	0.613	-16.02	658
820	10 10 49.0	-17 22 29.6	19.35	0.01	0.651	-16.02	431
2078	10 11 25.1	-17 19 47.1	19.36	0.01	1.013	-16.01	268
3819	10 12 22.7	-17 20 38.4	19.36	0.02	0.855	-16.01	609
2916	10 11 49.5	-17 01 55.5	19.37	0.02	0.883	-16.00	442
1687	10 11 14.0	-17 01 50.9	19.38	0.00	1.039	-15.98	362
3158	10 11 55.8	-17 09 38.8	19.38	0.05	0.812	-15.99	324
348	10 10 35.6	-16 59 17.3	19.39	0.03	0.943	-15.98	572
3724	10 12 21.9	-17 22 02.7	19.39	0.09	0.840	-15.98	628
674	10 10 44.8	-17 04 27.3	19.39	0.06	0.978	-15.98	387
927	10 10 51.5	-16 59 20.0	19.39	0.07	0.568	-15.98	500
1127	10 10 58.5	-17 19 13.5	19.40	0.01	0.972	-15.97	293
1390	10 11 04.7	-17 00 59.8	19.40	0.01	0.896	-15.96	406
2888	10 11 48.6	-16 57 22.8	19.40	0.07	0.920	-15.97	574
3826	10 12 21.7	-17 17 23.2	19.40	0.02	0.985	-15.97	555
1912	10 11 19.6	-17 10 02.0	19.41	0.05	0.853	-15.96	77
2304	10 11 32.5	-17 07 00.0	19.41	0.02	0.935	-15.95	216
3911	10 12 19.5	-17 06 56.0	19.41	0.04	0.906	-15.95	540
4124	10 12 26.6	-17 04 58.3	19.41	0.09	0.855	-15.96	621
1193	10 10 59.8	-17 01 03.1	19.42	0.02	0.672	-15.94	417
1370	10 11 04.0	-16 59 33.7	19.42	0.08	0.606	-15.94	455
579	10 10 41.8	-16 57 10.2	19.43	0.05	0.563	-15.94	604
922	10 10 51.8	-17 16 26.6	19.43	0.03	0.763	-15.94	263
1398	10 11 05.1	-17 21 22.6	19.44	0.04	0.808	-15.92	335
2043	10 11 23.6	-16 55 32.9	19.44	0.01	0.934	-15.93	581
2355	10 11 33.9	-17 01 11.5	19.44	0.04	1.023	-15.93	405
3530	10 12 14.7	-16 57 12.0	19.44	0.00	1.088	-15.92	702
4258	10 12 31.8	-17 23 36.4	19.44	0.00	0.984	-15.93	726

Table A.10: Candidate satellite galaxies in the field of MCG-03-26-030 (continued).

Number (1)	RA (J2000) (2)	DEC (J2000) (3)	R (mag) (4)	Class (5)	A (arcsec) (6)	M_R (mag) (7)	Dist (kpc) (8)
4412	10 12 26.3	-17 20 54.6	19.44	0.04	0.836	-15.93	640
1353	10 11 04.1	-17 18 01.8	19.46	0.05	0.823	-15.91	232
3649	10 12 05.6	-16 52 48.6	19.46	0.09	0.986	-15.90	781
470	10 10 39.1	-16 55 02.6	19.46	0.00	0.951	-15.90	679
739	10 10 47.8	-17 23 59.8	19.46	0.01	2.048	-15.91	480
1399	10 11 04.8	-16 54 41.8	19.47	0.00	1.154	-15.90	619
4143	10 12 30.0	-17 17 27.2	19.47	0.00	1.043	-15.89	622
2392	10 11 34.7	-16 53 30.3	19.49	0.01	0.880	-15.88	665
1779	10 11 16.5	-17 10 11.6	19.50	0.08	0.810	-15.87	72
3312	10 12 00.1	-16 54 27.6	19.50	0.08	0.856	-15.86	708
3968	10 12 17.2	-17 08 40.5	19.50	0.03	0.626	-15.87	504
1567	10 11 09.5	-17 11 22.0	19.51	0.05	0.748	-15.86	78
2123	10 11 25.8	-17 03 04.7	19.51	0.00	0.875	-15.86	324
4059	10 12 14.9	-17 07 32.9	19.51	0.00	0.974	-15.86	497
174	10 10 29.7	-17 00 40.6	19.52	0.05	0.852	-15.85	569
1941	10 11 20.7	-17 20 34.9	19.53	0.01	0.992	-15.84	290
3401	10 12 02.3	-17 20 16.4	19.53	0.04	0.901	-15.84	460
3533	10 12 13.4	-17 00 55.7	19.55	0.02	0.949	-15.82	603
4224	10 12 09.7	-17 05 49.0	19.55	0.01	0.851	-15.81	481
1261	10 11 01.7	-17 11 20.7	19.56	0.06	0.806	-15.81	141
1712	10 11 14.7	-16 54 28.8	19.57	0.02	0.775	-15.80	617
4460	10 12 20.5	-17 11 04.1	19.57	0.09	0.861	-15.80	518
4292	10 12 26.7	-17 13 29.0	19.60	0.06	0.766	-15.77	569
99	10 10 26.9	-16 57 08.2	19.60	0.04	0.708	-15.76	675
2793	10 11 46.2	-17 01 58.9	19.61	0.00	1.155	-15.76	425
4079	10 12 16.4	-17 09 57.7	19.61	0.00	0.743	-15.75	488
1433	10 11 05.5	-16 58 45.2	19.62	0.02	0.639	-15.75	480
773	10 10 47.8	-17 20 19.4	19.62	0.08	0.770	-15.75	377
1378	10 11 04.1	-16 59 35.0	19.63	0.06	0.512	-15.74	454
4357	10 12 07.1	-17 06 05.1	19.64	0.00	1.221	-15.73	458
3608	10 12 27.5	-16 54 49.0	19.65	0.00	1.038	-15.71	834
657	10 10 44.7	-17 13 01.4	19.65	0.00	1.332	-15.72	279
996	10 10 54.2	-16 54 25.1	19.65	0.00	0.940	-15.72	650
2953	10 11 50.9	-17 20 26.3	19.66	0.01	1.278	-15.71	393
3403	10 12 02.3	-17 19 27.5	19.66	0.09	0.722	-15.71	443
1174	10 10 59.4	-17 17 02.6	19.67	0.01	0.557	-15.70	229
3411	10 12 02.5	-17 15 46.5	19.67	0.07	0.928	-15.69	387
535	10 10 40.7	-17 19 53.2	19.67	0.09	0.717	-15.70	409
1327	10 11 03.1	-16 58 39.8	19.69	0.02	0.567	-15.67	488
3270	10 11 58.6	-16 56 28.9	19.69	0.02	0.663	-15.68	641
341	10 10 35.5	-17 14 09.6	19.70	0.00	1.019	-15.67	361
599	10 10 42.7	-17 14 40.8	19.70	0.00	0.999	-15.67	307
3838	10 12 13.4	-16 55 16.4	19.71	0.08	0.686	-15.66	746
653	10 10 44.2	-17 18 07.1	19.71	0.09	0.702	-15.65	348
944	10 10 52.3	-16 58 26.2	19.71	0.00	0.994	-15.66	525
1219	10 11 00.6	-17 17 58.7	19.72	0.00	0.825	-15.65	247
4096	10 12 14.5	-17 20 08.8	19.72	0.01	1.075	-15.65	541
1310	10 11 03.0	-17 19 50.9	19.73	0.04	0.886	-15.64	293
481	10 10 39.5	-17 17 56.6	19.73	0.00	0.877	-15.64	377
1482	10 11 06.9	-17 13 07.1	19.74	0.02	0.753	-15.63	98
4536	10 12 30.1	-17 13 28.6	19.74	0.04	0.736	-15.63	597
437	10 10 38.3	-17 20 34.4	19.75	0.08	0.742	-15.62	439
995	10 10 54.1	-17 05 05.7	19.75	0.01	0.767	-15.61	319
13	10 10 24.8	-16 58 34.1	19.76	0.01	0.889	-15.61	649
1471	10 11 06.8	-17 23 10.8	19.76	0.03	0.766	-15.61	392
2896	10 11 48.8	-17 05 12.1	19.76	0.08	0.895	-15.60	352
3423	10 12 02.8	-17 03 24.9	19.76	0.00	1.282	-15.61	480
455	10 10 38.7	-17 13 32.9	19.76	0.07	0.710	-15.60	331
798	10 10 48.8	-17 18 15.8	19.76	0.01	1.037	-15.61	321
1088	10 10 57.4	-17 11 30.8	19.77	0.00	0.877	-15.59	175
1537	10 11 08.1	-16 57 04.7	19.77	0.00	0.700	-15.59	533
701	10 10 45.3	-16 54 30.3	19.77	0.01	0.607	-15.59	673
1628	10 11 11.6	-17 11 54.8	19.78	0.05	0.531	-15.58	56
2374	10 11 34.2	-17 02 17.9	19.78	0.00	0.719	-15.58	369
1725	10 11 14.8	-16 53 07.0	19.79	0.05	1.265	-15.58	664
2730	10 11 44.3	-17 06 33.8	19.79	0.01	0.804	-15.58	292
1112	10 10 57.9	-17 10 10.6	19.80	0.07	0.721	-15.57	182
4370	10 12 05.0	-16 54 04.5	19.80	0.01	0.880	-15.57	740
2030	10 11 23.2	-16 54 39.4	19.81	0.00	0.975	-15.55	612
2547	10 11 39.3	-17 10 45.1	19.81	0.01	0.848	-15.56	182
293	10 10 33.5	-17 05 34.3	19.81	0.07	0.735	-15.56	437
3315	10 12 00.5	-17 13 13.9	19.81	0.07	0.773	-15.56	352
1802	10 11 16.8	-17 10 49.7	19.82	0.01	0.698	-15.55	50
2195	10 11 27.6	-17 03 25.2	19.82	0.09	0.812	-15.55	315
1812	10 11 17.0	-17 02 38.9	19.83	0.09	0.654	-15.54	333
2384	10 11 34.5	-17 02 59.5	19.84	0.00	0.735	-15.53	348
2945	10 11 49.7	-17 01 26.6	19.84	0.05	0.492	-15.53	456
2964	10 11 50.5	-17 06 41.5	19.84	0.09	0.729	-15.53	329
1474	10 11 06.5	-17 05 15.7	19.86	0.01	0.935	-15.51	261
3951	10 12 18.0	-16 58 38.0	19.86	0.00	0.993	-15.50	685
669	10 10 44.7	-17 10 44.2	19.86	0.00	0.822	-15.51	283
2597	10 11 40.6	-17 08 32.2	19.87	0.01	0.903	-15.50	225
3004	10 11 51.4	-16 56 29.7	19.88	0.01	0.841	-15.48	612
4018	10 12 16.4	-16 58 14.0	19.88	0.07	0.731	-15.49	685
4097	10 12 14.2	-16 59 16.3	19.88	0.09	0.752	-15.49	647
21	10 10 24.8	-17 22 05.5	19.89	0.01	0.622	-15.48	559
3718	10 12 23.5	-17 19 10.7	19.89	0.03	0.745	-15.48	592
593	10 10 42.4	-17 05 16.6	19.89	0.07	0.815	-15.48	383
3062	10 11 53.0	-17 17 19.2	19.90	0.03	0.745	-15.47	337
559	10 10 41.5	-17 20 18.7	19.90	0.00	0.835	-15.47	414

Table A.10: Candidate satellite galaxies in the field of MCG-03-26-030 (continued).

Number (1)	RA (J2000) (2)	DEC (J2000) (3)	R (mag) (4)	Class (5)	A (arcsec) (6)	M_R (mag) (7)	Dist (kpc) (8)
2332	10 11 32.8	-16 56 30.4	19.91	0.07	0.689	-15.45	559
1214	10 11 00.5	-17 13 45.5	19.93	0.00	0.817	-15.43	156
2614	10 11 40.7	-16 54 19.1	19.93	0.05	0.688	-15.44	649
2797	10 11 46.1	-17 15 04.7	19.93	0.05	0.713	-15.44	251
496	10 10 39.8	-17 03 03.5	19.93	0.00	0.883	-15.43	451
109	10 10 27.3	-17 03 12.3	19.95	0.01	0.774	-15.42	526
2192	10 11 27.4	-16 56 38.3	19.95	0.01	0.682	-15.42	547
1403	10 11 05.0	-17 20 28.0	19.96	0.09	0.663	-15.41	306
2685	10 11 43.3	-17 09 48.3	19.96	0.01	0.664	-15.40	224
3858	10 12 16.5	-17 17 39.1	19.96	0.08	0.708	-15.41	518
4028	10 12 17.2	-17 07 02.9	19.96	0.06	0.691	-15.41	521
1913	10 11 19.5	-16 54 11.2	19.97	0.03	1.020	-15.40	627
2734	10 11 44.1	-16 54 50.2	19.97	0.00	0.695	-15.40	641
3632	10 12 23.0	-17 00 38.7	19.97	0.01	0.495	-15.40	671
3886	10 12 18.4	-17 05 02.0	19.97	0.02	0.682	-15.40	558
2101	10 11 25.5	-17 15 45.2	19.98	0.01	0.764	-15.38	136
2231	10 11 28.8	-16 54 05.0	19.98	0.05	0.846	-15.38	636
2408	10 11 35.4	-17 15 41.4	20.00	0.08	0.740	-15.36	186
955	10 10 52.6	-17 22 34.7	20.00	0.07	0.627	-15.37	417
1217	10 11 00.6	-17 22 16.8	20.01	0.06	0.804	-15.35	378
1763	10 11 15.6	-17 04 38.1	20.01	0.09	0.541	-15.36	264
843	10 10 49.6	-17 05 54.7	20.01	0.00	0.789	-15.36	323
2046	10 11 23.7	-17 11 27.2	20.02	0.00	0.883	-15.34	52
2643	10 11 41.7	-16 54 01.4	20.02	0.03	0.647	-15.35	662
3695	10 12 08.6	-16 57 56.1	20.02	0.01	0.639	-15.35	649
2405	10 11 35.3	-17 09 49.2	20.05	0.00	0.717	-15.32	164
3053	10 11 52.4	-17 01 52.2	20.05	0.00	0.673	-15.31	458
3405	10 12 02.2	-17 12 31.0	20.05	0.04	0.713	-15.31	364
3650	10 12 06.1	-17 01 01.6	20.05	0.06	0.828	-15.32	556
1572	10 11 09.7	-17 21 49.5	20.06	0.02	0.750	-15.31	340
1864	10 11 18.7	-16 56 53.4	20.06	0.00	1.154	-15.31	533
2386	10 11 34.6	-17 02 14.5	20.06	0.00	0.593	-15.31	372
632	10 10 43.3	-17 11 07.5	20.06	0.01	0.775	-15.30	292
2499	10 11 38.1	-16 54 59.3	20.07	0.00	1.218	-15.30	621
1162	10 10 58.9	-17 02 47.8	20.08	0.06	0.612	-15.29	365
1410	10 11 05.2	-17 18 14.2	20.08	0.01	0.708	-15.29	234
2362	10 11 35.3	-17 01 41.2	20.08	0.03	0.701	-15.29	392
3577	10 12 27.0	-17 20 18.6	20.08	0.03	0.633	-15.29	635
213	10 10 31.1	-16 54 20.9	20.09	0.09	0.745	-15.28	734
3755	10 12 21.5	-17 17 31.4	20.09	0.01	0.647	-15.28	555
386	10 10 36.4	-17 06 59.9	20.09	0.06	0.588	-15.27	392
4078	10 12 23.4	-17 11 15.1	20.09	0.09	0.646	-15.28	541
4425	10 12 05.1	-17 05 53.4	20.09	0.05	0.806	-15.28	447
584	10 10 42.3	-17 08 26.3	20.09	0.05	0.888	-15.28	326
2534	10 11 38.9	-17 14 31.9	20.10	0.01	0.794	-15.26	189
1408	10 11 05.1	-17 23 50.9	20.11	0.00	0.658	-15.25	417
2296	10 11 31.9	-17 08 34.6	20.11	0.01	0.729	-15.26	170
3261	10 11 58.9	-17 20 51.8	20.11	0.04	0.819	-15.25	451
4201	10 12 12.0	-17 07 33.5	20.12	0.04	0.680	-15.24	475
160	10 10 29.0	-17 13 11.6	20.13	0.03	0.789	-15.24	409
204	10 10 30.8	-17 04 51.1	20.13	0.01	0.703	-15.24	470
2871	10 11 48.2	-17 20 47.8	20.13	0.07	0.591	-15.24	387
1995	10 11 22.2	-17 13 53.0	20.14	0.00	0.729	-15.23	65
2352	10 11 33.4	-16 53 58.4	20.14	0.00	0.806	-15.23	646
3321	10 12 00.6	-17 16 26.4	20.14	0.09	0.694	-15.23	380
3560	10 12 10.9	-17 13 29.8	20.14	0.09	0.622	-15.23	438
4329	10 12 07.1	-17 07 36.3	20.14	0.08	0.711	-15.23	436
2717	10 11 44.1	-17 17 35.2	20.15	0.00	0.728	-15.21	284
3340	10 12 00.8	-17 09 16.1	20.15	0.01	0.723	-15.22	368
480	10 10 39.3	-17 06 51.7	20.15	0.02	0.727	-15.22	373
1739	10 11 15.6	-17 23 03.1	20.17	0.08	0.637	-15.20	376
3183	10 11 56.1	-16 57 25.2	20.18	0.00	0.713	-15.19	603
3562	10 12 27.5	-17 12 41.6	20.18	0.00	0.893	-15.19	574
2664	10 11 42.7	-17 13 25.1	20.19	0.00	0.674	-15.18	207
4105	10 12 14.1	-17 03 37.4	20.19	0.07	0.723	-15.18	552
4273	10 12 06.0	-17 00 04.6	20.19	0.07	0.740	-15.18	579
79	10 10 26.3	-16 58 14.3	20.19	0.07	0.674	-15.18	649
1427	10 11 05.3	-17 02 23.9	20.20	0.01	0.641	-15.16	358
2843	10 11 47.2	-17 04 33.5	20.20	0.08	0.746	-15.17	359
3309	10 12 00.4	-17 17 33.4	20.20	0.05	0.677	-15.17	395
74	10 10 26.5	-17 19 36.1	20.20	0.00	0.691	-15.17	499
3566	10 12 25.5	-17 11 26.6	20.21	0.09	0.578	-15.16	559
1829	10 11 17.5	-16 54 25.2	20.22	0.00	1.037	-15.14	619
4026	10 12 11.1	-17 08 47.2	20.22	0.02	0.564	-15.15	454
1298	10 11 02.5	-17 17 20.4	20.23	0.01	0.618	-15.14	220
1654	10 11 12.5	-16 54 46.4	20.23	0.05	0.777	-15.14	608
2313	10 11 32.3	-17 05 03.3	20.23	0.07	0.497	-15.14	275
3220	10 11 56.9	-16 55 46.9	20.23	0.00	0.651	-15.14	655
3707	10 12 24.0	-17 17 32.8	20.23	0.03	0.751	-15.14	575
3892	10 12 19.7	-17 03 51.3	20.23	0.02	0.913	-15.14	587
904	10 10 51.2	-17 17 50.0	20.23	0.03	0.765	-15.14	296
3428	10 12 02.5	-17 08 02.1	20.24	0.07	0.614	-15.12	395
4389	10 12 05.4	-16 54 42.9	20.24	0.06	0.645	-15.13	724
2459	10 11 36.9	-17 20 44.5	20.25	0.01	0.528	-15.12	333
3584	10 12 25.2	-16 57 04.9	20.25	0.00	0.691	-15.12	765
675	10 10 44.6	-17 14 08.7	20.25	0.07	0.731	-15.11	286
2333	10 11 32.8	-16 53 23.7	20.26	0.01	0.658	-15.11	665
2701	10 11 43.4	-17 02 12.8	20.26	0.01	0.718	-15.11	405
3767	10 12 23.4	-17 23 05.7	20.27	0.03	0.694	-15.10	659
98	10 10 26.9	-17 07 04.8	20.27	0.07	0.583	-15.10	462

Table A.10: Candidate satellite galaxies in the field of MCG-03-26-030 (continued).

Number (1)	RA (J2000) (2)	DEC (J2000) (3)	R (mag) (4)	Class (5)	A (arcsec) (6)	M_R (mag) (7)	Dist (kpc) (8)
1730	10 11 15.2	-17 16 47.4	20.28	0.01	0.566	-15.09	160
2583	10 11 40.2	-16 55 21.7	20.28	0.05	0.839	-15.08	614
2735	10 11 44.6	-17 23 35.3	20.28	0.09	0.669	-15.09	451
1895	10 11 19.0	-17 10 17.4	20.29	0.00	0.691	-15.08	67
2339	10 11 33.2	-17 11 00.6	20.29	0.06	0.518	-15.08	130
844	10 10 49.6	-17 13 14.7	20.29	0.01	0.754	-15.08	239
1744	10 11 15.3	-16 55 43.0	20.30	0.09	0.730	-15.06	574
2462	10 11 36.8	-17 09 11.0	20.30	0.02	0.602	-15.07	186
1123	10 10 58.0	-17 00 32.7	20.31	0.00	0.705	-15.06	439
1329	10 11 03.4	-17 20 15.8	20.32	0.00	0.696	-15.04	304
2069	10 11 24.1	-16 52 37.8	20.32	0.01	0.799	-15.04	682
2633	10 11 41.8	-17 23 19.3	20.32	0.07	0.706	-15.04	431
3614	10 12 19.7	-17 12 01.6	20.32	0.00	0.693	-15.04	510
4475	10 12 26.3	-17 05 26.3	20.32	0.03	0.633	-15.05	612
319	10 10 34.3	-17 07 12.1	20.33	0.01	0.653	-15.04	404
4137	10 12 11.5	-17 17 20.9	20.33	0.00	0.760	-15.04	476
716	10 10 45.9	-16 52 57.0	20.33	0.02	0.756	-15.04	721
412	10 10 37.1	-17 03 41.8	20.34	0.05	0.707	-15.03	452
2413	10 11 35.6	-17 19 28.2	20.35	0.02	0.604	-15.01	289
2662	10 11 42.4	-16 58 54.2	20.35	0.05	0.680	-15.02	504
2948	10 11 50.0	-17 04 07.6	20.35	0.09	0.728	-15.02	386
4004	10 12 13.2	-17 18 39.5	20.35	0.02	0.551	-15.01	507
404	10 10 36.8	-17 07 32.5	20.35	0.04	0.592	-15.01	380
114	10 10 27.1	-16 56 33.1	20.36	0.01	0.617	-15.01	690
4005	10 12 16.8	-16 58 24.8	20.36	0.08	0.643	-15.01	683
4343	10 12 07.2	-17 18 17.3	20.36	0.09	0.701	-15.01	457
793	10 10 48.4	-17 19 46.7	20.36	0.01	0.628	-15.01	360
1733	10 11 15.1	-17 02 00.2	20.37	0.06	0.560	-15.00	356
4130	10 12 11.6	-17 04 29.4	20.37	0.01	0.749	-15.00	518
1057	10 10 56.1	-17 08 26.4	20.38	0.00	0.644	-14.99	226
1977	10 11 21.5	-17 07 32.1	20.38	0.07	0.635	-14.99	165
3788	10 12 13.1	-17 20 27.4	20.38	0.05	0.651	-14.99	537
796	10 10 48.3	-17 23 21.6	20.38	0.02	0.585	-14.99	459
1020	10 10 55.1	-17 10 29.9	20.39	0.04	0.642	-14.98	201
1134	10 10 58.7	-17 14 12.7	20.39	0.08	0.632	-14.98	176
189	10 10 30.2	-17 09 26.4	20.39	0.01	0.728	-14.98	410
3384	10 12 01.9	-17 19 37.8	20.39	0.00	0.622	-14.98	444
3691	10 12 04.7	-17 06 09.7	20.39	0.05	0.675	-14.98	439
621	10 10 43.0	-17 08 36.6	20.39	0.01	0.680	-14.98	318
684	10 10 44.9	-17 12 34.8	20.39	0.05	0.604	-14.97	276
3063	10 11 52.9	-17 15 31.8	20.40	0.04	0.678	-14.97	309
3581	10 12 21.2	-16 56 25.8	20.40	0.01	0.552	-14.97	758
3743	10 12 23.7	-16 56 28.1	20.40	0.04	0.677	-14.96	772
92	10 10 26.8	-17 11 26.0	20.41	0.01	0.567	-14.95	427
2764	10 11 45.3	-17 23 49.4	20.42	0.09	0.584	-14.95	460
2850	10 11 47.3	-16 59 31.3	20.42	0.03	0.566	-14.94	503
3955	10 12 17.1	-17 04 14.5	20.42	0.01	0.680	-14.95	562
1549	10 11 08.8	-17 21 08.3	20.45	0.01	0.697	-14.92	319
3194	10 11 56.4	-16 59 28.9	20.45	0.01	0.674	-14.91	544
3516	10 12 22.5	-16 52 36.3	20.45	0.03	0.696	-14.92	866
4072	10 12 14.8	-17 19 49.1	20.45	0.02	0.632	-14.92	538
43	10 10 25.6	-17 19 50.2	20.45	0.01	0.701	-14.92	510
3319	10 12 00.3	-17 12 46.2	20.46	0.01	0.572	-14.90	349
3685	10 12 06.4	-17 11 17.7	20.46	0.00	0.643	-14.91	401
1130	10 10 58.0	-17 08 45.6	20.47	0.09	0.528	-14.90	206
2949	10 11 49.9	-16 59 01.3	20.47	0.09	0.616	-14.90	529
373	10 10 36.3	-17 23 14.4	20.47	0.09	0.554	-14.90	517
91	10 10 26.7	-16 54 23.5	20.48	0.06	0.580	-14.89	753
2208	10 11 27.8	-17 04 21.1	20.49	0.01	0.604	-14.87	285
2357	10 11 33.6	-17 06 27.3	20.50	0.01	0.541	-14.87	237
316	10 10 34.3	-17 17 52.0	20.50	0.02	0.621	-14.87	413
3673	10 12 12.6	-17 03 29.0	20.50	0.09	0.673	-14.87	544
4058	10 12 29.0	-17 18 41.3	20.51	0.02	0.628	-14.86	628
4183	10 12 10.7	-17 02 51.6	20.51	0.01	0.632	-14.86	544
1317	10 11 02.8	-17 06 18.5	20.53	0.00	0.548	-14.84	242
2056	10 11 23.8	-17 00 51.8	20.53	0.01	0.749	-14.84	397
4266	10 12 32.4	-17 07 45.1	20.54	0.05	0.540	-14.83	634
457	10 10 38.4	-17 06 08.5	20.54	0.03	0.465	-14.83	392
1252	10 11 01.1	-17 18 07.8	20.55	0.02	0.545	-14.82	249
1401	10 11 04.6	-16 54 36.5	20.55	0.01	0.683	-14.82	622
3434	10 12 02.3	-16 52 39.0	20.55	0.00	0.684	-14.82	772
3266	10 11 58.6	-17 08 27.1	20.56	0.07	0.523	-14.80	360
3299	10 11 59.9	-17 05 45.7	20.56	0.00	0.625	-14.81	412
3410	10 12 02.1	-17 12 44.4	20.56	0.03	0.624	-14.80	364
3025	10 11 51.8	-17 17 45.6	20.58	0.00	0.672	-14.79	338
1034	10 10 55.4	-17 07 13.7	20.59	0.01	0.571	-14.78	257
1207	10 11 00.2	-17 16 29.3	20.59	0.02	0.528	-14.78	210
3143	10 11 55.4	-17 14 47.0	20.59	0.05	0.543	-14.77	320
4420	10 12 32.0	-16 57 50.3	20.59	0.05	0.619	-14.78	790
3170	10 11 55.9	-17 10 33.8	20.60	0.09	0.523	-14.76	317
4110	10 12 13.2	-16 59 26.5	20.60	0.05	0.601	-14.77	637
536	10 10 40.7	-17 05 38.4	20.60	0.01	0.790	-14.76	387
3149	10 11 55.2	-16 56 24.9	20.61	0.01	0.610	-14.76	629
3356	10 12 01.0	-16 59 15.5	20.62	0.05	0.569	-14.74	573
4200	10 12 25.8	-16 56 29.2	20.62	0.01	0.662	-14.75	783
532	10 10 40.6	-17 23 40.2	20.62	0.05	0.613	-14.75	505
622	10 10 43.0	-17 20 07.2	20.62	0.08	0.491	-14.75	400
3395	10 12 01.8	-17 09 15.9	20.63	0.08	0.550	-14.74	376
3543	10 12 03.6	-17 15 25.5	20.64	0.01	0.776	-14.73	392
3585	10 12 07.7	-16 59 04.5	20.64	0.01	0.526	-14.73	614

Table A.10: Candidate satellite galaxies in the field of MCG-03-26-030 (continued).

Number (1)	RA (J2000) (2)	DEC (J2000) (3)	R (mag) (4)	Class (5)	A (arcsec) (6)	M_R (mag) (7)	Dist (kpc) (8)
805	10 10 48.6	-17 19 53.9	20.66	0.08	0.604	-14.70	362
1575	10 11 09.7	-17 20 04.8	20.67	0.09	0.512	-14.70	281
408	10 10 36.8	-16 56 28.1	20.67	0.05	0.544	-14.70	647
609	10 10 42.8	-17 17 19.8	20.68	0.07	0.539	-14.69	343
1289	10 11 02.2	-17 20 43.2	20.69	0.04	0.504	-14.68	323
2496	10 11 37.8	-17 09 34.9	20.69	0.05	0.485	-14.68	186
54	10 10 25.8	-17 16 51.0	20.69	0.01	0.712	-14.68	463
4281	10 12 06.9	-17 17 55.6	20.70	0.01	0.605	-14.66	449
1381	10 11 04.3	-17 03 30.6	20.71	0.06	0.672	-14.66	324
3522	10 12 15.2	-17 03 47.6	20.71	0.02	0.523	-14.65	556
2424	10 11 35.6	-17 08 37.6	20.74	0.04	0.504	-14.63	190
1562	10 11 09.3	-17 22 09.9	20.77	0.05	0.590	-14.59	352
3448	10 12 02.9	-17 16 35.3	20.78	0.06	0.545	-14.59	400
3899	10 12 18.9	-17 14 23.7	20.78	0.02	0.481	-14.59	509
421	10 10 37.4	-17 13 59.1	20.78	0.02	0.618	-14.59	344
1901	10 11 18.9	-17 00 12.7	20.79	0.01	0.841	-14.58	417
3165	10 11 55.5	-16 57 49.9	20.81	0.01	0.483	-14.56	588
1295	10 11 02.2	-17 04 54.2	20.82	0.05	0.505	-14.55	287
2862	10 11 47.9	-17 15 11.5	20.83	0.02	0.537	-14.54	266
3542	10 12 12.6	-17 17 23.2	20.83	0.05	0.506	-14.53	485
1019	10 10 54.8	-17 09 21.7	20.85	0.01	0.571	-14.52	218
4063	10 12 14.8	-17 13 08.7	20.85	0.04	0.575	-14.52	470
4093	10 12 13.9	-17 04 22.7	20.87	0.09	0.492	-14.50	536
2154	10 11 26.3	-17 10 23.2	21.06	0.06	0.417	-14.30	92
2237	10 11 28.9	-16 58 31.1	21.10	0.08	0.564	-14.26	484
4513	10 12 31.7	-17 02 08.0	21.19	0.05	0.529	-14.18	703
94	10 10 27.1	-17 00 15.8	22.83	0.07	0.849	-12.54	594

Publications

The following publications have arisen from the work presented in this thesis.

1. *The photometric properties of isolated ealry-type galaxies* Reda F. M., Forbes D. A., Beasley M. A., O'Sullivan E. J., Goudfrooij P., 2004, MNRAS, 354, 851

2. *The fundamental plane of isolated early-type galaxies* Reda F. M., Forbes D. A., Hau G. K. T., 2005, MNRAS, 360, 693

3. *The spatially resolved stellar population of isolated early-type galaxies* Reda F.M., Proctor R. N., Forbes D. A., Hau G. K. T., Larsen S. S., astro-ph/0703545 (in press)